Exploring the relationship between white and grey matter damage in primary-progressive multiple sclerosis with structural magnetic resonance imaging

Benedetta Bodini

A thesis submitted to the University College of London for the degree of

Doctor of Philosophy

December 2012

UCL Institute of Neurology
Department of Brain Repair and Rehabilitation
Queen Square
London, WC1N 3BG
United Kingdom

Declaration

I, Benedetta Bodini, confirm that the work presented in this thesis is my own. Where information has been derived from other sources, I confirm that this has been indicated in the thesis.

Overview

In the first part of this thesis, an introduction of the main characteristics of the primary-progressive form of multiple sclerosis (PPMS) (Chapter I), and of the acquisition and post-processing of the conventional and quantitative magnetic resonance imaging techniques employed in the studies presented in this thesis (Chapter II), will be presented. In the second part of this thesis, several advanced imaging techniques will be employed to answer the following two key questions on PPMS: 1) Is there is a spatial and temporal link between the pathological processes occurring in the normal appearing white matter (WM) and in the grey matter (GM) of patients with PPMS?; 2) Which regions of WM and GM abnormalities significantly contribute to clinical progression and cognitive dysfunction over time in patients with PPMS?

To answer the first question, I first used tract-based spatial statistics (TBSS) and voxel-based morphometry (VBM), to explore the spatial relationship between the damage occurring in the normal-appearing WM and GM in patients with early PPMS (Chapter III). Then, I moved onto exploring the temporal relationship linking the pathological changes affecting the two compartments, employing magnetization transfer imaging (MTI) and diffusion-based tractography (Chapter IV).

To answer the second question, I first looked at the prognostic role of WM lesion location in a study conducted on a large population of patients with well-established PPMS who were followed-up for ten years in five different European centres (Chapter V). Then, using a novel approach which combines MTI and TBSS, I explored the regions of short-term accrual of microstructural damage in patients with early PPMS (Chapter VI). Finally, I moved onto examining the relative contribution of WM and GM damage to long-term motor and cognitive disability in PPMS (Chapter VII).

In the final Chapter, I will summarise the results of the studies presented in this thesis, provide an answer to the two key questions on PPMS, and propose future directions for research.

Acknowledgements

The work presented in this thesis was carried out in the Department of Brain Repair and Rehabilitation, UCL Institute of Neurology, which received a proportion of funding from the Department of Health's NIHR Biomedical Research Centres funding scheme and from the Multiple Sclerosis Society of Great Britain and Northern Ireland. My PhD was funded by fellowships I was awarded from the ENS, the AISM/FISM, and the MAGNIMS/ECTRIMS, and I would like to thank all these organisations for their generous support.

I am extremely grateful to my principal supervisor, Dr Olga Ciccarelli, for guiding me with tireless enthusiasm and motivation through the whole process of my research and writing up of this thesis. Over these years she has supported me in every single aspect of my life, and I could not have asked for a more inspirational mentor, for a more caring friend, and for a better auntie for my son. I would also like to warmly thank my second supervisor, Professor Alan J Thompson, from whom I learnt a great deal on identifying my goals and keeping focused on them, on dealing with academic writing and oral communications, and on enhancing emotional intelligence.

I would like to thank Dr Claudia Wheeler-Kingshott and Dr Mara Cercignani for sharing with me their deep knowledge of MRI physics (as well as countless meals chit-chatting in Italian, and fun nights out during conferences), and for making London a second home for me. I am also very grateful to Dr Declan Chard and Dr Ahmed Toosy, for helping me over the years in dealing with challenging clinical cases and with the even more challenging reviewers' comments to my papers. I wish to thank Professor David H Miller for his thoughtful comments to my papers and to my abstracts, and Dr Daniel Altmann, for his great input on the statistical part of my studies. I would also like to extend my gratitude to all the researchers who shared with me the infinite "chicken and egg project", which has finally come to an end, and is presented in Chapter IV. I

would like to warmly thank Dr Marco Battaglini, whose help was essential for carrying out the study presented in Chapter V, for finding our way out of the forest in Kauai, and for managing to submit our abstract for the last ECTRIMS conference exactly thirty seconds before the deadline.

A special thank goes to my friends and colleagues Dr Zhaleh Khaleeli, Dr Tom Jenkins, Dr Carmen Tur, Dr Nikos Gorgoraptis, and more recently Dr Amber Michelle Hill and Dr Khaled Abdel-Aziz, who at different times shared with me the small office on the 7th floor of Queen Square House, the Tuesdays in clinic, many nights out, my 30th birthday in New York, my pregnancy, the joys and the pains of my research, and all that made my years in London the most fun and unforgettable period of my life.

Many other people contributed directly or indirectly to my research, and I am very grateful to all of them for their valuable input and great support. In particular, I would like to mention the patients and the healthy volunteers who took part in the studies presented in this thesis, all the MRI physicists, the students of the Fellows' room, Ms Tracey Gibson, Ms Rowena Kemp, Ms Marie Braisher, Ms Tina Holmes, Ms Taira Bibi, Ms Navaeeda Naaem, Dr Elisabetta Cittadini, Ms Arianna Sanesi, Dr Antonella Ivaldi and all my wonderful friends in Rome, London and Paris.

My research would not have been possible without the help of my mother and my father, whose unconditioned love and infinite support sustained me throughout this long journey. Finally, I would like to thank my little Enrico, who was born just before I started writing this thesis, for always succeeding in getting a smile out of me with his irresistible laugh. Every page of this work is dedicated to him.

Publications associated with this thesis' work

Papers:

Bodini B, Khaleeli Z, Cercignani M, Miller DH, Thompson AJ, Ciccarelli O. Exploring the relationship between white matter and grey matter damage in early primary-progressive multiple sclerosis: an in vivo study with TBSS and VBM. *Human Brain Mapping*. 30(9):2852-61, 2009.

Bodini B, Battaglini M, De Stefano N, Khaleeli Z, Barkhof F, Chard D, Filippi M, Montalban X, Polman C, Rovaris M, Rovira A, Samson R, Miller D, Thompson A, Ciccarelli O. T2 lesion location really matters: a 10 year follow-up study in primary progressive multiple sclerosis. *Journal of Neurology, Neurosurgery and Psychiatry*. 82(1):72-7, 2011.

Dalton CM, **Bodini B**, Samson RS, Battaglini M, Fisniku LK, Thompson AJ, Ciccarelli O, Miller DH, Chard DT. Brain lesion location and clinical status 20 years after a diagnosis of clinically isolated syndrome suggestive of multiple sclerosis. *Multiple Sclerosis*. 82(9):1022-4, 2011.

Tozer DJ, Chard DT, **Bodini B**, Ciccarelli O, Miller DH, Thompson AJ, Wheeler-Kingshott CA. Linking white matter tracts to associated cortical grey matter: a tract extension methodology. *Neuroimage*. 59(4):3094-102, 2012.

Bodini B, Cercignani M, Khaleeli Z, Miller DH, Ron M, Penny S, Thompson AJ, Ciccarelli O. Corpus callosum damage predicts disability progression and cognitive dysfunction in primary-progressive MS after five years. *Human Brain Mapping*. Feb 13, 2012; [Epub ahead of print]

Bodini B, Cercignani M, Toosy A, De Stefano N, Miller DH, Thompson AJ, Ciccarelli O. A novel approach with "skeletonised MTR" measures tract-specific

microstructural changes in early primary-progressive multiple sclerosis. *Human Brain Mapping*, in press.

Bodini B, Chard D, Altmann D, Tozer D, Miller DH, Thompson AJ, Wheeler-Kingshott C, Ciccarelli O. White matter damage precedes and possibly causes later grey matter changes in early primary-progressive MS, in preparation.

Bodini B, Battaglini M, Eshaghi A, Gasperini C, Pozzilli C, Thompson AJ, De Stefano N, Ciccarelli O. Longitudinal microstructual and structural changes in relapsing and primary-progressive MS: lessons from the early phase, in preparation.

Book chapter:

Bodini B, Ciccarelli O. Diffusion MRI in neurological disorders. In: *Imaging brain pathways - Diffusion MRI: from quantitative measurement to in-vivo neuroanatomy.* Publisher: Academic (Elsevier), 2008. Editors: Heidi Johansen-Berg and Tim Behrens, University of Oxford.

Prize:

Bodini B. Corpus callosum damage predicts disability progression and cognitive dysfunction in primary-progressive MS after five years. Award for the best poster, Queen Square Symposium poster competition, London, 2010.

Table of contents

Chapter IV

List of tables

Chapter V

Chapter VI

Chapter VII

Appendix I

List of Figures

CHAPTER III

CHAPTER IV

CHAPTER V

CHAPTER VI

CHAPTER VII

List of formulas

CHAPTER II

List of abbreviations

AD	Axial diffusivity
ADC	Apparent diffusion coefficient
CC	Corpus callosum
CNS	Central nervous system
CSF	Cerebro-spinal fluid
CST	Cortico-spinal tract
DIR	Double inversion recovery
DTI	Diffusion tensor imaging
DWI	Diffusion-weighted imaging
EDSS	Expanded Disability Status Scale
EPI	Echo planar imaging
FA	Fractional anisotropy
FID	Free Induction Decay
FLAIR	Fluid attenuation inversion recovery
FOV	Field of view
FSE	Fast spin-echo
FSPGR	Inversion-prepared fast spoiled gradient recall
GCC	Genu of the corpus callosum
GE	Gradient echo
GM	Grey matter
IFOF	Inferior fronto-occipital fasciculus
IR	Inversion recovery

LEAP	Lesion automated pre-processing
LPM	Lesion probability map
MD	Mean Diffusivity
MRI	Magnetic resonance imaging
MS	Multiple sclerosis
MSFC	Multiple Sclerosis Functional Composite
MTI	Magnetisation transfer imaging
MTR	Magnetisation transfer ratio
NAGM	Normal appearing grey matter
NAWM	Normal appearing white matter
NHPT	Nine-Hole Peg Test
PASAT	Paced Auditory Serial Addition test
PD-w	Proton density weighted
PPMS	Primary-progressive multiple sclerosis
RF	Radio frequency
RD	Radial diffusivity
ROI	Region of interest
RRMS	Relapsing-remitting multiple sclerosis
SD	Standard deviation
SE	Spin-echo
SLF	Superior longitudinal fasciculus
SNP	Single nucleotide polymorphism
SPM	Statistical parametric mapping
SPMS	Secondary-progressive multiple sclerosis
T1-w	T1-weighted
T2-w	T2-weighted

TBSS	Tract-based spatial statistics
TE	Echo time
TI	Inversion time
TR	Repetition time
TWT	Timed Walk Test
VBM	Voxel-based morphometry
WM	White matter

The primary-progressive form of multiple sclerosis

Chapter I

In this first Chapter, the characteristics of the primary-progressive form of multiple sclerosis will be discussed. This chapter is divided into three parts. The first part is a review of epidemiology, aetiology, clinical presentation, diagnostic criteria, and therapy of this form of disease. The second section is a summary of this patient group main features that conventional and advanced imaging techniques have allowed to unveil. The final section of this Chapter describes the rationale for this thesis.

1.1 Primary-progressive multiple sclerosis

1.1.1 Multiple sclerosis and its primary-progressive form: overview and epidemiological data

Multiple sclerosis (MS) is a chronic neurological disease of the central nervous system (CNS) that primarily affects young adults, with a prevalence of between 1 in 500 and 1 in 1500 of the population in Europe, North America, and Australasia (Miller and Leary, 2007). It is an inflammatory demyelinating disease, which is characterised by the presence of typical white-matter (WM) lesions in the brain and spinal cord, although the importance of the neurodegenerative component of this disease is being increasingly acknowledged.

MS incorporates different subtypes of disease, each one characterised by a different course. The main clinical subtypes of MS were defined 20 years ago as *relapsing-remitting* (RRMS) and chronic progressive MS. The former is characterised by episodes of acute clinical deterioration (relapses), followed by periods of partial or complete recovery (remissions); the latter is characterised by a gradual, progressive deterioration in neurological functions over months or years. Most cases of chronic progressive MS start as RRMS (the so-called *secondary progressive* form, SPMS). According to epidemiological studies, most patients with RRMS eventually develop SPMS, entering a phase of progressive deterioration. However, in a subgroup of patients with MS, the disease course is characterised by a steady neurological deterioration from onset; this particular, rarer form of MS, has been labelled *primary-progressive*

(PPMS). About 10% of patients with PPMS have relapses (Andersson et al., 1999). Since 1996, there has been a formal classification of MS clinical subgroups according to clinical course, that includes RRMS, SPMS, and PPMS, which has become widely accepted (Lublin and Reingold, 1996) (Figure 1.1).

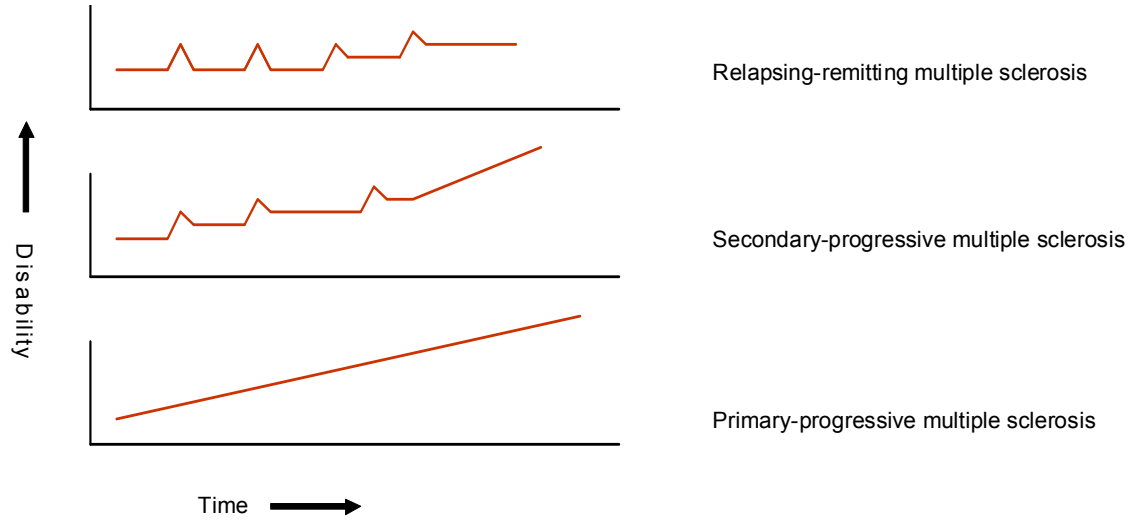

Figure 1.1. Graph representing the disease course of different types of multiple sclerosis.

A primary-progressive presentation is seen in approximately 10% of patients with MS (Koch et al., 2009). Most patients with PPMS come from areas where MS is common, such as North America and Europe, but an increasing number of studies have shown that this form of disease is also present in other parts of the world, such as South America and Africa (Idris et al., 2009; Ferreira Vasconcelos et al., 2010). In addition to its particular disease course, the PP form differs from the other subtypes of MS in other aspects. Symptom onset in patients with PPMS tends to occur at an older age compared with the RR form of disease (mean 40 years versus 30 years). In contrast to RRMS, where MS occurs between two and three times more frequently in women, there is no gender predominance in PPMS (Miller and Leary, 2007).

1.1.2 Genetic and environmental influence on the aetiology of PPMS

1.1.2.1 *Genetic factors*

To date, most studies have not reported evidence for genetic associations with the clinical forms of MS or the severity of the disease course (Ramagopalan et al., 2008; Jensen et al., 2010; Sawcer et al., 2011).

An association between the DR2 haplotype DRB1*15:01 in the class II region of the major histocompatibility complex on the short arm of chromosome 6 and the risk of developing MS, has been found both in patients with RRMS and PPMS (Barcellos et al., 2003; Miller and Leary, 2007; Ramagopalan et al., 2010). Moreover, an association with PPMS has been reported with other HLA haplotypes, such as DR4 - DQ8, DR7-DQw9 and DRw8-DQw4 haplotypes, and with DR3 (Ramagopalan et al., 2008). Data from a study conducted in a cohort of patients with PPMS showed a significant difference in the severity of the disease between HLA DRB1*1501-positive and negative patients, with the former deteriorating more quickly over time (Vasconcelos et al., 2009).

Over the years, genes outside the major histocompatibility complex with modest effect in MS have been identified, including interleukin-7 receptor α (IL7RA), interleukin-2 receptor α (IL2RA) and tumor-necrosis-factor receptor superfamily member 1A (TNFRSF1A) (Ramagopalan et al., 2010). A significant association with disease susceptibility was also found for chromosome 10 open reading frame (C10orf27), in a study conducted on 571 patients with RRMS and PPMS, and on healthy controls (Goertsches et al., 2008). Modestly powered studies found some evidence of an increased risk of developing the PP form of disease in patients with the Apolipoprotein E ε4 allele (Cocco et al., 2005), the Cytotoxic T Lymphocyte Antigen 4 G49 (Maurer et al., 2002), and the interleukin-4 E1(33) TT (Kantarci et al., 2003). An interesting study found an underexpression of the interleukin 7 receptor (IL7R, which is crucial for T cell maturation and proliferation) gene in patients with PPMS compared with those with SPMS, suggesting that IL7R may be a potential therapeutic target for PPMS. More recently, a study has confirmed the previously documented association between the perforin 1 gene and MS, and has reported that a subgroup of patients with

PPMS, mainly males, were characterized by not only a low perforin expression in peripheral blood cells, but also deficient expression in additional genes that code for proteins involved in cell killing by CD8+ T cell and NK cells, with mechanisms similar to perforin (Camina-Tato et al., 2010).

Recently, a genome-wide association study that included patients with MS from Europe, United States of America, Australia and New Zealand, replicated almost all of the previously suggested associations and identified further novel susceptibility loci, within genes such as VCAM1, CD65 or IL12B (Sawcer et al., 2011). Among the susceptibility genes proposed in this study, TMEM39A, IL12B and CBLB have been subsequently validated in another study on a large population of Spanish patients (Varade et al., 2012).

Finally, a recently published study on 590 Finnish patients investigated the association of specific single nucleotide polymorphisms (SNPs) in the genes of the melatonin pathway, and the risk of developing progressive MS. The Authors found an association between polymorphisms of the melatonin pathway genes and the risk of developing PPMS, as well as the risk of severe disability in PPMS (Natarajan et al., 2012).

1.1.2.2 *Environmental factors*

Epidemiological studies clearly demonstrate a prominent role for environmental factors in determining the disease risk for MS (Ramagopalan et al., 2010). There is strong evidence that Epstein-Barr virus (EBV) infection precedes MS onset and there is a dose dependent relationship between the risk of MS and the level of EBV specific antibodies (Lucas et al., 2011). A study conducted in 100 subjects, including 25 PPMS patients, showed that the pattern of serologic response to EBV was different between clinical subgroups, which may imply a different immunologic response to primary infection with EBV; this may determine/influence the clinical phenotype of the disease (Farrell et al., 2009)

Several retrospective and prospective studies have demonstrated an association between smoking and susceptibility to MS (Jafari and Hintzen, 2011). In particular, cigarette smokers have a higher risk of developing MS

compared with those who never smoke (Ascherio and Munger, 2007). Interestingly, a study conducted in 1465 MS patients, which included 63 patients with PPMS, found that the probability of a PP course of MS was significantly higher in current smokers or ex-smokers than that of an initially relapsing form of disease (Healy et al., 2009). This result is in line with data showing the neurotoxic effects of components of cigarettes, and the association of tobacco smoke components (such as cyanides) with demyelination in animal studies (Jafari and Hintzen, 2011).

Within temperate regions , MS incidence and prevalence increase with latitude, while living below 35° latitude for the first 10 years of one's life reduces this risk by approximately 50% (Ramagopalan et al., 2010). The association between sunlight exposure and vitamin D levels is a potential explanation for the association between MS incidence and latitude (van der Mei et al., 2003). It has been extensively documented that past sunlight exposure is inversely related to MS susceptibility, and higher vitamin D levels protect against MS (Munger et al., 2006). However, in a recent study comparing Vitamin D serum levels in patients with RRMS, PPMS and healthy controls, it was found that, differently from the RRMS group, where a significant reduction in Vitamin D levels compared to healthy controls was observed, in patients with PPMS the Vitamin D levels were similar to those observed in healthy individuals (Correale et al., 2011). A possible explanation for this finding is the different effect that Vitamin D could have on the pathogenic processes mediating brain damage in RRMS and PPMS.

1.1.3 Clinical presentation and disease course

The most common clinical presentation in patients with PPMS is a gradual and progressive, spastic paraparesis (usually lower limb asymmetric weakness and stiffness) (Cottrell et al., 1999), whilst in patients with RRMS the most frequent initial presentation is characterized by visual and sensory disturbances (Miller et al., 2012). Other (less frequent) presentations of PPMS include visual loss and cerebellar or brainstem disturbance. Usually, the clinical picture gradually deteriorates over months or years. However, in some cases symptoms can

remain stable for long periods. Urinary urgency and retention, bowel disturbances (including constipation and, less frequently, faecal urgency), as well as sexual dysfunction, are also common in PPMS.

Cognitive impairment is very frequent in MS, affecting up to 65% of patients, and is usually more common in the progressive forms of the disease (Amato et al., 2006). It has been well documented that cognitive dysfunction in PPMS is present in about 30% of patients, affecting a number of domains, including memory, attention/speed of information processing, and executive function (Camp et al., 1999; Camp et al., 2005; Ukkonen et al., 2009). Studies comparing the pattern and severity of cognitive impairment in different MS subtypes have reported more severe impairment in patients with progressive forms of MS than in those with RRMS (Huijbregts et al., 2004; Huijbregts et al., 2006), but only subtle differences in the pattern of neuropsychological deficit and in the severity of cognitive dysfunction have been seen between patients with PPMS and SPMS (Foong et al., 2000).

PPMS carries the worst prognosis of all MS subtypes. However, the speed of disability accumulation varies considerably among patients with this form of disease (Miller and Leary, 2007). Studies on the long-term natural history of patients with PPMS have shown that the speed of disability accumulation, as measured by the number of years taken to reach 6.0 on the Expanded Disability Status Scale (EDSS) (Kurtzke, 1983), varies considerably between different cohorts. In particular, while earlier studies reported a rapid disease progression (7.1 years to EDSS 6.0 in the Lyon cohort and approximately 8.5 years in the London, Ontario cohort) (Cottrell et al., 1999; Confavreux and Vukusic, 2006), data from the British Columbia MS cohort showed a much slower disease course (Tremlett et al., 2005); Koch et al. found that patients in this cohort took 14 years to reach EDSS 6.0 (Koch et al., 2009). Interestingly, a very recent study on the British Columbia MS cohort showed that 9.2% of PPMS patients showed a natural and innate improvement of ≥ 0.5 in EDSS over one year of follow-up (Tremlett et al., 2012).

Few clinical predictors of disease course have been identified in natural history

studies conducted on patients with PPMS. It has been shown that patients presenting at onset with involvement of three or more systems had a faster clinical deterioration over time compared with those with less than three systems involved (Cottrell et al., 1999). A worse prognosis has also been identified in patients presenting with cerebellar or brainstem symptoms (Tremlett et al., 2005). There is some evidence that in this form of disease the clinical decline is faster in men than in women (Cottrell et al., 1999; Confavreux and Vukusic, 2006) and in patients presenting with a faster rate of initial progression (Cottrell et al., 1999; Tremlett et al., 2005). More recently, in the British Columbia cohort, sensory symptoms at presentation and a younger age at disease onset were associated with a longer time to reach EDSS 6.0 (Koch et al., 2009). Two MAGNIMS (Magnetic Resonance Imaging in MS) multi-center studies, found that a shorter disease duration at baseline, male sex, and a more severe clinical disability at study entry, as measured by EDSS and timed-walk test (Cutter et al., 1999), were all independent predictors of a worse long-term clinical outcome in the large cohort of PPMS patients (Sastre-Garriga et al., 2005b; Khaleeli et al., 2008b).

1.1.4 Pathology of PPMS: differences and similarities with other forms of MS

1.1.4.1 *Pathological hallmarks of MS*

The pathological hallmarks of MS include inflammation, demyelination, remyelination, gliosis, neurodegeneration, which affect the WM and the GM both focally and diffusely (Lassmann et al., 2012). In particular, MS is characterised by multiple foci of inflammation (lesions) in the white matter, consisting of perivascular lymphocytic infiltrates, loss of oligodendrocytes and demyelination (Reynolds et al., 2011). Within the demyelinated lesions there is prominent astrogliosis. A degree of axonal damage has been reported to occur in active, inflammatory, demyelinating lesions (Trapp et al., 1998). In addition, demyelination is also present in both in the deep and cortical GM and is associated with neuronal loss (Bo et al., 2003; Geurts and Barkhof, 2008; Magliozzi et al., 2010). Recently, Lucchinetti and colleagues have studied cortical tissue from 138 patients with clinically isolated syndromes and early RRMS obtained with diagnostic stereotactic biopsy targeting WM lesions; they

demonstrated that even in the early stage of MS, cortical demyelinating lesions are frequent, and strongly associated with meningeal inflammation (Lucchinetti et al., 2011) (Figure 1.2). They also reported that the majority of the examined GM lesions were associated with inflammatory infiltrates. This is in contrast to previously reported data on the lack of lymphocytic infiltration, complement deposition and blood-brain barrier disruption in GM lesions (Geurts and Barkhof, 2008). In this respect, it is important to underline that the biopsy specimens under investigation in the study by Lucchinetti et al. originated from patients with atypical clinical and radiological presentations, and therefore the results may not generalise to typical MS cases (Lucchinetti et al., 2011). Cortical lesions are mainly localised in the subpial cortical layers in progressive MS, and active lesions are associated with activated microglia. Moreover, rims of activated microglia have been recently found at the border of cortical lesions in a subset of patients with more active WM inflammation and a worse disease course (Kooi et al., 2012).These data suggest that GM tissue damage may be driven by a soluble factor produced by meningeal inflammatory aggregates, which would cause tissue damage in the cortex either directly or indirectly through microglial activation (Howell et al., 2011; Lassmann et al., 2012).

Outside the macroscopically visible lesions, within the so called normal-appearing white matter (NAWM) and grey matter (NAGM), diffuse pathology has been demonstrated, consisting of axonal damage and loss (Kutzelnigg et al., 2005), microglial activation (Howell et al., 2010), changes at the nodes of Ranvier (Howell et al., 2011), and neuronal loss (Magliozzi et al., 2010). It has been shown that some degree of remyelination in demyelinated lesions may occur, but it is variable in extent (Patrikios et al., 2006; Patani et al., 2007).

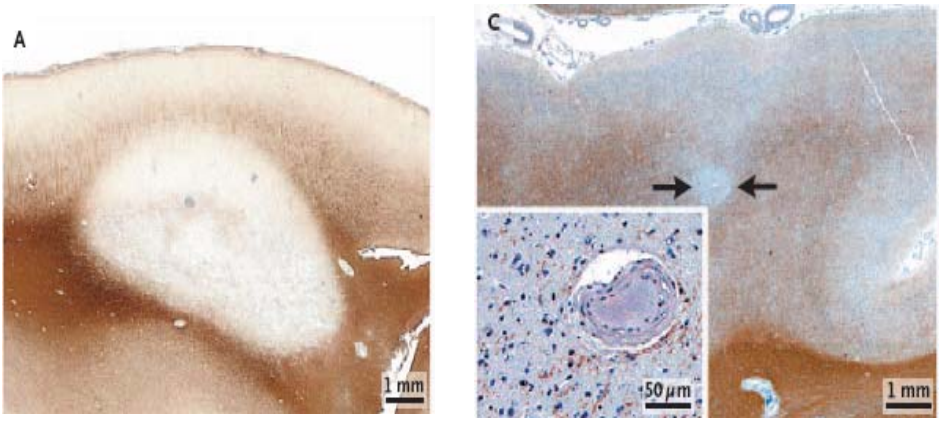

Figure 1.2 On the left, bioptic tissue showing a cortical demyelinating lesion in patients with early RRMS; on the right, the arrows indicate an area of intracortical demyelination, in which neurons are visible (inset) (*Adapted from Lucchinetti et al., 2011*).

1.1.4.2 *White matter and grey matter pathology in PPMS*

In a post-mortem study comparing the different subtypes of MS, it was found that the focal WM lesion load in PPMS was the lowest of all MS forms (Kutzelnigg et al., 2005). Moreover, while the most extensive inflammatory reaction was found in focal WM plaques in all disease subtypes, there was a mild, but *diffuse* inflammatory reaction in the NAWM of patients with progressive MS (Figure 1.3), which was significantly less pronounced in patients with RRMS. This inflammatory reaction was characterised by a diffuse infiltration of the tissue by T-lymphocytes, and by perivascular aggregates of mononuclear cells, and was associated with prominent microglial activation. Axonal damage and degeneration were present throughout the WM, although there was some increase around demyelinated plaques (Figure 1.3). Patients with progressive disease showed significantly more diffuse axonal injury in the NAWM compared with patients with acute or relapsing disease. Finally, no significant correlation was found between the focal lesion load and microglia activation or axonal injury in the NAWM, supporting the concept that diffuse WM pathology may develop independently from focal lesions in progressive MS (Kutzelnigg et al., 2005; Reynolds et al., 2011).

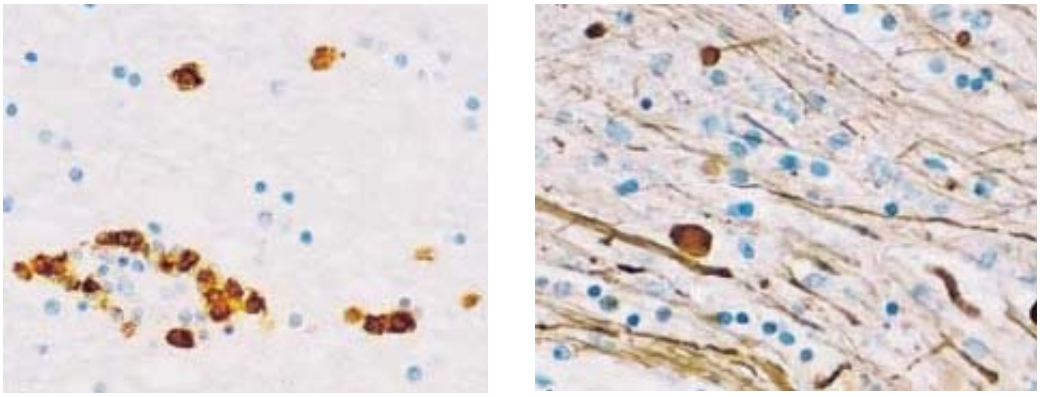

Figure 1.3 On the left, inflammation in the NAWM in PPMS (immunocytochemistry for CD8+ cells); on the right, diffuse axonal injury, reflected by axonal swellings and end bulbs in the NAWM of a PPMS patient (immunocytochemistry for neurofilament). (*Adapted from Kutzelnigg et al, 2005*).

On the other hand, in another histological study looking at the interdependence of inflammation, neurodegeneration and disease course, a highly significant association between inflammation and axonal injury was seen in the global MS population as well as in PPMS alone, supporting a close association between inflammation and neurodegeneration in all lesions and subtypes of MS (Frischer et al., 2009).

When comparing the cortico-spinal tract pathology of patients with PPMS with that of SPMS, Tallantyre et al. found that PPMS patients had a similar degree of axonal loss to SPMS patients, but presented a lower extent of demyelination in the WM. Therefore, PPMS patients presented a more pronounced axonal loss than SPMS patients within similarly demyelinated lesions (Tallantyre et al., 2009).

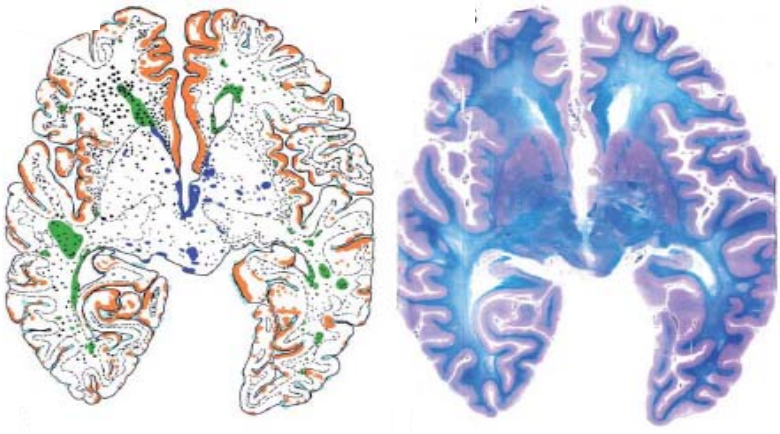

Figure 1.4 Cortical demyelination in PPMS. On the left, schematic illustration of pathological findings in a PPMS brain. In green: focal demyelinated plaques in the white matter; in red: cortical demyelination; in blue: demyelinated lesions in the deep grey matter; dark blue dots: inflammatory infiltrates in the brain; light blue dots: inflammatory infiltrates in the meninges. (*Adapted from Kutzelnigg et al, 2005*).

With regard to GM pathology, Kutzelnigg et al. demonstrated that demyelination in the cerebral cortex was significantly greater in patients with progressive MS than in those with relapsing MS. Demyelination mainly affected the subpial layers of the cerebral cortex, was associated with mononuclear inflammatory infiltrates in the meninges, and was significantly correlated with global inflammation and microglial activation in the NAWM (Kutzelnigg et al., 2005) (Figure 1.4). Recently, Choi et al. investigated the extent of WM perivascular and meningeal inflammation on post-mortem brain tissue from 26 cases of PPMS; they found that cases showing an increased level of meningeal inflammation exhibited a more extensive demyelination and neurite loss in the cortical grey matter, and were also those with a more severe disease course (i.e. shorted disease duration and younger age at death) (Choi et al., 2012). The Authors also reported a lack of tertiary lymphoid-like structures in PPMS brains.

When comparing GM pathology between patients with PPMS and SPMS, studies report different results. While early studies found that the degree of cortical GM demyelination was similar between PPMS and SPMS, or higher in PPMS than in SPMS (Bo et al., 2003; Kutzelnigg et al., 2005), Tallantyre et al. showed that the extent of GM demyelination was significantly lower in patients

with the PP form of the disease when compared with SPMS (Tallantyre et al., 2009). The formation of ectopic follicles in the cerebral meninges has been investigated in progressive MS and, while in a proportion of SPMS cases the presence of ectopic follicles was demonstrated, they were not seen in PPMS cases (Magliozzi et al., 2007).

In a post-mortem study in brains of all subtypes of MS (including 11 cases of PPMS), remyelination was seen in all forms of MS. This process consists of an increased number of oligodendrocytes within WM lesions, that results in a myelin density, which is intermediate between fully demyelinated lesions and healthy brain tissue. It has been demonstrated that remyelination can be extensive also in patients with long standing disease (Patani et al., 2007), and appears to be more prominent in the cortex than in the WM (Albert et al., 2007). Interestingly, when comparing patients with PPMS and with SPMS with regard to remyelination, Bramow et al. found that the proportion of remyelinated shadow plaques was higher in the former than in the latter form of disease (Bramow et al., 2010).

1.1.5 Diagnosing PPMS: a longstanding challenge

Diagnosing MS is a process that includes clinical and paraclinical laboratory assessments to demonstrate dissemination of lesions in space (DIS) and time (DIT) and to exclude alternative diagnoses. The Poser committee in 1983 formalised the diagnostic criteria for MS (Poser et al., 1983), which were based on clinical evidence of dissemination in time and space. For the first time, paraclinical evidence (a new lesion on MRI or altered evoked potentials) was accepted to replace clinical evidence. For a *laboratory supported* diagnosis, intrathecal syntesis of immunoglobulin G had to be detected in the cerebrospinal fluid (CSF) analysis. These criteria did not address appropriately the diagnostic difficulties posed by the PP form of MS, as in this subtype of disease the clinical picture is gradually deteriorating, and often affects one single system, at least in the early stages.

Thompson's criteria for diagnosing PPMS addressed this issue, defining three levels of diagnostic certainty (definite, probable, and possible) based on clinical findings, abnormal CSF, abnormalities on MRI of the brain and spinal cord, and visual evoked potentials (Thompson et al., 2000). To achieve a diagnosis of definite PPMS, in addition to a documented history of at least one year of clinical progression, evidence of intrathecal synthesis of immunoglobulin G together with one of the following three MRI criteria was required: (1) nine brain lesions, (2) two spinal cord lesions, (3) four to eight brain lesions and one spinal cord lesion. In all the studies presented in this thesis, the patients with PPMS have been recruited following Thompson's criteria. These criteria were largely integrated in the international diagnostic criteria for MS in 2001 (McDonald et al., 2001).

In 2005, Polman's revisions of McDonald's criteria simplified the original Thompson's criteria for PPMS, as positive CSF analysis was no longer mandatory for a definite diagnosis of PPMS (Polman et al., 2005). In particular, a diagnosis of PPMS could be achieved with a negative lumbar puncture, when both the spinal cord and brain MRI meet the criteria. Reviewing all the diagnostic algorithms proposed over the years, it has been recently reinforced the added value of a positive CSF analysis for the diagnosis of PPMS (Montalban et al., 2009b). In 2010, the International Panel of Diagnosis of MS formulated the 2010 Revisions to the McDonald Criteria (Polman et al., 2011). In these revised criteria, an attempt to harmonise MRI criteria for all forms of MS has been made, while considering the special diagnostic needs for PPMS (see Table 1.1) In particular, a diagnosis of PPMS can be made when there is one year of disease progression associated with dissemination in space (DIS) of asymptomatic lesions in the brain and in the spinal cord, or with DIS of lesions either in the brain or the spinal cord and a positive CSF.

PPMS may be diagnosed in a subject with:
1. One year of disease progression (retrospectively or prospectively determined)
2. Plus 2 of the 3 following criteria[a]:
A. Evidence for DIS in the brain based on >1 T2[b] lesions in at least 1 area characteristic for MS (periventricular, juxtacortical, or infratentorial)
B. Evidence for DIS in the spinal cord based on >2 T2[b] lesions in the cord
C. Positive CSF (evidence of oligoclonal bands and/or elevated IgG index)

[a] If a subject has a brainstem or spinal cord syndrome, all symptomatic lesions are excluded from the criteria
[b] Gadolinium enhancement is not required

Table 1.1 Diagnostic criteria for PPMS according to the 2010 Revisions to the McDonald Criteria

Very recently, a study from Kelly et al. compared the sensitivity of the diagnostic criteria for PPMS with particular reference to spinal cord criteria and the utility of the CSF oligoclonal bands (Kelly et al., 2012). The Authors found that the sensitivity of Thompson's criteria (Thompson et al., 2000) was 64%, while that of McDonald's 2010 revisions was 77%. They concluded that an alternative criterion requiring two of: (i) one or more lesions in two of three regions typical for demyelination on brain MRI; (ii) one T2-w spinal cord lesion typical for demyelination on spinal cord MRI; (iii) presence of CSF oligoclonal bands; would increase the diagnostic sensitivity for PPMS.

1.1.6 Failures and hopes in the therapy of PPMS

1.1.6.1 *Failures*

The treatment of patients with RRMS has made great progress over recent years, as new and effective disease-modifying and immunosuppressive drugs have been licensed or are in the final phases of clinical trials (Wiendl and

Hohlfeld, 2009). The same cannot be said for patients with PPMS, for whom no disease-modifying drug has been shown to be effective in slowing the clinical deterioration over time (Fitzner and Simons, 2010). The largest placebo-controlled trial conducted so far on this subtype of disease involved 943 patients with PPMS, and evaluated the immunomodulatory drug, *glatiramer acetate* (GA) (Wolinsky et al., 2007). This clinical trial had to be prematurely interrupted, as an interim analysis showed no effect on disease progression after two years. After the termination of the clinical trial, a post-hoc analysis showed a possible effect of GA in slowing disease progression in a subgroup of PPMS patients (i.e., male patients who showed more rapid progression when untreated).

Two small, single-centre placebo-controlled trials have been conducted in London and in Barcelona to test the efficacy of another immunomodulatory drug, *interferon beta* (IFN beta) in PPMS (Leary et al., 2003; Montalban, 2004). Both trials failed to demonstrate a reduced clinical progression in patients treated with the active medication. More recently, a phase II, placebo-controlled, single-center trial with IFN beta-1b in PPMS, showed statistically significant differences in the Multiple Sclerosis Functional Composite score (MSFC) (Cutter et al., 1999) and in T1 and T2 lesion volumes (Montalban et al., 2009a) between the placebo and the treatment arm which were favoring the treatment.

A small, phase II trial with *mitoxantrone*, an immunosuppressant agent, was conducted in patients with PPMS, using 12mg/m^2 of mitoxantrone or placebo every 3 months for 24 months. No benefit on time to sustained progression was demonstrated in patients on treatment versus those on placebo (Stuve et al., 2004).

Cladribrine, a synthetic deoxyadenosine analog, is an oral immunomodulatory agent that produces targeted, sustained reduction of T and B lymphocytes. This drug has been tested in patients with SPMS and PPMS, and failed to show a reduction in disease progression in both groups. However, there was sustained reduction in the number and volume of Gadolinium-enhancing lesions on MRI (Rice et al., 2000).

More recently, the B cell depleting monoclonal antibody *rituximab*, that showed an impact on disease activity in RRMS (Hauser et al., 2008) and neuromyelitis optica (Bedi et al., 2011), was tested in PPMS. In total, 439 PPMS patients received two 1,000 mg intravenous rituximab or placebo infusions every 24 weeks, through 96 weeks (4 courses). There was no effect on the primary endpoint (time to confirmed disease progression) in the group treated with rituximab, but a post-hoc subgroup analysis suggested that selective B-cell depletion may affect disease progression in younger patients, particularly those with inflammatory lesions (Hawker et al., 2009).

Several explanations have been proposed to justify the failure of all the clinical trials in PPMS (Fitzner and Simons, 2010). One possible reason is that the immunomodulatory and immunosuppressive drugs tested may not be able to target the inflammatory cells in progressive MS, as there could be a compartmentalization of the inflammatory cells inside the blood-brain barrier, which is not sufficiently permeable to most drugs. Also, specific inflammatory components that seem to be of particular relevance in the pathogenesis of progressive MS, such as cells belonging to the innate immune system (activated microglia and dendritic cells), are not the main targets of current therapies.

However, other reasons may have contributed to the failure of the reported clinical trials. Firstly, as PPMS is a relatively uncommon form of disease, patient cohorts are usually rather small, and therefore drawing meaningful conclusions from available data is often challenging. Secondly, the time frames of the clinical trials performed so far could be too short to observe clinically meaningful treatment effects in PPMS, considering the need for progression-based-only primary outcome measures in these patients. Finally, without reliable prognostic markers of progression, recruitment is unselected (i.e. not stratified according to the risk of progression), and it is very difficult to identify treatment effects in patients with a low risk of progressing rapidly. Therefore, the studies presented in Chapters V-VIII aim at looking for reliable (radiological and clinical) markers of clinical progression in PPMS, which in future may be used to recruit in clinical trials patients who are more likely to respond to treatments.

1.1.6.2 *Hopes*

Several clinical trials testing the efficacy of various drugs on slowing clinical progression in PPMS are currently ongoing, and a summary of the tested compounds, their mechanism of action, and the study design and status is provided in Table 1.2.

Fingolimod, a sphingosine 1-phosphate receptor agonist which, in addition to an effect on lymphocyte migration, has been shown to affect the maturation of dendritic cells (Brinkmann, 2009), is currently being assessed in PPMS patients (see Table 1.2). A modulation of the activation state of microglial cells may be obtained with *Minocycline*, a traditional antibiotic with profound anti-inflammatory and neuroprotective effects, which is now considered for treating PPMS (Chen et al., 2011).

Several studies in experimental autoimmune encephalomyelitis, the animal model of MS, have provided encouraging data on the neuroprotective effects of drugs that in future could be used in the treatment of PPMS (Fitzner and Simons, 2010; Fox et al., 2012).

With regard to symptomatic treatment of PPMS, two phase III studies involving patients with all forms of MS have recently demonstrated that *fampridine* (4-aminopyridine), a potassium channel blocker, has a significant effect in improving walking speed (one third of the patients improved of about 25% their walking speed) (Goodman et al., 2009; Goodman et al., 2010).

Drug	Action	Study Design	Status
Idebenone	Syntetic analogue of coenzyme Q10, is a potent antioxidant, protecting cell membranes and mitochondria from oxidative damage	Phase I/II	Recruiting
Masitinib	Selective tyrosine kinase inhibitor that targets the survival, differentiation, and degranulation of mast cells, thus indirectly controlling their array of proinflammatory and vasoactive mediators	Phase III	Recruiting
FTY720 (Fingolimod)	Modulates sphingosine-1-phosphate (S1P) receptors and has strong immunoregulatory features	Phase III	Ongoing, but not recruiting
Ocrelizumab	Recombinant humanised antibody selectively targeting CD20+ B cells	Phase III	Recruiting
Hydroxyurea	Inhibiting the synthesis of deoxynucleotides essential for viral transcription, suppresses the replication of Epstein-Barr virus	Phase II	Recruiting
Natalizumab	Monoclonal antibody that inhibits leukocyte migration across the blood-brain barrier	Phase II	Completed
Erythropoietin	Selective oral tyrosine kinase inhibitor, effectively inhibits the survival, migration and activity of mast cells	Phase II	Recruiting

Table 1.2 Ongoing clinical trials on patients with PPMS in December 2012 (source: *U.S. National Institutes of Health*).

1.2 Imaging primary-progressive multiple sclerosis

PPMS presents unique characteristics that are different from the other subtypes of disease (Thompson, 2004; Miller and Leary, 2007). Despite the irreversible accumulation of neurological disability, patients with PPMS have a relatively low lesion load and lesion activity, as detected on T2-weighted, T1-weighted, and Gadolinium-enhanced brain scans (Thompson, 2004). One explanation for the dissociation between the clinical picture and the radiological features, defined as the “clinico-radiological paradox” (Barkhof, 2002), has been provided by data obtained with advanced MRI techniques (Miller and Leary, 2007), which have allowed the detection of abnormalities occurring outside visible lesions,

thus contributing towards a more complete understanding of the mechanisms that underlie clinical progression in MS (Rocca et al., 2012a). This section is divided in three parts. In the first part, a summary of the main findings of the studies conducted on lesions (in the WM and in the GM) and on atrophy will be provided; in the second part, a review of previously published investigations, which used the advanced MRI techniques applied in the studies presented in this thesis (i.e. diffusion tensor imaging (DTI), and magnetization transfer imaging (MTI)), will be presented. In the third part, the main findings of the studies conducted in our cohort of patients with early PPMS will be summarized.

1.2.1 Studies on lesions and atrophy

1.2.1.1 *WM and GM lesions*

With regard to active lesions, it has been shown that in the early phase of progression, MR-visible inflammation is more frequent than in the later stages of the disease; however, this early inflammation does not seem to have a significant impact on the subsequent accumulation of clinical disability (Ingle et al., 2005; Khaleeli et al., 2010). T2-weighted lesions have been shown to have a small predictive value on the rate of clinical progression over 15 years in PPMS (Mostert et al., 2010). On the other hand, they have been found to have a complementary role with grey matter metrics in predicting clinical deterioration over time in PPMS (Tur et al., 2011a). T2-weighted lesions can be seen in both the brain and spinal cord; in the latter, diffuse (mild) hyperintensity, only weakly correlated with clinical disability scores, are often seen in PPMS (Lycklama et al., 2003).

The application of approaches, such as lesion probability mapping (LPM), described in the Chapter II of this thesis, has allowed researchers to explore the spatial location of T2-weighted and T1-weighted lesions in PPMS. Using LPM, it has been demonstrated that lesions are more frequently localized in the superior and posterior regions of the corona radiata in PPMS than in RRMS (Di Perri et al., 2008).

The application of double inversion recovery (DIR) sequences, diffusively used in MS to visualize cortical lesions in-vivo (Geurts et al., 2005; Calabrese et al., 2007; Geurts et al., 2011; Geurts et al., 2012), has shown that 80% of patients with PPMS have lesions in the cerebral cortex. Comparing the spatial location of cortical lesions in different patient groups, it has been found that there is no difference between PPMS and RRMS in their distribution across brain lobes, nor in their frequency and volume. However, the maximum probability of the occurrence of cortical lesions was demonstrated to be twice as high in PPMS than in RRMS patients (Calabrese et al., 2010). Importantly, in PPMS, the number and extent of cortical lesions correlated with clinical progression over two years (Calabrese et al., 2009). These data have been recently confirmed in a 5-year perspective study which included 44 patients with PPMS (Calabrese et al., 2012).

1.2.1.2 Atrophy

Global and fractional brain volume loss, as well as spinal cord atrophy, are visible on MRI scans from the earliest stage of PPMS (Sastre-Garriga et al., 2004; Rocca et al., 2012a), and have been shown to progress relentlessly over time in this patient group (Sastre-Garriga et al., 2005a; De Stefano et al., 2010; Laule et al., 2010). GM atrophy, as measured by MRI, probably reflects a combination of demyelination, neuroaxonal degeneration, and glial damage, but the relative contribution of each of these processes to cortical volume loss has yet to be conclusively established (Wegner et al., 2006; Pomeroy et al., 2008; Geurts et al., 2009).

Comparing patients with PPMS and SPMS, the Amsterdam group has recently reported that patients with PPMS have a higher GM volume, but a similar low WM volume, when compared with patients with SPMS (Roosendaal et al., 2011). This study also confirmed the presence of a relationship between GM atrophy and T2 lesion volume, that had been already reported in a previous study of a cohort of RR and PPMS patients (De Stefano et al., 2003).

The application of voxel-based morphometry (VBM, see Chapter II for technical details) (Ashburner and Friston, 2000), has allowed the localization of areas of

volume loss in patients with this form of disease. In particular, atrophy of the thalamic region has been demonstrated in PPMS in several studies (Sepulcre et al., 2006; Ceccarelli et al., 2009). In one of these studies, Sepulcre et al. demonstrated a loss of GM in the putamen, caudate, thalami, and cortical and infratentorial areas as the disease evolved over one year (Sepulcre et al., 2006). This study found a correlation between bilateral thalamic atrophy and T2 lesion load, confirming a previous observation of a correlation between regional GM volume loss (in the bilateral central sulci, left angular gyrus, and head of the left caudate nucleus) with focal WM damage (T1 lesion volume) (Pagani et al., 2005b). In the study presented in the Chapter III of this thesis I extended these data, exploring whether there was a link between regional GM volume loss, as measured using VBM, and regional WM damage localized *outside* focal lesions in PPMS.

Brain and cervical cord atrophy in PPMS have been shown to be clinically relevant and more pronounced in patients with motor disability (Rovaris et al., 2008). Moreover, the reduction of brain volume over two years has been demonstrated to predict long-term disease progression in a large, multicenter study, involving centers from the MAGNIMS consortium (Khaleeli et al., 2008b). Correlations between the localization of areas of GM volume loss and cognitive functional scores are of particular interest in this form of disease. Riccitelli et al. have recently demonstrated a significant GM loss in the anterior cingulated cortex and in the right superior temporal gyrus in cognitively impaired versus cognitively preserved PPMS patients (Riccitelli et al., 2011) (Figure 1.5).

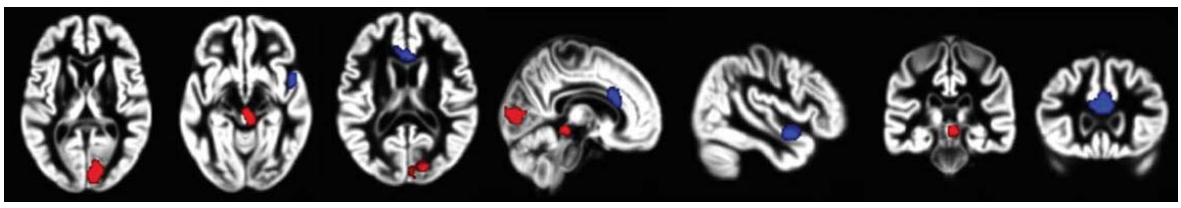

Figure 1.5 This picture shows the distribution of regions of significant GM atrophy (voxels in blue) and T2-visible lesions (voxels in red) in cognitively impaired versus cognitively preserved patients with PPMS (*Adapted from Riccitelli et al, 2011*).

Interestingly, Anderson et al. have found that hippocampal atrophy occurs both

in patients with RRMS and PPMS, but an association of hippocampal volume with memory performance was observed only in patients with PPMS (Anderson et al., 2010). Finally, a very recent study performing a voxel-wise analysis of cervical cord volume in patients with different subtypes of MS, found significant cord atrophy in PPMS, which correlated with clinical disability and motor impairment (Rocca et al., 2012b).

1.2.2 Studies using MTI and DTI

1.2.2.1 *Magnetisation transfer imaging (MTI)*

As discussed in detail in the second Chapter of this thesis, MTI provides an index, called magnetization transfer ratio (MTR), which reflects the extent of the magnetization exchange between the pool of free protons in tissue water and the pool of protons bound to macromolecules. MTR values are reduced in damaged brain tissues, and post-mortem studies have shown that reduced MTR correlate with the degree of demyelination and axonal loss in MS (van Waesberghe et al., 1999; Schmierer et al., 2004). Early studies have demonstrated that MTR values of lesions visible on T2-weighted images are significantly lower compared to those of the surrounding tissue in patients with PPMS (Gass et al., 1994; Leary et al., 1999). Both region-of-interest (ROI) and histogram-based analyses (see Chapter II for details) have shown reduced MTR in the NAWM of patients with PPMS when compared with healthy controls (Gass et al., 1994; Leary et al., 1999; Rovaris et al., 2008), and demonstrated that the damage in the NAWM is more severe in patients with the progressive form of MS than in those with RRMS (Filippi et al., 1999; Tortorella et al., 2000) However, when comparing the MTR values of the NAWM between patients with SPMS and PPMS, no significant difference was found (Rovaris et al., 2001). Interestingly, Rovaris et al. demonstrated that NAWM MTR values are only weakly correlated with T2- and T1-visible lesion load (Rovaris et al., 2001). This result is in line with the data emerging from post-mortem studies and discussed in the Pathology section of this Chapter, by confirming in vivo that NAWM damage could not derive exclusively from the Wallerian degeneration of axons transected in lesions, but also develops independently of focal and macroscopic WM damage.

With regard to the GM, several studies have demonstrated a significant reduction of MTR in PPMS compared with healthy controls, and correlations between lower MTR and greater clinical disability (Cercignani et al., 2001a; Dehmeshki et al., 2003; Ramio-Torrenta et al., 2006). A recent cross-sectional study focusing on the relationship between GM damage and cognitive impairment in this form of disease, has shown that GM MTR appears to be strongly correlated with overall cognitive dysfunction; this result highlights the role of abnormal GM integrity in determining cognitive impairment in PPMS (Tur et al., 2011b).

MTI has also been employed to investigate the damage in the cervical cord of patients with PPMS. In particular, an early study from the Amsterdam group found that a composite measure derived from a combination of cervical spine MTR and cross-sectional area (a measure of the spinal cord volume loss), correlated significantly with clinical disability, as measured by the EDSS (Nijeholt et al., 2000). Comparing SPMS with PPMS, the Milan group found that cord MTR histogram metrics were significantly worse in the former group (Rovaris et al., 2001). In the same study, by combining the cross-sectional area at the C2 level with the MTR histogram peak height, a significant correlation with disability was found.

1.2.2.2 *Diffusion tensor imaging (DTI)*

As discussed in detail in Chapter II, DTI allows quantitative (and in vivo) measurements of brain tissue microstructure. Among the DTI-derived measures, mean diffusivity (MD), which reflects the magnitude of diffusion, and fractional anisotropy (FA), which is a measure of tissue integrity and organization, have been widely employed to explore tissue damage in MS. Data from post-mortem analysis of MS brains showed that an increased MD and a lower FA correlate with a more pronounced degree of demyelination and, to a lesser extent, axonal loss (Schmierer et al., 2007; Moll et al., 2011).

In an early study that included patients with PPMS, Ciccarelli et al., using ROIs, found a significantly reduced anisotropy and a trend toward increased diffusivity

in both infratentorial and supratentorial NAWM of patients compared with controls. In the same study, the mean diffusivity in infratentorial NAWM correlated strongly with disease duration (Ciccarelli et al., 2001). When the lesional and WM diffusion metrics were compared between the different forms of MS, including PPMS, no significant differences were found (Droogan et al., 1999). This result was confirmed by Cercignani et al., who detected no difference between different MS subgroups in MD and FA histograms obtained from normal-appearing brain tissues and T2 visible lesions (Cercignani et al., 2001b). Different studies have investigated the relationship between NAWM DTI-derived metrics damage and T2 lesion load, and have found only a partial correlation between these variables (Rovaris et al., 2005). This supports the concept that the damage in the NAWM could not entirely depend upon retrograde degeneration of axons transected in T2 visible lesions.

DTI has also been employed to explore the GM of patients with PPMS. Bozzali et al. demonstrated that GM diffusion-derived metrics were abnormal in patients with MS, including a subgroup of PPMS, when compared with healthy controls, and that GM changes were more pronounced in patients with a progressive course than in patients with RRMS (Bozzali et al., 2002). Rovaris et al. showed that DTI abnormalities of the GM worsen over one year (Rovaris et al., 2005), and that GM diffusion abnormalities at baseline predict disability progression over five years (Rovaris et al., 2006). Mesaros et al. have recently found that the changes in DTI-derived metrics in the thalamus over fifteen months predict the long-term accumulation of disability in PPMS (Mesaros et al., 2011).

The voxel-wise analysis of DTI metrics has allowed the exploration of regional changes in PPMS in an unbiased way (see Chapter II for details). The Milan group, using a voxel-based approach, found abnormalities in DTI measures in brain areas associated with motor and cognitive functions (Ceccarelli et al., 2009) (Figure 1.6).

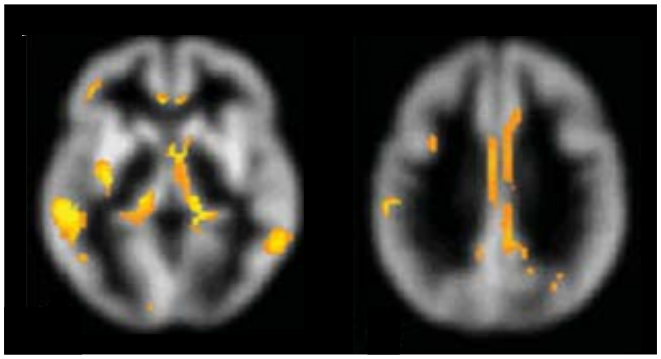

Figure 1.6 This picture shows statistical parametric mapping (SPM) regions (color-coded for t values) with increased GM mean diffusivity in PPMS patients compared with controls (*Adapted from Ceccarelli et al., 2009*)

An interesting voxel-wise approach that allows the detection of regional changes in FA along the main white matter tracts is tract-based spatial statistics (TBSS) (Smith et al., 2006), which is described in detail in the next Chapter. We have used this method for the first time in patients with early PPMS, as described in Chapter III, VI and VIII. In particular, in the study presented in Chapter III, we employed TBSS to compare the NAWM of early PPMS patients with healthy controls. In the study presented in Chapter VI, we combined TBSS and MTR to explore short-term WM changes in the same patients. Finally, in Chapter VIII we investigated whether WM FA at baseline predicts disability progression and cognitive dysfunction after five years in the same cohort of PPMS.

DTI has also been employed to investigate the damage in the spinal cord of patients with PPMS. MD and FA have been shown to be abnormal in patients with PPMS compared with healthy controls (Agosta et al., 2005). The Milan group studied the spinal cord of a group of MS patients, including 15 patients with PPMS, for two-years, and showed an increase in average MD and a decrease in average FA over the follow-up period. Moreover, while the increase in MD was independent of clinical course, the decrease in FA was more pronounced in PPMS than in patients with other forms of MS (Agosta et al., 2007).

1.2.3 Lessons from the early phase: the London studies in early PPMS

PPMS provides a useful model to study the mechanisms of progression in MS, as fixed disability progresses from disease onset and cannot be related to relapse activity. The important information obtained in the studies reported in the previous sections of this Chapter relate to patients with well established PPMS. However, data from natural history studies show that most patients attain high levels of disability in the first years after disease onset, while in the following years the accrual of disability slows down (Cottrell et al., 1999). Therefore, it is important to investigate patients with PPMS as early as possible in the course of disease, to explore the mechanisms underlying clinical progression which are responsible for the most clinically active phase of this form of disease. For this purpose, a cohort of 50 patients with PPMS in the early phase of disease (i.e. within five years of clinical onset) has been recruited in our Unit in London and followed-up for five years with clinical assessments and conventional and non-conventional MRI imaging. Here we summarise the main findings obtained from our studies in this unique cohort of patients, to give the clinical and radiological background to the studies presented in the Chapter III, IV, VI, and VII of this thesis.

Cross-sectional data on the London PPMS cohort, using different non-conventional imaging techniques, showed that brain abnormalities and volume loss are present since the early stages of the disease, affect both the GM and the WM, and are clinically relevant (Sastre-Garriga et al., 2004; Sastre-Garriga et al., 2005a; Ramio-Torrenta et al., 2006). Localised GM damage was described in a study by Khaleeli et al., who found a significant reduction of MTR in the right pre- and left pre- and post-central gyri, right middle frontal gyrus, left superior frontal gyrus, bilateral superior temporal gyri, left insula, right insula and visual cortex, and thalamus bilaterally, when compared with controls. In the same study, a correlation was found between the MTR values in the cortical areas of the motor network and the EDSS score, and between the MTR values of the cognitive network and the Paced Auditory Serial Attention Test (PASAT) scores (Khaleeli et al., 2007b). In addition to cortical regions, regional GM atrophy has been shown to affect also deep GM (Sepulcre et al., 2006).

Longitudinal studies in the same cohort showed that NAWM MTR predicts clinical progression over one year (Khaleeli et al., 2007a), while GM MTR, proposed as a potential surrogate marker of clinical progression, predicts clinical deterioration over three years (Khaleeli et al., 2008a) . A recent study has extended the follow-up to five years and showed that the combination of GM MTR and T2-weighted lesion load measured at baseline significantly predicts clinical progression after five years (Tur et al., 2011a). The relevance of GM MTR in predicting long-term clinical evolution in PPMS is further supported by Penny et al., who showed that a lower baseline GM MTR predicts a poorer performance on neuropsychological tests assessing attention, speed of information processing and executive function after five years (Penny et al., 2010). In summary, these studies reported a significant contribution of NAWM and GM pathology, as reflected by MTR changes, to clinical and cognitive impairment, but did not localise the regions that significantly contributed to the findings, as histogram metrics were derived from the whole GM and NAWM.

1.3 Two key unanswered questions on PPMS: rationale for this thesis

Against the background presented in this Chapter, this thesis focuses on addressing the following two questions, fundamental to the pathogenesis of progression in PPMS:

(1) Is there is a *spatial* and *temporal* link between the pathological processes occurring in the NAWM and in the GM of patients with PPMS? In other words, is GM damage secondary to axonal degeneration and demyelination in connected WM tracts or alternatively, does it represent the initial target of the disease process that leads to subsequent axonal degeneration in the WM?

(2) Which regions of WM abnormalities (within lesions and NAWM) and GM damage significantly contribute to clinical progression and cognitive deterioration?

The subsequent Chapters of this thesis will try to answer these two questions.

After Chapter II, which provides a description of the conventional and advanced MRI techniques applied in this thesis, the first question is addressed. In particular, in Chapter III, the *spatial* relationship between the damage occurring in the WM outside visible lesions and in the GM in patients with early PPMS is described, while the *temporal* relationship between NAWM and GM damage in the same cohort of patients will be presented in Chapter IV.

Chapters V-VII address the second question. In particular, the role of lesional WM damage in predicting clinical progression in patients with well established PPMS will be discussed in Chapter V. In Chapter VI, short-term changes in WM tract integrity, and their clinical relevance in patients with early PPMS, are explored. Finally, in Chapter VII, the contribution of early damage in WM and in GM to long-term clinical deterioration and cognitive dysfunction in this form of disease is investigated.

Principles of MRI, DTI, MTI, and notes on imaging analysis

CHAPTER II

This Chapter provides an overview of the physics principles of magnetic resonance imaging (MRI), and an introduction to the conventional and quantitative MRI techniques, diffusion tensor imaging (DTI) and magnetisation transfer imaging (MTI), and to the post-processing methods employed in the clinical studies presented in the subsequent Chapters of this thesis.

2.1 Principles of MRI

MRI generates images non-invasively with high spatial resolution. Since MRI does not emit ionizing radiation, it allows repeated *in vivo* imaging of an individual without the potential risk of neoplasia. MRI has been applied in many branches of science, but this discussion will focus on its application to brain imaging (Deoni, 2011).

2.1.1 Physics of MRI

As two thirds of the human body is made up of water, human tissue is rich in water hydrogen atoms. These are at the origin of the nuclear MR signal used to generate conventional MR images.

The nucleus of a hydrogen atom consists of a single proton surrounded by only one electron. In quantum mechanics, atomic nuclei such as protons have a fundamental property, defined *spin,* which is a type of angular momentum that results from the sum of the spins of the constituent particles. Protons have a positive electrical charge, and rotating around their own axis, they produce a small magnetic field. In presence of an externally applied magnetic field (B_0), all the nuclear spins tend to align with the magnetic field, showing a peculiar motion called *precession*, which is characterised by the circular movement of the spin axis forming a cone shape (Figure 2.1).

The precession frequency is described by the Larmor equation:

$$\omega_0 = \gamma B_0 \qquad (2.1)$$

where ω_0 is the Larmor frequency given in Hz or rad s^{-1}, B_0 is the strength of the externally applied magnetic field given in Tesla, and γ is the gyromagnetic ratio, given in Hz/Tesla. The Larmor equation states that the precession frequency is proportional to the external magnetic field, and this relationship is determined by the gyromagnetic ratio, which is different for different nuclei. For hydrogen, γ is 42.6 $MHzT^{-1}$. Therefore, in an MRI scanner with a magnetic field of 1.5 Tesla, such as the one used for all the studies presented in this thesis, the hydrogen nuclei precess at a frequency of around 64 MHz.

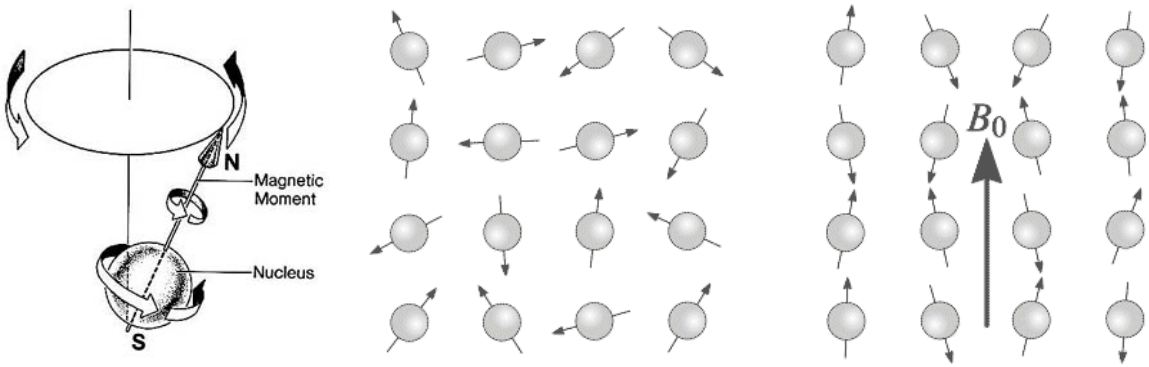

Figure 2.1. Proton behavior in an external magnetic field. The left side of the figure describes the precession movement. The right side of the picture shows that, when an external magnetic field B0 is applied to spinning protons with random orientations, their magnetic moments tend to align in a parallel or anti-parallel orientation with respect to B_0. The big arrow represents the net magnetisation (M) of the spinning protons.

Quantum mechanics tells us that the spin of each proton may have two different energy levels, which determine its alignment to the external magnetic field. In particular, at the low energy level a spin is aligned with the magnetic field, whereas at the high energy level the vector is anti-parallel to the field (Figure 2.1). At equilibrium, the population of anti-parallel spins is almost equivalent to that of parallel spins. However, there is a small population difference, due to the fact that the low energy state (parallel to the field) slightly dominates the high energy state.

This *equilibrium magnetisation* can be represented as a vector (M) pointing in the direction of the magnetic field (defined as the z-axis). The *equilibrium*

magnetisation cannot be measured, because it lies in the same direction as the main magnetic field. To measure the tissue magnetisation, we need to perturb the system and observe its return to equilibrium. This can be achieved by applying electromagnetic radiation to the system. In order to interact with the system, this radiation must be supplied at the Larmor frequency, and usually a radio frequency (RF) pulse is used. From a quantum mechanical point of view, the pulse provides the energy required for the transition of some of the spins in the low energy level to the high energy level. A more intuitive way of explaining this phenomenon can be derived from classical physics. Like every electromagnetic wave, the RF pulse has a magnetic field component, B_1. Assuming that the B_1 field is perpendicular to B_0, the net magnetisation M will start precessing around B_1 as well as around B_0. In order to simplify the description of the system, we can introduce a reference frame that rotates at the same angular frequency (the Larmor frequency) as the magnetisation. In this system, at equilibrium the net magnetisation M appears stationary.

2.1.2 From the spin-echo phenomenon to the generation of signal

During an RF excitation, the combined precession around both fields corresponds to a simple rotation towards the x-y plane. The angle by which M is rotated depends on the duration and the amplitude of the pulse, and it is called the flip angle. For example, a 90° pulse rotates completely M from the z to the x-y plane.
When the RF pulse is switched off, the spins return to equilibrium, releasing a signal that is detected by a coil that acts as an antenna, as described below. The spin-echo (SE) phenomenon was described by Erwin Hahn in his 1950 paper (Hahn, 1950), and was further developed by Carr and Purcell who pointed out the advantages of a 180° refocusing pulse (Carr and Purcell, 1954).

In the basic SE sequence, a RF 90° pulse (of magnitude given by the “flip angle”) applied along the y axis of the rotating frame (i.e. perpendicular to B_0), flips M into the horizontal (x-y) plane. This process produces a *transverse magnetisation*, because it causes protons 1) to perform a transition to a higher level of energy and 2) to precess in phase at the resonance (Larmor) frequency.

When the RF pulse is switched off, protons start losing phase coherence and the transverse magnetisation disappears. This process is called *transverse relaxation* or *spin-spin relaxation,* as it is caused by the interaction between the proton and other magnetic entities, such as other nuclear or electronic spins.

At the same time, protons start returning to a lower level of energy, and the longitudinal magnetisation returns to its original size in the direction of the magnetic field. This process is called *longitudinal relaxation* or *spin-lattice* relaxation, and is due to the spins releasing the energy obtained from the RF pulse to the surrounding lattice, and returning to their original equilibrium state (Bloch, 1946).

Two time constants describe these processes: 1) T2, which is the time constant for decay of the transverse magnetisation in a homogeneous static magnetic field; 2) T1, which is the time constant for the recovery of the longitudinal magnetisation. As transverse relaxation is faster than longitudinal relaxation, T2 is always shorter than T1 (Figure 2.2).

Different tissues, because of their different chemical constitutions and different physical states, will have different relaxation times.

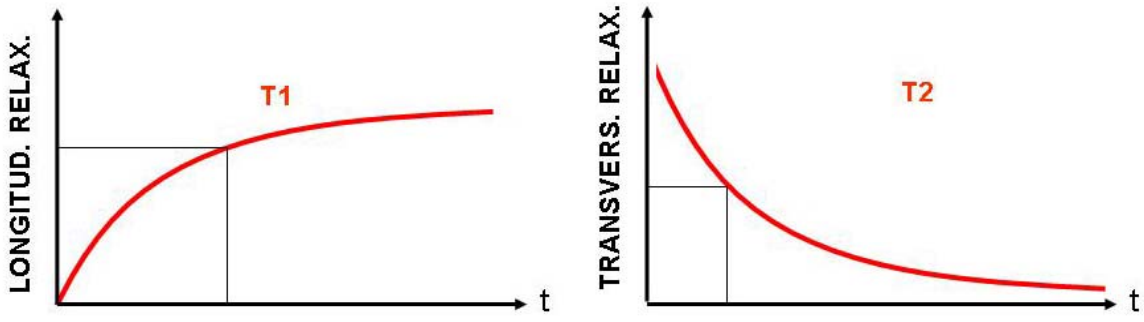

Figure 2.2. T1 recovery and T2 decay. The time needed for 63 % of the longitudinal magnetisation to recover after being flipped into the magnetic transverse plane by a 90° RF pulse is defined as T1 (left side of the figure); at a time equal to T2 after the occurrence of the transverse magnetisation, there has been a decay of the detectable signal to 37% of its original value (right side of the figure).

After a 90° pulse, local magnetic inhomogeneities in B_0 cause protons to resonate at slightly different frequencies at slightly different positions within

each voxel. This determines a faster dephasing than would be expected from spin-spin interactions alone, and therefore transverse magnetisation (and induced signal) is lost exponentially. This type of signal is called a *Free Induction Decay* (FID) signal, and is characterised by a reduction in intensity with time and by a constant frequency (Figure 2.3). The time constant of this decay is called T2*, and is always shorter than T2. In simple words, T2* incorporates T2 effects, but also some other causes of spin dephasing, such as field inhomogeneity, local susceptibility, etc. These latter effects can be compensated by using a 180° (refocusing) pulse, thus generating a SE.

In order to understand this, we can think that phase coherence is lost because different spins precess at slightly different frequencies, i.e., some will precess faster and others slower. After a given interval a 180° RF pulse is applied along the y axis. This second pulse reverses completely the phase of the protons. Spins will continue to precess at the same angular frequency; however, now their respective positions have been reversed. After an interval identical to the one between the 90° and the 180° pulse, they will be in phase again, producing a spin-echo signal (Hahn, 1950). Following the spin echo, coherence is again lost as the protons continue to resonate at slightly different frequencies due to non-uniformities in the main magnetic field. If another 180° pulse is applied, coherence can again be established for a second spin echo. Multiple spin echo signals can be produced if the original 90° pulse is followed by multiple 180° pulses (spin echo train) (Carr and Purcell, 1954). The main difference between T2 and T2* relaxation is that the T2* processes can be refocused, whereas the T2 processes cannot, as they result from random fluctuations in the Larmor frequency at the molecular level.

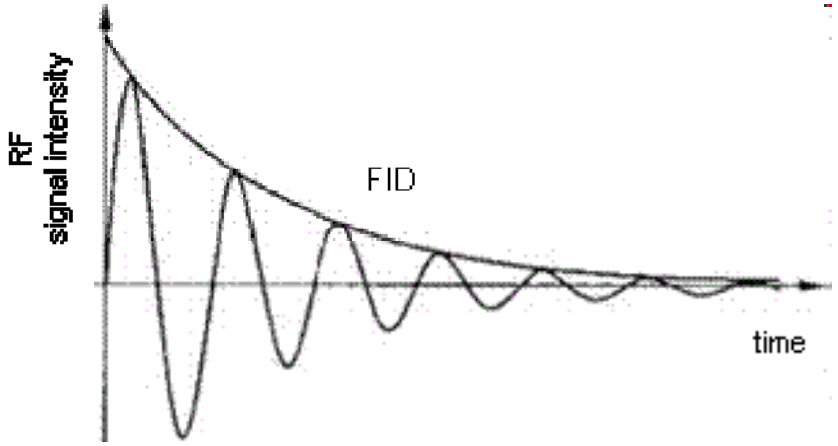

Figure 2.3. Free Induction Decay (FID). FID is the signal decay due the inhomogeneity of the local magnetic field, which in turn depends on 1) the non-uniformity of the external magnetic field due to imperfections in the windings of the coil itself and 2) the differences in magnetic susceptibility between adjacent regions. In a perfect magnetic field, the value of T2* can approach that of T2.

2.1.3 Spatial encoding

Spatial information is derived by three *gradient coils* which generate magnetic field gradients along three orthogonal axes that can be referred to as z, x, and y (Figure 2.4):

1) Slice select gradient (GSS, G_{slice}, "z")
2) Phase encoding gradient (GPE, G_{phase}, "y")
3) Frequency encoding (or readout) gradient (GFE, G_{read}, "x")

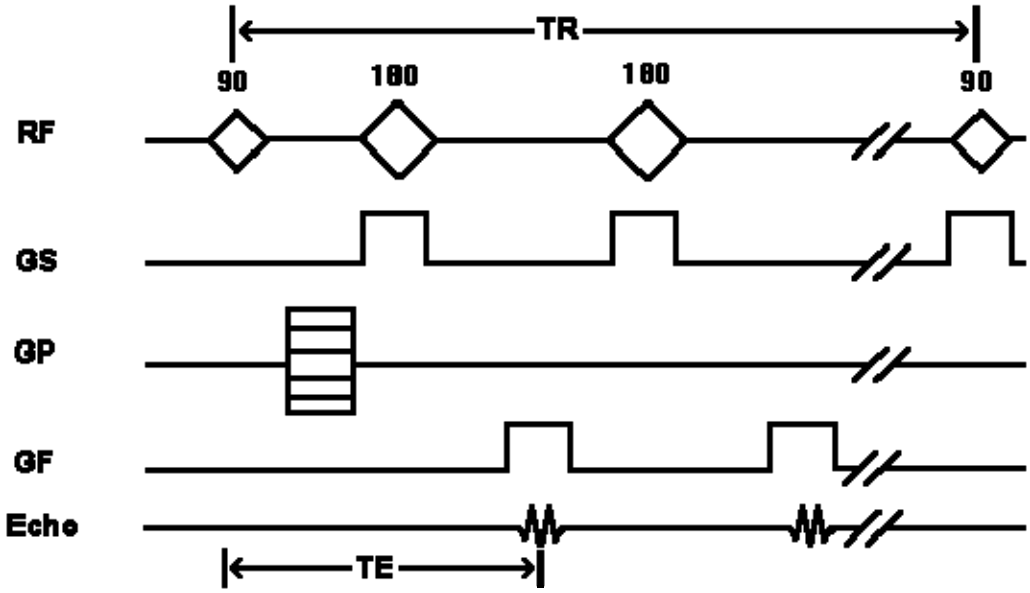

Figure 2.4. Dual spin echo sequence diagram, showing when the different gradients are applied. In the case of a dual spin echo sequence, a 90° excitation pulse is applied, followed by a 180° pulse refocusing pulse. This creates a spin echo which is the measured signal. A subsequent 180° refocusing pulse within the TR time generates a successive echo at a different TE.

For a two-dimensional (2D) image, frequency encoding is applied in one direction and phase encoding in the other. For a three-dimensional (3D) image, the slice selection is not employed, frequency encoding is applied in one direction and phase encoding in the other two. The 3D approach allows higher spatial resolution and higher signal-to-noise ratio compared with 2D scanning, but is characterised by a relatively long scan time.

The first step of spatial encoding consists in selecting the slice plane. To do this, the *slice select gradient (GSS)* is applied in the direction of the z axis, perpendicular to the desired slice plane. As a result, the protons localized at different physical positions along this direction precess at a slightly different Larmor frequency around the direction of B_0. In other words, adding this gradient to B_0, the protons of the selected slice will present a specific resonance frequency proportionate to GSS, according to the Larmor equation. A 90° RF pulse (*selective pulse*) is simultaneously applied, with the same frequency as that of the protons in the selected slice, and only those protons will be excited

and will contribute to the formation of a transverse magnetisation. At time t=TE/2 a 180° pulse is applied which rephases the protons that are getting out of phase and, at time TE, an echo is produced. As none of the protons located outside the selected slice plane are excited, they will not emit a signal. The RF bandwidth and the amplitude of the GSS determine the slice thickness, and sequential excitations select different slices to cover the tissue under investigation.

The second step in spatial encoding consists in applying a *phase encoding gradient (GPE)*, which is applied in the direction of the y axis (orthogonal to the GSS) after the 90° pulse and before acquisition in order to induce different phases to the echo signal. While it is applied, it modifies the spin resonance frequencies, inducing dephasing, which persists after the gradient is interrupted. This results in the protons at different positions in the gradient having accumulated different phases. In particular, the protons in the same row, perpendicular to the gradient direction, will all have the same phase. This phase difference lasts until the signal is recorded. On receiving the signal, each row of protons will be slightly out of phase, and this translates in their signals being more or less out of phase. In order to decipher the phase information, it is necessary to repeat this step with increasing phase encoding amplitude, so that spins at certain position will be characterised a unique combination of phases. Therefore, in order to obtain an image, the sequence of pulses and gradients required to generate an echo is repeated many times at regular intervals (as explained in section 2.1.4). The number of repetitions is equal to the number of rows in the image. In other words, for a spin echo sequence with « n » rows, we make « n » acquisitions each with a different phase encoding gradient.

The final step in spatial encoding is characterised by the application of a *frequency encoding gradient (GFE)* along the x direction when the signal is received. This last gradient applied during the signal acquisition, results in protons within the same column to precess with identical Larmor frequency, thus allowing the identification of their spatial location. The acquisition bandwidth determines the width of the acquisition window and together with the GPE it determines the in-plane resolution along the frequency or read-out

direction (Figure 2.4). The *image matrix* refers to the number of frequency encodes multiplied by the number of phase encodes.

2.1.4 Generation of tissue contrast

In order to characterize the contrast in a SE image, it is necessary to define the repetition time (TR) and the echo time (TE). We have seen that excitation (90° RF pulse) must be repeated several time in order to produce an image. TR is defined as the time between two successive excitations, i.e. from one 90° RF pulse to the next (Hahn, 1950). In order to have a full magnetisation recovery, it is necessary to allow a long relaxation time (equal to 5 times T1) before exciting the sample again. Changing TR, the contrast between tissues with different T1 relaxation times changes. For example, in the case of a short TR, the longitudinal magnetisation of a specific tissue with a long T1, which has to be flipped in turn by the second pulse, has not the time to recover totally, and it produces a smaller transverse magnetisation with a consequent lower signal. On the other hand, in case of a very long TR, all tissues will have recovered their longitudinal magnetisation.

The TE is defined as the time between the 90° RF pulse and the collection of the MR signal (Figure 2.4). In the case of a spin echo signal, TE is twice the time between the 90° and the 180° pulse. Changing TE, the contrast between tissues with different T2 relaxation times changes. This is because different tissues have different T2 relaxation time times and therefore they will be more or less dephased using a certain TE. In particular, with a short TE, the difference in signal intensity between two tissues with different T2 is very small, and both tissues can hardly be distinguished. Conversely, in the case of a long TE, the differences in signal intensity between tissues that have different T2 times, becomes evident. In order to produce images where the contrast is predictable, the TR and TE are selected to weight the image towards one contrast mechanism and away from the other (Westbrook, 2009), producing different degrees of contrast (intensity differences) between tissues. In particular, changing TR and TE we can obtain different types of sequences:

1) T1-weighted imaging (T1-w), which is characterised by short TE and short TR, is able to detect differences between tissues due to their difference in T1 relaxation times. Indeed, to reduce T2 effects, TE must also be short. In such images, fat (short T1) is bright, whereas water (longer T1) is dark.

2) T2-weighted imaging (T2-w), which is characterised by long TE and long TR, is able to detect differences between tissues due their difference in T2 relaxation times. T1 effects are diminished selecting a long TR, hence allowing full T1 recovery between successive excitations. In these images, fat (short T2) is dark and water (longer T2) is bright. Because many pathological processes (such as demyelinating lesions) increase water content and the mobility of water protons, they can often appear bright on T2-WI.

3) Proton-density weighted imaging (PD-w), which is characterised by short TE and long TR, is sensitive to detect differences in signal related to different proton density. These images are useful for showing pathological changes.

In the brain, the cerebro-spinal fluid (CSF) has high water content and has long T1 and T2. The white matter (WM) is highly structured and has short T1 and T2. Grey matter (GM) is less structured than the WM, but contains more macromolecules than CSF, and therefore has intermediate T1 and T2.

2.1.5 From MR signal to image reconstruction

The acquired MR echo containing the frequency- and phase-encoded spatial information necessary to construct an image is entered in what is referred to as *k-space,* a space that organizes spatial frequency information of an object (Gallagher et al., 2008). The signal acquisition is sampled along trajectories within *k-space*, which was described for the first time in 1983 by Tweig (Tweig, 1983) and Ljunggren (Ljunggren, 1983).

The *k-space* is defined by the space covered by phase and frequency encoding data. Within the *k-space*, a line of data corresponds to the digitized MR signal at

a particular phase encoding level. The position in *k-space* is directly related to the gradient across the object being imaged. By changing the gradient over time, the *k-space* data are sampled in a trajectory through Fourier space. In particular, the application of frequency encoding gradient moves the trajectory along the x axis, whereas the application of phase encoding gradient moves the trajectory along the y axis. During a single TR, data corresponding to a phase encoding step is stored, but more than one slice can be sampled with the same phase encoding gradient per TR. By convention, high spatial frequencies, required to describe rapid spatial variations of the object, such as sharp edges, are mapped at the periphery of *k-space*, whereas low spatial frequencies, required to reconstruct the overall form of the image, are mapped near the centre. The range of spatial frequencies in *k-space* is inversely proportional to the spatial resolution of the image. Many different k-space sampling schemes can be used and each of them has practical or theoretical advantages. For example, a small number of k-space trajectories are used to allow rapid acquisition of MR images, at the price of a lower resolution.

Subsequently, a *Fourier transform* of *k-space* decomposes the frequency- and phase-encoded spatial information, into a set of amplitudes at specific frequencies, which provide the image intensity at particular positions, resulting in the image we see (Gallagher et al., 2008).

The signal to noise ratio (SNR) is defined as the ratio of the amplitude of the MR signal to the amplitude of the background noise. SNR is relevant in determining the final quality of the image produced, and can be affected by the magnetic field strength, proton density, coil type and position, TR, TE, flip angle, number of signal averages, bandwidth and pixel volume.

The field-of-view (FOV) refers to the size of the area to be studied and is proportional to the acquisition bandwidth and inversely proportional to the readout gradient.

2.2 Conventional imaging sequences

This section outlines the main features of the conventional imaging sequences that have been employed in the clinical studies presented in the subsequent Chapters of this thesis.

2.2.1 Fast spin-echo (FSE) sequence

This is a much faster variant than the conventional SE sequence described above. In SE sequences, only one phase encode is performed during each TR. FSE performs the same total number of phase encodes, therefore maintaining resolution, but more than one phase encode is performed for each TR. A train of 180° refocusing pulses is employed, with each pulse producing one echo. The number of pulses and resulting echoes is referred to as the echo train length. Therefore, several lines of k-space can be filled for every TR instead of one per TR as in SE. Because k-space is filled more rapidly, scan time is reduced. FSE allows different TEs and therefore PD and T2 weighted imaging can be acquired from one sequence. FSE has the advantages of shorter scan times, high resolution imaging, and increased T2 weighting, and has been used in the studies presented in this thesis to acquire PD and T2 weighted images.

2.2.2 Gradient echo (GE)

In gradient recalled echo sequences, instead of the180° pulse used in SE sequences, a bipolar gradient pulse is used to generate an echo. A RF excitation pulse is followed by a relaxation period and a gradient reversal is used to produce rephasing of the spins. A transverse component of magnetisation is created. Often in GE imaging protocols a flip angle other than 90° is employed, hence only part of the longitudinal magnetisation is flipped to the transverse plane. The transverse magnetisation is dephased using a superimposed magnetic field gradient of known amplitude and duration. By reversing this magnetic field, the dephasing caused by the applied gradient is reversed, and a gradient echo is generated. Scan times are short, as GE sequences have shorter TEs and TRs than SE. After the RF pulse is withdrawn,

the loss of signal due to transverse relaxation (i.e. dephasing of spins) is produced immediately as a result of inhomogeneities in the local magnetic field. Therefore, the GE image intensity depends on T2* rather than on T2. Since dephasing of spins increases with increasing TE, GE imaging is acquired with very short TE (a few milliseconds) in order to reduce signal loss. GE imaging with short TR is used for rapid in vivo MRI to reduce scan time and motion artifacts (van der Meulen et al., 1985; Haase et al., 1986).

A *spoiled* GE is a sequence in which the transverse magnetization is spoiled at the end of each TR interval, before each RF excitation pulse, resulting primarily in T1 contrast images. An inversion-prepared fast spoiled gradient recall sequence (FSPGR), characterised by a single inversion RF pulse (see next section) followed by a spoiled and short TR gradient echo train acquiring the entire k-space, has been employed in all the studies presented in this thesis to acquire high-resolution T1-weighted images.

2.2.3 Inversion recovery (IR)

Inversion recovery (IR) sequences begin with a 180° pulse that inverts the net magnetisation M. When the pulse is removed, the net magnetisation starts to relax back to B_0. A 90° pulse at time interval TI (time from inversion) is then applied. A further 180° pulse refocuses the spins in the transverse plane to produce an echo. The TI is the main factor that determines the weighting in IR sequences.

Fast IR is a combination of IR and FSE and allows short scan times. A commonly used IR sequence in multiple sclerosis is FLAIR (fluid attenuation inversion recovery), which uses long TIs to null signal from CSF, thus producing CSF-suppressed images. Indeed, this sequence increases the delineation of periventricular lesions seen in multiple sclerosis.

2.2.4 Echo planar imaging (EPI)

EPI is a single-shot ultra-fast imaging sequence proposed by Mansfield in 1977

(Mansfield and Pykett, 1977), which collects all data required to fill all the lines of k-space from a single echo-train in one TR. The main echo is generated either by 180° rephasing pulses (spin echo EPI) or by gradient reversal (gradient echo EPI) (Figure 2.5). Images can be acquired in 50-80 ms and axial slices of the whole brain are feasible in 2-3s. EPI is particularly useful in functional MRI, cardiac imaging, and perfusion/diffusion imaging. EPI is sensitive to image artefacts and distortions, such as geometric distortions, which occur in regions where the magnetic field homogeneity is poor (frontal and temporal regions). In the studies presented in Chapter III, IV, VI, and VII, a spin-echo EPI sequence has been employed to acquire diffusion-weighted data.

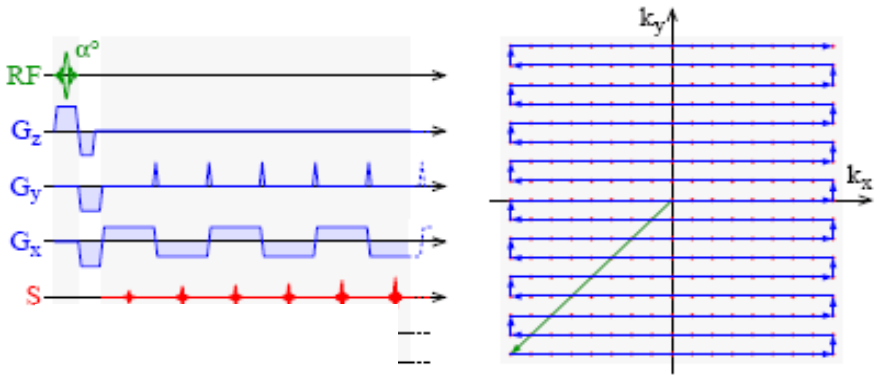

Figure 2.5. Gradient echo EPI pulse sequence and EPI k-space sampling.

2.3 Diffusion tensor imaging (DTI)

In this section, we will examine the basic principles of DTI, which has been employed in the studies presented in Chapters III, IV, VI and VII of this thesis, to explore the microstructural damage in patients with PPMS. Indeed, DTI can provide unique insights of tissue structure *in vivo*, using the information provided by the water diffusion. In particular, when a tissue is affected by pathology, the measures of diffusion change, and this is the reason why DTI has proven very useful in studying in vivo brain pathological damage.

2.3.1 The phenomenon of diffusion: basic principles

Diffusion is the random motion of molecules in any fluid system, including biological tissue, known as Brownian motion. When there is a gradient in the concentration (C) of a fluid, there is a macroscopic flux of fluid molecules from areas of high concentration to areas of low concentration, described by *Fick's first law of diffusion*:

$$F = - D \frac{\partial C}{\partial x} \qquad (2.2)$$

where F is the diffusion flux, D is the diffusion coefficient, and $\partial C / \partial x$ is the concentration gradient (the negative sign accounts for the flux direction being opposite to the increasing concentration)(Wheeler-Kingshott and Barker, 2003).

Conversely, when the concentration is uniform, diffusion can only be described statistically, by measuring the probability that a molecule travels a given distance in a given time. In an isotropic medium, such probability has a Gaussian distribution and all the molecules are free to diffuse in any direction without restrictions (Wheeler-Kingshott and Barker, 2003). In biological tissues, molecular mobility may not be the same in all directions. This *anisotropy* may result from the presence of obstacles that limit molecular movements in some directions, such as cell membranes and other intracellular and extracellular structures. In this context, different directional components of diffusion must be analysed separately, and the diffusion process can be described by a 3x3 tensor matrix. The diffusion tensor (DT) is characterised by 9 elements (Basser et al., 1994). However, it is symmetric about the diagonal, and therefore only six elements have to be measured to estimate the full DT. The on-diagonal elements are DTxx, DTyy, DTzz, which represent molecular mobility along axes x, y, and z, respectively. The remaining elements (DTxy, DTxz, and DTyz) are off-diagonal and indicate how strongly random displacements are correlated in the x, y and z directions.

$$DT = \begin{vmatrix} DTxx & DTxy & DTxz \\ DTyx & DTyy & DTyz \\ DTzx & DTy & DTzz \end{vmatrix} \quad (2.3)$$

2.3.2 Effects of diffusion on the MRI signal

Diffusion of protons can affect the MR signal (Wheeler-Kingshott and Barker, 2003). In particular, in a given tissue, there is a delay between the excitation and the refocusing of the magnetisation, during which spins are diffusing because of thermal agitation. In absence of motion or diffusion of water molecules, the dephasing that occurs after the first pulse is exactly rephased after the 180° pulse. If, instead, there is a random motion of the spins between dephasing and rephasing, then the refocusing of the spins is incomplete. As a consequence, there is a loss in the transverse magnetisation and a reduction in the signal amplitude. Diffusion effects are always present, but, as they are very small, they do not contribute substantially to signal attenuation in a standard spin-echo sequence. The sensitivity to diffusion must be increased using magnetic field gradients (as explained in section 2.3.3). The amount of signal attenuation in a diffusion-weighted sequence depends on: (i) the diffusion properties of the tissue, which determine the motion of the spins; (ii) the sequence parameters that determine the magnetic field gradients; and (iii) the time during which the diffusion process takes place.

2.3.3 The pulsed field gradient sequence

In 1965 Stejskal and Tanner proposed a practical scheme to introduce diffusion weighting in an MRI acquisition, i.e. to make MRI sensitive to diffusion along one or more directions (Stejskal and Tanner, 1965). This was obtained by adding a pair of pulsed magnetic field gradients in a SE sequence, positioning them around a 180° refocusing pulse. In particular, the first gradient pulse induces a phase shift for all spins, while the second reverses this phase shift. Therefore, the phase shift for static spins is cancelled, while the spins which

have changed location due to the diffusion of molecules during the time period between the two gradients (Δ in Figure 2.6) are not completely refocused by the second gradient pulse, and determine a signal attenuation (Pipe, 2009). In particular, the faster-moving water protons undergo a larger net dephasing.

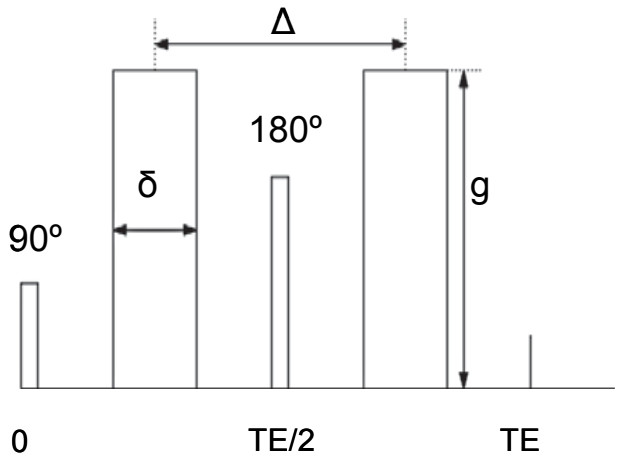

Figure 2.6. Diagram of the Stejskal-Tanner Pulse Field Gradient (PFG) sequence. The interval between the centres of the diffusion gradient lobes corresponds to the diffusion time (Δ). The strength of the diffusion weighting (i.e. the *b*-value) depends on the magnitude (g) and duration (δ) of the diffusion gradients, as well as the diffusion time, according to equation 2.5.

The resulting signal intensity of a voxel of tissue containing moving protons is equal to its signal intensity on a T2-weighted image decreased by an amount related to the rate of diffusion. If two acquisitions are performed, one without superimposed diffusion gradient (*b* value = 0), and one with diffusion gradient (i.e. b value ≠ 0), diffusion can be calculated using the equation of Stejskal and Tanner:

$$S = S_0 \, e^{-bD} \qquad (2.4)$$

Where *S* is the MRI signal in the presence of diffusion gradients, S_0 is the signal in the absence of diffusion gradients, D is the diffusion coefficient, and *b* is the diffusion weighting factor, introduced by Le Bihan et al. (Le Bihan et al., 1986):

$$b = (\gamma \; g \; \Delta)^2 \, (\Delta - \frac{\delta}{3}) \qquad (2.5)$$

where γ is the proton gyromagnetic ratio (267×10^6 $rad^{s-1}T^{-1}$), and g is the

strength of the diffusion sensitizing pulses. Therefore, the *b* factor depends on the amplitude of the diffusion gradient and on the diffusion times (δ and Δ). If the diffusion gradient is small (i.e. the *b* factor is small), there will be a small signal attenuation due to diffusion. If instead the diffusion gradient is very big (i.e. the *b* factor is big), there will be a much higher loss of signal.

2.3.4 Diffusion-weighted images and Apparent Diffusion Coefficient maps

The Pulse Field Gradient (PFG) method can be included in most MRI sequences to introduce diffusion weighting (DW) (i.e. sensitization of MRI images to diffusion) along multiple directions. This produces a reduced signal in the direction where there is the highest diffusion coefficient (Schaefer et al., 2000). For example, in anisotropic areas of white matter, where the diffusion is preferential along one direction, which generally corresponds to the main axis of axons, the signal attenuation is most evident when the diffusion gradients are applied along that direction, Conversely, the signal attenuation in isotropic areas of the brain is independent from the directions of diffusion gradients application (Figure 2.7).

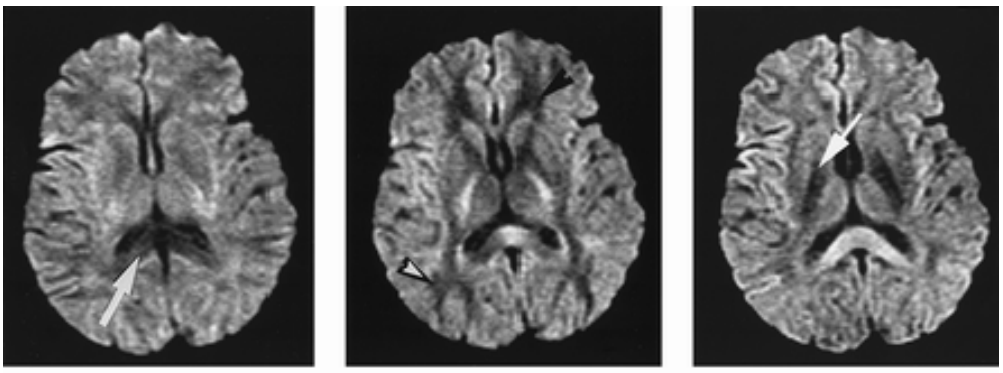

Figure 2.7. DW MR images, with diffusion gradients applied along the x (left), y (middle), and z (right) axes, demonstrating anisotropy in the brain. For example the corpus callosum (arrow on the left image) is hypointense when the gradient is applied in the x direction (right to left), the posterior white matter (arrowhead on the middle image) is hypointense when the gradient is applied in the y (anterior to posterior) direction, and the corticospinal tracts (arrow on the right image) are hypointense when the gradient is applied in the z (superior to inferior) direction. The ventricles are typical isotropic areas, presenting the same signal characteristics, independent of the direction of application of the diffusion gradients. (*Adapted from Schaefer et al., 2000*)

However, DWI is a qualitative type of image, which is very sensitive to the acquisition parameters and patient positioning in the scanner. Moreover, in DW images the MRI signal intensity remains sensitive to the T2 value of the tissue. For example, pathological conditions causing an increase in the T2 value of the affected brain area could result in an increased signal intensity of the DW images, which in turn could be erroneously interpreted as a reduction in diffusivity. To distinguish between diffusion and relaxation effects on image contrast, it is possible to obtain quantitative images of the diffusion coefficient, or more exactly the Apparent Diffusion Coefficient (ADC), which depends on the diffusion time and weighting used. Measuring the ADC is possible with a minimum of two measurements, one acquired without diffusion weighting and the other with diffusion weighting. If S and $S_{0,}$ together with the value of the b factor, are known for each voxel of the image, it is possible to calculate the diffusion coefficient voxel-by-voxel, using the equation 2.4. This procedure can generate a diffusion map where each voxel is the average diffusion coefficient of the tissue contained in that voxel, measured along the direction of application of the diffusion gradient.

This diffusion map (ADC map) has an intensity scale which is inverted relative to the DWI used to calculate it (i.e. areas with high mobility of water molecules along the direction of application of the diffusion gradient, which appear dark on DW images, appear bright on the ADC maps).

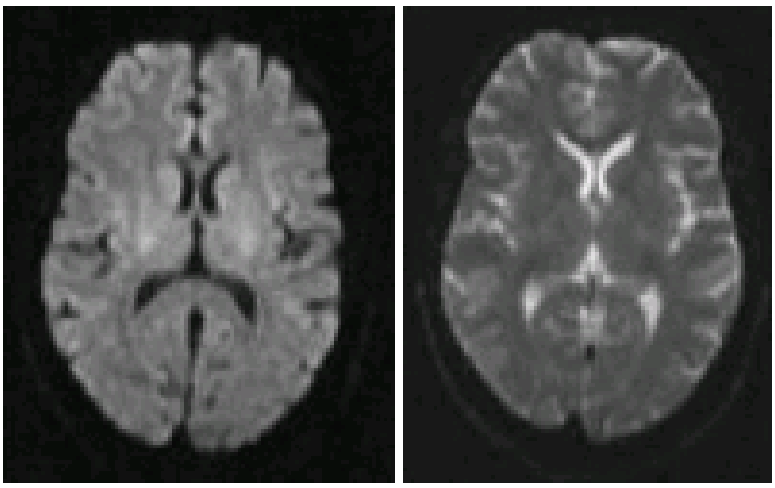

Figure 2.8. Inverted intensity scale of the ADC map (right) relative to the DWI (left) used to calculate it (normal brain of a 35 year old man).

2.3.5 Diffusion tensor and its indices

As mentioned above, in anisotropic tissues, the diffusion properties of a substance are better described by the diffusion tensor (DT) rather than a single diffusion coefficient. The main advantage of using the DT rather than just the ADC of the tissue is that the D reflects the underlying diffusion properties independently of the orientation of the tissue with respect to the direction of measurement (i.e. how the subject has been orientated within the scanner).

Calculation of the DT requires a non-diffusion-weighted image (i.e. a *b*=0 image) plus at least six DW measurements along non-collinear directions (Basser et al., 1994). The diffusion weighting is obtained by simultaneously applying diffusion gradients along combination of the three physical axes (e.g.,. x, y, z, xy, xz, yz). Knowing the six different components of the DT, shown in equation 2.3, it is possible to transform the DT into a new tensor, DT_1, (this process is called *tensor diagonalisation*) with all the off-diagonal elements equal to 0, and the diagonal elements reflecting the intrinsic properties of the tissue, independent of the coordinate system in which they were measured.

$$DT_1 = \begin{vmatrix} \lambda_1 & 0 & 0 \\ 0 & \lambda_2 & 0 \\ 0 & 0 & \lambda_3 \end{vmatrix} \qquad (2.6)$$

The D is characterized by three *eigenvectors* (ε_1, ε_2 and ε_3), which are orthogonal vectors in the scanner reference frame, representing three unique directions along which the displacement of water molecules is not correlated. λ_1, λ_2 and λ_3 are the corresponding ADC values, and they are defined as the D *eigenvalues*. In other words, the D eigenvalues correspond to the diffusion coefficients along the principal directions of the diffusion tensor. By convention, the eigenvalues are ordered with decreasing value of their eigenvalues ($\lambda_1 > \lambda_2 > \lambda_3$), so that ε_1 represents the principal direction of diffusivity characterised by $\lambda_1 > \lambda_2$ and $\lambda_2 > \lambda_3$. Therefore, if the DT has been acquired and diagonalised, ε_1 will always be aligned with the axis of the fibres and λ_1 will be the diffusion coefficient along ε_1, corresponding to the maximum diffusion in each voxel,

regardless how the head is oriented in the scanner reference frame. Several rotationally-invariant indices (or parameters) can be extracted from the DT to describe the behavior of diffusion within each voxel.

The *mean diffusivity* (MD) is the simplest way to summarise the diffusion properties of a voxel, and is given by the average of the eigenvalues of the DT within a voxel:

$$MD = \frac{\lambda 1 + \lambda 2 + \lambda 3}{3} \qquad (2.7)$$

Another index derived from the DT is *fractional anisotropy* (FA), which is equal to the ratio between the square root of the variance of the eigenvalues and the square root of the sum of the squares of the eigenvalues (Basser and Pierpaoli, 1996). Therefore FA estimates what proportion of diffusion is due to anisotropic diffusion:

$$FA = \frac{\sqrt{\left(\lambda 1 - \langle D \rangle\right)^2 + \left(\lambda 2 - \langle D \rangle\right)^2 + \left(\lambda 3 - \langle D \rangle\right)^2}}{\sqrt{\lambda 1^2 + \lambda 2^2 + \lambda 3^2}} \qquad (2.8)$$

FA is of special interest in the study of brain tissues, as it is different between the grey and white matter, being low in the former and high in the latter (Pierpaoli and Basser, 1996). Indeed, FA=1 for a cylindrically symmetric anisotropic medium with $\lambda_1 >> \lambda_2 = \lambda_3$, and FA=0 for complete isotropy (a sphere) where $\lambda_1 = \lambda_2 = \lambda_3$. An example of a brain MD and FA maps is provided in Figure 2.9.

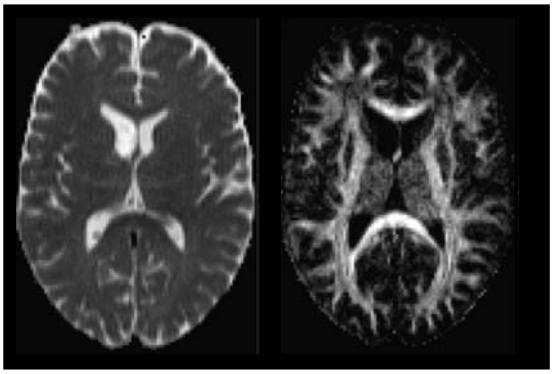

Figure 2.9. Diffusion tensor-derived maps. On the left a mean diffusivity (MD) map is displayed. On the right a fractional anisotropy (FA) map is displayed.

The diffusion ellipsoid is another way of visualising the DT within each image voxel. This ellipsoid is a surface representing the distance that a molecule will diffuse to with equal probability from the origin. The principal axes of the ellipsoid are given by the eigenvectors of the DT, and the lengths are given by the diffusion distance in a given time t . The shape of the ellipsoid reflects the degree of anisotropy (it is a sphere for isotropic voxels), and its main axis, if eccentric, represents the principal direction of the greatest diffusivity, as displayed in Figure 2.10.

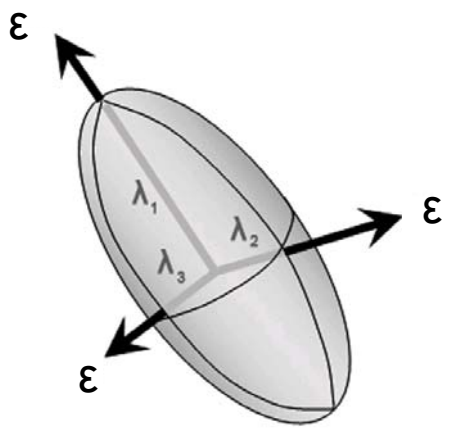

Figure 2.10. The diffusion ellipsoid in an anisotropic voxel is characterised by a cylindrically symmetric shape, with $\lambda_1 >> \lambda_2 = \lambda_3$, where λ_1 represents the greatest diffusivity along the principal direction.

2.3.6 Artifacts in the acquisition of diffusion-weighted images

DW imaging (DWI) is inherently sensitive to motion, and thus suffers from motion artifacts. Furthermore, DTI requires the collection of several images with gradients applied along non-collinear directions. For both motivations, DTI requires fast acquisition sequences, and typically EPI is used. EPI, however, is characterised by a low bandwidth in the phase encoding direction and thus is sensitive to a number of artifacts.

I. *Eddy currents*: Large, rapidly switched magnetic field gradients produced by gradient coils during a pulse sequence induce eddy currents in the electrically conductive structures of the MRI scanner which, in turn, produces additional unwanted magnetic fields (Jones, 2009). This can result in the generation of geometrical distortions. A number of different approaches have been developed for warping each DW image to a common template and remove distortions. One of the most commonly used method to correct for eddy-currents, which we have applied in the studies presented in Chapter III, IV, VI and VII, takes into account the bulk motion that is related to scanning live subjects. It consists of a full affine rigid-body approach to align whole diffusion-weighted volumes to the non-diffusion-weighted images, using the FLIRT package (Jenkinson and Smith, 2001).

II. *Magnetic susceptibility gradients*: Large discontinuities in bulk magnetic susceptibility, such as those occurring at tissue/air interfaces, produce local magnetic fields that can degrade and distort DWI, particularly during echo-planar imaging. Susceptibility effects are particularly acute in the brain regions adjacent to the sinuses (Jones, 2009).

III. *Cardiac pulsation*: Another source of artifacts is the physiological motion that arises from cardiac pulsation. It has been known for a long time that the pulsation of the brain, caused by the systolic part of the cardiac cycle, leads to additional phase dispersion in the brain parenchyma, which increases the apparent diffusivity (Jones, 2009). Several methods have been developed to remove these artifacts. One of the most commonly used is the method

consists of triggering the acquisition from the heart cycle of the participant with a peripheral gating device, to avoid the arrival of the pressure wave in the brain (Wheeler-Kingshott et al., 2002). This cardiac gating method has been employed in the studies presented in Chapter III, IV, VI and VII.

2.4 Magnetisation transfer imaging (MTI)

In this section, we will discuss the basic principles of magnetisation transfer imaging (MTI) (Tofts, 2003), which has been employed in the studies presented in the Chapters IV and VI of this thesis. MTI was first introduced by Wolff and Balaban in 1989 (Wolff and Balaban, 1989).

2.4.1 Basic principles of MTI

In brain tissue, protons exist in two states: a *free* state, in which they are very mobile, and a *bound* state, where they are associated with macromolecules such as proteins and lipids (for example in the context of cell membranes or myelin sheaths). MTI allows us to explore the properties of protons bound to macromolecules.

The relaxation characteristics of protons change depending on which compartment or proton pool they are in. Free water protons have faster average rotational frequency and, as a consequence, less fixed protons that may cause local field inhomogeneities. Because of this uniformity, most free water protons have resonant frequencies lying in a narrow range around the Larmor frequency of 63 MHz (at 1.5 Tesla). The high rotational frequency also results in fewer interactions with the environment so that dephasing of the transverse magnetisation is slower and the T2 of the free pool is long.

Conversely, bound protons are slowed down by extensive interactions with the protons in the local macromolecules and therefore magnetic field inhomogeneities are generated that lead to a wider resonance frequency spectrum (they absorb energy at frequencies not included in the narrow water resonance spectrum). The interactions with other protons result in faster

dephasing of the spins and therefore much shorter T2 values (<20 μs). This rapid loss of signal makes it impossible to image the bound proton pool directly. As discussed previously in this Chapter, in conventional MRI, the frequency of the RF pulse must match the resonant frequency of free water to obtain a signal from the free protons. With MTI, there is an additional pulse with a frequency off-set from water resonance, and this pulse saturates only the bound pool due to the much larger range of resonant frequencies of the bound pool (i.e. the magnetization of the bound proton pool is reduced) while having little effect on the free proton pool (Figure 2.11).

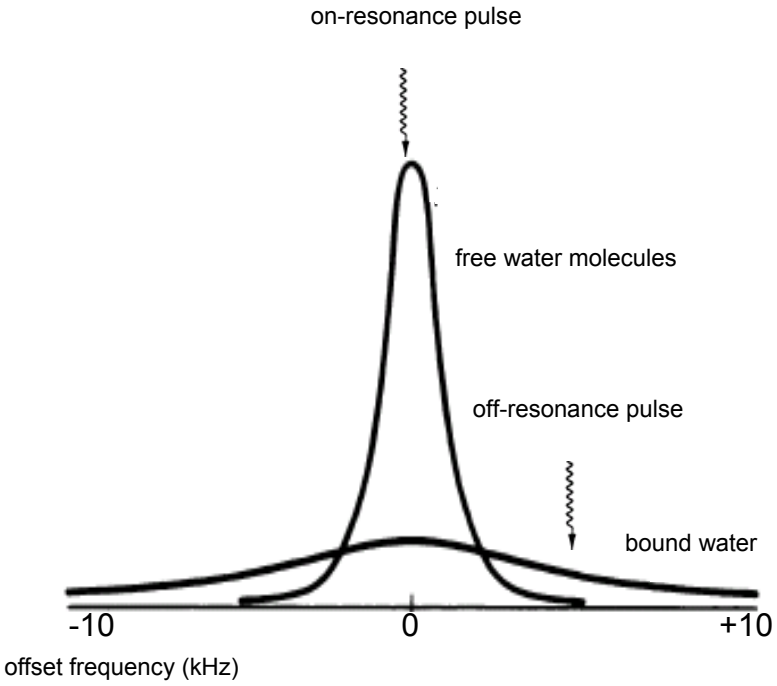

Figure 2.11. This diagram illustrates that the two different pools of protons (free and bound) resonate a different frequencies. As a consequence, the bound protons are selectively saturated by an off-resonance pulse that does not significantly affect the free water protons.

We can then indirectly measure the saturation of the bound pool via the effect this has on the free pool. The two pools exchange magnetization with each other, therefore applying an off-resonance pulse to excite protons in the bound pool has a detectable effect on the signal received from the free water molecules. After irradiating the bound pool, there is a *magnetisation transfer* between the two pools, which results in a reduction of longitudinal

magnetisation in the free pool. This causes an increase in the T1 of the free water and reduced signal from the free proton pool in tissues in which the magnetisation transfer mechanism is present. In other words, the reduction in signal depends on the exchange rate between the free and bound protons.

2.4.2 Magnetisation transfer ratio (MTR)

If images of the same slice are produced with and without an MT presaturation pulse, the MT ratio (MTR), which provides a measure of the saturation effect on a given tissue, can be calculated as follows:

$$MTR = \frac{\left[M_0 - M_s\right]}{M_0} \times 100 \qquad (2.9)$$

where M_0 is the signal intensity without MT presaturation, and M_s is the signal intensity with MT presaturation. MTR is therefore the percentage reduction in the signal when the saturation is applied, and is usually expressed in percentage units (pu).

The greater the MTR, the greater the reduction in signal and, therefore, the greater the bound water pool size, although many other factors contribute to the MTR. It should also be noted that the MTR is only 'semi-quantitative', in that it depends heavily on sequence acquisition parameters and MT pulse details, therefore MTR values are not necessarily comparable between different centres.

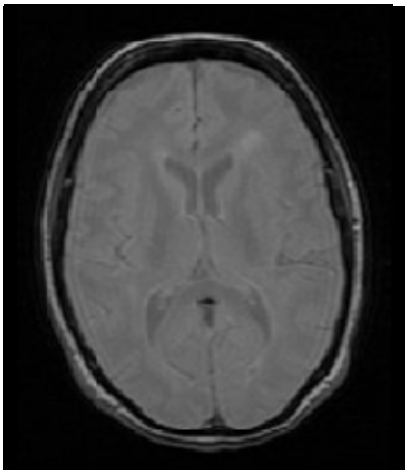

Figure 2.12. Example of an MTR map, derived from one of our patients with primary-progressive multiple sclerosis, involved in the study presented in Chapter VI.

2.5 Imaging analysis

In this section of the Chapter, the post-processing techniques which have been employed in the studies presented in this thesis will be described. The analysis methods applied to conventional images (i.e. GM volume analysis and lesion probability mapping) will be discussed first, and will be followed by a description of the post-processing techniques used to analyse DT and MT images.

2.5.1 Post-processing of conventional images

2.5.1.1 *Voxel-based morphometry (VBM)*

VBM is a fully automated technique which allows to perform voxel-wise analysis of the local concentration of GM (Ashburner and Friston, 2000; Ashburner and Friston, 2005). A VBM-style post-processing approach has been employed in the studies presented in Chapters III and VII of this thesis, to explore the role played by GM volume in the pathogenesis of early PPMS, and in the long-term prognosis of this disease. After an introduction of the basic VBM procedure, in this section we will review the optimisations and the improvements that we have included in the studies presented in this thesis. The basic VBM approach consists of the following steps:

I. *Spatial normalisation*: all subject's structural images are aligned to a standard space template image (such as a study-specific template or the standard MNI152, which we have used in the studies presented in this thesis). This step usually involves a first linear registration, which is followed by a non-linear transformation. This spatial normalization is not an attempt to match every cortical feature exactly, instead is aimed to correct for global brain shape differences.

II. *Segmentation:* each subject's structural image is segmented into different tissue types (GM, WM, and CSF), generating GM, WM, and CSF masks. Two sources of information are used to classify the image into the three tissue types: spatial prior probability maps (to which the original image is compared), and image intensities (each voxel in the original image has an intensity which corresponds to a specific probability of it being in one of the three tissue types).

III. *Smoothing:* Segmentation output data (GM mask) are then smoothed with an isotropic Gaussian kernel. As a result of this procedure, each voxel in the smoothed image contains the average concentration of GM from around the voxel. This is done for several reasons: (i) the smoothing helps reduce the effects of misalignment of structures when the registration is not completely accurate; (ii) smoothing can increase sensitivity if the extent of smoothing matches the size of an effect of interest; (iii) finally, smoothing makes the data more normally distributed, improving the validity of parametric statistical tests. The size of the smoothing kernel sensitizes the analysis to differences of comparable size as the kernel (Rosenfeld and Kak, 1982). In the study presented in Chapter III, a 12-mm FWHM Gaussian kernel has been employed, while in the study presented in Chapter VII, GM images were smoothed using both 12-mm FWHM and 8-mm FWHM Gaussian kernels.

IV. *Voxelwise statistics:* Statistical analysis using the General Linear Model (GLM) is then carried out voxel by voxel using one of the standard statistical parametric procedures. For example, to identify regions of GM concentration that are significantly different between two groups (e.g. patients versus

controls) it is possible to carry out a *t*-test or a *F*-test whereas, to identify GM areas related to a particular effect under study (e.g. areas where the GM concentration is related to specific clinical variables, such as disease severity or various clinical scores) it is possible to perform a regression analysis. A design matrix and a contrast of interest have to be defined. For example, for an independent two-sample t-test, such as the one we have used in the study presented in Chapter III to test for differences in GM volume between patients (group 1) and controls (group 2), a t-contrast of [-1 1] will correspond to a right-tailed (group2 > group1) t-test, while a contrast of [1 -1] to a left-tailed (group1 > group2) t-test. It is also possible to take into account the role of possible confounding factors (for example age and gender) in the relationship between the GM concentration and a specific variable of interest (for example clinical test scores), including in the model the relevant covariates (which will be set as "0" in the the contrast matrix). The resulting set of voxels from each contrast represents a statistical parametric map of the *t*-statistic (or *F*-statistic).

V. *Thresholding:* The resulting statistical parametric image includes the result of many statistical tests, and it is necessary to correct for these multiple comparisons. In the studies presented in Chapters III and VII of this thesis, we have used a family-wise error (FWE) correction at $p<0.05$ for multiple comparisons at voxel level across the whole brain (i.e. it is assumed that less than 5% of the resulting statistical parametric maps contain false positive voxels).

VBM is fully automated, simple to apply, and its main advantage is that it offers the opportunity to investigate the whole brain without the need to generate an a priori hypothesis. The main limitation of this approach relates to problems caused by possible alignment inaccuracies, that can lead to a misinterpretation of results in voxels that in fact are not localized in the same position in all subjects included in a study, and by the arbitrariness of the spatial smoothing, which can influence the results of the analysis.

In the studies presented in this thesis, VBM has been carried out using the

Statistical Parametric Mapping (SPM) software package (www.fil.ion.ucl.ac.uk/spm/software/, Wellcome Department of Cognitive Neurology, London, UK). Over the years, SPM has proposed a number of improvements and optimizations of the original VBM protocol, which we have included in the studies presented in this thesis. The *optimised* VBM protocol (Good et al., 2001) introduced with SPM99 and SPM2, in which the GM segmentation is used to drive the registration (instead of the raw structural images), to improve the results of the spatial normalization, has been employed in the studies presented in Chapter III and VII. Moreover, in both these studies, the *modulation* option offered by SPM has been used, that allows to correct the segmentation output after non-linear registration (i.e. voxel intensities are multiplied by the local value in the deformation field from normalization), so that the total amount of GM in the modulated GM remains the same as it would be in the original image. This procedure allows us to make inferences about GM volume, instead of GM concentration. In April 2009, a major update to the SPM software, called SPM8, has been released. In this updated version of the SPM software, which has been employed in the study presented in Chapter VII, the VBM protocol consists of an iterative combination of segmentations and normalizations to produce a GM probability map (Ashburner and Friston, 2005). Finally, as the presence of lesions in the WM has recently shown to significantly affect brain segmentation (Nakamura and Fisher, 2009) and registration (Sdika and Pelletier, 2009), which are key steps in VBM, in the study presented in Chapter VII we applied the recently developed lesion automated preprocessing (lesion automated preprocessing, LEAP) (Chard et al., 2010) technique to the T1-weighted images, before feeding them into the VBM procedure. Briefly, LEAP is an “in-painting” technique developed in our Unit, which replaces lesional voxels with values derived from the intensity distribution within the WM outside visible lesions in the presegmentation phase (Chard et al., 2010). This technique minimises lesion-associated segmentation biases that may significantly affect VBM results.

2.5.1.2 *Lesion Probability Mapping (LPM)*

LPM is a method that, applied to conventional T2-weighted and T1-weighted images, allows defining the probability of each image voxel to be lesional (Di

Perri et al., 2008). In the study presented in the Chapter V of this thesis, we generated LPMs on both T2-w and T1-w images, in order to explore the role of lesion location in predicting long-term clinical outcome in patients with PPMS.

The LPM method which has been applied in Chapter V consists of the following steps:

I. *Lesion mask:* PD hyperintense and T1 hypointense lesions were contoured, with reference to the co-registered T2 weighted images, using a semiautomated technique (Plummer, 1992). Binary lesion masks were then produced and individual lesion loads calculated.

II. *Template construction:* Each patient's T1 scan was registered to the Montreal Neurological Institute (MNI152) template using a fully affinetransformation (12 parameters), as previously described in patient groups with a variety of neurological conditions (Karagulle Kendi et al., 2008; Ginestroni et al., 2009; Vellinga et al., 2009). All of the resulting transformed images were averaged to obtain our “internal” T1 template.

III. *Transformation of individual scans and lesion masks into T1 template:* Each patient's PD weighted scan was registered to the corresponding T1 scan in native space using a rigid body transformation and trilinear interpolation. The transformation parameters were then applied to the T2 lesion masks, bringing them into alignment with the individual T1 scans. Each patient's T1 scan was then registered to the T1 template, using non-linear registration, and the resulting transformation parameters were applied to the T1 and T2 lesion masks, which had been previously registered onto the individual T1, using trilinear interpolation. In order to maintain the volume of the transformed lesion masks as close as possible to those in the native brain images, after the trilinear interpolation, the lesion masks were thresholded using a value of 0.5.

IV. *Generation of T2 and T1 LPMs:* T2 and T1 LPMs were generated by averaging the T2 and T1 lesion masks, at each voxel, in standard space. For

each map, the resulting voxel intensity indicates how frequently the voxel in question is within a lesion across all patients, ie, the probability of that voxel being lesional. Regions containing the peaks of lesion probability were localised using the Johns Hopkins University DTI-based white matter tractography atlas (Mori, 2005).

2.5.2 Post-processing of DTI and MTI images

2.5.2.1 *Methodological considerations*

From a methodological point of view, the DTI- and MTI-derived parameters can be measured in the brain in clinical studies using different post-processing approaches, which can be summarised as follows:

I. *Region-of-interest analysis:* This methodology consists of drawing ROIs in specific areas of the brain, and then quantifying DTI or MTI parameters (FA and MTR, for example) within those areas. The main advantages of this approach are that the regions can be chosen on the basis of a priori hypotheses, and can be located in a specific part of the brain. On the other hand, this approach can miss significant abnormalities in regions that are not selected, and it is highly dependent on the observer and on the anatomical clues used in positioning the regions. The registration process and its related methodological issues must be carefully considered when images from different modalities are co-registered to allow the transfer of regions. It is also necessary to reposition the ROIs in exactly the same location in longitudinal studies. In the study presented in the Chapter IV of this thesis, tractography has been employed to identify ROIs (tracts of interest, in this specific case), from which the mean MTR was extracted.

II. *Histogram analysis:* An alternative approach to the ROI is the histogram analysis. This methodology has been used widely in patients with neurological disorders, such as MS and brain tumors, to investigate the differences between patients and controls and to explore correlations between MRI parameters and clinical disability. The histogram of DTI and MTI parameters is a frequency distribution showing the number of voxels with

a particular range of parameter values. From the histogram of each parameter, the following variables can be derived: the mean; the peak height (the proportion of voxels at modal value); the peak location (the location of the modal value). These variables are then used in statistical tests, for example comparing patients and controls. The histogram analysis allows the characterisation of the parameters in the whole brain in a fully automated way. Histograms of WM or GM only can also be obtained. In contrast to the ROI approach, it does not retain any information about location of abnormalities, and avoids any pre-judgment about which parts of the brain is investigated. However, this approach does not allow to localise regional abnormalities, as it provides a measure of the global tissue changes.

III. *Voxel-wise analysis:* More recently, a voxel-wise approach, similar to the one described in the VBM section of this Chapter, has been proposed to analyse both DTI- and MTI-derived metrics on a voxel-by-voxel basis. This approach allows us to localise changes in these metrics related to tissue abnormalities, and allows to combine the ability of ROIs to be spatially specific with the ability of histograms to be unbiased. In simple terms, it involves co-registration of the DTI-and MTI-derived metrics maps (FA or MTR maps, for example), into a standard space, and then making comparisons of diffusion parameter values between groups or testing for correlations with an external variable, such as disability or age. Advantages of this approach are that all locations across the brain are tested in an unbiased way, and that location of significant group differences or correlations is automatically shown. As previously discussed, the limitations of this approach relate to the possible inaccuracy of the registration algorithms and to the arbitrariness of the spatial smoothing. To overcome some of these limitations, in the studies presented in the Chapter III, VI and VII of this thesis tract-based spatial statistics (TBSS) (Smith et al., 2006) has been employed to analyse FA maps and MTR maps (see next section of this Chapter for a full description of the method).

2.5.2.2 *Tract-based spatial statistics (TBSS)*

Tract-based spatial statistics (TBSS) is a fully automated method that allows a

voxelwise analysis of multi-subject diffusion data which aims to solve some of the issues related to the VBM approach (Smith et al., 2006). This is achieved by generating a *group mean FA skeleton* (Figure 2.13), which represents the centre of all WM tracts that are common across all the subjects included in a study. Each subject's FA map is then projected onto the mean FA skeleton in such a way that each skeleton voxel takes the FA value from the local centre of the nearest relevant tract, thus resolving issues of alignment and correspondence of voxels and, in turn, ensuring reliable results.

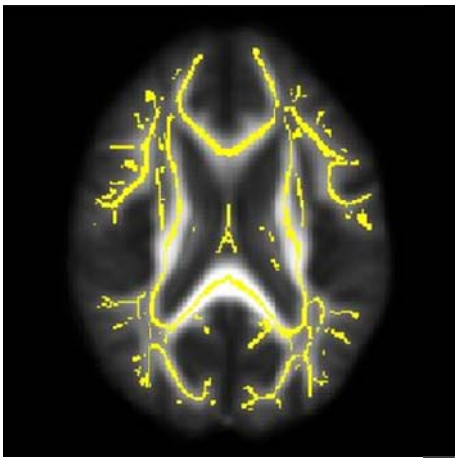

Figure 2.13. The image sh ows the mean FA skeleton of the cohort of patients with PPMS investigated in Chapter VII, which represents the core of all white matter tracts that are common across all patients, and is overlaid onto the mean patients' FA image.

The TBSS approach consists of the following steps:

I. *Non-linear alignment:* All subjects' FA images are aligned to a common target using a linear registration first (FLIRT) (Jenkinson and Smith, 2001), and then a non-linear registration (FNIRT) (www.fmrib.ox.ac.uk/fsl/fnirt). The target image used in the registrations can either be a pre-defined target, or can be automatically chosen to be the most "typical" subject in the study, i.e. to be the target image which minimizes the amount of warping required for all the other subjects to align to it. In the studies presented in this thesis we followed the recommendation of FSL website (www.fmrib.ox.ac.uk/fsl/tbss), using as target image the FMRIB58_FA 1x1x1mm standard-space image. At

this stage, a perfect alignment is not expected nor required.

II. *Mean FA image and FA skeleton:* The transformed images are then averaged to obtain a mean FA image. To achieve skeletonisation, the local surface perpendicular direction is estimated, and then a search is carried out in this direction to identify the voxel with the highest FA, which is considered to be the centre of the tract. This FA skeleton, which represents the different tract structures in the mean FA image, is then thresholded to exclude from further analysis those voxels where it is unsafe to assume good tract correspondence across subjects (Figure 2.13). Then, the mean FA is thresholded to exclude voxels which are in the GM or in the CSF in the majority of subjects and to ensure that the skeleton does not run to the outermost edges of the cortex, where the most variable tracts across subjects are not well aligned (in the studies presented in this thesis a threshold of 0.2 was used).

III. *Projection of each subject's FA onto the mean FA skeleton:* Each subject's aligned FA image is then projected onto the mean FA skeleton, to account for the residual misalignments after the initial non-linear registration. Then, at each point in the skeleton, each subject's FA image is searched in the perpendicular tract direction to find the maximum FA value, and this value is assigned to the skeleton voxel. At this stage the skeleton has been filled, for each subject, with FA values from the centers of the nearest relevant tracts.

IV *Voxel-wise statistics:* Finally, voxel-wise statistics across subjects is performed on the skeleton-space FA data. To perform the statistical analysis, a design matrix to perform a specific test has to be generated (for example a *t*-test to search for differences in FA between patients and controls, as in the study presented in Chapter III), together with a contrast matrix which specifies the contrast of interest (in the example of the Chapter III study, the contrast of interest was control group FA> patient group FA). It is also possible to correct for possible confounding factors.

2.5.2.3 *White Matter tractography*

As previously discussed, the diffusion tensor (DT) can be defined as a mathematical description of the magnitude and the directionality of the diffusion of water molecules in a three-dimensional space (Basser, 1995). White matter tractography (WMT) algorithms use this information extracted from the DT to estimate the connectivity patterns between different brain regions, by inferring the continuity of fibre paths from voxel to voxel (Ciccarelli et al., 2008; Lazar, 2010). To date, a large number of WMT algorithms have been proposed, that can be classified into deterministic, probabilistic, and global optimization algorithms (Lazar, 2010).

The *deterministic algorithms* generate a unique trajectory for each seed point. In this case, a trajectory is calculated from the seed point in both forward and reverse directions of the fiber orientation field in a stepwise fashion (i.e. at each step, the trajectory is advanced along the estimated tract direction) (Figure 2.14).

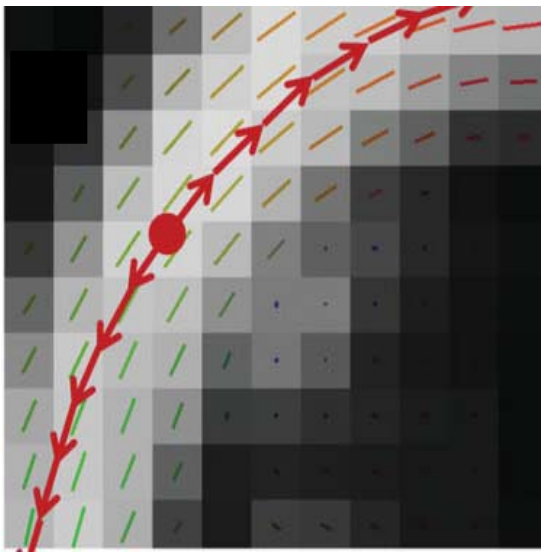

Figure 2.14. The deterministic algorithms define fiber trajectories following fiber direction estimates from voxel to voxel starting from a seed point, indicated with a dot in the picture.

Several strategies can be employed to step along the trajectory, including a constant step size with the propagation direction estimated at the beginning of the step, or calculated along the step, or a variable step size. The propagation

of the fiber trajectory is stopped when a previously established stopping criteria is met (e.g. exiting the brain space, the intersection with voxels characterised by low anisotropy values such as the GM or the CSF, or large local curvature of the trajectory) (Bick et al., 2012). In this approach the point reached is not known a priori, but the tracking process, being deterministic, is fully repeatable. In contrast to deterministic algorithms, which estimate WM connectivity by assuming a unique fiber principal direction within a voxel, *probabilistic algorithms* generate a set of possible propagation directions for a given voxel. For each seed point, a set of possible trajectories is obtained, each one generated in a streamline fashion, with the propagation direction at each step being chosen at random from the distribution of directions available at the step's corresponding voxel. A probability of connection between the seed voxel and other voxels or regions of the brain is defined as the density of the trajectories, where the density is calculated as the number of connecting trajectories normalized by the total number of trajectories. A higher density of trajectories between two regions of the brain indicates a higher probability of connection between those two regions. To map the extent of a tract, connectivity is then thresholded, such that voxels with low probability of connection are not included in the estimated tract volume.

Finally, *global optimisation algorithms* reconstruct the most probable paths in the brain space, such as the path trajectories that are consistent with the underlying diffusion data and satisfy specific constraints. The first constraint is to consider path optimization between two regions, i.e. a seed point and a target point. Often, path smoothness is used as additional constraint to find optimal trajectories.

WMT has been used extensively with various applications (Lazar, 2010). In particular, WMT has proved useful in (i) demonstrating the in vivo mapping of the brain WM tracts; (ii) generating new information regarding brain organization and internal connection; (iii) identifying specific WM tracts and using them as regions of interest; (iv) segmenting GM regions on the basis of their connectivity patterns; (v) presurgical planning.
In the study presented in Chapter IV, probabilistic tractography on healthy

controls data has been employed, to identify the route of the tracts of interest (see below) and to investigate these fibre bundles in patients with PPMS. In particular, the tractography algorithm from the Camino toolkit (www.camino.org) was used and the probabilistic index of connectivity (PICo) (Parker et al., 2003)) was computed using 5000 iterations and no interpolation. Importantly, no FA thresholds were included to constrain the outcome of the tractography. As discussed above, a curvature threshold was used such that each run of the tractography stops if there is curvature of more than 80° between adjacent voxels; connectivity maps were thresholded at a connectivity value of 0.02 (Toosy et al., 2004). Seed regions and exclusion masks were defined, and used to constrain the tracts to anatomically plausible regions of the brain, to extract the following tracts: i) the left and right cortico-spinal tracts (CST), ii) the genu of the corpus callosum (GCC), and (iii) The left and right optic radiations (OR).

2.5.2.4 *Linking WM tracts to associated cortical GM: a tract-extension methodology*

A new method to extend WM tracts into the cortical GM has been developed in our Unit and has been employed in the study presented in Chapter IV to identify the “cortical targets” of the three WM tracts, extracted following the steps described in the previous section (i.e. CST, GCC and OR) (Tozer et al., 2012).

This new method is based on geometrical, rather than diffusion information, and starts from a WM tract, as defined by a diffusion-based tractography algorithm, and extends it through to the outer edge of the cortical GM ribbon, to the boundary between brain and CSF, as defined from segmented T1-weighted volumes (or other segmented images) in the same space. The tractography algorithm and the seed voxel used for the tractography, as well as the segmentation method used to generate the GM ribbon will determine the starting point for the tract extension method. The tract extension method itself, though, is independent of the method used to determine the starting point.

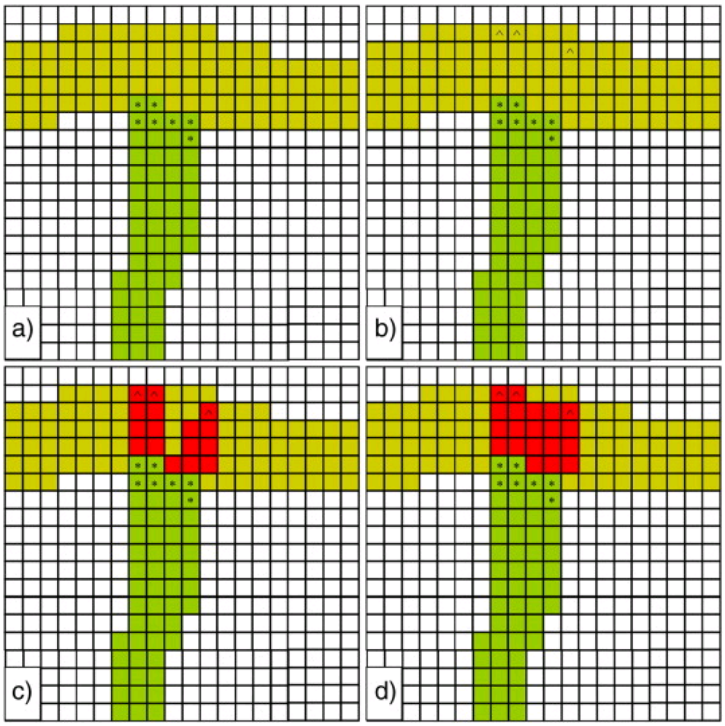

Figure 2.15. A schematic representation of the tract extension method. In all parts the original tract is in green, the GM is in sandy yellow and the extended tract in shown in red. a) Shows the start points of the extension method, marked with a *, being the points on the edge of the tract within or adjacent to the GM. In b) end points have been identified, marked as ^, which are the closest points to each of the start points. c) Shows the voxels in a straight line between the start and end points and d) shows the final extension after the dilation/erosion step.

The steps to define the GM extension of a WM tract are as follows (Figure 2.15):

I. Definition of a starting point (SP):

A starting point is a voxel satisfying two criteria: (i) the voxel is on the boundary of the original tract; (ii) the voxel is either within the GM, or on the GM/WM boundary, such that the voxel adjacent to the tract boundary voxel is within the GM);

II. Definition of an end-point (EP):

For each SP found by step I, the EP must be a voxel on the outer edge of the GM, i.e. on the boundary between tissue and CSF surrounding the brain. For each SP, the EP is chosen by satisfying two criteria: (i) the straight line connecting SP and EP must be the shortest possible; (ii) the line connecting SP

and EP must not pass through non-tract WM or non-brain tissue voxels. The process performed in the study presented in Chapter IV was performed in a multiplanar 2-dimensional (2D) manner, where three EPs, were defined for each SP, one in each of three orthogonal representations of data with the EP being chosen in plane only.

III. WM tract extension to include GM voxel selection:
The voxels that lie on the straight line between each SP and the corresponding EP are then classified as part of the GM most likely to be connected with the tract. The results of the extension in the three directions were then combined to produce the GM extension and then with the original tract to produce a mask of the entire tract (WM and GM).

IV. Erosion–dilation steps:
The combined WM tract and resulting GM region generated in step II was dilated and eroded by 2 voxels, in 3 dimensions, to fill in gaps and then masked with both a GM mask and the original WM tract, to remove any non-brain and non-tract WM voxels. This masking can also be used to divide the extended tract into the original WM portion and a GM portion, so the WM tract parameters can then be analysed alongside their associated cortical GM values.

2.5.2.5 *"Skeletonised MTR": a novel approach to explore microstructural WM changes*

In the study presented in Chapter VI, a novel method is proposed to explore WM microstructural changes over one year in patients with PPMS, which consists of a combination of TBSS and MTR (see previous sections of this Chapter for further details on TBSS and MTR). In summary, a common skeleton of patients' WM tracts was created using the standard TBSS approach, and then the MTR value,corresponding to each voxel of the skeleton, was extracted. To obtain a "skeletonised" MTR image for each patient, the following steps were followed:

I. MT was first co-registered with DTI data, by matching the non-MT weighted

volume with the b0 volume, after skull-stripping, with an affine transformation using FLIRT (FMRIB's Linear Image Registration Tool, part of FSL) (Smith et al., 2004).

II. The transformation was then applied to the MTR map.

III. Finally, the transformed MTR map underwent the same projection as the FA data onto the common FA tract skeleton (which had been previously created using TBSS), to obtain a "skeletonised" MTR image for each subject at each time point of the study (i.e. baseline and one year).

2.6 Conclusions

This Chapter reviewed the basic principles of conventional and non-conventional imaging techniques, as well as the post-processing methods that have been employed in the clinical studies presented in this thesis. In the final part of the Chapter, two novel imaging analysis methods have been described: the "tract-extension" methodology and the "skeletonised MTR" approach. Both methods have been employed for the first time in the clinical studies shown in this thesis.

After these two introductory Chapters, the next part of the thesis will discuss the results of the clinical studies that have been performed to answer the two main questions presented at the end of Chapter I. In particular, Chapter III will address the first question, i.e. the relationship between WM and GM damage in PPMS, through an investigation of cross-sectional links between the damage occurring in the two compartments, and will assess their clinical relevance.

Exploring the relationship between white matter and grey matter damage in PPMS

Chapter III

This Chapter addresses the first question presented in Chapter I, investigating whether there is a spatial relationship between the damage occurring in the normal appearing WM (NAWM) and in the GM of patients with PPMS at the earliest stage of their disease. The cross-sectional spatial link between the abnormalities affecting the two compartments will be explored using TBSS (Smith et al., 2006) and an optimized VBM approach (see Chapter II for technical details on methods).

3.1 Introduction

As reported in Chapter I, MRI studies have consistently reported structural abnormalities in the NAWM of patients with PPMS, even in the early stages of the disease; these abnormalities have been shown to be clinically relevant (Rocca et al., 2012a). One of the MRI measures most commonly employed to assess the integrity and orientation of WM tracts is FA, which is derived from the diffusion tensor (Basser et al., 1994). Reduced FA, which reflects underlying demyelination and axonal loss (Schmierer et al., 2007; Moll et al., 2011) has been described in the WM of PPMS using various approaches, including ROIs and histogram analyses (Ciccarelli et al., 2001; Vrenken et al., 2006). These results are consistent with the data coming from post-mortem studies in PPMS (see Chapter I), which have demonstrated widespread demyelination and axonal injury in the NAWM in the brain of patients with PPMS (Kutzelnigg et al., 2005). In addition, it has been suggested that activated microglia and microglial nodules may explain reduced FA in the WM of patients with MS (Moll et al., 2011).

As discussed previously, GM damage and, in particular, GM atrophy, has been detected in PPMS (Sastre-Garriga et al., 2004; Sepulcre et al., 2006; Roosendaal et al., 2011), but the precise pathological substrate of GM atrophy, as measured in vivo with MRI, remains unknown. However, a post-mortem study has suggested a correlation between MRI-measured atrophy and neuronal and glial loss (Wegner et al., 2006). In addition, in histological studies, extensive GM demyelination has been described in progressive MS patients (Kutzelnigg et al., 2005; Bo et al., 2007).

Since GM tissue does not have strong directionality, FA is generally considered not to be useful as a measure of local GM abnormalities. On the other hand, VBM (Ashburner and Friston, 2000) and histogram analysis of T1-weighted images have outlined regions of GM atrophy in patients with PPMS when compared with controls (De Stefano et al., 2003; Ramio-Torrenta et al., 2006; Khaleeli et al., 2007b), which progress relentlessly throughout the course of the disease (De Stefano et al., 2010) predicting clinical evolution over time .

The important question addressed in the study presented in this Chapter is whether NAWM damage correlates with abnormalities in connected GM or the two compartments are affected independently in early PPMS. Previous histological studies addressing this question have been inconclusive. Kutzelnigg et al. (Kutzelnigg et al., 2005) reported a weak correlation between diffuse WM inflammation and GM demyelination, whereas Bo et al. (Bo et al., 2007) found no association between abnormalities in the grey and white matter compartments. MRI studies, on the other hand, have focused on the relationship between lesions in the WM and GM damage in patients with PPMS and other forms of MS (De Stefano et al., 2003; Pagani et al., 2005b; Ramio-Torrenta et al., 2006; Sepulcre et al., 2006; Charil et al., 2007; Bendfeldt et al., 2010; Roosendaal et al., 2011), and have suggested that at least a proportion of cortical pathology may be secondary to WM abnormalities.

The investigation focused on the relationship between NAWM damage and GM atrophy in vivo in patients with early PPMS, who are probably in the most clinically active phase of the disease (Thompson, 2004), combining the results of TBSS (Smith et al., 2006), which localised areas of reduced FA in the NAWM of patients, with the results of an optimized VBM approach (Good et al., 2001), which detected areas of GM atrophy in patients (see Chapter II for more details). As previously discussed, both techniques test the whole brain without requiring any specific a priori hypothesis.

A similar methodology of combining TBSS and VBM has been applied to healthy individuals of different age (Giorgio et al., 2010; Moy et al., 2011), as well as to patients with psychiatric and neurological diseases, such as

adolescent-onset schizophrenia (Douaud et al., 2007), bipolar disorder (Haller et al., 2011), Friedreich's ataxia (Della Nave et al., 2008), cluster headache (Absinta et al., 2011), RRMS (Roosendaal et al., 2009) and clinically isolated syndromes suggestive of MS (CIS) (Raz et al., 2010a; Raz et al., 2010b). In the study presented here, this methodology was applied in order to investigate the *quantitative* relationship underlying the anatomical correspondence between GM and WM damage in patients with early PPMS. In particular, the aim of this study was to assess whether: (i) there was an anatomical correspondence between reduced FA in the NAWM and GM atrophy; (ii) FA values of abnormal tracts correlated with the GM volume of connected atrophic regions; and (iii) NAWM FA or GM volume independently correlated with disability.

3.2 Methods

3.2.1 Subjects

Thirty-six patients with a diagnosis of PPMS according to Thompson's criteria (Thompson et al., 2000) within 5 years of symptom onset (15 females, 21 males, mean age 45.3 years, and SD 11.32) underwent an imaging and clinical assessment protocol approved by the Joint Medical Ethics Committee of the National Hospital for Neurology and Neurosurgery and the Institute of Neurology, London (see Appendix I). Written and informed consent was obtained from all participants. One patient was later excluded from the analysis (as discussed below), leaving a total of 35 patients.

All patients were assessed on the day of scanning using the EDSS (Kurtzke, 1983) and the Multiple Sclerosis Functional Composite (MSFC) subtests: Paced Auditory Serial Addition Test (PASAT), Nine-Hole Peg Test (NHPT), and Timed Walk Test (TWT) (Cutter et al., 1999).

Two different groups of controls were used, as this was a retrospective analysis performed on previously acquired data, which were combined for the purpose of this study. The first group included 18 healthy subjects, who were age-matched to the patient group (8 females, 10 males, mean age 41.5 years, and SD 12.63)

and were used for the localization of WM abnormalities. The second group included 23 healthy subjects (12 females, 11 males, mean age 35.1 years, and SD 7.9), who were used for the localization of regions of GM atrophy. The difference in age between this second group of controls and the patient group were adjusted for, at each stage of the analysis. The patients' and controls demographic, clinical and radiological characteristics are summarised in Table 3.1.

Characteristics	Patients	Controls 1st group	Controls 2nd group
Number	36	18	23
Age, years (SD)	44.8 (11.13)	41.5 (12.63)	35.1 (7.9)
Gender, female/male	15/20	8/10	12/11
EDSS, median (range)	4.5 (1.5–7.0)	-	-
Disease duration, years (SD)	3.3 (0.9)	-	-
T2 lesion load, ml (SD)	31.56 (24.79)	-	-
PASAT score, mean (SD)	47.65 (11.24)	-	-
NHPT score, mean (SD)	22.48 (3.69)	-	-
TWT score, mean (SD)	8.63 (8.37)	-	-

Table 3.1 Patients' and healthy controls' characteristics.

3.2.2 Image acquisition and analysis

All imaging was obtained using a 1.5-T GE Signa scanner (General Electric, Milwaukee, IL), with maximum gradient strength of 22 mT m−1. Images were displayed on a Sun workstation (Sun Microsystems, Mountain View, CA) for analysis.

3.2.2.1 *Dual-echo images, lesion load, and creation of a mean lesion mask*

All subjects had a fast spin echo scan that collects PD and T2-weighted images (repetition time [TR] 2000 ms; echo times [TEs] 17/92 ms; matrix size 256 ×

256; field of view [FOV] 240 × 180 mm2; 28 contiguous axial slices of 5 mm thickness). Lesions were delineated by a single observer (who was blinded to the clinical details) on the PD images, with reference to the coregistered T2-w images, using a semiautomated contour thresholding technique (Plummer, 1992), and used to calculate each subject's lesion load and lesion mask. Each individual binary lesion mask was obtained by setting the signal within lesion boundaries to one and the remainder of the brain to zero.

Each subject's T2-weighted image was registered to the Montreal Neurological Institute (MNI) template using an affine transformation (FLIRT, part of FSL www.fmrib.ox.ac.uk/fsl) (Jenkinson and Smith, 2001). The same transformation parameters were then applied to the lesion mask. The individual, normalized lesion masks were then averaged to obtain a mean lesion map indicating the proportion of the cohort having a lesion in each voxel. Finally, this map was binarised to retain only voxels with a value higher than 0.1 (indicating that at least 10% of the subjects had a lesion in a given voxel).

3.2.2.2 *Diffusion-tensor imaging and TBSS analysis*

All patients and the first group of 18 age-matched controls underwent a whole-brain, cardiac-gated Spin Echo Diffusion Weighted Echo Planar Imaging (SE-DW-EPI) sequence (Wheeler-Kingshott et al., 2002). Full brain coverage was obtained with three separate acquisitions, each collecting 14 axial slices of 3 mm thickness, which were interleaved off-line. The data was acquired with the following parameters: FOV 240 × 240 mm2, matrix size 96 × 96 (reconstructed to 128 × 128), image resolution 2.5 × 2.5 × 3 mm (reconstructed to 1.9 × 1.9 × 3 mm), TE 95 ms, TR 7RRs, and maximum b factor 1000 sm m−2. Diffusion gradients were applied along 25 optimized directions (Jones et al., 1999). Three images with no diffusion weighting (b0) were also acquired.

After correction for eddy-current-induced distortions, the diffusion tensor was calculated on a voxel-by-voxel basis (Basser et al., 1994), and FA maps were generated using DTIfit provided by the fMRIB Diffusion Toolbox [part of FSL; www.fmrib.ox.ac.uk/fsl; (Smith et al., 2004)]. TBSS (Smith et al., 2006) was used to create a mean FA skeleton, following the procedure described in

Chapter II. Since the focus of the study was the investigation of NAWM only, the final binary lesion mask was subtracted from the skeleton in order to produce a NAWM only significant skeleton.

Voxel-wise differences in projected FA between patients and controls were tested using a two sample t-test. Two contrasts, patients greater than controls' FA and controls greater than patients, were estimated. The resultant statistical maps were thresholded at $p < 0.05$ corrected at cluster level for multiple comparisons using a permutation-based approach (Nichols and Holmes, 2002). In particular, a cluster-forming threshold $t > 2$ was used (the threshold-free cluster enhancement was not available at the time of this study), and the null distribution of maximum values (across the image) of the test statistic was estimated. A similar cluster-forming threshold had been used in the only TBSS study of patients with MS published at the time of this study (Cader et al., 2007).

3.2.2.3 *T1-weighted volumetric images and SPM2-VBM analysis of GM*

All patients and the second group of 23 controls underwent a three-dimensional inversion-prepared fast spoiled gradient recall (3D FSPGR) T1-weighted sequence of the brain [FOV 300 × 225 mm, matrix size 256 × 160 (reconstructed to 256 × 256 for a final in plane resolution of 1.17 mm), TR 13.3 ms, TE 4.2 ms, inversion time 450 ms, 124 contiguous axial slices, slice thickness of 1.5 mm].

Pre-processing of T1-weighted images was performed according to the previously described optimized VBM-style protocol (Good et al., 2001) (see Chapter II for details) using the segmentation and registration tools available in the statistical parametric mapping software (SPM2, as SPM5 had recently being released at the time of the analysis, and the same software used in previous studies on the same group of patients was employed in this case). The protocol was modified to account for the presence of WM lesions in patients, as described by Khaleeli et al. (Khaleeli et al., 2007b). The procedure will now be briefly summarised. The 3D FSPGRs of all subjects were segmented in native space. Lesions masks were applied to the GM partitions to remove lesions erroneously classified as GM. GM volume was estimated for every subject, and

the images normalized onto the SPM GM template. Lesion masks were used to weight the normalization. The normalization parameters were then applied to the T1-volumes, and the normalized images were segmented and masked again to produce GM segments. One patient was excluded from the study because of segmentation failure due to a high lesion load. All data were then smoothed using a 12-mm FWHM Gaussian kernel.

To localize areas where GM volume was significantly lower in patients compared with controls, an analysis of covariance adjusted for age and for total GM volume was performed. A family-wise error correction at $p < 0.05$ for multiple comparisons at voxel level across the whole brain was used. Regions comprising clusters of less than 100 voxels were excluded from the analysis.

3.2.2.4 *Anatomical correspondence and quantitative relationship between NAWM and GM abnormalities*

In patients, areas of *anatomical correspondence* between tracts of lower FA and adjacent regions of GM atrophy were visually identified by overlaying the results of the two different analyses on the same anatomical image (Douaud et al., 2007). To assess whether there was a *quantitative correlation* underlying this anatomical relationship, for each area of anatomical correspondence, the mean FA value of the cluster of significantly lower NAWM FA and the mean volume of the cluster of significantly lower GM volume were extracted. The relationship between mean FA and mean GM volume of these areas was quantified using the Spearman's correlation coefficient (using SPSS 11.5 for Windows).

3.2.2.5 *Correlation between NAWM and GM abnormalities and disability*

The Z-score (z) for each MSFC subtest was calculated using our own sample as reference (Cutter et al., 1999). Patients were also divided into three categories of roughly similar size on the basis of disability as follows: (i) EDSS ≤ 3.5 = Group 1 (patients with minimal disability and fully ambulatory); (ii) EDSS between 4.0 and 5.5 = Group 2 (patients with moderate disability and restricted ambulation); and (iii) EDSS ≥ 6.0 = Group 3 (patients with severe disability who required unilateral or bilateral assistance to walk).

In patients, for each region where a quantitative relationship between NAWM

FA and GM volume was found, the association between clinical scores and NAWM and GM changes was assessed using (i) multiple linear regression analysis for the zPASAT, zHPT, zTWT and (ii) multiple ordinal logistic regression analysis for the EDSS categories, as the EDSS is not a linear scale and was not normally distributed.

To identify which MRI variable (i.e., GM volume and NAWM FA) was associated with disability, independently from the other and from age and gender, each disability score (i.e., EDSS, zPASAT, zHPT, zTWT) was selected, in turn, as dependent variable, whilst NAWM FA, GM volume, age, and gender were selected as independent variables. We chose not to analyse the impact of MRI changes on the global MSFC, but rather on the individual MSFC subtests, which can be more informative than the global MSFC score, as this is obtained by calculating the mean of the three subtest z-scores. Results with p values < 0.05 were reported.

3.3 Results

3.3.1 Reduced FA of NAWM tracts

Patients showed reduced FA compared with controls in the NAWM along the corticospinal tracts bilaterally (posterior limb of the internal capsule, corona radiata, and WM adjacent to primary motor cortex), in the WM adjacent to the premotor cortex bilaterally, and in the entire corpus callosum (i.e., rostrum, genu, body, and splenium).

FA was also significantly reduced in patients than in controls in the following areas bilaterally: (i) thalamic radiation, (ii) optic radiation, (iii) fornix, (iv) fasciculus arcuatus, (v) inferior longitudinal fasciculus, and (vi) WM of the temporal and frontal lobe (Figure 3.1).

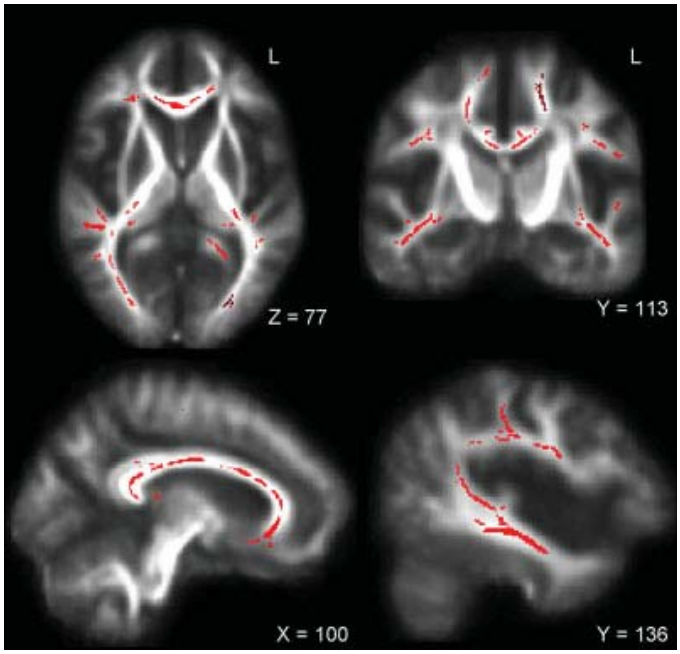

Figure 3.1 Results of the TBSS analysis: significant reduction in FA along the bilateral corticospinal tract, the bilateral optic radiation, the bilateral corona radiata, the corpus callosum, and the left arcuate fasciculus in patients when compared with controls, displayed on the mean FA map (*from Bodini et al., 2009*).

3.3.2 GM atrophy

The cortical regions which showed the most extensive and significant reduction in volume in patients compared with controls were the sensory motor cortex bilaterally, followed by the insula bilaterally, the GM around the left sylvian fissure, and the right superior temporal gyrus.

Patients also showed significantly reduced GM volume in the deep GM regions, including the bilateral thalamus and the left cerebellar hemisphere. Other regions with lower GM volume in patients included the left precuneus and the right angular and cingulate gyrus (Figure 3.2, Table 3.2).

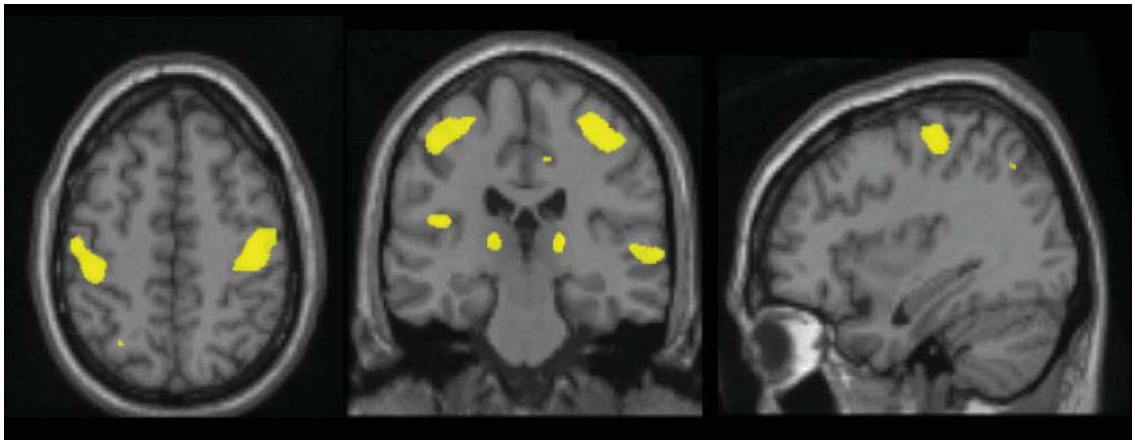

Figure 3.2 Results of SPM-VBM results: significant reduction in grey matter volume (yellow voxels) in the bilateral sensory-motor cortex, in the bilateral thalamus, in the right superior temporal gyrus, and in the left grey matter around sylvian fissure in patients when compared with controls, displayed on the Montreal Neurological Institute (MNI) template. (*from Bodini et al., 2009*).

Region	Side	MNI coordinates of local maxima			Number of voxels	Local maximum *t*-value
Sensory-motor cortex	L	−49	−18	56	2793	6.84
Sensory-motor cortex	R	42	−21	53	4196	6.62
Inferior frontal gyrus	L	−61	−6	31	184	5.58
Inferior frontal gyrus	R	55	−15	20	52	5.38
Middle frontal gyrus	R	43	−2	58	73	5.52
Superior temporal gyrus	R	67	−22	2	697	5.95
Middle temporal gyrus	L	−62	−4	−8	185	5.08
GM around sylvian fissure	L	−42	−23	17	858	6.30
Precuneus	L	−12	−69	44	101	5.47
Cerebellar hemisphere	L	−20	−80	−38	375	5.88
Angular gyrus	R	34	−63	45	74	5.54
Cingulate gyrus	R	15	−65	14	72	5.38
Thalamus	L	−18	−29	5	1599	6.30
Thalamus	R	−20	−28	5	1220	6.57
Insula	L	−36	5	1	726	6.53
Insula	R	33	9	0	61	5.28

Table 3.2 List of regions showing a lower GM volume in patients when compared with controls.

3.3.3 Anatomical correspondence between NAWM and GM abnormalities

Anatomical correspondence was observed between the reduced NAWM FA of the corticospinal tract and the GM atrophy in the sensory-motor cortex, bilaterally. Similarly, a topographic correspondence was found between reduced FA in the NAWM adjacent to (i) the left inferior frontal gyrus, (ii) the right superior temporal gyrus, (iii) the left middle temporal gyrus, (iv) the left GM around sylvian fissure, (v) the left precuneus, (vi) the right angular gyrus, (vii) both thalami, and (viii) the left insula, and the atrophy of the same GM regions (Figure 3.3 A,B).

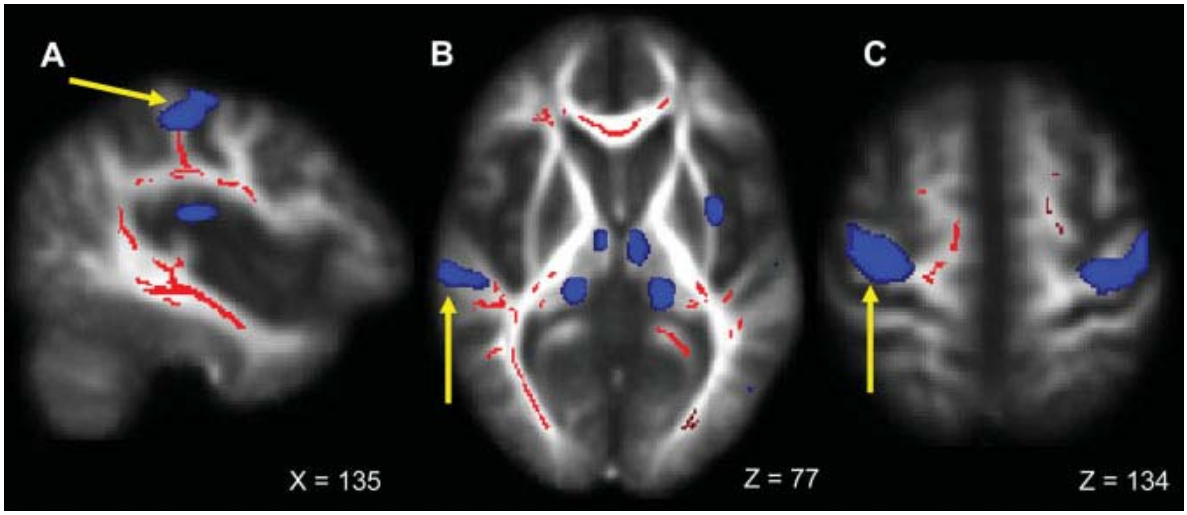

Figure 3.3 Examples of regions where anatomical (A and B) or anatomical and quantitative correlations (C) between NAWM damaged tracts (voxels in red) and GM atrophy (areas in blue) have been found in patients. This figure shows: In (A), the left corticospinal tract projecting onto the left sensory-motor cortex (see yellow arrow); in (B), the NAWM immediately adjacent to the GM of the right superior temporal lobe (see yellow arrow); and in (C), the right corticospinal tract and the connected sensory-motor cortex (see yellow arrow) *(from Bodini et al., 2009*).

3.3.4 Quantitative relationship between anatomically related NAWM and GM abnormalities

Out of the eleven regions showing anatomical correspondence between abnormal NAWM FA and GM volume, four areas showed also a quantitative relationship (Table 3.3):

(1) Reduced FA in the corticospinal tract correlated with greater GM atrophy in

the adjacent right sensory-motor cortex (Figure 3.3 C);
(2) Reduced FA of the thalamic radiations correlated with greater GM atrophy of both thalami (Figure 3.3 B);
(3) Reduced FA of the tracts immediately adjacent to the left insula correlated with greater GM atrophy of the insula (Table 3.3, Figure 3.3 B).

Region	FA, mean (SD)	Volume (ml), mean (SD)	r	p value
Right sensory-motor	0.48 (0.04)	4.52 (0.30)	0.53	0.001
Left thalamus	0.43 (0.04)	5.79 (0.59)	0.70	0.0001
Right thalamus	0.54 (0.03)	5.60 (0.53)	0.64	0.0001
Left insula	0.42 (0.04)	7.6 (0.21)	0.51	0.002

Table 3.3 Regions where grey matter atrophy was significantly correlated with FA reduction in the adjacent NAWM in patients.

3.3.5 Correlation between NAWM and GM abnormalities and disability

Either the NAWM FA or the GM volume of the four regions showing a quantitative relationship between NAWM and GM damage correlated with disability independently from the other, and from age and gender.

In particular, patients with greater GM atrophy in the right sensory-motor cortex had greater upper limb disability, as measured by zNHPT ($p = 0.01$, coeff. = 1.27, 95% confidence interval (CI) 0.26, 2.28), independently from the NAWM FA of the right corticospinal tract. The NAWM FA of the left and right thalamic radiations was lower in patients with greater cognitive impairment, as measured by zPASAT ($p = 0.0001$, coeff. = 0.001, 95% CI 0.001, 0.002 and $p = 0.0001$, coeff. = 0.002, 95% CI 0.001, 0.002, respectively), independently from the GM thalamic volume. We also found that the NAWM FA of the tracts adjacent to the left insula was associated with zPASAT ($p = 0.0001$, coeff. = 0.001, 95% CI 0.001, 0.002), independently from the insular GM volume.

No correlation was found between either NAWM or GM damage and the categorized EDSS.

3.4 Discussion

3.4.1 NAWM and GM abnormalities

In this study, tracts of reduced FA in the NAWM of patients with early PPMS were localised using TBSS (Smith et al., 2006). This was the first time that this technique was used to map FA changes in the NAWM of patients with PPMS when compared with controls and to investigate whether they related to the GM atrophy of connected regions, measured using a VBM approach. This study was particularly focused on the investigation of the NAWM, as a correlation between T2 lesion load and GM pathology had already been demonstrated in this form of disease (De Stefano et al., 2003; Ramio-Torrenta et al., 2006; Sepulcre et al., 2006; Roosendaal et al., 2011). Moreover, the diffuse NAWM abnormalities in PPMS are known to be only partially explained by axonal destruction in the plaques, followed by secondary Wallerian degeneration (Pelletier et al., 2003; Kutzelnigg et al., 2005).

In this study, patients with early PPMS showed reduced FA than controls in several NAWM tracts, in line with data obtained in patients with well established PPMS, with other forms of MS and in CIS (Cader et al., 2007; Roosendaal et al., 2009). Using VBM (Ashburner and Friston, 2000), extensive and focal areas of GM atrophy were detected early in the disease course of PPMS, confirming results obtained in RRMS (Morgen et al., 2006; Prinster et al., 2006) and in our larger cohort of PPMS patients (Khaleeli et al., 2007b).

3.4.2 Anatomical and quantitative relationship between NAWM damage and GM atrophy

When the topographic distribution of reduced NAWM FA and GM atrophy in patients was investigated, eleven regions of clear anatomical correspondence between the two compartments were identified. For example, there was a

reduced FA in the bilateral corticospinal tract and a reduced GM volume in both connecting sensory-motor cortices. Conversely, other abnormal WM tracts did not show any anatomical correspondence with areas of GM atrophy. Similarly, a number of regions of GM atrophy were not adjacent to any regions of reduced NAWM FA.

Interestingly, out of these eleven regions with visible anatomical correspondence, only four areas showed a significant quantitative correlation between GM atrophy and reduced NAWM FA in the connected tracts. These areas were the right sensory-motor cortex and the connected corticospinal tract, both thalami and the adjacent thalamic radiations, and the left insula and the adjacent WM. This suggests that in these regions there may be a link between the pathological processes occurring in the two compartments. For example, it is possible that the GM atrophy is secondary to degeneration of WM tracts resulting from transection of axons in inflammatory WM lesions (Trapp et al., 1998). Alternatively, the GM may be the primary target of the disease process, resulting in secondary axonal degeneration and demyelination in WM (the “inside out” model of MS) (Tsunoda and Fujinami, 2002; Geurts et al., 2009). Finally, a combination of the above mechanisms could also occur. In the next Chapter of this thesis, these hypotheses will be explored in further detail. The remaining seven regions, where a quantitative correlation was not found, suggest that the pathological processes occurring in the NAWM and in the GM could to some extent develop independently from each other (Geurts and Barkhof, 2008; Geurts et al., 2009; Geurts et al., 2012), at least in some areas of the brain and in the early stages of the disease.

It should be noted here, for clarity, that the term “anatomical correspondence” was used in this study to indicate areas which appear contiguous on visual inspection, while more sophisticated approaches, such as DT tractography, would be needed to confirm the connection between the identified NAWM and GM areas..Indeed, this technique was employed in the study presented in Chapter IV of this thesis, and confirmed the connection between the WM tracts of interest and their cortical targets.

From a methodological point of view, the quantitative approach applied in this study has proven valuable in providing additional information not available from a purely qualitative and anatomical analysis. For example, the finding that only a minority of anatomically associated areas showed a quantitative correlation between the MRI measures, may help explain the minimal or absent correlations between the damage affecting the two compartments reported in histological studies (Kutzelnigg et al., 2005; Bo et al., 2007).

This study, however, has a major limitation, as the analysis of the differences in NAWM FA and GM volume between patients and controls was performed using two different groups of controls, with differing mean age. Further investigations based on data from the same control group are warranted to confirm the reported findings. However, the age of the two control groups was not significantly different from each other ($p = 0.07$, using the two-sample t-test), and the difference in age between patients and the group of 23 controls was corrected for, at each stage of the analysis. Furthermore, the mapping of regions of reduced FA and increased atrophy is consistent with what has been reported in previous studies, as discussed above. Another methodological limitation of this study lies in the coregistration of DTI and FSPGR images, which have different slice thicknesses, within the same anatomical image, during post-processing procedures. These aspects, together with the smoothing of the images, which is needed in the VBM analysis to render the data normal for statistical purposes, may have influenced the reported results by compromising accurate localization of abnormal regions and subsequent identification of areas of anatomical correspondence.

3.4.3 Contribution of NAWM and GM abnormalities to disability

Interestingly, all four areas of visually identified and quantitatively confirmed correlation between NAWM damage and GM atrophy were clinically eloquent, and in each area an independent contribution from one of the two compartments to disability was observed. In particular, the GM atrophy in the right sensory-motor cortex correlated with the upper limb function, as measured by the NHPT, independently from the NAWM damage in the right corticospinal

tract. These findings indicate that, in this area, GM damage has a role in determining motor disability, which is greater than, and independent from, the injury of the connected corticospinal tract. This finding confirms the relationship between atrophy in the motor cortical areas and disability that was already documented in a previous study on this same cohort of early patients with PPMS (Khaleeli et al., 2007b).

In this study it was also found that reduced FA in the thalamic radiations and in the tracts adjacent to the left insula was independently associated with poor performance on the PASAT test in patients; this association was independent of the GM atrophy of the thalamus and insula, respectively. These data suggest an important contribution from these tracts to cognitive function, as the PASAT test is a complex working memory task involving several distinct brain areas that interact simultaneously. This is in line with other reports of a correlation between WM tract injury and PASAT score in patients with MS (Ozturk et al., 2010; Van Hecke et al., 2010; Yu et al., 2012).

The lack of correlation with EDSS, on the other hand, could be explained by the limitations of this scale (Hobart et al., 2000). However, it is important to take into account that NAWM and GM damage in the brain are not the only contributors to clinical disability in PPMS. WM lesions, GM lesions, and spinal cord atrophy (which were not included in this investigation) are also known to significantly contribute to clinical disability in this form of disease (Rocca et al., 2012a), and the interpretation of the presented results shall not disregard these important aspects of MS pathology.

3.5 Conclusions

In conclusion, this study has demonstrated that NAWM damage and GM atrophy in early PPMS are strictly interdependent in specific, clinically relevant brain regions. This suggests that that there may be a link between the mechanisms of damage occurring in the two compartments in these areas in the early phase of progression, and it is noteworthy that damage in these regions was associated with disability. However, another possible interpretation

of our results is that the pathological processes affecting the two compartments develop independently of each other (as suggested by the evidence in the presented data of NAWM regions where a significant difference between patients and controls was found, which was not paralleled by significant changes affecting the connected GM areas, and viceversa) reaching a similar (correlated) degree of damage in few, specific areas of the brain.

In the next Chapter, the spatial and temporal characteristics of the changes occurring in the NAWM tracts and in the connected GM areas will be explored, in order to establish whether there is a directionality in the pathological changes affecting these two compartments over time in the same cohort of patients with early PPMS.

Exploring the temporal relationship between white and grey matter pathology in early PPMS

Chapter IV

Moving from the data presented in Chapter III on the cross-sectional spatial relationship between WM and GM damage in early PPMS, in this Chapter I aim to complete the answer to the first question of this thesis, describing the temporal relationship between the pathological changes occurring in the WM tracts and those occurring in the connected cortical areas. My aim was to establish the temporal sequence and the directionality of the pathological processes affecting the two compartments, in our cohort of patients with early PPMS followed-up for two years. In particular, the two following hypotheses on the pathogenesis of the early phase of PPMS were tested: (i) the damage in the WM tracts, as reflected by MTR, precedes that occurring in the connected GM areas ("primary WM damage model"); (ii) pathological changes, as reflected by MTR, originate in the cortex, and subsequently spread to the connected WM tract ("primary GM damage model").

4.1 Introduction:

As discussed in the first Chapter of this thesis, the pathological changes affecting both the white (WM) and the grey matter (GM) are known to contribute to the complex pathogenesis of primary-progressive multiple sclerosis (PPMS), from the early stage of the disease (Antel et al., 2012; Rocca et al., 2012a). Post-mortem studies, and in-vivo investigations using different quantitative magnetic resonance imaging (MRI) techniques, have contributed to the characterization of the damage occurring within focal lesions in both WM and GM, and to the description of the pathological changes affecting normal-appearing brain tissues (Filippi et al., 2012).

The study presented in Chapter III has shown that, at least in some clinically relevant brain areas, the pathological processes affecting the WM tracts and their anatomically adjacent GM regions were interdependent, suggesting a relationship between the mechanisms of damage occurring in the two compartments in the early phase of clinical progression (Bodini et al., 2009). However, the temporal relationship (i.e. the directionality) linking the damage occurring in the WM tracts to that affecting the connected cortical areas, remains unknown. There are two alternative hypotheses that can describe the

pathogenic processes leading to WM and GM changes in progressive MS (Geurts et al., 2009): the first hypothesis (which I will refer to as "primary WM damage model" herein after) is that the cortical changes are secondary to continuing damage in the connected WM tracts (both focal and in the NAWM), where the pathology would originate, through anterograde (Wallerian) or retrograde degeneration (Bjartmar and Trapp, 2001), or as a result of both. In contrast, the second hypothesis (the "primary GM damage model"), postulates that the GM damage could represent an important and initial target of the disease, which would subsequently spread to the connected WM tract, resulting in a "whole brain" pathology (Geurts et al., 2009). Obviously, both models may coexist, but this would represent a third hypothesis that was not tested in this study.

In order to assess the validity of these two models in describing the pathogenesis of PPMS in its early phase, it is necessary to follow-up structural changes as detected by MRI over time, from completely intact WM and GM areas to damaged regions (Filippi et al., 2012). This has been explored in this study, using tissue-specific MTR as a measure of microstructural tissue damage (Schmierer et al., 2004; Moll et al., 2011), along with tissue-specific volumetric measures, in our cohort of patients with early PPMS, which was compared with a group of healthy controls followed-up for two years. In keeping with the aim to test both the "primary WM damage" and the "primary GM damage" models in-vivo, we sampled three "tract-cortex pairs" of anatomically connected WM-GM regions, each one consisting of a WM tract and its associated GM cortical target, at baseline and after two years. The WM (or tract) component of each tract-cortex pair is composed of both NAWM tissue and tract-specific WM lesions, which have been investigated separately from each other.

4.2 Methods:

4.2.1 Subjects

Forty-seven patients with a diagnosis of PPMS according to Thompson's criteria (Thompson et al., 2000) within five years of symptom onset underwent a

clinical and imaging protocol at study entry, and after 24 months, which was approved by the Joint Medical Ethics Committee of the National Hospital for Neurology and Neurosurgery and the Institute of Neurology, London (see Appendix I). At each time point, patients were assessed and scored with the Expanded Disability Status Scale (Kurtzke, 1983) (see Table 4.1 for the patients' clinical, demographic and radiological characteristics at study entry), and then performed the MRI protocol described below.

Since this was a retrospective analysis performed on previously acquired data, MTR and DTI images were not available in the same group of healthy controls. Therefore, MTR data were available for 18 healthy subjects (Group A), and DTI data were found to be available for 23 healthy controls (Group B) (see Table 4.1 for their demographic characteristics).

Characteristics	Patients	HC Group A	HC Group B
Number	47	18	23
Age, years (mean (SD))	43.9 (11.2)	35.2 (6.02)	35.1 (7.9)
Gender, female/male	18/29	11/7	12/11
Disease duration, years (mean (SD))	3.4 (0.9)	-	-
EDSS, median (range)	4.5 (1.5-7)	-	-
T2 lesion load, ml (mean (SD))	15.4 (17.3)	-	-
Spinal cord area, mm^3 (mean (SD))	70.3 (9.4)	-	-

Table 4.1 Demographic and radiological characteristics of patients and healthy controls (HC) at study entry.

4.2.2 Image Acquisition

The imaging protocol was performed using a 1.5-T GE Signa scanner (General Electric, Milwaukee, IL), with maximum gradient strength of 22 mT m^{-1}. Images were displayed on a Sun workstation (Sun Microsystem, Mountain View, CA) for

analysis.

4.2.2.1 *Brain imaging*

At baseline and after two years, all subjects had a three-dimensional inversion-prepared fast spoiled gradient recall (3D FSPGR) T1-weighted (T1-w) sequence of the brain [field of view (FOV) 300 x 225mm^2, matrix size 256 x 160 (reconstructed to 256 x 256 for a final in plane resolution of 1.17 mm), repetition time (TR) 13.3 ms, echo time (TE) 4.2 ms, inversion time 450 ms, 124 contiguous axial slices, slice thickness of 1.5 mm].

At both time-points, all patients and the Group A of healthy controls underwent:
(i) a fast spin echo scan that collects proton-density-weighted and T2-weighted (T2-w) images (TR 2000 ms ; TE 17/92 ms ; matrix size 256 x 256; FOV 240 x 180 mm^2 ; 28 contiguous axial slices of 5 mm thickness);
(ii) magnetisation transfer (MT) dual echo interleaved spin-echo sequence (28 contiguous axial slices, TR 1720 ms, TE 30/80 ms, number of excitations 0.75, acquired matrix 256×128, reconstructed matrix 256×256, FOV 240×240 mm), including PD and T2-weighted images, acquired with and without a MT presaturation pulse to calculate the MT ratio (MTR) images from the short echo data. A Hamming-apodised three-lobe sinc MT pulse (duration 16 ms, peak amplitude 23.2 μT, bandwidth 250 Hz, 1 kHz off-water resonance) was employed.

At baseline, the healthy controls of Group B underwent a whole-brain, cardiac-gated, spin echo diffusion-weighted (DW) echo planar imaging sequence [FOV 240x240mm², matrix size 96x96 (reconstructed to 128x128), image resolution 2.5x2.5x3mm (reconstructed to 1.9x1.9x3mm), TE 95ms, TR 7RRs, maximum b-factor 1000 smm^{-2}; three series, each collecting 14 axial slices of 3mm thickness, which were interleaved off-line; diffusion gradients were applied along 25 optimised directions, and three images with no diffusion weighting were also acquired, which was used to generate a DTI template in standard space.

4.2.2.2 *Spinal cord imaging*

In patients, volumetric images of the spinal cord were also acquired, using a standard phased array spinal coil. In particular, a volume acquired inversion prepared fast spoiled gradient echo was performed (60 1 mm “partitions”, TI 450 ms, TE 4.2 ms, TR 15.6 ms, flip angle 20°, FOV 24x24 cm, matrix 246x256). Five contiguous 3 mm axial slices from the caudal landmark of the C2/3 intervertebral disc were reformatted from the volume data set and a coil radiofrequency uniformity correction was applied.

4.2.3 Image analysis

4.2.3.1 *White matter lesions*

In patients, white matter lesions (WML) were delineated with a semi-automated contour thresholding technique (Plummer, 1992) by a single rater on the PD images. The co-registered T2-w images were always used as a reference to increase confidence in lesion identification. Lesion masks were obtained by setting the signal intensity equal to 1 for all voxels within a lesion and zero outside lesions. The same procedure was performed on the baseline and the follow-up scans.

4.2.3.2 *Generation of the DTI template, reconstruction of tracts and tract extension in standard space*

After correction for eddy current distortions using a software tool (eddy_correct) provided by FSL (www.fmrib.ox.ac.uk/fsl/), the DW images from the healthy controls of Group B were used to generate a high-resolution diffusion tensor (DT) dataset (voxel size=1×1×1 mm^3), constructed by averaging the DT data into the EPI equivalent of the MNI standard space (Mazziotta et al., 2001).

To briefly summarise the procedure, each subject’s fractional anisotropy (FA) map was nonlinearly registered to the FA map in standard space provided by the FSL library, using the flirt/fnirt functions (Woolrich et al., 2009). The transformations were applied to the individual tensor components using the preservation of principal direction algorithm (Alexander et al., 2001), which were then averaged (using the mean) and diagonalised to give the mean DT in

standard space.

The probabilistic tractography algorithm, called PICo (probabilistic index of connectivity) provided by the Camino toolkit (www.camino.org) (Parker et al., 2003) was used to reconstruct five tracts, as described below, on the high-resolution DTI dataset. 5000 iterations of the FACT algorithm were used. No interpolation and no FA thresholds were included to constrain the outcome of the tractography, while a curvature threshold was used, such that each run of the tractography stops if there is a curvature of more than 80° between adjacent voxels; connectivity maps were thresholded to a connectivity value of 0.02 (Toosy et al., 2004). Seed regions and exclusion masks, used to constrain the tracts to anatomically plausible regions of the brain, were defined to reconstruct the following tracts:

(i) The left and right cortico-spinal tracts (CST) were obtained by placing seed regions (size= 60 voxels) in the posterior limb of the internal capsule. The exclusion mask sheets divided the images in the sagittal plane through the interhemispheric fissure, and axially at the level of the interior margin of the genu of the corpus callosum (Figure 4.1, voxels in light blue-blue).
ii) The genu of the corpus callosum (GCC) was generated using a seed mask (size= 64 voxels) in the genu of the corpus callosum. The exclusion mask sheets divided the brain in the coronal plane immediately posterior to the genu of the CC, in the axial plane immediately inferior to the genu of the CC, and in the sagittal plane starting anteriorly to the genu of the CC (Figure 4.1, voxels in green).
iii) The optic radiations (OR) were generated using a seed mask (size= 52 voxels) in the region posterior and lateral to the lateral geniculate nucleus (LGN). The exclusion mask contained four planar sheets, a complete mid sagittal sheet dividing the two hemispheres, a complete coronal sheet anterior the LGN, an axial sheet touching the inferior margin of the occipital lobes and extending anteriorly to the level of the splenium of the CC, and another axial sheet starting in the splenium of the CC and extending posteriorly (Figure 4.1, voxels in pink).

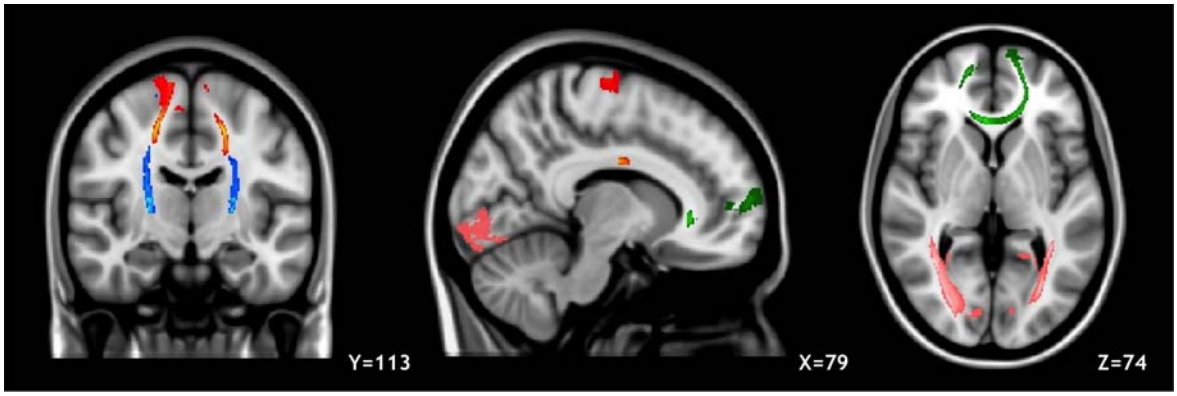

Figure 4.1 Reconstructed tracts and corresponding cortical targets in standard space, overlayed onto the MNI T1-w template: CST (voxels in light blue-blue) and precentral/postcentral cortex (voxels in red); GCC (voxels in light green-green) and frontal cortex (voxels in green); OR (voxels in light pink-pink) and occipital cortex (voxels in pink).

To define each tract's anatomically connected cortical region (the "cortical target"), each point on the tract boundary, which is either within or abutting the GM, was extended geometrically to the corresponding outer boundary of the cortex following a straight line, employing the novel « tract-extension» approach described in Chapter II (Tozer et al., 2012), (see Chapter section 2.5.2.4 and Figure 2.15). Each tract (CST, GC, OR) went through the tract-extension procedure in standard space using tissue templates derived from the segmentation of the MNI template using SPM8 (www.fil.ion.ucl.ac.uk/spm) and the maximum likelihood algorithm to assign each voxel to a tissue type.

After these steps, we obtained three "tract-cortex (T-C) pairs" of anatomically connected WM-GM regions, each one consisting of a WM tract and its associated GM cortical target: (i) right and left motor pair (CST and connected GM in the pre- and post-central cortex); (ii) callosal pair (genu of the CC and its connected GM region in the frontal lobe); and (iii) right and left optic pair (OR and its connected GM area in the occipital cortex).

4.2.3.3 MTR map calculation and transformation of extended tracts into native space

In all patients and in the Group A of healthy controls, at each time point, the MTR map was calculated in the subject-specific space (native space) on a voxel-by-voxel basis from the short echo data from the MTR sequence according to the standard equation (Grossman et al., 1994).

At each time point, each extended tract reconstructed in standard space was transformed into native space, using algorithms from the FSL software package (http://www.fmrib.ox.ac.uk/fsl/), as follows:

i) The individual (and native) short echo non-MT weighted data was registered to the native T1-w image using a linear transformation algorithm (FLIRT) from the FSL library;

ii) The native T1-w images were registered to the T1-weighted MNI template provided by the FSL software library, using a non-linear registration algorithm (FNIRT);

iii) The two registration steps (i and ii) were combined and then the transformation from standard space to native space (MNI2map) was calculated;

iv) The MNI2map transformation parameters were applied to the extended tracts in order to transform them into native space.

4.2.3.4 *Segmentation of extended tracts in native space and extraction of WM and GM MTR values*

In order to segment the WM tracts from the corresponding cortical targets in native space, we followed the steps below:

(i) The native T1-w scans were registered to native MTR map space (which will be referred to as “MTR map space” herein after) by applying the inverse transformation of the FLIRT registration described in the previous section. We maintained a high resolution (e.g., 1×1×1 mm3) for the T1-w registered images in order to reach a better segmentation, rather than matching the MTR map resolution (e.g. 0.97×0.97×5 mm3) at this step.

ii) The T1-w scans in MTR map space, obtained in (i), were then segmented into WM, GM and CSF probability maps using SPM8 (www.fil.ion.ucl.ac.uk/spm/).

iii) The WM and GM probability maps, obtained in (ii), were then down-sampled to match the resolution of the MTR map space, which was 0.97×0.97×5 mm3.
iv) Tissue segments were then produced from the down-sampled probability maps by applying the maximum likelihood algorithm.
v) The WM and GM maps obtained in step (iv) were then used to mask the extended tracts in native MTR map space, resulting in WM and GM segments of each tract-cortex pair for each subject and at each time point (Figure 4.2).

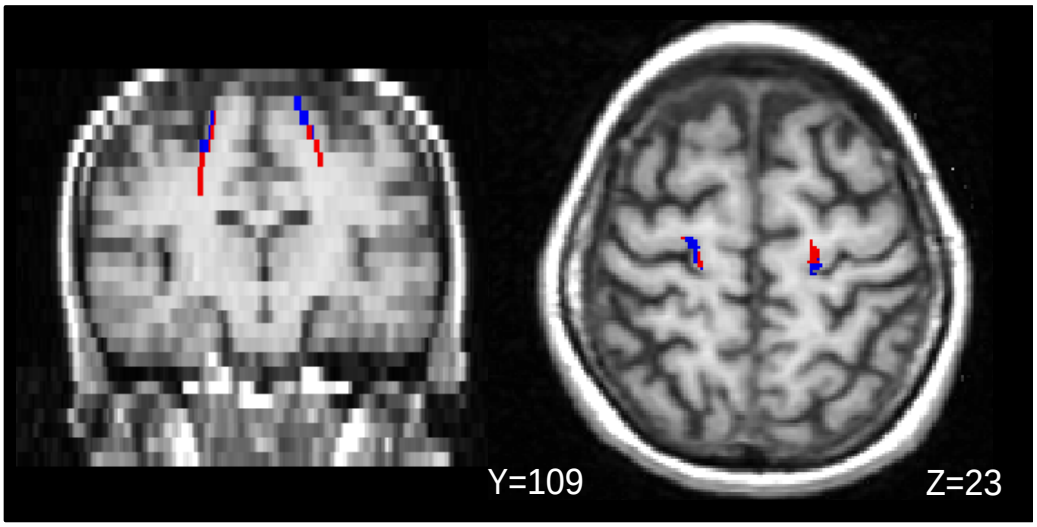

Figure 4.2 Left and right CST (voxels in red), and associated voxels in the precentral/postcentral cortex (voxels in blue) in a single patient, overlayed onto the patient's T1-w image in native space.

In patients, and for each tract, the WM lesion masks were used to mask the WM tracts, to obtain a mask for normal-appearing white matter (NAWM) and a tract-specific lesional tissue mask. The tract-specific lesion load was calculated in all tracts at each time-point.

At each time-point, the WM and GM segments of each T-C pair were then used as region-of-interests (ROIs) and applied to the MTR map to calculate:
(i) in patients, the mean MTR values of the tract NAWM, of the tract-specific lesional tissue, and of the connected cortex;
(ii) in controls, the mean MTR values of both the WM and GM. The mean MTR

values of the whole WM and of the whole GM were also calculated.
The maps of WM tracts and of connected GM areas were then used to calculate the corresponding tissue volume, by multiplying the number of non-zero voxels by the voxel volume.

4.2.3.5 *Cord cross-sectional area*

In patients, cord cross-sectional area at the C2-3 level was calculated using a semi-automated technique previously described by Losseff and colleagues (Losseff et al., 1996). This level was selected as it offers several anatomical advantages for measuring cord cross-sectional area, with high cord-to-cerebrospinal fluid contrast, limited inter-subject variability in cord cross-sectional area at this level and a low probability of disc protrusions.

4.2.4 Statistics

Statistical analysis was carried out using Stata 12.1 statistical software (Stata Corporation, College Station, Texas, USA). Results with p value < 0.05 were considered statistically significant.

4.2.4.1 *Comparison of WM and GM MTR between patients and controls*

Cross sectional differences in mean MTR between patients and controls at the two time points were obtained using a multivariate regression, which is based on four simultaneous regressions for each pair (i.e. NAWM MTR regressed against GM MTR and viceversa, for the two time-points), using subject group, age and gender as common covariates. This was performed using the Structural Equation Modelling (SEM) command in Stata, using the Maximum Likelihood for Missing Values (MLMV) estimation method. An advantage of this method is that correlations between the variables are taken into account to smooth out the effect of different missing values at different time points in different variables; this yields estimates which are less prone to bias than the separate regressions under the assumption a) that regression residuals are multivariate normal; and b) that the missing values are either Missing Completely At Random (MCAR) or Missing at Random (MAR) (Schott and

Bartlett, 2012): briefly this assumption is that values are missing either completely randomly or in a way that is dependent only on observed values.

4.2.4.2 *Evolution of NAWM, WML and GM values over time in patients*

To assess the evolution of NAWM, WML and GM values over the follow-up period in patients, changes in mean MTR of tract NAWM, of WM lesions and of connected GM cortex from baseline to 24 months were estimated using a single multivariate regression for each tract-cortex pair (this is equivalent to simultaneously performing the three paired t-tests, for NAWM MTR, WM lesions MTR and GM MTR, for each tract-cortex pair).

4.2.4.3 *Cross-sectional relationship between NAWM and GM values at each time-point*

In patients, at each time point a multivariate regression was performed over the five tract-cortex pairs (corresponding to five simultaneous regressions at a time point); each regression was between that tract-cortex pair's NAWM mean MTR and the corresponding GM target's mean MTR, giving standardised regression coefficients and p-values to assess each association. To investigate whether any tract-cortex pair specific baseline GM vs WM MTR associations were explained by age, gender, disease duration, whole WM or GM mean MTR, NAWM or GM volumes, lesion MTR or volume, or spinal cord area, these variables were entered in turn as covariates into the regressions.

4.2.4.4 *Temporal relationship between tract-specific NAWM and GM values: the "primary WM damage" and the "primary GM damage" model*

(i) Primary WM damage model: In order to investigate whether, in each pair, the baseline NAWM MTR predicted the GM MTR at 24 months, *independently of baseline GM MTR* (as the GM MTR at 24 months is expected to significantly correlate with the GM MTR at baseline), a multivariate regression was performed over the five tract-cortex pairs using for each pair the NAWM MTR at baseline as independent variable and GM MTR at 24 months as dependent variable; the multivariate regression was then repeated adjusting for GM MTR at baseline.

(ii) Primary GM damage model: Similarly, in order to investigate whether, in each pair, the baseline GM MTR predicted the NAWM MTR at 24 months, *independently of baseline NAWM MTR* (as the NAWM MTR at 24 months is expected to significantly correlate with the NAWM MTR at baseline), a multivariate regression was performed over the five tract-cortex pairs using for each tract-cortex pair the GM MTR at baseline as independent variable and NAWM MTR at 24 months as dependent variable; the multivariate regression was then repeated adjusting for NAWM MTR at baseline.

To examine whether other potential confounders (age, gender, disease duration, whole WM or GM mean MTR, NAWM or GM volumes, tract-specific lesion MTR or volume, or spinal cord area) explained the two models, these variables were added singly as covariates in the models.

4.2.4.5 *The role of lesions: post-hoc analysis on the correlation between baseline lesion MTR and later NAWM and GM MTR*

To assess in further detail the role of early lesions in contributing to later NAWM and GM damage, in addition to examining whether baseline tract-specific lesion MTR explained the “primary WM damage” or the “primary GM damage” model, as described above, multivariate regressions were performed over the tract-cortex pairs, using WML MTR at baseline as independent variable and the tract-specific NAWM and corresponding GM area’s MTR at 24 months as dependent variables.

4.3 Results:

The mean MTR in NAWM, GM, and lesions in patients, and the mean MTR in WM and GM in healthy controls (Group A) are reported for each tract-cortex pair at the two time points in Table 4.2.

	Left motor pair mean MTR				Right motor pair mean MTR				Callosal pair mean MTR				Left optic pair mean MTR				Right optic pair mean MTR			
month	patients		controls		patients		controls		patients		controls		patients		controls		patients		controls	
	GM	NAWM	GM	WM	GM	NAWM	GM	WM	GM	NAWM	GM	WM	GM	NAWM	GM	WM	GM	NAWM	GM	WM
M 0	3513	3622	3568	3719	3392	3612	3534	3698	3242	3807	3364	3953	3122	3407	3263	3550	3221	3438	3364	3612
M 24	3443	3633	3509	3708	3347	3625	3512	3717	3234	3849	3361	3937	3120	3424	3259	3509	3236	3456	3359	3619

Table 4.2 Each tract-cortex pair's mean MTR in NAWM and GM in patients, and in WM and GM in healthy controls, at baseline and year 2.

4.3.1 Comparison of WM and GM MTR between patients and controls

At baseline, there was a significantly reduced mean MTR in patients compared with controls in the NAWM of the CST, bilaterally (p=0.001 in the left CST, p=0.002 in the right CST), while there was no significant difference between patients and controls in the GM of the corresponding motor areas. At baseline, in the callosal pair and in the optic pair, bilaterally, there was a significant reduction in both NAWM and corresponding GM mean MTR in patients compared with controls (except in the NAWM of the left OR, where the difference between patients and controls was only borderline significant) (Table 4.3). At year 2, there was a significant reduction in MTR in patients compared with controls in the NAWM and in the GM of all the tract-cortex pairs except in the motor area on the left side, and in the NAWM of the OR on the left side (Table 4.3).

	T-C pair 1 left		T-C pair 1 right		T-C pair 2		T-C pair 3 left		T-C pair 3 right	
	patients – controls mean diff, p-value		patients – controls mean diff (p-value)		patients – controls mean diff (p-value)		patients – controls mean diff (p-value)		patients – controls mean diff (p-value)	
	GM	NAWM	GM	NAWM	GM	NAWM	GM	NAWM	GM	NAWM
M 0	-52 P=0.444	-128 P=0.001	-76 P=0.289	-105 P=0.002	-116 P=0.002	-193 P<0.001	-137 P=0.004	-105 P=0.053	-144 P<0.001	-168 P=0.001
M 24	-164 P=0.140	-128 P=0.001	-211 P=0.044	-154 P<0.001	-127 P=0.004	-151 P<0.001	-195 P<0.001	-97 P=0.142	-167 P<0.001	-164 P=0.004

Table 4.3 Comparison of mean MTR between patients and healthy controls (mean difference and p-value) adjusted for age and gender, at baseline and year 2.

4.3.2 Evolution of NAWM, WML and GM damage over time in patients

In both CSTs, there was no suggestion of progressive change in NAWM MTR over the follow-up period (Table 4.4), while in the corresponding motor areas, a progressive reduction of GM mean MTR was found, though this was not statistically significant. In the callosal pair, there was no suggestion of progressive damage in the NAWM of the GCC nor in the corresponding frontal GM mean MTR over two years (Table 4.4). In the optic pair, there was no evidence for a significant progressive change in the mean MTR of NAWM in the bilateral OR over two years.

On the other hand, while the right occipital cortex showed no suggestion of progressive change in mean MTR over two years, we found a progressive and significant reduction in mean MTR in the left occipital cortex over two years (p=0.017, Table 4.4).

	Left motor pair			Right motor pair			Callosal pair			Left optic pair			Right optic pair		
	GM	**WM**	**lesions**	**GM**	**WM**	**lesions**	**GM**	**WM**	**lesions**	**GM**	**WM**	**lesions**	**GM**	**WM**	**lesions**
M0 to M24	-63.6	-4.2	-45.9	-45.4	-4.3	-77.2 P=0.084	-19.3	-16.3	15.7	-42.8 P=0.017	-20.7	-15.6	-31.5	-4.6	-38.1

Table 4.4 Mean MTR change in the NAWM and GM of all the tract-cortex pairs over the follow-up (p value indicated where mean MTR change was significantly different between baseline and month 24).

4.3.3 Cross-sectional relationship between NAWM and GM damage at each time-point

At baseline, there was a significant correlation between the mean MTR of each tract's NAWM and the mean MTR of the corresponding GM target, in the left motor pair (p=0.023), in the callosal pair (p=0.002), and in the optic pair, both on the left (p=0.001) and on the right (p=0.001), where the resulting association was the strongest. On the other hand, at baseline the mean NAWM MTR of the right CST was not significantly associated with the mean MTR of the corresponding motor cortex (p=0.288). In the callosal and in the optic pairs, when included in the model, neither age, gender, disease duration, baseline lesion MTR and volume, baseline spinal cord area, global WM and GM MTR, NAWM or GM volumes, affected the reported baseline associations. However, when including the global WM in the model in the left motor pair, the association between the mean NAWM MTR of the left CST and the mean MTR of the left motor cortex lost significance (p=0.358) while, when including baseline spinal cord area in the model in the right motor pair, the association between the mean NAWM MTR of the right CST and the mean MTR of the right motor cortex, showed a trend towards a statistical significance (p=0.086).

At year 2, there was a significant association between the mean MTR of each tract and the mean MTR of the corresponding GM region in all tract-cortex pairs, except for the left motor pair, where the correlation between the mean MTR in the CST NAWM and the mean MTR in the motor cortex did not reach statistical significance independently of baseline whole WM MTR.

4.3.4 Temporal relationship between tract-specific NAWM and GM damage

4.3.4.1 *"Primary WM damage" model*

In the motor pair and in the optic pair bilaterally, the baseline mean MTR of each tract's NAWM was a significant predictor of the corresponding GM area's mean MTR at year 2 (Table 4.5). The association between NAWM mean MTR at baseline and GM mean MTR at year 2, was not significant in the callosal pair (p=0.274). When repeating the significant regressions including the baseline GM region's mean MTR in the model, all the abovementioned regressions remained significant apart from the left optic pair where the association lost significance.

	Left motor pair	Right motor pair	Callosal pair	Left optic pair	Right optic pair
NAWM0	0.320, P=0.034	0.444, P=0.004	0.612, P=0.274	0.112, P=0.290	0.231, P=0.022

Table 4.5 Standardised regression coefficients and p-values for each tract-cortex pair's "primary WM model" regression, adjusted for baseline GM area's MTR (i.e. baseline NAWM mean MTR as independent variable, and corresponding GM area's mean MTR as dependent variable, adjusted for baseline GM area's MTR).

When age, gender, disease duration, baseline NAWM and GM volumes, baseline lesion MTR and volume, and baseline spinal cord area, were included in the model, in all tract-cortex pairs the "primary WM damage model" regressions remained significant. When correcting for baseline whole WM and GM mean MTR, in all tract-cortex pairs the "primary WM damage model" regressions remained significant, except in the optic pair, bilaterally, where the "primary WM damage model" regression lost significance (p=0.322 on the right, p=0.19 on the left).

4.3.4.2 *"Primary GM damage" model*

In the motor pair bilaterally, the baseline mean MTR of the motor cortex was not a significant predictor of the CST's NAWM mean MTR at year 2. On the other hand, in the callosal pair and frontal cortex, the mean MTR at baseline

significantly predicted the GCC's NAWM mean MTR at year 2. In the right optic pair, bilaterally, the baseline mean MTR of the occipital cortex significantly predicted the mean MTR of the OR's NAWM at year 2 (Table 4.6). When repeating the significant regressions including the baseline NAWM tract's mean MTR in the model, the regression in the callosal pair and in the left optic pair lost significance (p=0.107 and p=0.119, respectively), while that in right optic pair became borderline significant (p=0.045). When adjusting for spinal cord, all the regressions lost statistical significance.

	Left motor pair	Right motor pair	Callosal pair	Left optic pair	Right optic pair
GM0	0.001, P=0.992	0.062, P=0.260	0.563, P<0.001 0.178, P=0.158	0.216, P=0.099 0.114, P=0.127	0.425, P=0.001 0.206, P=0.045

Table 4.6 Standardised correlation coefficient and p-values for each tract-cortex pair's "primary GM model" regression, adjusted for NAWM MTR at baseline (i.e. baseline GM region mean MTR as independent variable, and corresponding NAWM tract's mean MTR as dependent variable, *adjusted for baseline tract's NAWM MTR*).

4.3.4.3 *Comparison between the "primary WM damage" and the "primary GM damage" model*

The direct comparison of coefficients between the "primary WM model" and the "primary GM damage model" reached the statistical significance in the motor pair on both sides (p=0.03 on the left, p=0.007 on the right). The direct comparison of coefficients between the "primary WM" and the "primary GM damage model" in the callosal pair and in the right optic pair (in which both models resulted significant), did not provide significant evidence of a difference (p=0.201 in the callosal pair, and p=0.422 in the right optic pair). However, in terms of the size of the standardised regression coefficients, and the p-values, the "primary GM damage model" regression appeared to be weaker than the corresponding "primary WM damage model" regression.

4.3.4.4 *The role of lesions: correlation between baseline lesion MTR and later WM and GM MTR*

In the left motor cortex, a higher baseline WML volume showed a trend towards a significant correlation with a lower MTR in the NAWM at 24 months (r=- 0.316,

p=0.081). In the right motor cortex, both baseline lesion MTR and volume were significantly associated with NAWM MTR of the CST at 24 months (r=0.522, p=0.046 and r=-0.808, p<0.001, respectively). In the callosal pair, only baseline WML MTR was significantly associated with NAWM MTR of the GCC at 24 months (r=0.97, p<0.001). In the optic pair bilaterally, there was no significant association between lesion MTR or volume at baseline, and NAWM MTR at 24 months. Finally, in all tract-cortex pairs, no significant association was found between tract-specific lesion metrics at baseline, and the corresponding cortical area's GM MTR at 24 months.

4.4 Discussion

In this study on the pathological mechanisms underlying the early phase of PPMS, the early microstructural damage in the NAWM of the bilateral pyramidal tract (where pathological changes were already present at baseline, in contrast to the motor cortices, which resulted relatively spared at study entry), was found to precede and significantly predict the pathological changes later affecting the connected motor cortex bilaterally. This was independent of focal lesion load and spinal cord area. In addition, data from the other two tract-cortex pairs of WM tracts and their anatomically connected GM areas, were also compatible with the same temporal relationship. Overall, these preliminary data suggest that cortical pathology in the early phase of clinical progression, rather than reflecting a primary target of the disease, may originate from ongoing damage in the connected WM tracts, as described by the "primary WM model" hypothesis.

At study entry, there was a significant decrease in MTR in patients compared with healthy controls, reflecting microstructural damage consisting of demyelination and axonal loss (Schmierer et al., 2004) in the NAWM of all tracts and in the correspondent GM targets (with the exception of the motor cortex bilaterally). This finding is in agreement with previous studies on this same cohort, which showed structural damage affecting both WM and GM from the early stage of the disease (Sepulcre et al., 2006; Ramio-Torrenta et al., 2006; Khaleeli et al., 2007b; Bodini et al., 2009). On the other hand, the patients'

motor cortex on both sides, which was showed to be atrophic in previous studies on this same cohort (Khaleeli et al., 2007b; Bodini et al., 2009) did not present any significant MTR reduction in our analysis, when compared with healthy controls. A possible explanation for this may lie in the novel approach we used in this study to identify the specific cortical target of the motor tracts (consisting in the geometrical extension of each point of the tract boundary into the GM) (Tozer et al., 2012), which defined specific regions within the motor areas, not entirely overlapping with those analysed and discussed in previous reports from this same cohort. In addition, previous studies only focused on a subgroup of the same cohort, whilst here we included all 37 patients who participated in the study.

Looking at the tissue-specific evolution of NAWM and GM damage over time, there was no evidence for a significant progressive MTR reduction in the NAWM of all tracts, whilst a significant reduction in MTR over time was demonstrated in all cortical targets (with the exception of the right occipital cortex). Our data could reflect the temporal sequence of the pathological damage described by the “primary WM model” hypothesis, with the disease initially affecting the WM tracts, and then spreading progressively over time to the connected GM regions (Geurts et al., 2009). Interestingly, the notion that GM atrophy proceeds relentlessly over the course of the disease, has already been reported in all subtypes of MS, including PPMS (De Stefano et al., 2010).

When the cross-sectional relationship between NAWM and GM damage at each time-point was investigated, a significant correlation between the damage occurring in the two compartments, which was independent of all the confounding variables (including baseline lesion load and spinal cord area), was found in all tract-cortex pairs. These data are in agreement with what was previously reported in this same cohort in Chapter III (Bodini et al., 2009), and support the notion that the pathological processes affecting the two compartments are strictly interconnected, at least in some clinically relevant brain areas and at specific stages of the disease. Interestingly, the findings here reported suggest that there is a continuing damage between the NAWM and the GM, which evolves, at least to some extent, independently of the changes

secondary to WM lesions and spinal cord damage. A possible interpretation of this result could be that pathological processes primarily affecting the NAWM tracts (i.e. not resulting from focal lesion/ spinal cord damage), have the potential to spread along the axons back to the neuronal soma, resulting in secondary effects within the cortex (Filippi et al., 2012). On the other hand, in the motor pair, at both time-points, the association between the damage affecting the NAWM in the CST and that occurring in the corresponding motor cortex was weaker (i.e. either it was non significant, or was significantly influenced by other covariates). These data suggest that in the motor pair, at the time of the study, the disease had not yet spread to the two compartments, and had not reached in both the same degree of extent and severity; as a result, the analysis of the damage affecting this specific tract-cortex pair, gave us the unique opportunity to follow-up directly the temporal sequence of the pathological processes affecting the two compartments, as they were first appearing, and then developing over time.

When we explored the temporal relationship between the damage in the tract-specific NAWM and the abnormalities in the connected GM areas, we found that overall, the “primary WM damage model” described more accurately than the “primary GM model” the temporal evolution of the pathological processes in our cohort of patients with early PPMS. Indeed, in all tract-cortex pairs (except the callosal pair and the left optic pair), the tract-specific microstructural damage in the NAWM at baseline, as measured by the mean MTR, significantly correlated with the damage affecting the connected GM area after two years, independently of the baseline GM area’s mean MTR, and of all the other confounding variables included in the model, including T2-w lesion load and MTR, and spinal cord area. According to the “primary WM model” hypothesis, the pathological processes initially affecting the WM tracts, over time start spreading to their connected cortical areas, resulting in subsequent GM pathology. Different pathogenic mechanisms potentially underlying the temporal sequence described by the “primary WM damage model” have been proposed, and are currently under investigation (Geurts and Barkhof, 2008). Indeed, several different pathogenic processes affecting the WM tracts (including glutaminergic excitotoxicity, disrupted intra-axonal transport, and mythocondrial

dysfunction), may cause an axonal pathology associated with a dying-back axonopathy along the tract. This axonopathy could result in a secondary damage to the cortical regions connected with the tracts (Geurts and Barkhof, 2008; Filippi et al., 2012). The “primary WM damage model” regressions remained significant when T2-w lesion load and MTR, as well as spinal cord area, were included in the model. Our results could be interpreted in the light of an intriguing pathogenic hypothesis which has been recently proposed to explain the pathogenesis of MS. This suggests that a degenerative mechanism within the NAWM (affecting the axons, or the oligodendrocytes, or both) might be the earliest event, which then triggers an immunitary response (whose severity varies in different MS subtypes, being less pronounced in PPMS) that is responsible, in turn, of the inflammatory reaction that is found in the WM (Stys et al., 2012).

Interestingly, the “primary WM damage model” hypothesis did not explain the temporal evolution of the disease processes in the case of the callosal pair. This could be because, in this particular brain region, the damage had already reached an advanced stage at baseline, with the sequence of pathological events (i.e. early damage accrual in the WM tract followed by the secondary occurrence of abnormalities in the connected GM area) being already completed at study entry.

On the other hand, when the “primary GM damage model” was tested, this was not significant in the motor pair, bilaterally, and in the left optic pair. In the callosal pair and in the right optic pair, it resulted to be significant ($p<0.001$ and $p=0.001$), when no covariates were included in the model. However, when the “primary GM damage model” regression was repeated adjusting for baseline occipital cortex mean MTR, it became borderline significant in the right optic pair ($p=0.045$), while it lost significance in the left optic pair ($p=0.119$). This suggests that the abovementioned correlations were not completely genuine, as they seemed to be induced by the strong association existing between the MTR values at the two time-points in the occipital cortex.

The statistical comparison between the two proposed models showed that the

"primary WM damage model" was significantly stronger than the "primary GM damage model" in the motor pair, bilaterally. In the callosal pair and in the optic pair, bilaterally, although the direct comparison between the two models did not reach statistical significance, there was a suggestion that the "primary WM damage model" was stronger than the "primary GM damage model" one, in terms of both the standardised regression coefficients, and the p-values. This suggests that, in the early phase of PPMS, the main sequence of pathological events seems to consist of primary damage of the WM tracts which precedes, and possibly causes, the pathological changes occurring in the connected GM areas. However, data from the callosal and the optic pair, suggest that this sequence of events may coexist, in specific brain regions, with a concurrent pathogenic mechanisms, consisting of a primary neurodegenerative damage affecting the GM (possibly due to meningeal inflammation (Magliozzi et al., 2007; Choi et al., 2012), gradually leading to a subsequent axonal retraction and, in turn, to a degeneration of the resulting empty myelin sheaths along the WM tracts (Geurts et al., 2009).

When we looked at the impact of tract-specific WM lesions on the spatial and temporal relationship between the damage of WM tracts and that of the cortical regions connected to them, we obtained rather interesting results. We found that, although the damage of tract-specific WM lesions (in terms of both mean MTR and volume), clearly correlated with the concurrent and subsequent changes affecting the NAWM of the tracts, the cross-sectional and longitudinal association between the changes affecting the two compartments were independent of lesional damage. Our data are in line with the hypothesis that the pathological changes occurring in the NAWM, may partly depend on retrograde degeneration of axons that are transected in WM lesions (Trapp et al., 1998) but, to some extent, they may be also attributable to independent processes primarily originating within the NAWM itself (Geurts et al., 2010).

4.5 Conclusions

In conclusion, we described, for the first time in-vivo, the temporal sequence of pathological events affecting the WM and the GM in the early phase of PPMS.

The results presented in this study may suggest that, at least in the early phase of clinical progression in this subtype of disease, the tract NAWM could represent the initial target of the disease, as described by the “primary WM damage model”. I showed that microstructural damage affecting the NAWM, as reflected by MTR, precedes and predicts that occurring in the connected cortical areas. However, it is noteworthy to underline the limitations of the hypothesis-driven approach employed in this study to test the “primary WM damage” and the “primary GM damage” models. In particular, the presented results could simply reflect the temporal sequence of the pathological events affecting the two compartments, and they do not imply any causal relationship between them. Secondly, our study does not exclude the possibility that MS is a “whole brain disease”, where WM and GM are affected independently of each other, or where both the two models (“primary WM damage” and “primary GM damage” models) are valid and can accurately describe the temporal sequence of events, each one possibly prevailing on the other at different stages of disease and/or in different brain areas. Future work applying the methodology described in this study, will explore the temporal sequence of pathological events, as well as the role of T2-w lesions in contributing to WM and GM pathology over time, in the relapsing-onset forms of disease.

With the studies presented in Chapter III and Chapter IV, I tried to answer the first question of this thesis. In the following Chapters, the second question presented in Chapter I will be addressed, exploring the relative contribution of the two compartments to short-term and long-term clinical progression.

The role of focal WM damage in predicting clinical progression over 10 years in PPMS

Chapter V

The study presented in this Chapter will address the second question proposed in the Chapter I of this thesis, investigating the role of WM lesions (and in particular their spatial location) in predicting long-term clinical deterioration in PPMS. DThe data presented in this Chapter are is the result of a 10-year follow-up of a large cohort of patients with PPMS recruited in five European centres (Amsterdam, Barcelona, Bordeaux, London and Milan), all members of the MAGNIMS (MRI in MS) consortium.

5.1 Introduction

As discussed in the Chapter I of this thesis, predicting long term clinical outcome in patients with PPMS has important clinical implications, since this can affect the recruitment criteria for treatment trials (that would benefit from an appropriate stratification of risk for patients at study entry) and, in future, provide prognostic advice to individual patients.

Whole brain T2 and T1 lesion loads, which are objective measures of visible tissue damage, have been studied as potential predictors of long-term clinical outcome in a previous MAGNIMS study, where a large cohort of PPMS patients was followed-up for 10 years (Khaleeli et al., 2008b). The results of this study showed that neither T2 nor T1 lesion load at study entry predicted clinical deterioration over 10 years. This is surprising, since T2 lesion volume has been shown to predict disability after 20 years in patients who presented with clinically isolated syndrome (Fisniku et al., 2008), and suggests differences in the mechanisms of tissue damage between RRMS and PPMS.

In searching for other features of T2 and T1 brain lesions, which could predict long term outcome in PPMS, Khaleeli et al. also examined the short-term increase in T2 and T1 lesion loads over 2 years, finding that this also failed to predict progression over 10 years (Khaleeli et al., 2008b). On the other hand two other studies, one from the MAGNIMS PPMS cohort and one from the London early PPMS cohort, indicated a more promising role for the short-term change in T2 and T1 lesion loads in predicting clinical progression over 5 years (Ingle et al., 2003; Sastre-Garriga et al., 2005b). This suggests that

accumulation of visible lesions over a short time showed no advantage over total lesion load at study entry when it came to predicting progression at 10 years. Thus, predictors which are promising in short-term follow-up studies, may not be as compelling in long-term studies.

Another, mostly unexplored, feature of lesions, which may be relevant to predicting long-term clinical progression, is their topographic distribution. Therefore, the study presented in this Chapter aimed to investigate whether the location of T2 and T1 lesions at baseline predicts progression over 10 years, performing a retrospective study in the same MAGNIMS cohort of patients with well-established PPMS previously studied by Khaleeli et al. (Khaleeli et al., 2008b). To explore lesion location, in the study presented here I employed the Lesion Probability Mapping (LPM) approach was employed, whichthat provides a voxel-wise, quantitative description of the topographic distribution of brain lesions (Di Perri et al., 2008).

Among the other possible limitations of previous studies, which explored predictors of progression, there could be the use of step-changes of EDSS as the outcome measure in this form of disease (Kragt et al., 2008). In the attempt to address this issue, the time (in years) taken to require bilateral support in order to walk was defined in this study as a measure of the individual progression rate. Then, a time to event (TTE) analysis was performed and combined with LPM.

Although cervical cord cross sectional area at study entry did not predict clinical outcome at 10 years in this cohort of PPMS patients (Khaleeli et al., 2008b), spinal cord damage is thought to play an important role in determining disability in PPMS (Nijeholt et al., 1998; Rovaris et al., 2001; Bieniek et al., 2006); therefore, the LPM analysis presented here was corrected for baseline cord cross-sectional area. Moreover, it was tested whether regional T2 and T1 lesion loads located in specific, clinically strategic areas, were significant predictors of TTE.

5.2 Methods

5.2.1 Patients

Out of 101 patients with PPMS who were followed-up for 10 years in five European centres (Amsterdam, Barcelona, Bordeaux, London and Milan) (Khaleeli et al., 2008b), 80 participants, whose baseline imaging data were available, were included in this study (see Appendix I). All of these patients were clinically assessed using the EDSS (Kurtzke, 1983) at baseline (see Table 5.1 for baseline demographic, clinical and radiological characteristics), 76 after 1 year, 59 after 2 years, 75 after 5 years and 79 after 10 years. Of the 79 patients assessed after 10 years, 36 were scored using the EDSS telephone interview (Lechner-Scott et al., 2003). Four patients scored 10 on the EDSS, as their death was due to MS; one death occurred between years 2 and 5, and three between years 5 and 10. All subjects gave informed, written consent before the study, which was approved by the local Ethics Committees in each one of the participating centres.

Characteristics	Amsterdam	Barcelona	Bordeaux	London	Milan
Patients, number	20	22	4	22	12
Age, years (mean (SD))	53.5 (76–34)	45.7 (31–64)	48.7 (43–59)	52.7 (29–74)	45.1 (32–50)
Gender, female/male	10/10	9/13	3/1	1 1/11	2/10
EDSS, median (range)	6.0 (2–8)	5.5 (2–7.5)	5.0 (4–6)	6.0 (2.5–8.5)	4.0 (2–8.5)
Disease duration, years (mean (SD))	11.7 (2–32)	8.8 (3–24)	9.0 (2–11)	10.3 (1–24)	6.8 (2–17)
T2 lesion load, ml (SD)	8.4 (11.0)	15.8 (16.0)	12.6 (17.7)	15.3 (17.5)	7.7 (5.7)
T1 lesion load, ml (SD)	3.4 (4.9)	5.6 (7.2)	6.0 (7.7)	4.7 (7.7)	3.8 (6.6)
Spinal cord area (mm2) (mean (SD))	72.3 (10.1)	77.9 (8.2)	–	70.3 (9.4)	77.4 (8.1)

Table 5.1 Demographic, clinical and radiological characteristics of the patients studied in each centre, at study entry.

5.2.2 MRI acquisition

Patients underwent the same imaging protocol in each centre at study entry. In London, data were acquired using a 1.5 T GE Signa scanner, whereas at the other four sites a 1.5 T Siemens scanner was used. The protocol included T1-w and dual echo (T2- and proton density (PD)-w spin echo) imaging of the brain (see Table 5.2 for the acquisition parameters in each centre). Volumetric images of the spinal cord were also acquired, as described in Chapter IV (Stevenson et al., 1999).

Acquisition parameters T2/PD	**Amsterdam**	**Barcelona**	**Bordeaux**	**London**	**Milan**
Repetition time, ms	2500	3000	3000	3000	2500
Echo time, ms	45/90	14	19	15/90	30
Continuous axial slices, n	44	46	45	44	44
Slice thickness, mm	3	3	3	3	3
Acquisition parameters T1					
Repetition time, ms	620	690	600	600	550
Echo time, ms	15	15	14	20	10
Continuous axial slices, n	44	46	45	44	44
Slice thickness, mm	3	3	3	3	3

Table 5.2. Acquisitions parameters for T2-w/PD and T1-w sequences performed in each centre at study entry.

5.2.3 MRI processing

5.2.3.1 *Lesion probability map (LPM)*

A detailed description of the LPM approach is given in Chapter II. Here, the main steps relevant to this specific study are summarised. The imaging tools

available in the Functional MRI of the Brain's Software Library (FSL, http://www.fmrib.ox.ac.uk/fsl) were used.

1. Lesion masks

A single observer, who was blinded to the clinical details, contoured the PD hyperintense and T1-w hypointense lesions, with reference to the co-registered T2-w, using a semiautomated technique (Plummer, 1992). Binary lesion masks were then produced and individual lesion loads calculated.

2. Template construction

Each patient's T1-w scan was registered to the Montreal Neurological Institute (MNI152) template using a fully affine transformation (12 parameters) (FLIRT - FMRIB's Linear Image Registration Tool), as per previous work in patient groups with a variety of neurological conditions (Karagulle Kendi et al., 2008; Ginestroni et al., 2009; Vellinga et al., 2009). All of the resulting transformed images were averaged to obtain an internal T1-w template.

3. Transformation of individual scans and lesion masks into T1-w template

Each patient's PD weighted scan was registered to the corresponding T1-w scan in native space using a rigid body transformation and trilinear interpolation (with FLIRT). The transformation parameters were then applied to the T2-w lesion masks, bringing them into alignment with the individual T1-w scans. Each patient's T1 scan was then registered to the T1 template, using non-linear registration (FNIRT-FMRIB's Non Linear Image Registration Tool), and the resulting transformation parameters were applied to the T1 and T2 lesion masks, which had been previously registered onto the individual T1, using trilinear interpolation. In order to maintain the volume of the transformed lesion masks as close as possible to those in the native brain images, after the trilinear interpolation, lesion masks were thresholded using a value of 0.5. Two observers independently checked all the co-registered lesions masks.

4. T2 and T1 LPMs

T2 and T1 LPMs were generated by averaging the T2-w and T1-w lesion masks, at each voxel, in standard space. For each map, the resulting voxel

intensity indicates how frequently the voxel in question is within a lesion across all patients, ie, the probability of that voxel being lesional. Regions containing the peaks of lesion probability were localised using the Johns Hopkins University DTI-based white matter atlas, provided by FSL (Mori, 2005).

Since male gender has been associated, in this patient cohort, with a worse long term outcome (Khaleeli et al., 2008b), the differences in the probability of each voxel being lesional between male and female patients were assessed using an unpaired t-test and corrected for multiple comparisons at cluster level (t 2, $p<0.05$) using permutation based inference (Nichols and Holmes, 2002).

5.2.3.2 *Cord cross-sectional area*

Cord cross-sectional area at the C2–3 level was measured using a semiautomated technique previously described by Losseff and colleagues (Losseff et al., 1996).

5.2.4 Statistical analysis

5.2.4.1 *Correlation between lesion location and time to event*

For each patient, the time (in years) taken from disease onset to reach the level of disability that requires a constant bilateral support to walk (i.e., EDSS=6.5) was defined as the TTE and was used as a measure of progression rate. An EDSS of 6.5 was chosen as it is easy to recognise and represents a clinically meaningful stage in the progression of disability. It was also appropriate for the selected cohort, whose median EDSS at study entry was 5.7 (range 2–8.5). In cases where the EDSS was scored as equal or greater than 6.5 at a follow-up visit for the first time, it was assumed that the patient reached this score midway between the date of the visit and the preceeding assessment.

Patients were divided into three groups of similar size on the basis of their TTE, as follows: (1) patients who reached EDSS 6.5 before entering the study (n=23); (2) patients who reached EDSS 6.5 between the baseline assessment and year 5 (n=23); and (3) patients who reached EDSS 6.5 between year 5 and year 10 (n=13) and those who had not reached the event at the end of the study (n=21).

To identify regions where the probability of each voxel being lesional in T2-LPM and T1-LPM correlated with TTE, an ordinal multiple regression was used, with an indicator of the three TTE categories as regressor, and age, gender, disease duration at baseline, centre and cord cross-sectional area as additional covariates. Corrections for multiple comparisons at cluster level (t 2, $p<0.05$) were performed using permutation-based inference (Nichols and Holmes, 2002).

5.2.4.2 *Predictors of progression rate*

A Cox regression analysis was performed, entering TTE as the dependent variable, and the number of lesional voxels (or regional lesion loads) extracted from tracts that encompassed regions showing significant associations in the previous analysis, as independent variables. T2 and T1 total lesion loads, cord cross-sectional area, gender, age, disease duration and centre were entered as additional, independent variables. In particular, each independent variable was entered individually into the model. Subsequently, significant and borderline predictors were modelled together to determine the best, independent predictor. This analysis was performed using Stata 9.2 (http://www.stata.com) (Stata-Corp, College Station, Texas, USA), and results with $p<0.05$ were considered significant.

5.3 Results

5.3.1 T2 and T1 lesion probability maps

The brain locations that showed the highest probability of detecting T2 hyperintense and T1 hypointense lesions were the superior and posterior regions of the corona radiata (Figure 5.1). The maximum local probability was higher in T2-LPM compared with T1-LPM (42% vs 26%).

No significant differences in the probability of a voxel being lesional in T2-LPM and T1-LPM between men and women were found.

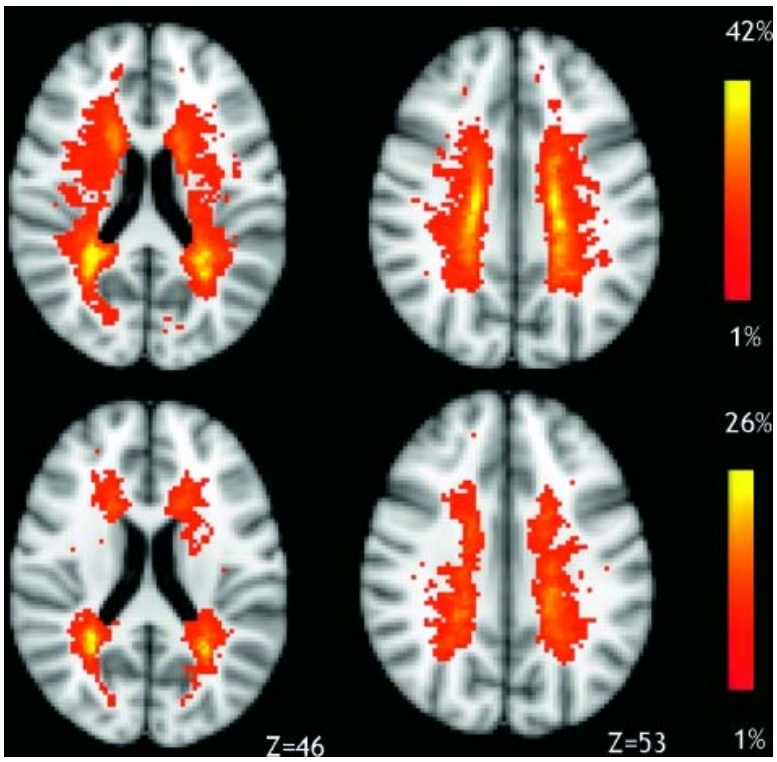

Figure 5.1. T2-Lesion probability map (LPM) (top row) and T1-LPM (bottom row); the colour code indicates the probability of a voxel being lesional. The maximum probability was found in the superior and posterior regions of the corona radiata, and was higher in T2-LPM compared with T1-LPM (42% vs 26%).

5.3.2 Correlation between lesion location and time to event

Of the 80 patients included in the study, 59 (73.7%) reached the event (EDSS=6.5) either before entering the study (23 patients, 28.7%) or during the course of the study (36 patients, 45%), while 21 (26.3%) had not reached the event when the study terminated. The median of the TTE calculated on those who reached EDSS 6.5, was 11.5 years (range 3–29 years).

There was a significant correlation between a higher probability of a voxel being lesional on T2-LPM and a shorter TTE ($p<0.05$) in the following three regions: the bilateral corticospinal tract (CST) (from the cortex to the corona radiata), the bilateral superior longitudinal fasciculus (SLF) and the right inferior fronto-occipital fasciculus (IFOF) (Figure 5.2). Conversely, there was no correlation between lesion probability on T1-LPMs and TTE, although a statistical trend towards a significant association was found in a region in the right posterior corona radiata, which included the CST and the SLF ($p<0.08$).

5.3.3 Predictors of progression rate

The number of lesional voxels and corresponding regional lesion loads extracted from tracts containing regions that showed an association between lesion location and TTE are summarised in Table 5.3.

Measures of regional lesional damage	Bilateral CST	Bilateral SLF	Right IFOF
Number of lesional voxels mean, SD	37.6 (58.8)	38.4 (76.1)	30.1 (47.4)
Lesion load (ml) mean, SD	0.3 (0.5)	0.3 (0.6)	0.2 (0.4)

Table 5.3. Number of lesional voxels and corresponding regional lesion loads extracted from the three tracts containing regions that showed an association between lesion location and time to event (CST, corticospinal tract; IFOF, inferior fronto-occipital fasciculus; SLF, superior longitudinal fasciculus).

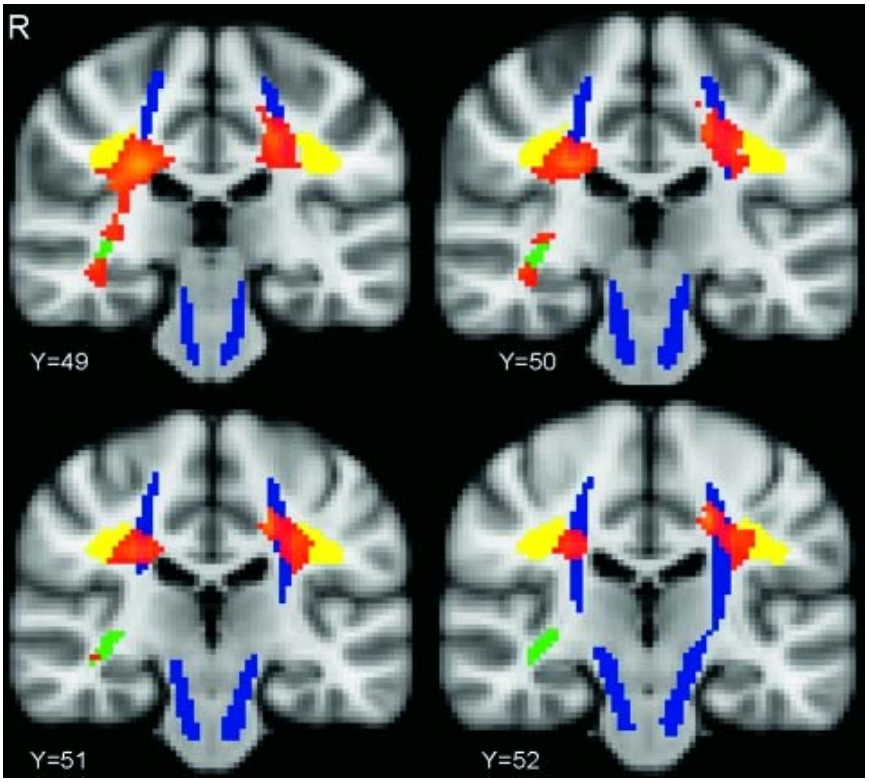

Figure 5.2. Red–orange voxels show the regions on the regression maps where a higher probability of a voxel being lesional on T2 images was significantly associated with a shorter time to event. These regions are: the bilateral corticospinal tract (CST) (from the cortex to the corona radiata), the bilateral superior longitudinal fasciculus (SLF) and the right inferior fronto-occipital fasciculus (IFOF). In blue, yellow and green are displayed the courses of the three white matter tracts (bilateral CST, bilateral SLF and right IFOF, respectively).

When predictors were entered individually into the Cox regression model, it was found that a greater number of T2 lesional voxels extracted from the right IFOF was associated with a shorter TTE (p=0.01, hazard ratio (HR) 1.00689, 95% CI 1.00158 to 1.01225); in other words, for every extra ml of lesions within the right IFOF, the time taken to reach EDSS 6.5 was halved.

The number of T2 lesional voxels extracted from the bilateral CST showed a trend towards a correlation with TTE (p=0.07, HR 1.002, 95% CI 0.99981 to 1.00442); in this case, for every extra ml of lesions localised within the CSTs, the time taken to reach the event was reduced by 30%. The number of lesional voxels in the bilateral SLF did not predict TTE.
Among the other variables tested individually in the Cox regression, it was found that: (i) the whole brain T1-w hypointense lesion load was significantly associated with TTE (p=0.04, HR 1.00004, 95% CI 1.000001 to 1.00007); in other words, for every extra ml in total T1-w lesion load, the time taken to reach the event was reduced by 0.5%; and (ii) there was a borderline significant association between gender and TTE (p=0.062, HR 1.62, 95% CI 0.96 to 2.73), so that the time taken for men to reach the event was reduced by 60%.

When all significant and borderline predictors were entered together into the Cox regression model, the number of T2-w lesional voxels in the right IFOF was the best independent predictor of TTE (p=0.016, HR 1.00652, 95% CI 1.00121 to 1.01186). The number of T2-w lesional voxels in the bilateral CST (p=0.07, HR 1.0022, 95% CI 0.99979 to 1.00461) and the whole brain T1-w hypointense lesion load (p=0.07, HR 1.00003, 95% CI 0.99999 to 1.00006) became borderline independent predictors, while gender became non-significant.

5.4 Discussion

The study presented in this Chapter showed that the location of T2-w lesions at baseline is associated with the rate of progression in PPMS over a 10 year period. In particular, a relationship between a higher probability of a voxel being lesional and a faster progression rate was found in the motor tract (ie, the bilateral CST) and two associative tracts (ie, the bilateral SLF and the right

IFOF). These results extend the findings of previous cross-sectional studies that have found correlations between mobility and regional MRI abnormalities localised within the motor tract in MS (Wilson et al., 2003; Reich et al., 2008; Gorgoraptis et al., 2010).

Furthermore, the SLF and the IFOF are two associative tracts, which are part of the longitudinal association fibre system that connects each frontal lobe with other regions in the same hemisphere. In particular, the SLF connects the parietal and the frontal lobe, whereas the IFOF mediates the connection between the frontal and the occipital lobe (Catani et al., 2002; Martino et al., 2010). Both SLF and IFOF are known to be involved in the regulation of high order aspects of motor function, including conveyance of somatosensory and kinesthetic information and initiation and guidance of motor activity (Schmahmann and Pandya, 2007; Jang and Hong, 2012). Therefore, a possible interpretation of these findings is that disruption of long associative tracts, due to the presence of lesions, causes a disconnection syndrome that may contribute to a more rapid deterioration of mobility, as previously proposed (He et al., 2009; Vellinga et al., 2009). In fact, it is known that disrupted white matter pathways, which play a crucial role in the coordination of information flow between different grey matter regions, are likely to lead to an altered functional connectivity between regions and, ultimately, to clinical impairment (Rocca et al., 2005). Furthermore, damage in these tracts may reduce the cortical reorganisation that originates from activation of regions connected through these pathways, thus resulting in a reduced ability of the brain to limit the clinical impact of structural damage. Recent data from the Milan cohort of patients with PPMS, obtained combining functional MRI (fMRI) and structural imaging data, support this interpretation of data, showing a correspondence between the extent of damage to specific tracts and fMRI changes in corresponding networks (Ceccarelli et al., 2010).

In the study presented in this Chapter, the relationship between lesion location in the IFOF and TTE was found to be statistically significant on the right side only. This is in agreement with the reports of asymmetry in MS brain pathology

(Reich et al., 2007). In future, the contribution of handedness to these results needs to be further explored.

The association between a higher probability of a voxel being lesional and a faster progression rate, was independent of spinal cord atrophy (the mean value of cord cross-sectional area in patients is similar to that previously reported in PPMS) (Rovaris et al., 2001). Interestingly, when the correlation between lesion location and TTE was investigated using both EDSS equal to 6 and EDSS equal to 7 as events, the same motor and associative tracts showed significance (results not shown), suggesting that the location of T2 brain lesions in these tracts is an important factor in contributing to disability progression in PPMS.

When the best predictors of TTE were investigated, the regional T2 lesion volume measured in the right IFOF was found to be the best, independent predictor of progression. Conversely, the T2-w lesion load in the bilateral CST became a borderline predictor, and that in the SLF became non-significant, suggesting a preferential role of the right IFOF, perhaps through the infero- and dorso-lateral frontal, and occipital cortices that it connects (Catani et al., 2002; Martino et al., 2010). Indeed, the IFOF constitutes the inferior part of the fronto-occipital fasciculus, that is thought to be involved in the use of visual information for the purpose of guiding movements and controlling motor actions (Schmahmann and Pandya, 2007).The clinical relevance of IFOF in MS is further supported by the results of a recent study conducted on a cohort of patients who were followed up 20 years after presenting with a CIS, where (using the same LPM procedure described here) it was found that patients who converted to clinically defined MS had a greater probability of having lesions in the right IFOF when compared with those who did not (Dalton et al., 2011).

As previously demonstrated, the whole brain T2-w lesion load did not correlate significantly with the progression rate, supporting the concept that in MS a proportion of the total lesion load is clinically silent (Miki et al., 1999; Li et al., 2006; Rudick et al., 2006) and is not as relevant in determining progression as other lesions localised in strategic areas.

In contrast with the reported data about T2-w lesions, no significant association was found between the T1-w hypointense lesion probability and progression rate. A possible interpretation for this finding is that the T1-w lesion load is considerably smaller than the T2-w lesion load and, therefore, tracts are less likely to contain T1-w compared with T2-w lesions. This, in turn, means that the range of lesion loads within a given region is smaller for T1-w compared with T2-w lesions, reducing the possibility of a correlation with clinical outcomes. Interestingly, it was found that whole brain T1-w lesion load was a borderline independent predictor of progression rate. This is not surprising, since T1-w hypointense lesions are known to be histopathologically associated with severe tissue destruction (van Walderveen et al., 1998) and T1-w total lesion load correlates with clinical disability in MS more strongly than T2-w lesion load (Truyen et al., 1996; O'Riordan et al., 1998).

Moreover, the areas most likely to contain lesions were similar in the T2-LPMs and T1-LPMs, and included the superior and posterior regions of the corona radiata. This is interesting, since a large number of axonal projections that contribute to the generation of the CST converge in this region (Wakana et al., 2004), and PPMS is typically characterised by a progressive decline in motor function. A previous study reported that patients with PPMS had a greater probability of a lesion occurring in these regions, compared with RR patients (Di Perri et al., 2008).

Interestingly, a TTE analysis which had been limited to clinical trials (Panitch et al., 2004; Montalban et al., 2009a), was included in this study. In fact, TTE analysis can be easily adapted to different events as long as the event in question is temporally defined and clinically meaningful (Allen et al., 1999). When the event cannot be specifically dated, it is acceptable to use the midpoint between the visit at which the event is noted and the previous one, as the time of the event (Law and Brookmeyer, 1992).

However, due to our study design, the interval between visits varied between 1 and 5 years, and 13 patients (16%) reached the event during the 5 years which elapsed between the last two time points. When the analysis was repeated

without these patients, the results were found to be very similar to those presented here (results not shown); therefore, it is possible to conclude that the variability in follow-up intervals has not significantly distorted the results. Furthermore, the progression rate observed in the population presented in this study, was similar to the one previously reported in epidemiological studies in PPMS patients (Cottrell et al., 1999), suggesting that despite the retrospective design of the study and the suboptimal frequency of assessments, the definition of the clinical outcome was appropriate. Another limitation of this study lies in the fact that 28.3 % of the patient cohort had already reached the event (EDSS 6.5) before entering the study. This implies that the design of the study, (which can be considered as being prospective for the 71% of the cohort which reached the event after entering the study), has necessarily to be defined as retrospective for this sub-group of patients. Future analysis should take into account this substantial difference, and the presented results should be confirmed in larger cohorts by repeating the analysis separately for the "prospective" and the "retrospective" sub-groups.

In this study, a large number of PPMS patients recruited in five European centres, was studied over a very long follow-up period. A potential limitation of this study is that, with the available data, we were not able to look for grey matter lesions that may be very relevant in contributing to long term clinical disability, as discussed in the Chapter I of this thesis (Calabrese et al., 2012). Another possible limitation of this study is the potential for registration errors and consequent lesion location inaccuracies related to the LPM technique. Two observers, rather than one (Di Perri et al., 2008; Vellinga et al., 2009b), inspected registered lesion masks and were in agreement in all cases. While it is to be expected that there will be some residual misalignments, in the context of a lesion probability analysis, their effects will be negligible.

5.5 Conclusions

The study presented in this Chapter has demonstrated that the focal damage localised in motor and associative tracts, might have the potential to significantly contribute to clinical progression, independently of spinal cord atrophy, in

patients with PPMS. Furthermore, the time to bilateral support has been demonstrated to be a useful approach to identify patients who progress more rapidly.

Having described the role of focal WM damage in predicting long-term clinical outcome in this form of disease, the next Chapter of this thesis will continue to address the question of which regions of WM and GM abnormalities significantly contribute to clinical progression, exploring the role of short-term accrual of WM damage (within and outside focal lesions) in determining clinical disability in patients with early PPMS.

Short-term microstructural changes in white matter tracts in early PPMS

Chapter VI

The study presented in this Chapter will further address the second question proposed in Chapter I of this thesis, exploring the tract-specific, short-term accrual of microstructural damage in PPMS, and its impact on clinical progression, by using a novel methodology, called “skeletonised MTR”, which combines TBSS and MTR.

6.1 Introduction

As discussed in Chapter I, MTI has proved valuable in identifying and quantifying in-vivo tissue changes including demyelination and remyelination, that occur within and outside visible lesions on T2-w scans (Ropele and Fazekas, 2009). In particular, decreased MTR values, which post-mortem studies have shown to be sensitive to a reduced myelin content, in addition to axonal loss (Schmierer et al., 2004), have been demonstrated in patients with RRMS and progressive forms of MS when compared with controls, since the early stages of the disease (Filippi and Agosta, 2010).

Previous MTR studies in patients with MS have employed histograms in a priori selected areas, such as segmentation-based masks or hand-drawn regions (Filippi and Agosta, 2010). In the study presented in Chapter IV, tract-specific MTR changes have been measured using tractography-based strategies that determine the WM tract of interest, and a similar approach has been previously employed both in healthy controls and in patients with psychiatric and neurological disorders (Reich et al., 2006; Reich et al., 2007; Dalby et al., 2010; de Zeeuw et al., 2011). However, tractography-based ROI approaches do not allow the investigation of the whole brain, and require the a priori selection of the tract(s) of interest.

On the other hand, as discussed in Chapter II and Chapter III, TBSS is a fully automated, voxel-wise method that is able to carry out voxel-wise cross-subject statistics on diffusion derived metrics without requiring an a priori hypothesis (Smith et al., 2006). By addressing the challenges of inter-subject data alignment, TBSS has been widely employed to localise WM changes related to normal brain development (Giorgio et al., 2008) and ageing (Giorgio et al.,

2010), as well as neurological diseases, including Alzheimer's disease (Damoiseaux et al., 2009; Stricker et al., 2009; Serra et al., 2010)(Damoiseaux et al., 2009; Stricker et al., 2009; Serra et al., 2010), epilepsy (Focke et al., 2008; Nguyen et al., 2011), multiple sclerosis and clinically isolated syndrome (Roosendaal et al., 2009; Raz et al., 2010a; Raz et al., 2010b; Kern et al., 2011). In particular, as described in detail in Chapter II, TBSS uses each subject's FA to produce an alignment-invariant tract structure, representing the core of whole-brain WM tracts, known as the "skeleton". This step is followed by the projection of FA values from the main WM tracts of every subject onto the skeleton, achieved by searching perpendicular to the local skeleton structure for the maximum FA value. This value is assumed to represent the nearest relevant tract centre. This step ensures the alignment of WM tracts rather than that of macroscopic features (e.g., the boundary between tissues or the sulci shape, as in standard voxel-based approaches).

In this study, TBSS was employed to create an FA-based "skeleton", and then the same "projection" procedure was applied to co-registered MTR data to create a "skeletonised" MTR map for every subject. This novel approach was employed to explore the microstructural abnormalities reflected by one year changes in diffusion-derived parameters and MTR values along the core of WM tracts, within and outside T2-w lesions, in patients with the early PPMS. The other aim of this study was to assess whether these WM changes were clinically relevant, by performing correlations with changes in clinical scores over the same follow-up.

6.2 Methods

6.2.1 Patients

Twenty-one patients diagnosed with PPMS according to Thompson's criteria (Thompson et al., 2000) (11 women, 10 men, mean age 46.6 yrs, SD 9.6), within 5 years of symptom onset, underwent a neurological assessment and a whole brain imaging protocol, including diffusion weighted imaging and MT imaging, at both study entry and after 12 months (see Appendix I). These

patients were part of a larger cohort of 50 subjects. A subset had diffusion and MT data at both, baseline and year 1, and was included in the current study. One patient was being treated with oral corticosteroids every four months. Clinical assessment included measuring the EDSS (Kurtzke, 1983), and the MSFC subtests (Cutter et al., 1999): PASAT, NHPT, and TWT.

The study was approved by the Joint Medical Ethics Committee of the National Hospital for Neurology and Neurosurgery and the UCL Institute of Neurology, London. Written and informed consent was obtained from all participants.

6.2.2 Image acquisition

Patients were imaged using a 1.5T GE Signa scanner (General Electrics, Milwaukee, IL). MRI acquisition and protocol were as follows:

(a) Three-dimensional inversion-recovery fast spoiled gradient recall (3D FSPGR) T1-weighted sequence of the brain (FOV 300x225 mm, matrix size 256x160 (reconstructed to 256x256 for a final in plane resolution of 1.17 mm), repetition time 13.3 ms, echo time 4.2 ms, inversion time 450 ms, 124 axial slices, 1.5 mm thickness).

(b) Whole-brain, cardiac-gated, Spin Echo Diffusion-Weighted (DW) Echo Planar Imaging sequence [FOV 240x240mm², matrix size 96x96 (reconstructed to 128x128), image resolution 2.5x2.5x3mm (reconstructed to 1.9x1.9x3mm), TE 95ms, TR 7RRs, maximum b-factor 1000 smm-2; three series, each collecting 14 axial slices of 3mm thickness, which were interleaved off-line; diffusion gradients were applied along 25 optimised directions (Jones et al., 1999), and three images with no diffusion weighting were also acquired.

(c) Magnetisation transfer (MT) dual echo interleaved spin-echo sequence (Barker et al., 1996) (28 contiguous axial slices, slice thickness 5 mm, repetition time [TR] 1720 ms, echo time [TEs] 30/80 ms, number of excitations [NEX] 0.75, acquired matrix 256×128, reconstructed matrix 256×256, field of view [FOV] 240×240 mm). A Hamming-apodised three-lobe sinc MT pulse (duration

16 ms, peak amplitude 23.2 μT, bandwidth 250 Hz, 1 kHz off-water resonance) was used. The sequence collects inherently co-registered proton density (PD) (30 ms echo) and T2-weighted images (80 ms echo) before and after the saturation pulse.

6.2.3 Image post-processing

6.2.3.1 *Lesions*

Lesions were delineated with a semi-automated contour thresholding technique (Plummer, 1992) by a single rater on the unsaturated PD images of the MT protocol. The T2-weighted images, which were inherently co-registered with the PD-weighted images (both acquired with the same dual-echo sequence), were always used as a visual reference to increase confidence in lesion identification. Lesion masks were obtained by setting the signal intensity equal to 1 for all voxels within a lesion and zero outside lesions. The same procedure was performed on the baseline and the follow-up scans.

6.2.3.2 *From "skeletonised" FA, AD, RD, to "skeletonized MTR"*

After correction for eddy-current induced distortions, the diffusion tensor was calculated on a voxel-by-voxel basis, and FA maps were generated using DTIfit, that is part of the FMRIB Software Library 4.1 (FSL, FMRIB Image Analysis Group, Oxford, UK) (Smith et al., 2004). FA maps were fed into TBSS (Smith et al., 2006) to generate a common FA tract skeleton onto which every subject's FA was then projected (see Chapter II for details). As some animal work suggests that axial diffusivity (AD) (coincident with the largest eigenvalue of the diffusion tensor, i.e., diffusion coefficient along the direction of maximum diffusion) and radial diffusivity (RD) (the average diffusion coefficient in the orthogonal directions) are more specific than FA to microstructural changes involving axons and myelin (Song et al., 2005), a TBSS analysis of these indices was also performed, as follows: AD and RD maps for all patients at baseline and follow-up were generated by fitting a tensor model to the raw diffusion data. By applying the original non-linear registration of each patient's FA map to standard space, the axial and radial diffusivity maps were projected onto the mean FA skeleton generated with TBSS, to obtain a "skeletonised AD"

and a “skeletonised RD” for each patient at each time point.

MTR maps were calculated from the inherently co-registered PD images of the MT sequence in native space, by subtracting the saturated from the unsaturated signal, using the formula MTR=[(Mo- Ms)/Mo]×100 percent units (pu) on a pixel-by-pixel basis. These short-echo images were chosen because the resulting MTR map has higher signal-to-noise ratio than that from the 80-ms echo. To obtain a “skeletonised” MTR image for each subject, MT data were first co-registered with DTI by matching the native non-MT weighted volume (inherently co-registered with the MTR maps) with the native b0 volume, after skull-stripping, with an affine transformation using FLIRT (FMRIB's Linear Image Registration Tool, part of FSL), using normalised mutual information as the cost function. The transformation was then applied to the native MTR map. Finally, the transformed MTR map underwent the same projection as the FA data onto the common FA tract skeleton, to obtain a “skeletonised” MTR image in MNI space, for each subject at each time point.

6.2.4 Statistical analysis

6.2.4.1 *Assessment of clinical progression over one year*

To assess whether there was a significant deterioration in EDSS score over the follow-up period, the EDSS scores at baseline and at year one were compared using the Wilcoxon matched-pairs signed rank test. Changes in EDSS scores were then converted into steps by considering 1 step change equal to 1 point increase for values of EDSS of 5.5 or lower, and to 0.5 increase for values of EDSS higher than 5.5 (Wingerchuk et al., 1997). To measure if changes in MSFC subtests were significant over the follow-up, all the scores were first transformed into z-scores (z-NHPT, z-TWT and z-PASAT), using our baseline sample as reference. A paired t-test between the z-scores at the two time points was then performed for each MSFC subtest.

6.2.4.2 *Changes in skeletonised FA, AD, RD and MTR over one year*

To assess the presence of any regional change in FA, AD, RD and MTR over the follow-up period, the skeletonised FA, AD, RD maps and MTR maps, at

baseline were compared with those at follow-up, using permutation tests (2000 iterations). Age, gender and disease duration at baseline were added as covariates of no interest. Correction for multiple comparisons was performed using threshold free cluster enhancement (TFCE) (Smith and Nichols, 2009). Differences were considered significant if $p<0.05$.

Tract specific FA, AD, RD, and MTR values were obtained and reported from every subject's skeletonised maps. The John Hopkins University white matter tractography atlas provided with FSL was used to identify the forceps major, the forceps minor, and 9 bilateral tracts: anterior thalamic radiation, cortico-spinal tract, cingulum bundle (split into cingulate and hippocampal parts), inferior fronto-occipital fasciculus, inferior longitudinal fasciculus, superior longitudinal fasciculus (split into fronto-parietal and temporal parts), and uncinate fasciculus.

6.2.4.3 *Correlation between changes in FA, AD, RD and MTR, and clinical changes over one year*

In order to assess the association between the changes in FA, AD, RD and in MTR and the clinical variables, a map of the difference between baseline and follow-up skeletonised images was computed for every patient. Patients were divided into three groups of similar size on the basis of their step-change in EDSS over one year: (1) patients who had no change in EDSS; (2) patients whose EDSS step-change was equal to 0.5; (3) patients whose EDSS step-change was greater than 0.5. To identify regions of significant correlation between FA and principal diffusivities changes and changes in the EDSS, the voxel-wise DTI parameters and MTR differences between baseline and follow-up were regressed against the three groups of EDSS step-change. In addition, to assess the correlation between the areas of FA (and principal diffusivities) and MTR changes and the changes in MSFC subtests over one year, three linear multiple regression analyses were performed (one for each of the MSFC subtests), using the changes in z-NHPT, z-TWT and z-PASAT as regressors. In all the regressions, age, gender, and disease duration at baseline were included as additional covariates. Correction at $p < 0.05$ for multiple comparisons was performed using TFCE.

6.2.4.4 *Post-hoc analysis*

(i) The role of lesions

To create a mask of "new and enlarged lesions" which developed during one-year follow-up, the lesion mask obtained from the T2-weighted images at baseline was subtracted from the lesion mask computed from the T2-weighted image at one year. This map includes both the new lesions, developed by patients during the follow-up period, and the portions of older lesions which have enlarged during follow-up. A lesion probability map was then created, in which a colour scale indicated the percentage of patients who had developed a new/enlarged lesion in a given voxel. To establish whether the areas of significant change in FA and MTR over one year were part of the "new/enlarged T2-weighted lesions" or were localised within the normal-appearing white matter (NAWM), the areas of significant decrease in FA and MTR, and the "new/enlarged T2-weighted lesion probability mask" were overlaid on the same anatomical image and then visually inspected.

Finally, to assess the contribution of the change in T2-weighted lesion load over the follow-up period to the significant changes found in the skeletonised FA/MTR, the lesion load increase over one year was first computed for each patient. Then, the correlation between the average skeletonised FA/MTR changes (i.e., the mean FA/MTR differences between baseline and one year in the areas that showed a significant change over one year) and the T2 lesion load difference was calculated, using Pearson's correlation coefficient.

(ii) The role of total GM MTR

To assess the correlation between total GM MTR changes over one year and clinical changes during the same period, the mean GM MTR value was computed for each patient at each time point using the following procedure. First SPM8 (Ashburner and Friston, 2005) was used to segment the T1-weighted volumes into WM, GM and CSF in native space. The GM probability maps were thresholded (to retain only voxels with probability of more than 75% of belonging to the GM (Khaleeli et al., 2007b). These GM masks were applied to the whole brain MTR maps to obtain GM MTR maps. The mean GM MTR values were calculated for every patient at both baseline and follow-up. The

difference between these two values (mean GM MTR at baseline – mean GM MTR at follow-up) was calculated. Finally, the correlations between GM MTR changes and clinical changes (i.e., changes in EDSS, NHPT, TWT, and PASAT) were assessed using Pearson's correlation coefficient.

(iii) Correlation between FA changes and MTR changes in regions that showed correlation between MTR changes and clinical function

To assess whether there was a correlation between FA changes and MTR decrease in the regions that showed a significant association between MTR decrease and clinical changes, we extracted the mean skeletonised FA and MTR values from these areas at baseline and at follow-up, calculated the difference between these two values and tested for significant correlations between FA and MTR changes in these regions using the Pearson's correlation coefficient (results with p values < 0.05 were considered significant).

6.3 Results

6.3.1 Clinical progression over one year

Patients showed weak evidence towards a significant progression of disability between baseline and year 1, as measured by EDSS (p = 0.08); there was a change in the MSFC subtest scores during the follow-up period, but it was not statistically significant. The clinical tests results at baseline and at one year are summarised in Table 6.1.

Clinical tests	Baseline assessment	Year one assessment	p-value (baseline vs 1 year)
EDSS (median, range)	4.5, 3.5-7.0	5.25, 2-7.5	0.08
PASAT score (mean, SD)	43.3, 13.3	44.9, 14.2	0.3
NHPT score (mean, SD)	33.2, 16	33.3, 18	0.9
TWT score (mean, SD)	14.2, 20	15.8, 26.8	0.4

Table 6.1. Clinical test scores at baseline and year one.

6.3.2 Changes in skeletonised FA, AD, RD, and MTR over one year

There was no significant change in skeletonised FA and AD between baseline and one year.

A significant increase in RD over time was found. The main changes were located within the cortico-spinal tract (CST) at the level of the cerebral peduncles (bilaterally) and the corona radiata (left hemisphere), the inferior longitudinal fasciculus and the inferior fronto-occipital fasciculus (right hemisphere), the left cingulum bundle and the anterior thalamic radiation (bilaterally) (Figure 6.1).

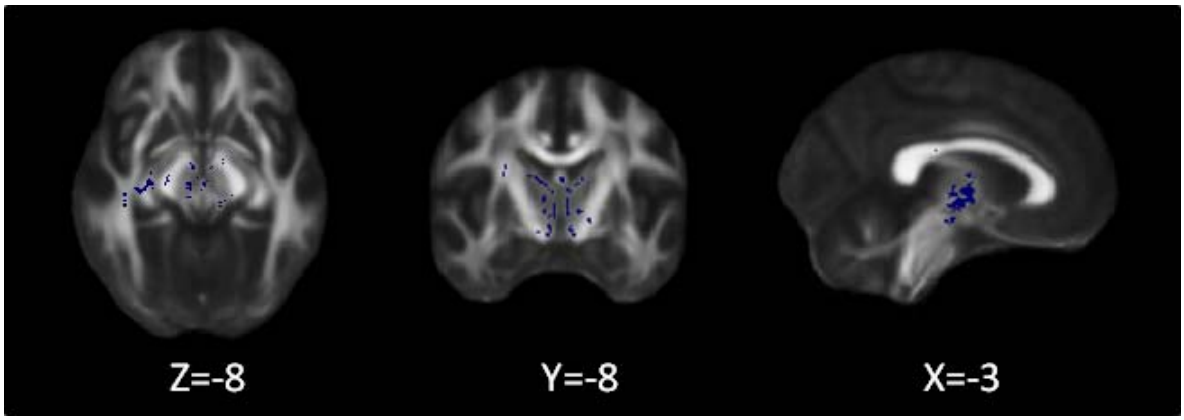

Figure 6.1: WM tracts showing a significant increase in RD over the follow-up (voxels in blue), overlaid onto the FSL fractional anisotropy template in MNI coordinates.

Patients showed a significant reduction in skeletonised MTR over the same follow-up period in the WM along the bilateral CST (posterior limb of the internal capsule and cerebral peduncle), and in the genu and the body of the corpus callosum (CC) ($p < 0.01$) (Figure 6.2).

A significant decrease in MTR over time was also detected bilaterally in the thalamic radiation, and in the superior and inferior longitudinal fasciculi ($p<0.01$) (Figure 6.2).

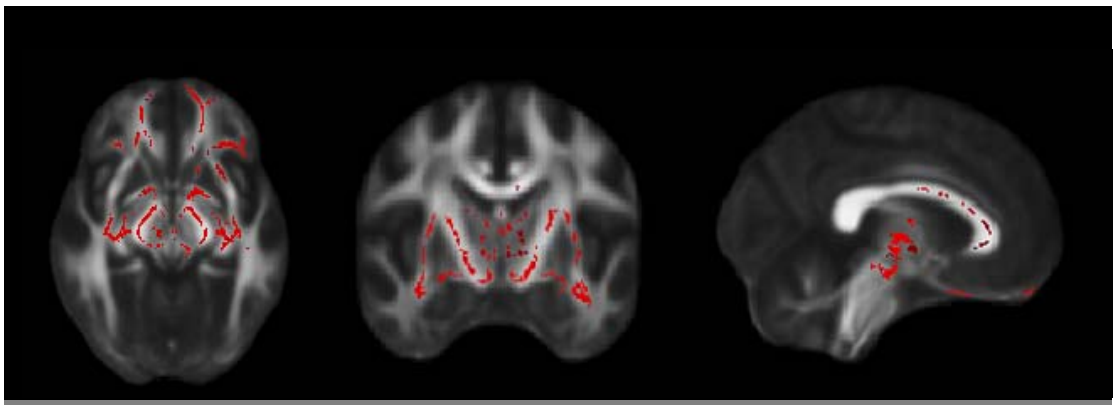

Figure 6.2: Red voxels show the regions of significant reduction in skeletonised MTR over one year, overlaid onto the FSL fractional anisotropy template in MNI coordinates.

Within the areas of significant change, the average difference in MTR between baseline and one year, computed across the skeleton, was 2% (mean value [SD] at baseline = 35.4 [3.1] pu, mean value [SD] at one year = 34.7 [3.3] pu). Tract specific FA and MTR values obtained from skeletonised maps at baseline and one year are shown in Table 6.2.

Tract	baseline		Year 1	
	mean FA (SD)	mean MTR [pu] (SD)	mean FA (SD)	mean MTR [pu] (SD)
Left ATR	0.407 (0.028)	34.14 (2.81)	0.402 (0.033)	33.58 (3.28)
Right ATR	0.420 (0.032)	34.47 (2.68)	0.416 (0.042)	33.87 (3.62)
Left CST	0.521 (0.029)	35.94 (1.48)	0570 (0.032)	35.59 (1.76)
Right CST	0.582 (0.027)	35.87 (1.44)	0.577 (0.031)	35.44 (1.59)
Left Cingulum	0.517 (0.051)	37.32 (1.45)	0.508 (0.057)	36.87 (1.60)
L Cingulum (HP)	0.456 (0.038)	33.10 (2.36)	0.456 (0.046)	31.53 (3.28)
R Cingulum (HP)	0.450 (0.043)	33.96 (1.60)	0.445 (0.054)	33.42 (1.79)
Forceps Major	0.598 (0.057)	34.48 (2.05)	0.590 (0.071)	34.58 (2.20)
Forceps Minor	0.480 (0.038)	37.46 (1.50)	0.473 (0.044)	36,96 (1.68)
Left IFOF	0.455 (0.042)	35.93 (2.09)	0.450 (0.050)	35.59 (2.17)
Right IFOF	0.455 (0.041)	35.61 (2.29)	0.449 (0.047)	35.35 (2.50)
Left ILF	0.430 (0.040)	35.65 (2.21)	0.427 (0.045)	35.49 (2.44)
Right ILF	0.447 (0.037)	35.80 (1.97)	0.440 (0.044)	35.78 (2.13)
Left SLF	0.434 (0.041)	36.84 (2.00)	0.429 (0.048)	36.51 (2.35)
Right SLF	0.445 (0.032)	36.70 (2.10)	0.441 (0.038)	36.58 (2.08)
Left UNC	0.431 (0.039)	35.67 (1.86)	0.428 (0.047)	35.44 (1.95)
Right UNC	0.448 (0.051)	35.25 (1.74)	0.446 (0.066)	35.28 (2.30)
L SLF (temporal)	0.471 (0.059)	37.11 (1.56)	0.468 (0.068)	36.83 (1.84)
R SLF (temporal)	0.505 (0.043)	36.91 (1.90)	0.496 (0.053)	36.76 (2.04)

Table 6.2. Tract-specific FA and MTR values obtained from skeletonised images in patients at baseline and one-year follow-up. List of Abbreviations: ATR = anterior thalamic radiation; CST = cortico-spinal tract; HP = hyppocampal part; IFOF = inferior fronto-occipital fasciculus; ILF = inferior longitudinal fasciculus; SLF = superior longitudinal fasciculus; UNC = uncinate fasciculus; R=right; L=left.

6.3.3 Correlation between changes in FA, AD, RD, and MTR, and clinical changes over one year

Changes in FA over the follow-up period did not significantly correlate with any change in the clinical variables.

AD decreases in the left CST (next to the primary motor cortex) and CC (genu, body and splenium) over one year correlated with changes in upper limb function, as measured by the z-NHPT scores (Figure 6.3). On the other hand, changes in AD did not correlate with the changes in TWT z-score nor with the changes in PASAT z-score.

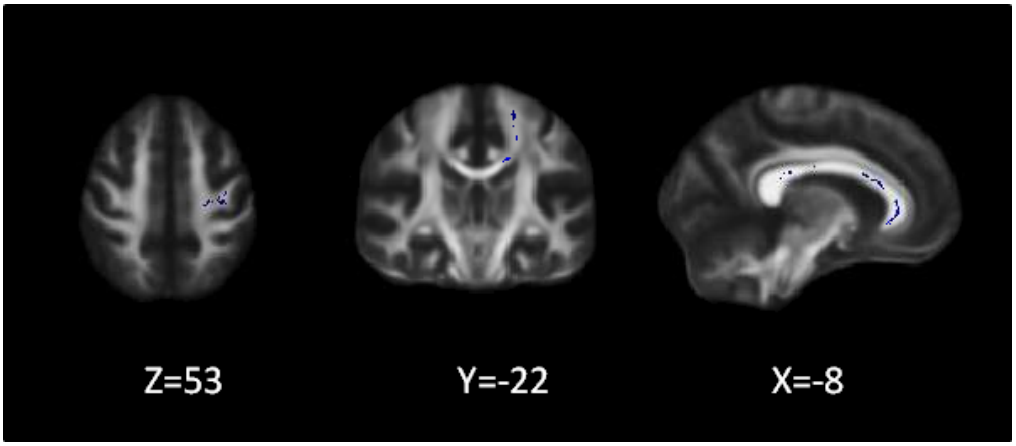

Figure 6.3: In blue are displayed areas of significant associations between a reduction in axial diffusivity and reduction in NHPT z-score over 1 year overlaid onto the FSL fractional anisotropy template in MNI coordinates.

Widespread significant inverse correlations were found between changes in the z-NHPT scores and changes in RD. These correlations were located in the right CST (at the level of the internal capsule), in the CC (genu, body and splenium), in the inferior longitudinal fasciculus (bilaterally), in the uncinate (bilaterally), in the anterior thalamic radiations, and in the cerebellar peduncles (Figure 6.4).

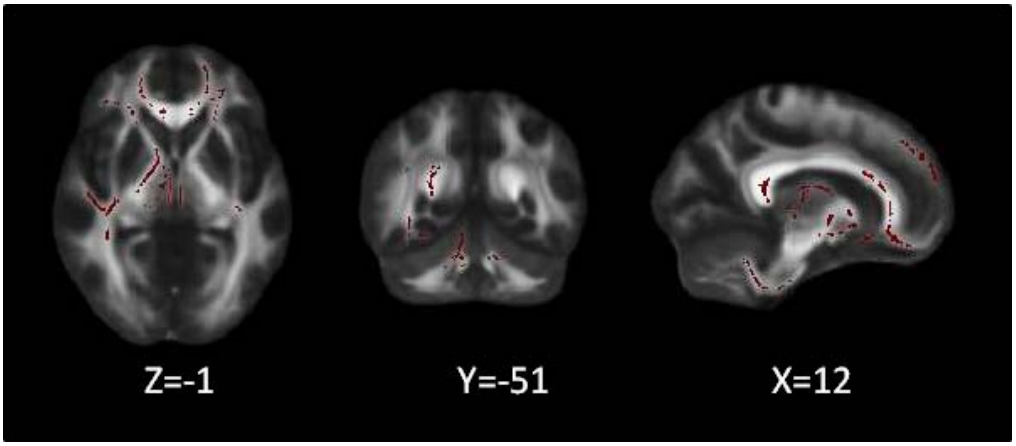

Figure 6.4: Voxels in red show the areas of significant associations between an increase in radial diffusivity and a reduction in NHPT z-scores, overlaid onto the FSL fractional anisotropy template in MNI coordinates.

There was a significant inverse correlation between changes in z-PASAT and changes in RD in the left cingulum, in the left anterior thalamic radiation, in the body of the CC, in the inferior fronto-occipital fasciculus bilaterally, and in the left CST (Figure 6.5).

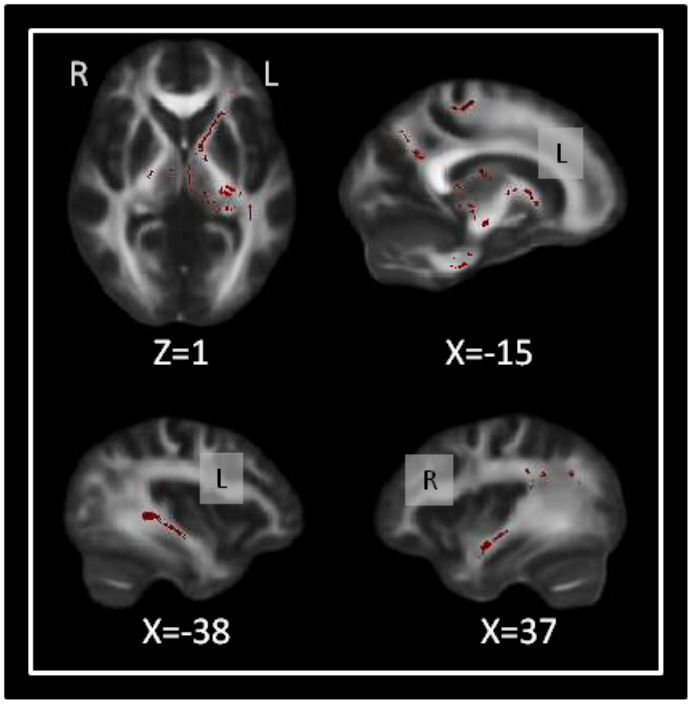

Figure 6.5: Voxels in red show areas of significant association between an increase in radial diffusivity and a reduction in PASAT z-scores, overlaid onto the FSL fractional anisotropy template in MNI coordinates.

In patients, a decrease in skeletonised MTR in the genu and the body of the CC, and in the superior part of the right CST (corona radiata) was significantly correlated with reduced upper limb function, as measured by the z-NHPT scores, over the follow-up period ($p<0.05$) (Figure 6.6). The decrease in MTR over one year was not significantly associated with changes in EDSS, in z-TWT or in z-PASAT.

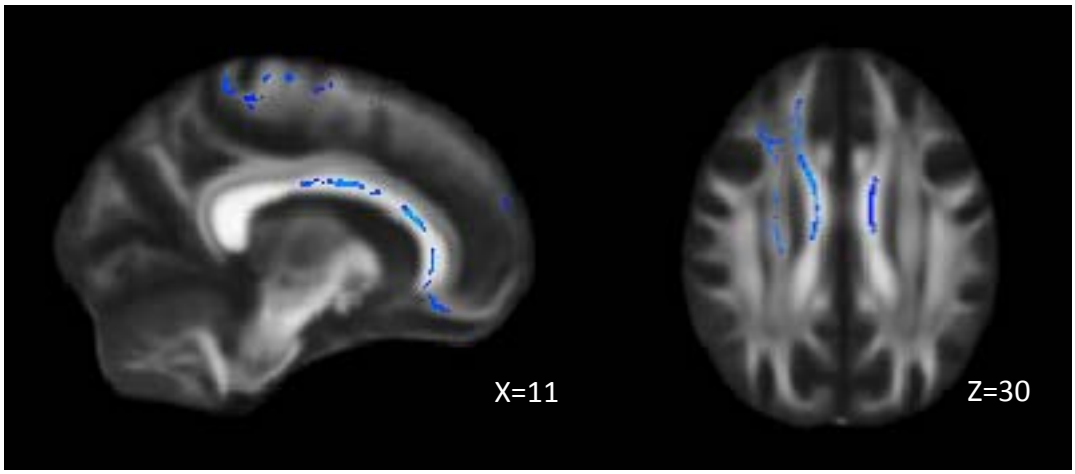

Figure 6.6:. Blue voxels indicate the areas of significant correlation between the decrease in skeletonised MTR over the follow-up period and the changes in upper limb function scores (z-NHPT). The map is overlaid onto the FSL fractional anisotropy template in MNI coordinates.

6.3.4 Post-hoc analysis

6.3.4.1 *The role of lesions*

The areas of significant change in MTR were localised in part within the "new/enlarged T2 lesions" which developed over the follow-up period, but also outside them, in the NAWM (Figure 6.7).

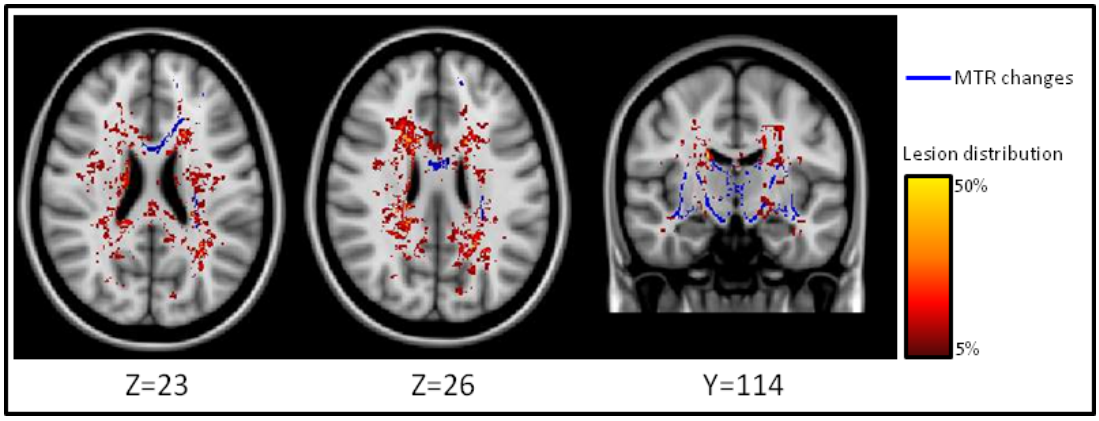

Figure 6.7: Significant MTR changes over one year (blue) and probabilistic distribution of new/enlarged lesions over the same follow-up period in the patient group (red-yellow). The red-yellow colour scale indicates the percentage of patients who developed a new/enlarged lesion in a given voxel. This figure shows that MTR changes were not confined to areas of new/enlarged lesions, but were also detectable in the NAWM, possibly through mechanisms of Wallerian degeneration. The maps are overlaid onto the FSL T1 template in MNI coordinates.

There was a significant correlation between the average MTR decrease over one year in the genu and the body of the CC, and in the superior part of the right CST, and the total T2 lesion load increase over the same follow-up period ($r=0.49$, $p<0.033$). This corresponds to an $r2=0.24$, i.e. the increase in T2 lesion load can explain 24% of the variance in MTR decrease in these brain areas.

6.3.4.2 *The role of total GM MTR*

No significant correlation was found between the changes in total GM MTR over one year and the changes in clinical scores during the same period.

6.3.4.3 *Correlation between FA changes and MTR decrease in regions that showed correlation between MTR changes and clinical function*

No significant correlation was found between the mean FA change and the mean MTR decrease extracted from the regions of significant association between changes in MTR and changes in z-NHPT scores (i.e., the genu and the body of the CC, and from the superior part of the right CST).

6.4 Discussion

In this study, a combination of MT imaging and TBSS has been employed for the first time to ”skeletonise” the MTR maps and explore tract-specific microstructural changes in the London cohort of patients with early PPMS, recruited within five years of symptom onset. Indeed, it is known that PPMS patients are particularly prone to show dynamic changes in their conditions in the early phase of the disease. This study shows a significant decrease in MTR along WM tracts, such as the CST, the CC, the SLF and the ILF over one year follow-up. RD (which is the average of the second and third eigenvalues of the DT) also significantly increased over time in similar regions, whilst AD (which is the principal eigenvalue of the DT) and FA did not change. These very early changes were localised within the NAWM and the new or enlarged lesions visible on T2-w scans, which developed over the same follow-up period. Moreover, this study showed that the significant decreases in MTR in the body and genu of the CC and the MTR decreases in the superior part of the CST correlated with a deterioration in the upper limb function occurring over one

year. Similarly, RD increases in several tracts, including the CC and the right CST (internal capsule) correlated with deterioration in the upper limb function.

As reported in Chapter II, the MT effect is generated by the interaction between protons localised in a relatively free environment and those whose motion is restricted (Tofts, 2003), and MT-based imaging has been proposed as a sensitive and reliable surrogate marker of myelin content (Filippi et al., 1998; Filippi, 1999; Zivadinov, 2007). Brain areas with low MTR values (reflecting reduced efficiency in the exchange of magnetisation occurring between macromolecules and the surrounding water molecules) have been shown to correlate strongly with pathological changes in MS (Deloire-Grassin et al., 2000; Chen et al., 2007; Chen et al., 2008). In particular, post-mortem analysis of MS has demonstrated that MTR is remarkably sensitive to myelin content, in addition to axonal loss (Schmierer et al., 2004; Moll et al., 2011).

Given its sensitivity to the degree of tissue damage, MTR has been acquired in all subtypes of MS to investigate pathological changes in vivo (Filippi and Agosta, 2010). To date, most of the assessments have been based on the histogram-based analysis of the whole brain (Filippi et al., 2000; Dehmeshki et al., 2001) or on the investigation of a priori selected regions of interest (ROIs), such as the normal-appearing WM (NAWM), NAGM,, tractography-selected WM tracts or user-defined anatomical masks (Filippi et al., 1998; Santos et al., 2002; De Stefano et al., 2006; Reich et al., 2007; Lin et al., 2008; Tur et al., 2011a). In several cross-sectional studies, these approaches demonstrated significant and clinically relevant abnormalities in the NAWM of patients with PPMS (Leary et al., 1999b; Tortorella et al., 2000b; Dehmeshki et al., 2003). A histogram-based approach has also been employed in longitudinal studies, which showed that normal-appearing brain tissues MTR at baseline predicted the deterioration of disability over time (Khaleeli et al., 2007a; Khaleeli et al., 2008a). However, there have been several attempts to develop an effective approach for performing a voxel-wise analysis of MTR images, assessing the GM compartment only or the whole brain (Audoin et al., 2007; Dwyer et al., 2009). The attractiveness of voxel-based approaches lies in the fact that they provide information about the sites of abnormality as a result of the analysis.

The steps involved in image normalization and smoothing, however, might compromise the accurate localization of changes.

In order to overcome some of these limitations, in this study a novel methodology has been proposed, that combines the sensitivity provided by MTR in detecting disease- related pathological changes with the accurate spatial information offered by TBSS. This technique allowed identification of early accrual of tract-specific microstructural abnormalities in PPMS, specifically affecting WM tracts involved in motor function control, such as the bilateral CST, the SLF and the ILF. Indeed, the CST is the main WM pathway controlling voluntary movements, whereas the SLF and the ILF are associative tracts that have been shown to play a key role in integrating multiple functions within the complex network system that controls the precise execution of fine movements. In particular, the SLF mediates the interaction between the parietal lobe and the motor and premotor areas, which are crucial in planning movement precision in space (Koch et al., 2010), whereas the ILF, connecting the occipital cortex with the temporal cortex, is thought to be involved in the use of visual information for the purpose of guiding movements and controlling motor actions (Schmahmann and Pandya, 2007). Moreover, a significant reduction in skeletonised MTR over the follow-up period was found in the genu and the body of the CC, where the WM fibres interconnecting motor and cognitive networks between the two hemispheres are localised. Indeed, the early disruption of the inter-hemispheric callosal pathways may result in a disconnection syndrome that contributes to long-term physical and cognitive disability. Also, in the cross-sectional study in this same patient cohort presented in Chapter III, patients showed a diffusively reduced FA compared with controls in the NAWM; the areas of significant FA decrease in patients at baseline included the bilateral CST, the CC, the thalamic radiations and the inferior longitudinal fasciculus, which are the same regions showing a further accrual of damage during the first year of follow-up. In the future it would be of interest to investigate whether there is a difference in the location and in the extent of the skeletonised MTR short-term changes between PPMS and relapse-onset MS, whose WM changes may be more related to the presence of lesions than PPMS.

Contrary to the MTR results, no significant FA changes were found over the 12 month follow-up. This suggests that MTR and FA offer complementary information when studying the evolution of brain diseases, since FA is sensitive to the detection of differences between patients and controls (as demonstrated in the study presented in Chapter III), whereas changes in MTR correlate with changes in clinical function over one year. The findings reported in this cohort of PPMS suggest that MTR is a more sensitive marker of disease progression in early PPMS than FA. Interestingly, when looking at changes in RD and AD over the same follow-up period, a significant increase in RD over one year was found in regions which overlapped with those found using MTR, although the MTR changes were more widespread, whilst no significant changes in AD were found. This suggests that the analysis of the directional diffusivities may reflect underlying pathological changes more accurately than FA, which is obtained by combining the three eigenvalues. The results of an interesting study which investigated the pathological correlates of quantitative MRI measures in MS brains study showed that, while both MTR and DTI changes significantly correlated with myelin integrity within T2-w visible lesions, in non-lesional WM they were correlated with activated microglia, but not with axonal or myelin integrity (Moll et al., 2011). Therefore, although it is tempting to suggest that the observed RD and MTR changes over one year reflect increased demyelination, at least inside WM lesions (Moll et al., 2011) and especially in view of the animals studies using directional diffusivities (Song et al., 2005) and post-mortem analysis (Schmierer et al., 2004), it is likely that other processes, including axonal loss and activated microglia, are reflected by in vivo RD and MTR changes (van Waesberghe et al., 1999; Cader et al., 2007; Zhang et al., 2009). As mentioned above, changes in MTR and RD were almost overlapping, which suggests that MTR probably does not allow the detection of specific pathological processes in the WM which are invisible to other currently available imaging measures. However, with this study it has been demonstrated the technical feasibility of combining TBSS with other imaging measures, which itself shows a great potential. Indeed, in future it will be possible to combine the accuracy in spatial location offered by TBSS with the pathological specificity offered by novel imaging techniques (such as [C-11] PIB, which has been

recently demonstrated to be highly accurate in detecting demyelination in MS) (Stankoff et al., 2011).

With respect to correlations between imaging and clinical changes, we found that changes in skeletonised MTR, RD, and AD in the CST and in the CC significantly correlated with the deterioration in upper limb function, as measured by the z-NHPT (Cutter et al., 1999). These results extend to the PPMS population the findings of correlation between altered diffusion metrics within the pyramidal tract and motor dysfunction previously demonstrated in CIS and RRMS (Wilson et al., 2003; Pagani et al., 2005a; Lin et al., 2007). Moreover, these findings support the key role played by the disruption of callosal fibres in mediating the functional impairment of fine motor control (Larson et al., 2002; Johansen-Berg et al., 2007; Bonzano et al., 2008; Kern et al., 2011), probably through a mechanism of reduced inhibitory input (Kern et al., 2011). In addition, RD increases in the inferior longitudinal fasciculus, uncinate fasciculus, thalamic radiations and cerebellar peduncle, correlated with a deterioration of the upper limb function. These data suggest that motor dysfunction may result from the damage to a complex network of systems in MS, including the visual-motor coordination system, in which is implicated the inferior longitudinal fasciculus (Catani et al., 2003), and the control system of fine-tuning of movements during motor execution, mediated by the cerebellar structures (Voogd, 2003). In future, studies employing the TBSS-MTR methodology in combination with scores aimed at assessing individual neurological functions, such as the pyramidal and sensory scores, may test system-specific hypotheses in MS.

In addition, a significant inverse correlation between changes in the z-PASAT score and changes in RD in the left cingulum, left anterior thalamic radiation, body of the CC, inferior fronto-occipital fasciculus bilaterally, and in the left CST, was demonstrated. The PASAT test is a complex working memory task involving several distinct brain areas that interact simultaneously, and is known to be heavily influenced by the disruption of connecting WM fibres in MS (Audoin et al., 2005).

On the other hand, no significant correlation between changes in total GM MTR and clinical changes over one year was demonstrated. This finding is in line with he results of previous studies on this same cohort of patients, which reported that while total GM MTR was shown to be a useful predictor of clinical progression over a long-term follow-up period (Tur et al., 2011a), WM MTR seemed to correlate better than GM MTR with short-term clinical changes (Khaleeli et al., 2007a).

Looking more closely at the results of this study, it is worth mentioning that significant changes in skeletonised MTR not only included areas of newly developed or enlarged WM lesions, but also regions of NAWM. In particular, T2-w lesion load increase over one year explained 24% of the variance in MTR decrease, suggesting that new/enlarging T2-w lesions are relevant for the observed MTR drop, although they are not the only factor. These results confirm data emerged in several studies conducted on all subtypes of MS that demonstrated the occurrence and the clinical relevance of the WM damage localised outside visible T2-w lesions when using other quantitative MRI techniques (Filippi and Agosta, 2010). In addition, these data showed the development of new T2-w lesions and the enlargement of pre-existing ones within the areas of significant and clinically eloquent changes in skeletonised MTR, suggesting that T2-w lesion load increase may contribute to the MTR decrease. This finding further underlines the already reported contribution of T2-w lesions to the occurrence of the clinically relevant WM abnormalities that are detected by changes in MTR (Vrenken et al., 2007).

A limitation of this study is that only 21 out of 50 patients included in the original cohort of 50 patients with early PPMS performed both DWI and MTR data at both baseline and one year and the lack of age- and gender-matched controls who performed the same protocol at the same time points. This limitation derives from analysis of data which were not originally acquired for the development of this specific methodology. Moreover, the differing slice thickness used for DTI and MT images should be considered as a limitation of this study, as it could potentially affect the co-registration between these images, thus compromising the accurate anatomical localisation based on

TBSS. However, in order to minimise these issues, the intra-subject co-registration was optimised by the use of a cost function known to work well for images of different contrasts, namely normalised mutual information. Finally, our results need to be confirmed by future studies employing more recent, and potentially more sensitive, diffusion data acquisition protocols.

6.5 Conclusions

In conclusion, using the 'skeletonised MTR' approach presented in this Chapter, it has been demonstrated the short-term accrual of microstructural damage in specific WM tracts that may contribute to clinical impairment in early PPMS. This study gave me also the opportunity to face the technical challenges of combining TBSS with a different imaging technique. Using a similar technical approach, the combination of the accurate spatial information provided by TBSS with the sensitivity of different imaging techniques (such as PET imaging) in detecting disease-related pathological changes, could offer the opportunity of new insights into the pathogenesis of progression in MS. This novel method could be applied in future to explore regional microstructural WM changes in cross-sectional and longitudinal studies in patients with other forms of MS, and with other neurological diseases. Moreover, the combination of 'skeletonised MTR' and voxel-wise measures of GM damage could be employed to explore the spatial and temporal relationship between the WM and the GM damage in MS as well as in other brain diseases.

Moving from the analysis of short-term pathological changes in PPMS, in the next Chapter I will address the second question of this thesis by investigating the contribution of early damage in WM and in GM to long-term clinical deterioration and cognitive dysfunction in this type of disease.

The relative contribution of WM and GM damage to long-term disability progression and cognitive dysfunction

Chapter VII

To complete the investigation on the impact of WM and GM damage on long-term clinical outcome in PPMS, trying to address the second question presented in Chapter I, this Chapter moves to exploring the relative contribution of the regional damage occurring in the two compartments in predicting long-term disability progression and cognitive dysfunction in patients with early PPMS. In the study presented here, the same techniques described in the study presented in Chapter III were applied, following-up the London population of early PPMS patients for five years.

7.1 Introduction

As discussed in Chapter I, quantitative MRI has the potential to provide prognostic indicators of clinical disability and cognitive dysfunction for patients with PPMS, whose disease course can vary widely (Cottrell et al., 1999; Tremlett et al., 2005; Koch et al., 2009). Over recent years, DTI and volumetric MRI techniques have been employed to establish the clinical relevance of in-vivo brain WM and GM abnormalities in MS (Bakshi et al., 2008). In particular, as previously discussed, FA has been extensively used to quantify the integrity of WM tracts in MS; a reduction of this measure implies demyelination, axonal loss and migroglia activation (Schmierer et al., 2004; Moll et al., 2011). Despite being a measure which is pathologically non-specific, FA has been shown to correlate significantly with cognitive scores in MS (Roosendaal et al., 2009) and predict motor impairment in RRMS (Kern et al., 2010). With regard to GM, the most commonly used measure is GM volume, which, if reduced, reflects irreversible tissue loss (or atrophy) (Wegner et al., 2006), and has been demonstrated to proceed relentlessly throughout the course of the disease (De Stefano et al., 2010) and to correlate with disability progression and cognitive performance in MS (Fisher et al., 2008; Riccitelli et al., 2011).

As discussed in Chapter II and Chapter III, several methods for detecting patient-control differences based on MRI parameters are available. TBSS (Smith et al., 2006) and VBM (Ashburner and Friston, 2000) are able to identify, respectively, WM regions of reduced FA and areas of GM atrophy in patients when compared with healthy controls.

The advantage of these two techniques is that they localise specific brain regions of WM damage and GM volume loss in patients compared with healthy controls without the need to generate an a priori hypothesis. In the cross-sectional study of patients with early PPMS (i.e. patients who were studied within 5 years of symptom onset) presented in the Chapter III of this thesis, these two techniques have been combined, and allowed to find a reduced FA in extensive WM regions including the whole corpus callosum and the cortico-spinal tracts in patients when compared with healthy controls, and a diffuse reduction of GM volume in patients, in areas such as the sensory-motor cortex bilaterally and the right superior temporal gyrus. In a subsequent longitudinal study in the same patient population, MTI histogram and volumetric analyses of WM and GM were employed, and allowed to demonstrate that WM lesion load is the most important predictor of subsequent cognitive dysfunction, but whole GM MTR also contributed (Penny et al., 2010). Despite evidence of damage in both tissue compartments, and of their role in the accumulation of disability, it is unknown whether the factors responsible for clinical progression in PPMS are the whole (diffuse) GM tissue pathology or abnormalities in specific GM and WM regions, above and beyond the contribution provided by WM lesion load. As discussed in Chapter I, this is an important question to address in order to understand the mechanisms underlying clinical deterioration, which is known to be quite variable in this type of MS.

In the study presented in this Chapter, the specific location of grey and WM areas was hypothesised to play a relevant role in predicting long-term physical and cognitive disability in patients with early PPMS. Therefore the same longitudinal dataset obtained in the London cohort of early PPMS patients was re-analysed, and TBSS and VBM techniques were employed, for the first time, to identify specific areas of WM and GM which predict progression of physical disability over five years and cognitive dysfunction after five years.

7.2 Methods

7.2.1 Study design

Thirty-two patients with PPMS (Thompson et al., 2000) within five years of symptom onset (13 women, mean age 44.5 yrs, SD 10.3) (see Table 7.1 for clinical, radiological and demographic characteristics) underwent a whole brain imaging protocol, including diffusion sequences, and were clinically assessed on the EDSS (Kurtzke, 1983) at study entry (see Appendix I).

After five years, they were again assessed on the EDSS and invited to undergo an extensive neuropsychological assessment, which was also performed on a group of healthy controls.

Characteristics	
Number	32
Age, years (mean (SD))	44.5 (10.3)
Gender, female/male	13/19
Disease duration, years (mean (SD))	3.3 (0.9)
EDSS, median (range)	4.5 (1.5-4.5)
T2 lesion load, ml, (mean (SD))	23.5 (17.3)
Years of education*, (mean (SD))	13 (2.9)
Premorbid IQ*, (mean (SD))	109.4 (9.6)

•values calculated on the subgroup of 25 patients who underwent the neuropsychological testing at five years

Table 7.1 Patients' clinical, radiological and demographic characteristics at baseline.

7.2.2 Neuropsychological assessment

Out of 32 patients recruited at baseline, 25 (11 women, mean age 51.3 years, (range 31-68), mean years of education 13.0 (range 10-19)) underwent an extensive neuropsychological assessment five years after entry into the study. Out of the seven patients who were not cognitively assessed, four male patients were too physically impaired (they were very dysarthric and ataxic) to provide valid results for a significant proportion of the tests, and therefore were excluded; one female and one male patient declined to take part in the neuropsychological tests. The remaining female patient was not contactable.

Thirty-one age- and gender-matched healthy controls (14 women, mean age 48.9 years, (range 30-65), mean years of education 13.4 (range 10-19)) also underwent the same neuropsychological tests. The exclusion criterion applied to all subjects was a history of other neurological or systemic illness, of impaired cognition, of psychiatric illness, of head injury resulting in loss of consciousness, or of alcohol or drug abuse.

The cognitive assessment included the following tests: (i) the National Adult Reading Test (NART) (Nelson HE, 1982) to estimate each patient's premorbid intellectual functioning; (ii) the immediate and delayed conditions of the Story (SRT) and Figure Recall (FRT) subtests of the Adult Memory and Information Processing Battery (Coughlan AK and Hollows AK, 1985), to assess verbal and visual recall memory function; (iii) the Paced Auditory Serial Addition Test (3-second version) (PASAT-3) (Cutter et al., 1999) and the Symbol Digit Modalities Test (SDMT) (Smith A, 1982), to evaluate attention and speed of information processing; (iv) the Hayling Sentence Completion Task (HSCT) (Burgess PW and Shallice T, 1997) a test of verbal response generation and inhibition, and the Brixton Spatial Anticipation Test (Burgess PW and Shallice T, 1997), a spatial reasoning, rule detection and rule change task, to test executive functions. The whole neuropsychological assessment of both patients and controls was performed by an experienced neuropsychologist (S.P.).

Patients had not previously received any of these tests with the exception of the PASAT, which had been administered up to seven times in earlier follow-ups.
This study was approved by the Joint Medical Ethics Committee of the National Hospital for Neurology and Neurosurgery, London. Written and informed consent was obtained from all participants.

7.2.3 Processing of clinical and cognitive data

Analysis was performed using Stata version 9.2 (Stata Corporation, College Station, Texas) and results with a $p<0.05$ were considered significant.

Significant changes in EDSS between baseline and five years were assessed using the Wilcoxon Signed Ranks Test. Since the EDSS is an ordinal (non-continuous scale), parametrical statistical methods cannot be used to analyze changes in the EDSS score, and, for this reason, the mean raw change in the EDSS score is considered to be an inappropriate statistical endpoint (Wingerchuk et al., 1997). In addition, it is important to underline that the meaning of the changes in EDSS is not equivalent throughout the scale. For example, the difference between EDSS 0.5 and 1.0 is 0.5, as well as the difference between EDSS 6.0 and 6.5 is 0.5; however, this 0.5 difference does not reflect the same extent of clinical deterioration. Finally, there is a variable mean duration at different EDSS levels, as the frequency of progression is usually lower at higher levels of disability on the EDSS than at lower levels (Weinshenker et al., 1991). Therefore, to assess disability progression over the follow-up period, the recommendation to calculate the EDSS step-change in each patient was followed: one step deterioration on the scale was defined as an increase of 1 if the baseline EDSS was less than or equal to 5, or an increase of 0.5 if it was greater than 5. This approach is more sensitive in detecting significant clinical deterioration in the upper part of the scale (i.e., in more disabled patients), and has also been recommended for clinical trials (Wingerchuk et al., 1997).

As far as the neuropsychological scores are concerned, the raw scores of all the measures, except premorbid IQ, were converted to z-scores referenced to

the control group, and these multiplied by -1 when appropriate, so that a lower score always indicated a poorer performance. A z-score ≤ -2 in a test was considered to be abnormal. Age, years of education and premorbid IQ were compared between patients and healthy controls using t-tests; gender was compared between groups using a chi-square test.

To investigate the difference in cognitive performance between patients and healthy controls, a multiple linear regression model was used, entering each cognitive measure, in turn, as dependent variable, and a binary group indicator, together with age, gender, years of education and premorbid IQ, as covariates. Since the primary goal of this study was to identify predictors of cognitive dysfunction, only the neuropsychological test scores that showed a significant difference between patients and healthy controls, or a trend towards a difference ($p<0.08$), were entered in the subsequent steps of the analysis.

Differences between male and female patients in EDSS scores at five years and in all neuropsychological tests scores were also tested for, using Mann-Whitney test and independent samples t tests, respectively.

7.2.4 Image acquisition and post-processing

Patients were imaged at study entry using a 1.5T GE Signa scanner (General Electrics, Milwaukee, IL). The MRI protocol, which included fast spin echo scans, Diffusion-Weighted Echo Planar Imaging and T1 volumetric sequences (SPGR), and imaging analysis to obtain a TBSS skeleton were described in Chapter III.

In this study, the SPGR volumes were segmented and normalized to obtain GM, WM and cerebro-spinal fluid volumes using SPM8 software (Wellcome Department of Cognitive Neurology, London, UK), according to the VBM protocol (Ashburner and Friston, 2005). As the presence of WM lesions is known to significantly affect brain segmentation (Nakamura and Fisher, 2009) and registration (Sdika and Pelletier, 2009), which are key steps in VBM, the recently developed lesion automated preprocessing (lesion automated

preprocessing, LEAP) (Chard et al., 2010) technique was applied to the T1w images, before feeding them into the VBM procedure. As described in detail in Chapter II, LEAP is an “in-painting” technique, which replaces lesional voxels with values derived from the intensity distribution within the WM outside visible lesions in the presegmentation phase (Chard et al., 2010). This technique minimises lesion-associated segmentation biases that may significantly affect VBM results. As the smoothing kernel sensitises the analysis to differences of comparable size as the kernel (Rosenfeld and Kak, 1982) GM images were modulated and smoothed using both 12-mm FWHM and 8-mm FWHM Gaussian kernels.

7.2.5 Investigation of predictors of physical deterioration and cognitive dysfunction

7.2.5.1 *White matter FA analysis*

To investigate whether FA was associated with EDSS step-change and neuropsychological tests scores, a voxel-wise linear regression analysis was performed, adjusting for age, gender, years of education and NART (the last two variables were used only when predicting neuropsychological scores). As mentioned above, only tests that identified abnormality in patients compared with healthy controls were used. The analysis was based on permutation-based inference, and corrected for multiple comparisons using Threshold-Free Cluster Enhancement (TFCE) ($p<0.05$) (Smith and Nichols, 2009).

To investigate the effect of gender on significant findings, the voxel-wise linear regression analysis was repeated by modelling the interaction between gender (male or female) and each clinical and neuropsychological score, using permutation-based inference, and correcting for multiple comparisons using TFCE ($p<0.05$).

In order to understand the contribution of WM lesions to the results, where significant associations were found between baseline FA and clinical /neuropsychological variable, the regression analysis was repeated by including, in turn, the total LL and the tract-specific LL, as additional covariate.

This tract-specific LL was calculated by using the Johns Hopkins University (JHU) DTI-based white matter atlas, provided by FSL (Mori, 2005), which provides a probabilistic reconstruction of the main WM tracts. Each subject's T2-w scan was co-registered with the atlas, and the same transformation was applied to the lesion mask. Lesions belonging to a specific tract were identified to obtain the tract-specific LL.

7.2.5.2 *Grey matter volumetric analysis*

A voxel-wise multiple regression analysis was used to investigate the association between regional GM volume and EDSS step-change and neuropsychological tests, adjusting for the same variables as those used for TBSS, and correcting for multiple comparisons with family-wise error rate. P-values<0.05 were considered to be significant.

7.3 Results

7.3.1 Patients' clinical and neuropsychological assessment

Patients showed progression of disability on the EDSS during the follow-up period (median EDSS at baseline= 4.5 (range 1.5-4.5), at five years= 6.4 (range 1.5-9), p=0.001).

There were no significant differences between patients and healthy controls in age, gender, years of education or premorbid IQ. The neuropsychological test results, the number of patients who failed on each test, and the comparison between patient and control groups in all tests are summarised in Table 7.2, and have been previously reported in detail (Penny et al., 2010).

Eighteen patients had abnormal scores on at least one test (six patients failed on one test only, six on two tests, and six on three or more tests). The neuropsychological tests on which patients performed significantly worse than healthy controls, and which were therefore retained for the subsequent part of the analysis, were the immediate and delayed Story Recall tests (SRT) and Figure Recall tests, the SDMT, and the HSCT.

There was no significant difference between male and female patients in EDSS scores at five years, and in all neuropsychological tests scores.

Clinical and neuropsych. score at follow-up	No. of voxels per significant white matter cluster	MNI Atlas coordinates x, y, z	Significant regions	p value
Immediate Story Recall Test	6025	106, 82, 80	Splenium of CC	P=0.003
	1084	74, 171, 59	Anterior part of genu of CC	
Delayed Story Recall Test	4471	105, 84, 80	Splenium of CC	P=0.003
	2466	69, 173, 71	Anterior part of right thalamic radiation and genu of CC	
	651	103, 112, 105	Body of CC	
Symbol Digit Modalities Test	2265	94, 104, 97	Body of CC	P=0.05
	86	99, 84, 86	Splenium of CC	
Hayling Sentence Completion Task	1065	76, 161, 84	Genu of CC	P=0.003
	873	56, 80, 102	Right posterior corona radiata	
	456	107, 71, 121	Left posterior corona radiata	
	243	91, 135, 95	Body of CC	
	177	78, 122, 100	Body of CC	

Table 7.2 Neuropsychological test results and comparisons of patient and control groups.

7.3.1 White matter FA as predictor

When looking for a significant association between FA across the whole skeleton and disability progression, a lower baseline FA in the splenium of the corpus callosum (CC) was found to be associated with greater progression of disability over five years, as measured by the EDSS step-change (MNI coordinates, x=83, y-90, z=92, no. voxels= 8307, $p<0.05$) (Figure 7.1).

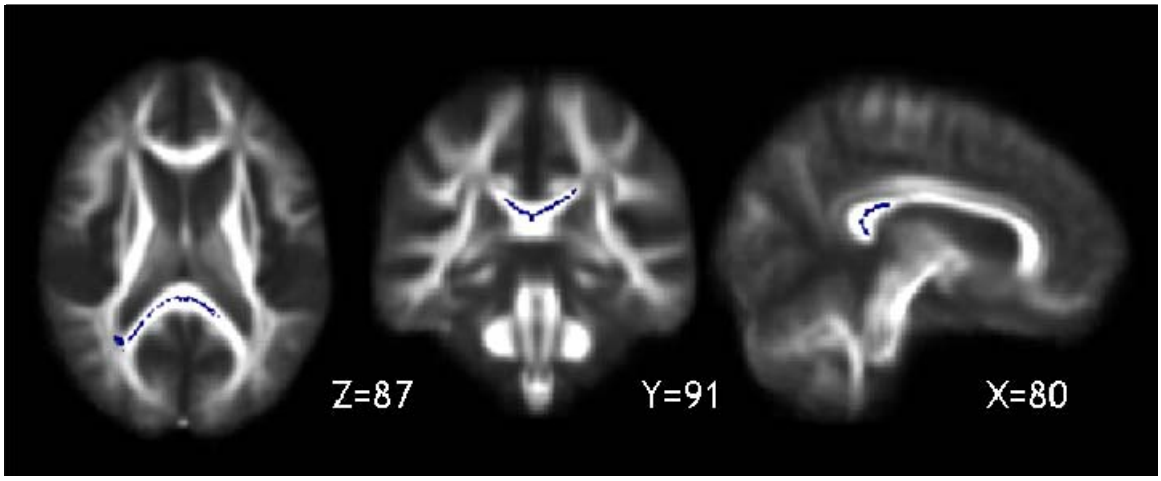

Figure 7.1 The callosal regions along the TBSS skeleton, whose FA at study entry was associated with progression of physical disability over 5 years, are shown in blue and overlaid onto the patients' mean FA image ($p<0.05$).

With regard to the prediction of cognitive dysfunction, the strongest (and most consistent) association between lower FA at baseline and worse cognitive performance at five years was found in the CC (see Table 7.3 for cluster sizes and coordinates).

In particular:

(i) lower FA in the splenium and genu of the CC was associated with worse immediate verbal memory function, as measured by the immediate SRT ($p=0.003$) (Figure 7.2 A);

(ii) lower FA in the splenium, body and genu of the CC (with extension into the right thalamic radiation) was associated with worse delayed verbal memory function, as measured by the delayed SRT ($p=0.003$);

(iii) lower FA in the body and splenium of the CC was associated with worse attention and speed of information processing, as measured by the SDMT ($p<0.05$) (Figure 7.2 B);

(iv) lower FA in the genu and body of the CC (and in the bilateral corona radiata) was associated with worse executive functions, as measured by the HSCT ($p=0.003$) (Figure 7.2 C).

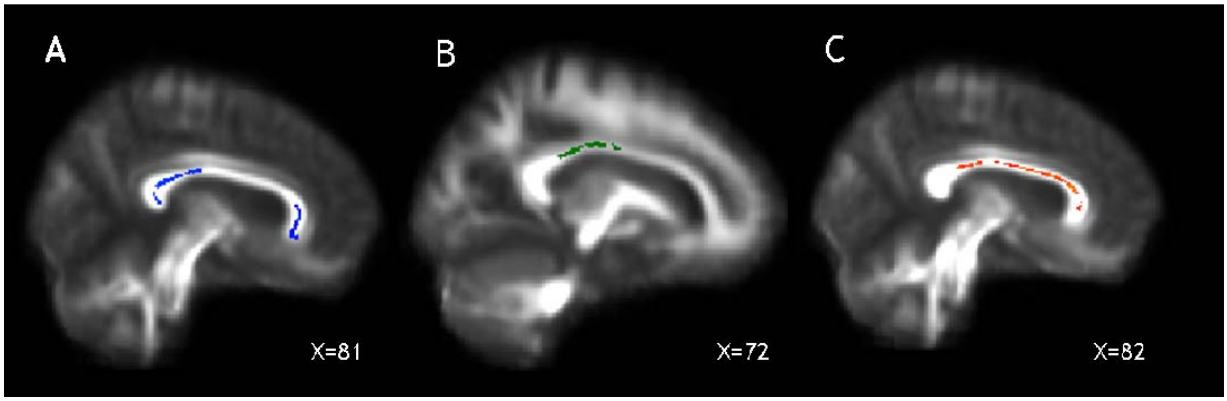

Figure 7.2 Association between FA values at study entry and cognitive scores at five years. The callosal areas, whose FA at study entry were associated with immediate verbal memory scores (as measured by SRT, $p<0.003$), are shown in blue (A), those predicting attention and speed of information processing scores (SDMT, $p<0.05$) at five years in green (B), and those whose FA was associated with executive function scores (as measured by HSCT, $p<0.003$) are shown in red (C), and overlaid onto the patients' mean FA image.

When less stringent thresholds for significance were used ($p<0.05$), associations between FA and the immediate and delayed SRT and HSCT were also found in multiple areas of the skeleton, including the frontal and parietal WM (Figure 7.3), and the brainstem.

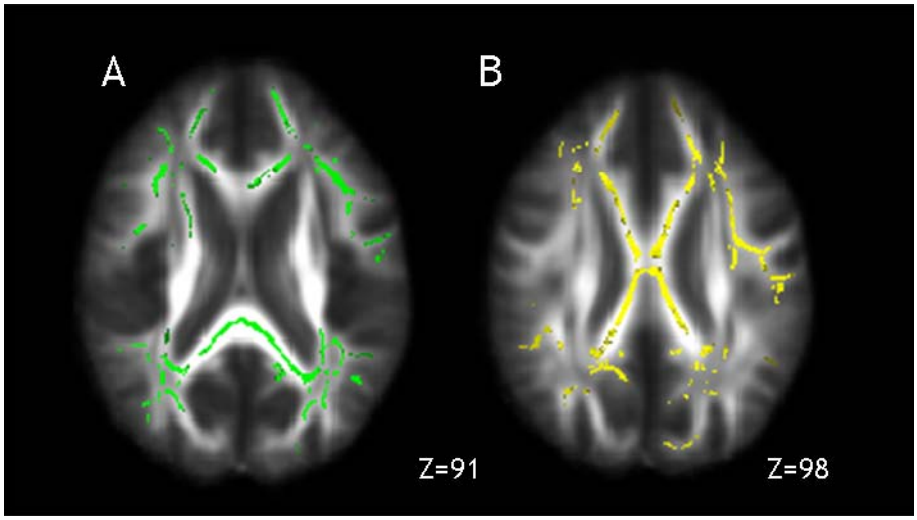

Figure 7.3 White matter regions showing an association between lower baseline FA and immediate SRT (voxels in green, A) and HSCT (voxels in yellow, B) scores at five years, when a threshold for significance of $p<0.05$ was used (results overlaid onto patients' mean FA).

No significant gender-related differences in the EDSS and neuropsychological tests at five years were seen; no significant interactions between gender and EDSS or neuropsychological score were found.

7.3.2 Contribution of WM lesions

When repeating the analyses adjusting for total LL, the association between lower FA in the genu and body of the CC and the executive functions (HSCT) at five years remained significant ($p<0.05$), whilst the associations between FA and disability progression and the performance on immediate and delayed verbal memory tests (SRT) and attention and speed of information processing (SDMT) did not.

The mean volume of lesions localised in the CC (the region that showed the strongest association with clinical and neuropsychological variables) was 1.3 cc (SD1.47). When repeating the analyses adjusting for this CC lesion load, FA in the splenium of the CC no longer predicted disability progression, and lower FA in the splenium and body of the CC no longer predicted a poorer performance in attention and speed of information processing (SDMT).

By contrast, the FA of the splenium of the CC at study entry remained significantly associated with a worse performance on immediate and delayed verbal memory tests (SRT) ($p<0.05$), and the FA of the body of the CC was associated with a poorer performance on a test of executive function (HSCT) ($p<0.05$) (Figure 7.4) at five years.

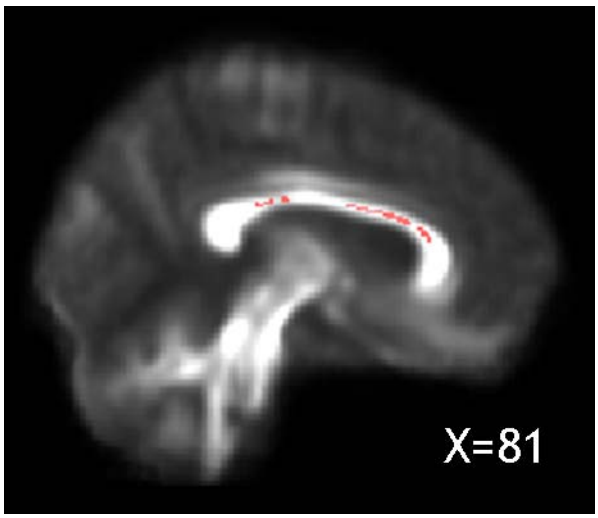

Figure 7.4 The callosal area, whose FA at baseline significantly correlated with executive function scores (HSCT) at five years, after adjusting for corpus callosum T2 lesion load, is displayed in pink ($p<0.05$) and overlaid onto the patients' mean FA image.

7.3.3 Grey matter volume as predictor

Baseline GM volume did not significantly predict EDSS step-change or any cognitive impairment at 5 years (with either 8-mm or 12-mm FWHM smoothing Kernel).

7.4 Discussion

In the study presented in this Chapter, a combination of TBSS and VBM (after a lesion filling procedure) was applied to the baseline FA and volumetric scans of patients with early PPMS. The reported data showed that the baseline FA of the CC, previously shown to be reduced in the same cohort of patients compared to that of healthy controls (see data shown in Chapter III), was significantly associated with long-term progression of physical disability, as measured by the EDSS step-change, and the occurrence of cognitive dysfunction at five years, in the domains of immediate and delayed verbal memory, executive function, and attention and speed of information processing, where patients performed significantly worse than controls. These findings were interpreted as indicative that lower CC FA at baseline was a predictor of both disability progression and cognitive dysfunction at five years. Future studies will address the question

whether CC FA is also relevant to the progression of cognitive impairment, which has been reported in MS (Langdon, 2011).

The CC ensures effective communication between motor and cognitive networks in the two brain hemispheres (Bogen et al., 1965); in particular, the anterior parts of the CC (rostrum and genu) connect the orbitofrontal, lateral and medial frontal cortices, whereas the body and splenium connect parietal, temporal and occipital homotopic regions (Abe et al., 2004). The primary motor cortices, necessary for performing highly skilled motor movements, and several premotor areas, involved together with the supplementary motor areas in the initiation, planning and regulation of movement, are connected between hemispheres through the CC (Chao et al., 2009). The disconnection of these motor networks has been shown to result in a deterioration of motor function and upper limb function (Ozturk et al., 2010; Kern et al., 2010; Srikanth et al., 2010). In our cohort, it was found that lower FA in the splenium of the CC predicted the accumulation of motor disability over the follow-up period and, similarly, the raw EDSS at five years ($p=0.02$; results not shown). The splenium of the CC is known to interconnect temporal and occipital cortices (Park et al., 2008), mainly underlying the transfer of auditory and visual information. However, the connections between its superior segment and Brodmann's area 5 (Chao et al., 2009), that is implicated in the earliest stages of sophisticated movement planning (Andersen and Buneo, 2002), could explain why its early damage predicts long-term disability progression in our patients.

Furthermore, the correlation found between a lower baseline FA of the CC and a worse cognitive performance at five years, extends previous findings on the relevant role of the CC in ensuring effective interhemispheric cooperation, which is necessary to perform cognitive tasks that require the activation of cortical areas in both hemispheres. In particular, considerable evidence from functional neuroimaging studies showed that bilateral temporo-parietal cortices are implicated in performing episodic memory tests (Buckner and Wheeler, 2001; Rugg et al., 2002), and that complex tasks, such as those related to attention/speed of information processing, and executive function, require bilateral frontal and parietal involvement (Gazzaniga, 2005; Buchsbaum et al.,

2005). Evidence from several cross-sectional studies investigating different subject populations supports the findings reported here (Jokinen et al., 2007; Roosendaal et al., 2009; Voineskos et al., 2012). For example, a reduction in the white matter integrity of the splenium correlated with worse age-related memory and executive function in a sample of 53 healthy subjects (Voineskos et al., 2010), and atrophy of the CC fibres correlated with poor performance in tests assessing speed of mental processing, and attention and executive functions, in patients with age-related white-matter hyperintensities (Jokinen et al., 2007).

Cross-sectional studies have demonstrated that tissue damage localised in the CC plays a role in contributing to concurrent motor disability and cognitive dysfunction in different phenotypes of MS (Mesaros et al., 2009; Roosendaal et al., 2009; Ozturk et al., 2010; Kern et al., 2011). The data presented here extend these results by demonstrating that CC damage has an important role in predicting long-term disability. The underlying mechanism may be the occurrence of a disconnection syndrome (He et al., 2009), whereby damage to structural connectivity (either through focal lesions or normal appearing white matter (NAWM) pathology) may, in turn, lead to an altered functional connectivity between GM regions and, ultimately, to clinical impairment and cognitive dysfunction in MS (Dineen et al., 2009). The possibility of a disconnection syndrome is further supported by the findings that, when lower thresholds for significance were used for the analysis, the association between FA and cognitive performance on immediate and delayed verbal memory tests (SRT) and executive functions (HSCT) was found to extend to multiple regions of the skeleton, including frontal, temporal and parietal WM, which are regions involved in memory (Buckner and Wheeler, 2001; Rugg et al., 2002) and executive function (Gazzaniga, 2005). The finding of significant association between FA of the brainstem and executive function suggests that the disruption to brain stem-hemisphere interactions may further contribute to the disconnection syndrome, in agreement with reports of cognitive dysfunction in patients with isolated brain stem insult (Garrard et al., 2002).

When the association between FA and cognitive performance was corrected for

total lesion load, FA in the genu and body of the corpus callosum remained significantly associated with performance on a executive function test (HSCT); similarly, FA of the body of the CC still predicted performance on the HSCT when adjusting for callosal lesion load (LL). Whilst the association between genu FA and executive function is expected to remain significant despite correction for the total LL, the association between more posterior portions of the CC and the performance on the HSCT is less obvious. The HSCT score is determined to some extent by general speed, and involves verbal processing and word generation. These cognitive functions require an effective interhemispheric connection between temporal and parietal cortical areas that are connected through more posterior regions of the CC. When adjusting for callosal LL, FA in the splenium of the CC predicted performance on immediate and delayed verbal memory tests (SRT), confirming that the reduced integrity of posterior callosal regions is linked to verbal memory dysfunction independently of local lesions. Overall, this persistence of significant correlations between FA and cognitive performance after corrections for LL supports the important role played by the normal-appearing WM (NAWM) damage in contributing to cognitive dysfunction in MS (Mesaros et al., 2009); as previously hypothesised, the injury to the NAWM of the CC may result from a degeneration of axons transected in local T2 lesions and distal lesions whose related fibres cross the CC, through a mechanism of Wallerian degeneration (Coombs et al., 2004; Mesaros et al., 2009; Dziedzic et al., 2010). However, as discussed in Chapter IV, the contribution of grey matter injury and primary damage to axons (i.e., primary axonopathy) (Geurts et al., 2010) to axonal degeneration in the NAWM has yet to be conclusively established.

In a previously published work on this same cohort, where the whole WM and GM matter histogram metrics and volumes were analysed with a traditional approach, it was found that whole brain GM MTR predicted the PASAT score, whereas whole brain GM and WM volume predicted performance on the Brixton test (Penny et al., 2010). Here, the scores on both the PASAT and the Brixton have been excluded from the analysis, as they did not differ significantly between patients and healthy controls. Rather surprisingly, in the present study, no GM region significantly predicted clinical outcome, when using a VBM

approach. Since the extent of the areas being investigated is in principal unknown, two different smoothing kernels were used, but the results were consistently negative. As discussed previously, the pathological correlates of GM atrophy are still unclear, and may reflect demyelination, loss of dendrites, axons, and synapses, possibly in combination. Even in early PPMS patients, GM atrophy has been identified in the pre- and post-central gyri, and in the temporal cortex, and this has been reported to be relevant for concurrent clinical disability (Khaleeli et al., 2007b; Bodini et al., 2009).

The lack of correlation between GM atrophy and disability progression is in contrast with the results of other studies, performed on patients with other forms of MS (Jasperse et al., 2007). This could be a consequence of the regional distribution of atrophy in PPMS, which seems to differ from the pattern described in other forms of MS when using VBM (Ceccarelli et al., 2008). This difference in regional distribution of atrophic GM areas could perhaps help to explain the lack of significant association between regional GM volumes at baseline and long-term clinical outcomes in the London cohort of PPMS. Moreover, in RRMS, it has been reported a significant correlation between early changes in regional GM volume and clinical outcome (Jasperse et al., 2007). It is possible that looking at regional changes in GM volume, rather than using baseline regional GM volumes only, could prove more useful in finding significant correlations with long-term clinical outcomes.

Finally, when investigating potential predictive measures of clinical outcome, MRI measures other than GM volume, for example those able to explore the microstructural damage occurring in the early stage of the disease, such as MTR, or sequences that allow detection of GM lesions, may provide significant results.

From a technical point of view, in this work a novel approach was employed to remove lesion-related segmentation bias before VBM. Preliminary results of the applications of this method shows that without region filling the GM volume is in general overestimated (because the WM lesions have signal intensity similar to that of the cortex) (Chard et al., 2010). Therefore, the application of this method

should ensure that the segmented GM does not include the lesional tissue.

7.5 Conclusions

In conclusion, in this study the relative contribution of WM and GM damage to long-term disability in PPMS has been established, and with the data presented in this Chapter the answer to the second question of this thesis has been completed. In particular, it has been demonstrated that WM damage localised in the CC, both in terms of WM lesions and NAWM, is a relevant determinant of progression of motor disability and future cognitive dysfunction, while GM regional damage may not be as important. Furthermore, it is possible to propose the disconnection of relevant brain regions as a potential mechanism underlying clinical progression in MS. However, it may be important to mention that two different regional measures of damage in the WM and in the GM were employed in this study: in the first case we used FA, while in the case of GM we looked at atrophy, and this relevant difference in the predicting measures may explain the surprising lack of predictive value of GM metrics on motor and cognitive disability in the results of this study. As a more general consideration, the prediction of cognition impairment overall (which can result from the damage to multiple brain areas) by the use of regional measures (which also differ for WM and GM in the case of this study, as mentioned above) is challenging and could potentially provide misleading results. These limitations should be taken into account in the interpretation of the data presented in this study.

Conclusions and future directions

Chapter VIII

In this final Chapter, the conclusions drawn from all the studies presented in this thesis will be summarised, and the answer to the two key questions proposed in Chapter one will be provided; finally, future research perspectives that could originate from the results reported in this thesis will be presented.

8.1 The answer to the two key questions on PPMS

(1) Is there is a *spatial* and *temporal* link between the pathological processes occurring in the NAWM and in the GM of patients with PPMS? In other words, is GM damage secondary to axonal degeneration and demyelination in connected WM tracts or alternatively, does it represents the initial target of the disease process that leads to subsequent axonal degeneration in the WM?

With regard to the spatial link between the pathological processes occurring in the NAWM and in the GM of patients with early PPMS, the study presented in Chapter III showed that NAWM damage (as detected by DTI) and GM atrophy in adjacent areas are interdependent in some specific and clinically eloquent brain regions. These data suggest that there might be a *spatial* link between the mechanisms of damage occurring in the two compartments in the early phase of progression. However, another possible interpretation of the presented results is that the pathological processes affecting the two compartments develop independently of each other (as suggested by the evidence in our data of NAWM regions where a significant difference between patients and controls was found, which was not paralleled by significant changes affecting the connected GM areas, and viceversa) reaching a similar (correlated) degree of damage in few areas of the brain.

In the study presented in Chapter IV, the temporal sequence of the pathological processes affecting NAWM and GM in early PPMS was explored. The results presented in this thesis may suggest that, at least in the early phase of clinical progression in this subtype of disease, the tract NAWM could represent the initial target of the disease, as described by the “primary WM damage model”. I showed that microstructural damage affecting the NAWM, as reflected by MTR,

precedes and predicts that occurring in the connected cortical areas. However, it is noteworthy to underline the limitations of the hypothesis-driven approach employed in this study to test the “primary WM damage” and the “primary GM damage” models. In particular, the presented results could simply reflect the temporal sequence of the pathological events affecting the two compartments, and they do not imply any causal relationship between them. Secondly, this study does not exclude the possibility that MS is a “whole brain disease”, where WM and GM are affected independently of each other, or where both the two models (“primary WM damage” and “primary GM damage”) are valid and can accurately describe the temporal sequence of events, each one possibly prevailing on the other at different stages of disease and/or in different brain areas.

(2) Which regions of WM abnormalities (within lesions and NAWM) and GM damage significantly contribute to clinical progression and cognitive deterioration?

To answer this question, I first looked at the role of WM lesions, in the study presented in Chapter V, which was conducted in patients with well-established PPMS who were followed-up for ten years in five different centres. The focal WM damage localised in motor and associative tracts (the cortico-spinal tract , the bilateral superior longitudinal fasciculus, and the right inferior longitudinal fasciculus) was found to be the major determinant of clinical progression, independent of spinal cord atrophy.

In the study presented in Chapter VI, where changes in WM tracts over one year were investigated, I showed that the short-term accrual of microstructural damage in specific WM tracts, such as the cortico-spinal tract, the corpus callosum, and the superior and inferior longitudinal fasciculus may contribute to clinical impairment in early PPMS. In the study presented in Chapter VII, I moved onto examining the relative contribution of WM and GM damage to long-term motor and cognitive disability in PPMS. I demonstrated that WM damage localised in the corpus callosum, both in terms of lesions and NAWM, is a relevant determinant of progression of motor disability and future cognitive

dysfunction, while GM regional damage may not be as important. However, it may be important to mention that two different regional measures of damage in the WM and in the GM were employed in this study: in the first case we used FA, while in the case of GM we looked at atrophy, and this relevant difference in the predicting measures may explain the surprising lack of predictive value of GM metrics on motor and cognitive disability in the results of this study. As a more general consideration, the prediction of cognition impairment overall (which can result from the damage to multiple brain areas) by the use of regional measures (which also differ for WM and GM in the case of this study, as mentioned above) is challenging and could potentially provide misleading results. These limitations should be taken into account in the interpretation of the data presented in this study.

In conclusion, the answer to the second question of this thesis is that the WM damage plays a key role in contributing to motor and cognitive impairment in patients with PPMS and that this appears to be more significant than the pathology in GM regions. In particular, damage to strategic WM regions (both in terms of lesional change, and abnormalities affecting the NAWM), such as the cortico-spinal tract, the corpus callosum, and the associative tracts, could be a major determinant of short- and long-term clinical progression in patients with this type of disease. It is therefore possible that the mechanisms underlying clinical progression in PPMS include the damage in WM tracts, which are essential for ensuring the normal neurological functions of the body (such as the cortico-spinal tract for the motor function). Additionally, the structural disconnection of relevant brain regions may, in turn, result in an abnormal functional connectivity between GM regions and, ultimately, lead to motor and cognitive impairment in PPMS.

8.2 Future directions

A recent international initiative, the International Collaborative in Progressive MS, has highlighted the needs of developing an effective strategy to improve the treatments of patients with progressive MS. This strategy includes five keys areas and biomarkers discovery is one of them. The studies presented in this

thesis show that novel imaging techniques have the potential to serve as biomarkers and to improve our understanding of the pathogenesis of progression, which is a key step in the development of new opportunities for therapeutic intervention. Therefore, to continue along the strategy lines proposed by the International Collaborative in Progressive MS, I would propose the following research projects.

Firstly, it would be very important to move from the results presented in Chapter III, combining the "skeletonized MTR" method described in Chapter VI with novel methods to explore regional GM volume changes, such as Tensor Based Morphometry (TBM) (Friston et al., 2006), to investigate whether the spatial relationship between WM microstructural damage and GM abnormalities in PPMS changes over time.

Moreover, it would be extremely interesting to explore whether the "primary WM damage model" presented in Chapter IV, which seems to describe accurately the temporal sequence of pathological events in PPMS, proves valuable in describing the sequence of events in other forms of demyelinating disease, such as CIS and RRMS. Should this be the case, it will be of considerable interest to establish the relative contribution of WM lesions and NAWM damage in determining GM pathology in the other forms of disease.

The results presented in Chapter V and Chapter VII, where specific locations of WM damage were demonstrated to be major determinants of long-term motor and cognitive disability in PPMS, offer the opportunity to investigate further the MRI prognostic factors identified in this thesis, in the attempt to extrapolate the results shown here to individual cases. To this aim, lesion load in the cortico-spinal tract, the bilateral superior longitudinal fasciculus, and the right inferior longitudinal fasciculus, as well as diffusion metrics in the corpus callosum, should be included in the MRI features used to train Support Vector Machines (SVMs), an innovative computer-based technology which can be applied to associate MRI features with clinical outcomes on an individual basis (Ciccarelli et al., 2012). This research field could lead to an accurate individual prognosis in patients with PPMS, which would be extremely important for appropriate risk

stratification when designing clinical trials for this form of disease.

Moreover, to further explore the pathological processes leading to clinical progression in PPMS, it would be very interesting to replicate the data presented in this thesis using imaging measures which could be more pathologically specific than MTR or diffusion-derived parameters. To this aim, a great opportunity is offered by molecular imaging with Positron Emission Tomography (PET), which allows directly marking and therefore quantifying specific components of the central nervous system, such as the myelin (Stankoff et al., 2011). Combining PET with advanced MRI imaging could offer the unique opportunity to understand in further detail the mechanisms underlying clinical progression in PPMS.

Finally, another major challenge which has to be faced in the investigation of the pathogenesis of PPMS, as well as in the identification of relevant prognostic factors of future motor and cognitive progression in this group of patients, is the quantitative assessment in vivo of spinal cord damage. Indeed, novel technical approaches in the field of spinal cord imaging, such as the use of combined glutamate-glutamine spectroscopy, or the integration of accurate quantification of DTI and MTR measures, have the potential to explore in further detail the key role played by spinal cord damage in determining clinical progression in MS.

Appendix I

Different cohorts of patients and controls included in the studies presented in this thesis

Except for the study presented in Chapter V, which involved a large cohort of well-established PPMS patients from the MAGNIMS cohort, all the data presented in this thesis come from the investigation of the London cohort of 50 early PPMS patients, recruited within 5 years of clinical onset and followed-up for five years with clinical and radiological assessments. Since all the studies presented in this work result from a retrospective analysis performed on previously acquired data, not all the MRI sequences were available in all the patients at all time-points, and this is the reason why in each study the number of patients included is different, although they all belong to the same “early PP” cohort. For the same reason, volumetric, MTR and DTI images were not available in the same group of healthy controls, and therefore two different groups of healthy subjects were included in both the studies presented in Chapter III and Chapter IV.

A table summarising the details of the patients and the healthy controls included in each study is presented below:

	Chapter III	Chapter IV	Chapter V	Chapter VI	Chapter VII
Patients	36 patients from the London early PPMS cohort (those with both DTI and volumetric images at baseline)	47 patients from the London early PPMS cohort (those with both MTI and volumetric images at baseline and after two years)	80 patients from the MAGNIMS cohort of well-established PPMS patients (those with T1w and T2w scans at baseline and a 10 year clinical follow-up)	21 patients from the London early PPMS cohort (those with DTI and MTI images at baseline and after 1 year)	32 patients from the London early PPMS cohort (those with both DTI and volumetric images at baseline, and a clinical follow-up after five years)
Controls	2 different control groups: one of 18 subjects with DTI images, and one with 23 subjects with volumetric images	2 different control groups: one of 23 subjects with DTI images at baseline, and one with 18 subjects with MTI and volumetric images at baseline and after two years)	-	-	31 controls (recruited at the same time of the patients' 5-year follow-up, to undergo the neuropsychological assessment)

Table AI Patient and healthy control groups included in the studies presented in this thesis

References

Abe O, Masutani Y, Aoki S, Yamasue H, Yamada H, Kasai K, Mori H, Hayashi N, Masumoto T, Ohtomo K. 2004 Jul. Topography of the human corpus callosum using diffusion tensor tractography. J Comput Assist Tomogr 28(4):533-539.

Absinta M, Rocca MA, Colombo B, Falini A, Comi G, Filippi M. 2011 Dec. Selective decreased grey matter volume of the pain-matrix network in cluster headache. Cephalalgia.

Agosta F, Benedetti B, Rocca MA, Valsasina P, Rovaris M, Comi G, Filippi M. 2005 Feb. Quantification of cervical cord pathology in primary progressive MS using diffusion tensor MRI. Neurology 64(4):631-635.

Agosta F, Absinta M, Sormani MP, Ghezzi A, Bertolotto A, Montanari E, Comi G, Filippi M. 2007 Aug. In vivo assessment of cervical cord damage in MS patients: a longitudinal diffusion tensor MRI study. Brain 130(Pt 8):2211-2219.

Albert M, Antel J, Bruck W, Stadelmann C. 2007 Apr. Extensive cortical remyelination in patients with chronic multiple sclerosis. Brain Pathol 17(2):129-138.

Alexander DC, Pierpaoli C, Basser PJ, Gee JC. 2001 Nov. Spatial transformations of diffusion tensor magnetic resonance images. IEEE Trans Med Imaging 20(11):1131-1139.

Allen C, Jiang K, Malbecq W, Goadsby PJ. 1999 Jul. Time-to-event analysis, or who gets better sooner? An emerging concept in headache study methodology. Cephalalgia 19(6):552-556.

Amato MP, Zipoli V, Portaccio E. 2006 Jun. Multiple sclerosis-related cognitive changes: a review of cross-sectional and longitudinal studies. J Neurol Sci 245(1-2):41-46.

Andersen RA, Buneo CA. 2002. Intentional maps in posterior parietal cortex. Annu Rev Neurosci 25:189-220.

Anderson VM, Fisniku LK, Khaleeli Z, Summers MM, Penny SA, Altmann DR, Thompson AJ, Ron MA, Miller DH. 2010 Sep. Hippocampal atrophy in relapsing-remitting and primary progressive MS: a comparative study. Mult Scler 16(9):1083-1090.

Andersson PB, Waubant E, Gee L, Goodkin DE. 1999 Sep. Multiple sclerosis that is progressive from the time of onset: clinical characteristics and progression of disability. Arch Neurol 56(9):1138-1142.

Antel J, Antel S, Caramanos Z, Arnold DL, Kuhlmann T. 2012 May. Primary progressive multiple sclerosis: part of the MS disease spectrum or separate disease entity? Acta Neuropathol 123(5):627-638.

Ascherio A, Munger KL. 2007 Jun. Environmental risk factors for multiple sclerosis. Part II: Noninfectious factors. Ann Neurol 61(6):504-513.

Ashburner J, Friston KJ. 2000 Jun. Voxel-based morphometry--the methods. Neuroimage 11(6 Pt 1):805-821.

Ashburner J, Friston KJ. 2005 Jul. Unified segmentation. Neuroimage 26(3):839-851.

Audoin B, Au Duong MV, Ranjeva JP, Ibarrola D, Malikova I, Confort-Gouny S, Soulier E, Viout P, Ali-Cherif A, Pelletier J, Cozzone PJ. 2005 Mar. Magnetic resonance study of the influence of tissue damage and cortical reorganization on PASAT performance at the earliest stage of multiple sclerosis. Hum Brain Mapp 24(3):216-228.

Audoin B, Davies G, Rashid W, Fisniku L, Thompson AJ, Miller DH. 2007 May. Voxel-based analysis of grey matter magnetization transfer ratio maps in early relapsing remitting multiple sclerosis. Mult Scler 13(4):483-489.

Bakshi R, Thompson AJ, Rocca MA, Pelletier D, Dousset V, Barkhof F, Inglese M, Guttmann CR, Horsfield MA, Filippi M. 2008 Jul. MRI in multiple sclerosis: current status and future prospects. Lancet Neurol 7(7):615-625.

Barcellos LF, Oksenberg JR, Begovich AB, Martin ER, Schmidt S, Vittinghoff E, Goodin DS, Pelletier D, Lincoln RR, Bucher P, Swerdlin A, Pericak-Vance MA, Haines JL, Hauser SL. 2003 Mar. HLA-DR2 dose effect on susceptibility to multiple sclerosis and influence on disease course. Am J Hum Genet 72(3):710-716.

Barkhof F. 2002 Jun. The clinico-radiological paradox in multiple sclerosis revisited. Curr Opin Neurol 15(3):239-245.

Basser PJ, Mattiello J, LeBihan D. 1994 Mar. Estimation of the effective self-diffusion tensor from the NMR spin echo. J Magn Reson B 103(3):247-254.

Basser PJ. 1995 Nov. Inferring microstructural features and the physiological state of tissues from diffusion-weighted images. NMR Biomed 8(7-8):333-344.

Basser PJ, Pierpaoli C. 1996 Jun. Microstructural and physiological features of tissues elucidated by quantitative-diffusion-tensor MRI. J Magn Reson B 111(3):209-219.

Bedi GS, Brown AD, Delgado SR, Usmani N, Lam BL, Sheremata WA. 2011 Oct. Impact of rituximab on relapse rate and disability in neuromyelitis optica. Mult Scler 17(10):1225-1230.

Bendfeldt K, Blumhagen JO, Egger H, Loetscher P, Denier N, Kuster P, Traud S, Mueller-Lenke N, Naegelin Y, Gass A, Hirsch J, Kappos L, Nichols TE, Radue EW, Borgwardt SJ. 2010 Oct. Spatiotemporal distribution pattern of

white matter lesion volumes and their association with regional grey matter volume reductions in relapsing-remitting multiple sclerosis. Hum Brain Mapp 31(10):1542-1555.

Bick AS, Mayer A, Levin N. 2012 Jan. From research to clinical practice: implementation of functional magnetic imaging and white matter tractography in the clinical environment. J Neurol Sci 312(1-2):158-165.

Bieniek M, Altmann DR, Davies GR, Ingle GT, Rashid W, Sastre-Garriga J, Thompson AJ, Miller DH. 2006 Sep. Cord atrophy separates early primary progressive and relapsing remitting multiple sclerosis. J Neurol Neurosurg Psychiatry 77(9):1036-1039.

Bjartmar C, Trapp BD. 2001 Jun. Axonal and neuronal degeneration in multiple sclerosis: mechanisms and functional consequences. Curr Opin Neurol 14(3):271-278.

Bloch F. 1946. Nuclear induction. Phys Rev 70:460.

Bo L, Vedeler CA, Nyland HI, Trapp BD, Mork SJ. 2003 Jul. Subpial demyelination in the cerebral cortex of multiple sclerosis patients. J Neuropathol Exp Neurol 62(7):723-732.

Bo L, Geurts JJ, van d, V, Polman C, Barkhof F. 2007 Jan. Lack of correlation between cortical demyelination and white matter pathologic changes in multiple sclerosis. Arch Neurol 64(1):76-80.

Bodini B, Khaleeli Z, Cercignani M, Miller DH, Thompson AJ, Ciccarelli O. 2009 Sep. Exploring the relationship between white matter and gray matter damage in early primary progressive multiple sclerosis: an in vivo study with TBSS and VBM. Hum Brain Mapp 30(9):2852-2861.

Bogen JE, Fisher ED, Vogel PJ. 1965 Dec. Cerebral commissurotomy. A second case report. JAMA 194(12):1328-1329.

Bonzano L, Tacchino A, Roccatagliata L, Abbruzzese G, Mancardi GL, Bove M. 2008 Mar. Callosal contributions to simultaneous bimanual finger movements. J Neurosci 28(12):3227-3233.

Bozzali M, Cercignani M, Sormani MP, Comi G, Filippi M. 2002 Jun. Quantification of brain gray matter damage in different MS phenotypes by use of diffusion tensor MR imaging. AJNR Am J Neuroradiol 23(6):985-988.

Bramow S, Frischer JM, Lassmann H, Koch-Henriksen N, Lucchinetti CF, Sorensen PS, Laursen H. 2010 Oct. Demyelination versus remyelination in progressive multiple sclerosis. Brain 133(10):2983-2998.

Brinkmann V. 2009 Nov. FTY720 (fingolimod) in Multiple Sclerosis: therapeutic effects in the immune and the central nervous system. Br J Pharmacol 158(5):1173-1182.

Buchsbaum BR, Greer S, Chang WL, Berman KF. 2005 May. Meta-analysis of neuroimaging studies of the Wisconsin card-sorting task and component processes. Hum Brain Mapp 25(1):35-45.

Buckner RL, Wheeler ME. 2001 Sep. The cognitive neuroscience of remembering. Nat Rev Neurosci 2(9):624-634.

Burgess PW, Shallice T. 1997. The Hayling and Brixton Tests. Bury St Edmunds, Suffolk.

Cader S, Johansen-Berg H, Wylezinska M, Palace J, Behrens TE, Smith S, Matthews PM. 2007 May. Discordant white matter N-acetylasparate and diffusion MRI measures suggest that chronic metabolic dysfunction contributes to axonal pathology in multiple sclerosis. Neuroimage 36(1):19-27.

Calabrese M, De SN, Atzori M, Bernardi V, Mattisi I, Barachino L, Morra A, Rinaldi L, Romualdi C, Perini P, Battistin L, Gallo P. 2007 Oct. Detection of cortical inflammatory lesions by double inversion recovery magnetic resonance imaging in patients with multiple sclerosis. Arch Neurol 64(10):1416-1422.

Calabrese M, Rocca MA, Atzori M, Mattisi I, Bernardi V, Favaretto A, Barachino L, Romualdi C, Rinaldi L, Perini P, Gallo P, Filippi M. 2009 Apr. Cortical lesions in primary progressive multiple sclerosis: a 2-year longitudinal MR study. Neurology 72(15):1330-1336.

Calabrese M, Battaglini M, Giorgio A, Atzori M, Bernardi V, Mattisi I, Gallo P, De SN. 2010 Oct. Imaging distribution and frequency of cortical lesions in patients with multiple sclerosis. Neurology 75(14):1234-1240.

Calabrese M, Poretto V, Favaretto A, Alessio S, Bernardi V, Romualdi C, Rinaldi F, Perini P, Gallo P. 2012 Oct. Cortical lesion load associates with progression of disability in multiple sclerosis. Brain 135(Pt 10):2952-2961.

Camina-Tato M, Morcillo-Suarez C, Bustamante MF, Ortega I, Navarro A, Muntasell A, Lopez-Botet M, Sanchez A, Carmona P, Julia E, Tortola MT, Audi L, Oksenberg JR, Martin R, Montalban X, Comabella M. 2010 Nov. Gender-associated differences of perforin polymorphisms in the susceptibility to multiple sclerosis. J Immunol 185(9):5392-5404.

Camp SJ, Stevenson VL, Thompson AJ, Miller DH, Borras C, Auriacombe S, Brochet B, Falautano M, Filippi M, Herisse-Dulo L, Montalban X, Parrcira E, Polman CH, De SJ, Langdon DW. 1999 Jul. Cognitive function in primary progressive and transitional progressive multiple sclerosis: a controlled study with MRI correlates. Brain 122 (Pt 7):1341-1348.

Camp SJ, Stevenson VL, Thompson AJ, Ingle GT, Miller DH, Borras C, Brochet B, Dousset V, Falautano M, Filippi M, Kalkers NF, Montalban X, Polman CH, Langdon DW. 2005 Dec. A longitudinal study of cognition in primary progressive multiple sclerosis. Brain 128(Pt 12):2891-2898.

Carr HY, Purcell EM. 1954. Effects of diffusion on free precession in nuclear magnetic resonance experiments. Phys Rev.

Catani M, Howard RJ, Pajevic S, Jones DK. 2002 Sep. Virtual in vivo interactive dissection of white matter fasciculi in the human brain. Neuroimage 17(1):77-94.

Catani M, Jones DK, Donato R, Ffytche DH. 2003 Sep. Occipito-temporal connections in the human brain. Brain 126(Pt 9):2093-2107.

Ceccarelli A, Rocca MA, Pagani E, Colombo B, Martinelli V, Comi G, Filippi M. 2008 Aug. A voxel-based morphometry study of grey matter loss in MS patients with different clinical phenotypes. Neuroimage 42(1):315-322.

Ceccarelli A, Rocca MA, Valsasina P, Rodegher M, Pagani E, Falini A, Comi G, Filippi M. 2009 Sep. A multiparametric evaluation of regional brain damage in patients with primary progressive multiple sclerosis. Hum Brain Mapp 30(9):3009-3019.

Ceccarelli A, Rocca MA, Valsasina P, Rodegher M, Falini A, Comi G, Filippi M. 2010 Apr. Structural and functional magnetic resonance imaging correlates of motor network dysfunction in primary progressive multiple sclerosis. Eur J Neurosci 31(7):1273-1280.

Cercignani M, Bozzali M, Iannucci G, Comi G, Filippi M. 2001 Mara. Magnetisation transfer ratio and mean diffusivity of normal appearing white and

grey matter from patients with multiple sclerosis. J Neurol Neurosurg Psychiatry 70(3):311-317.

Cercignani M, Inglese M, Pagani E, Comi G, Filippi M. 2001 Mayb. Mean diffusivity and fractional anisotropy histograms of patients with multiple sclerosis. AJNR Am J Neuroradiol 22(5):952-958.

Chao YP, Cho KH, Yeh CH, Chou KH, Chen JH, Lin CP. 2009 Oct. Probabilistic topography of human corpus callosum using cytoarchitectural parcellation and high angular resolution diffusion imaging tractography. Hum Brain Mapp 30(10):3172-3187.

Chard DT, Jackson JS, Miller DH, Wheeler-Kingshott CA. 2010 Jul. Reducing the impact of white matter lesions on automated measures of brain gray and white matter volumes. J Magn Reson Imaging 32(1):223-228.

Charil A, Dagher A, Lerch JP, Zijdenbos AP, Worsley KJ, Evans AC. 2007 Jan. Focal cortical atrophy in multiple sclerosis: relation to lesion load and disability. Neuroimage 34(2):509-517.

Chen JT, Kuhlmann T, Jansen GH, Collins DL, Atkins HL, Freedman MS, O'Connor PW, Arnold DL. 2007 Jul. Voxel-based analysis of the evolution of magnetization transfer ratio to quantify remyelination and demyelination with histopathological validation in a multiple sclerosis lesion. Neuroimage 36(4):1152-1158.

Chen JT, Collins DL, Atkins HL, Freedman MS, Arnold DL. 2008 Feb. Magnetization transfer ratio evolution with demyelination and remyelination in multiple sclerosis lesions. Ann Neurol 63(2):254-262.

Chen X, Ma X, Jiang Y, Pi R, Liu Y, Ma L. 2011 Jun. The prospects of minocycline in multiple sclerosis. J Neuroimmunol 235(1-2):1-8.

Choi SR, Howell OW, Carassiti D, Magliozzi R, Gveric D, Muraro PA, Nicholas R, Roncaroli F, Reynolds R. 2012 Aug. Meningeal inflammation plays a role in the pathology of primary progressive multiple sclerosis. Brain.

Ciccarelli O, Werring DJ, Wheeler-Kingshott CA, Barker GJ, Parker GJ, Thompson AJ, Miller DH. 2001 Apr. Investigation of MS normal-appearing brain using diffusion tensor MRI with clinical correlations. Neurology 56(7):926-933.

Ciccarelli O, Catani M, Johansen-Berg H, Clark C, Thompson A. 2008 Aug. Diffusion-based tractography in neurological disorders: concepts, applications, and future developments. Lancet Neurol 7(8):715-727.

Ciccarelli O, Kwok PPWV, Chard D, Stromillo ML, De Stefano N, Thompson AJ, Miller DH, Alexander DC. 2012. Predicting clinical conversion to multiple sclerosis in patients with clinically isolated syndrome using machine learning techniques.

Cocco E, Sotgiu A, Costa G, Murru MR, Mancosu C, Murru R, Lai M, Contu P, Marrosu MG. 2005 Feb. HLA-DR,DQ and APOE genotypes and gender influence in Sardinian primary progressive MS. Neurology 64(3):564-566.

Confavreux C, Vukusic S. 2006 Mar. Natural history of multiple sclerosis: a unifying concept. Brain 129(Pt 3):606-616.

Coombs BD, Best A, Brown MS, Miller DE, Corboy J, Baier M, Simon JH. 2004 Aug. Multiple sclerosis pathology in the normal and abnormal appearing white matter of the corpus callosum by diffusion tensor imaging. Mult Scler 10(4):392-397.

Correale J, Ysrraelit MC, Gaitan MI. 2011 Dec. Vitamin D-mediated immune regulation in Multiple Sclerosis. J Neurol Sci 311(1-2):23-31.

Cottrell DA, Kremenchutzky M, Rice GP, Koopman WJ, Hader W, Baskerville J, Ebers GC. 1999 Apr. The natural history of multiple sclerosis: a geographically based study. 5. The clinical features and natural history of primary progressive multiple sclerosis. Brain 122 (Pt 4):625-639.

Coughlan AK, Hollows AK. 1985. The Adult Memory and Information Processing Battery. Leeds.

Cutter GR, Baier ML, Rudick RA, Cookfair DL, Fischer JS, Petkau J, Syndulko K, Weinshenker BG, Antel JP, Confavreux C, Ellison GW, Lublin F, Miller AE, Rao SM, Reingold S, Thompson A, Willoughby E. 1999 May. Development of a

multiple sclerosis functional composite as a clinical trial outcome measure. Brain 122 (Pt 5):871-882.

Dalby RB, Frandsen J, Chakravarty MM, Ahdidan J, Sorensen L, Rosenberg R, Videbech P, Ostergaard L. 2010 Oct. Depression severity is correlated to the integrity of white matter fiber tracts in late-onset major depression. Psychiatry Res 184(1):38-48.

Dalton C, Bodini B, Samson R, Battaglini M, Fisniku L, Thompson A, Ciccarelli O, Miller D, Chard D. 2011 Aug. Brain lesion location and clinical status status 20 years after a diagnosis of clinically isolated syndrome suggestive of multiple sclerosis. Mult Scler.

Damoiseaux JS, Smith SM, Witter MP, Sanz-Arigita EJ, Barkhof F, Scheltens P, Stam CJ, Zarei M, Rombouts SA. 2009 Apr. White matter tract integrity in aging and Alzheimer's disease. Hum Brain Mapp 30(4):1051-1059.

De Stefano N, Matthews PM, Filippi M, Agosta F, De LM, Bartolozzi ML, Guidi L, Ghezzi A, Montanari E, Cifelli A, Federico A, Smith SM. 2003 Apr. Evidence of early cortical atrophy in MS: relevance to white matter changes and disability. Neurology 60(7):1157-1162.

De Stefano N, Battaglini M, Stromillo ML, Zipoli V, Bartolozzi ML, Guidi L, Siracusa G, Portaccio E, Giorgio A, Sorbi S, Federico A, Amato MP. 2006 Aug. Brain damage as detected by magnetization transfer imaging is less

pronounced in benign than in early relapsing multiple sclerosis. Brain 129(Pt 8):2008-2016.

De Stefano N, Giorgio A, Battaglini M, Rovaris M, Sormani MP, Barkhof F, Korteweg T, Enzinger C, Fazekas F, Calabrese M, Dinacci D, Tedeschi G, Gass A, Montalban X, Rovira A, Thompson A, Comi G, Miller DH, Filippi M. 2010 Jun. Assessing brain atrophy rates in a large population of untreated multiple sclerosis subtypes. Neurology 74(23):1868-1876.

de Zeeuw P, Mandl RC, Hulshoff Pol HE, van EH, Durston S. 2011 Aug. Decreased frontostriatal microstructural organization in attention deficit/hyperactivity disorder. Hum Brain Mapp.

Dehmeshki J, Silver NC, Leary SM, Tofts PS, Thompson AJ, Miller DH. 2001 Mar. Magnetisation transfer ratio histogram analysis of primary progressive and other multiple sclerosis subgroups. J Neurol Sci 185(1):11-17.

Dehmeshki J, Chard DT, Leary SM, Watt HC, Silver NC, Tofts PS, Thompson AJ, Miller DH. 2003 Jan. The normal appearing grey matter in primary progressive multiple sclerosis: a magnetisation transfer imaging study. J Neurol 250(1):67-74.

Della Nave R, Ginestroni A, Tessa C, Salvatore E, Bartolomei I, Salvi F, Dotti MT, De MG, Piacentini S, Mascalchi M. 2008 Mar. Brain white matter tracts degeneration in Friedreich ataxia. An in vivo MRI study using tract-based spatial statistics and voxel-based morphometry. Neuroimage 40(1):19-25.

Deloire-Grassin MS, Brochet B, Quesson B, Delalande C, Dousset V, Canioni P, Petry KG. 2000 Sep. In vivo evaluation of remyelination in rat brain by magnetization transfer imaging. J Neurol Sci 178(1):10-16.

Deoni SC. 2011. Magnetic resonance relaxation and quantitative measurement in the brain. Methods Mol Biol 711:65-108.

Di Perri C, Battaglini M, Stromillo ML, Bartolozzi ML, Guidi L, Federico A, De SN. 2008 Feb. Voxel-based assessment of differences in damage and distribution of white matter lesions between patients with primary progressive and relapsing-remitting multiple sclerosis. Arch Neurol 65(2):236-243.

Dineen RA, Vilisaar J, Hlinka J, Bradshaw CM, Morgan PS, Constantinescu CS, Auer DP. 2009 Jan. Disconnection as a mechanism for cognitive dysfunction in multiple sclerosis. Brain 132(Pt 1):239-249.

Douaud G, Smith S, Jenkinson M, Behrens T, Johansen-Berg H, Vickers J, James S, Voets N, Watkins K, Matthews PM, James A. 2007 Sep. Anatomically related grey and white matter abnormalities in adolescent-onset schizophrenia. Brain 130(Pt 9):2375-2386.

Droogan AG, Clark CA, Werring DJ, Barker GJ, McDonald WI, Miller DH. 1999 Jun. Comparison of multiple sclerosis clinical subgroups using navigated spin echo diffusion-weighted imaging. Magn Reson Imaging 17(5):653-661.

Dwyer M, Bergsland N, Hussein S, Durfee J, Wack D, Zivadinov R. 2009 Jul. A sensitive, noise-resistant method for identifying focal demyelination and remyelination in patients with multiple sclerosis via voxel-wise changes in magnetization transfer ratio. J Neurol Sci 282(1-2):86-95.

Dziedzic T, Metz I, Dallenga T, Konig FB, Muller S, Stadelmann C, Bruck W. 2010 Sep. Wallerian degeneration: a major component of early axonal pathology in multiple sclerosis. Brain Pathol 20(5):976-985.

Farrell RA, Antony D, Wall GR, Clark DA, Fisniku L, Swanton J, Khaleeli Z, Schmierer K, Miller DH, Giovannoni G. 2009 Jul. Humoral immune response to EBV in multiple sclerosis is associated with disease activity on MRI. Neurology 73(1):32-38.

Ferreira Vasconcelos CC, Santos Thuler LC, Cruz dos Santos GA, Papais AM, Papais AM, Gomes Camargo SM, Papais Alvarenga RM. 2010 May. Differences in the progression of primary progressive multiple sclerosis in Brazilians of African descent versus white Brazilian patients. Mult Scler 16(5):597-603.

Filippi M, Rocca MA, Martino G, Horsfield MA, Comi G. 1998 Jun. Magnetization transfer changes in the normal appearing white matter precede the appearance of enhancing lesions in patients with multiple sclerosis. Ann Neurol 43(6):809-814.

Filippi M. 1999. Magnetization transfer imaging to monitor the evolution of individual multiple sclerosis lesions. Neurology 53(5 Suppl 3):S18-S22.

Filippi M, Iannucci G, Tortorella C, Minicucci L, Horsfield MA, Colombo B, Sormani MP, Comi G. 1999 Feb. Comparison of MS clinical phenotypes using conventional and magnetization transfer MRI. Neurology 52(3):588-594.

Filippi M, Inglese M, Rovaris M, Sormani MP, Horsfield P, Iannucci PG, Colombo B, Comi G. 2000 Oct. Magnetization transfer imaging to monitor the evolution of MS: a 1-year follow-up study. Neurology 55(7):940-946.

Filippi M, Agosta F. 2010 Apr. Imaging biomarkers in multiple sclerosis. J Magn Reson Imaging 31(4):770-788.

Filippi M, Rocca MA, Barkhof F, Bruck W, Chen JT, Comi G, DeLuca G, De SN, Erickson BJ, Evangelou N, Fazekas F, Geurts JJ, Lucchinetti C, Miller DH, Pelletier D, Popescu BF, Lassmann H. 2012 Apr. Association between pathological and MRI findings in multiple sclerosis. Lancet Neurol 11(4):349-360.

Fisher E, Lee JC, Nakamura K, Rudick RA. 2008 Sep. Gray matter atrophy in multiple sclerosis: a longitudinal study. Ann Neurol 64(3):255-265.

Fitzner D, Simons M. 2010 Sep. Chronic progressive multiple sclerosis - pathogenesis of neurodegeneration and therapeutic strategies. Curr Neuropharmacol 8(3):305-315.

Focke NK, Yogarajah M, Bonelli SB, Bartlett PA, Symms MR, Duncan JS. 2008 Apr. Voxel-based diffusion tensor imaging in patients with mesial temporal lobe epilepsy and hippocampal sclerosis. Neuroimage 40(2):728-737.

Foong J, Rozewicz L, Chong WK, Thompson AJ, Miller DH, Ron MA. 2000 Feb. A comparison of neuropsychological deficits in primary and secondary progressive multiple sclerosis. J Neurol 247(2):97-101.

Fox RJ, Thompson A, Baker D, Baneke P, Brown D, Browne P, Chandraratna D, Ciccarelli O, Coetzee T, Comi G, Feinstein A, Kapoor R, Lee K, Salvetti M, Sharrock K, Toosy A, Zaratin P, Zuidwijk K. 2012 Nov. Setting a research agenda for progressive multiple sclerosis: The International Collaborative on Progressive MS. Mult Scler 18(11):1534-1540.

Frischer JM, Bramow S, Dal-Bianco A, Lucchinetti CF, Rauschka H, Schmidbauer M, Laursen H, Sorensen PS, Lassmann H. 2009 May. The relation between inflammation and neurodegeneration in multiple sclerosis brains. Brain 132(Pt 5):1175-1189.

Friston KJ, Penny WD, Ashburner JT, Kiebel SJ, Nichols.T.E. 2006. Statistical Parametric Mapping: The Analysis of Functional Brain Images. Elsevier Science.

Gallagher TA, Nemeth AJ, Hacein-Bey L. 2008 May. An introduction to the Fourier transform: relationship to MRI. AJR Am J Roentgenol 190(5):1396-1405.

Garrard P, Bradshaw D, Jager HR, Thompson AJ, Losseff N, Playford D. 2002 Aug. Cognitive dysfunction after isolated brain stem insult. An underdiagnosed cause of long term morbidity. J Neurol Neurosurg Psychiatry 73(2):191-194.

Gass A, Barker GJ, Kidd D, Thorpe JW, MacManus D, Brennan A, Tofts PS, Thompson AJ, McDonald WI, Miller DH. 1994 Jul. Correlation of magnetization transfer ratio with clinical disability in multiple sclerosis. Ann Neurol 36(1):62-67.

Gazzaniga MS. 2005 Aug. Forty-five years of split-brain research and still going strong. Nat Rev Neurosci 6(8):653-659.

Geurts JJ, Pouwels PJ, Uitdehaag BM, Polman CH, Barkhof F, Castelijns JA. 2005 Jul. Intracortical lesions in multiple sclerosis: improved detection with 3D double inversion-recovery MR imaging. Radiology 236(1):254-260.

Geurts JJ, Barkhof F. 2008 Sep. Grey matter pathology in multiple sclerosis. Lancet Neurol 7(9):841-851.

Geurts JJ, Stys PK, Minagar A, Amor S, Zivadinov R. 2009 Jul. Gray matter pathology in (chronic) MS: modern views on an early observation. J Neurol Sci 282(1-2):12-20.

Geurts JJ, Kooi EJ, Witte ME, van d, V. 2010 Nov. Multiple sclerosis as an "inside-out" disease. Ann Neurol 68(5):767-768.

Geurts JJ, Roosendaal SD, Calabrese M, Ciccarelli O, Agosta F, Chard DT, Gass A, Huerga E, Moraal B, Pareto D, Rocca MA, Wattjes MP, Yousry TA, Uitdehaag BM, Barkhof F. 2011 Feb. Consensus recommendations for MS cortical lesion scoring using double inversion recovery MRI. Neurology 76(5):418-424.

Geurts JJ, Calabrese M, Fisher E, Rudick RA. 2012 Dec. Measurement and clinical effect of grey matter pathology in multiple sclerosis. Lancet Neurol 11(12):1082-1092.

Ginestroni A, Battaglini M, Della NR, Moretti M, Tessa C, Giannelli M, Caffarra P, Nacmias B, Bessi V, Sorbi S, Bracco L, De SN, Mascalchi M. 2009 Jun. Early structural changes in individuals at risk of familial Alzheimer's disease: a volumetry and magnetization transfer MR imaging study. J Neurol 256(6):925-932.

Giorgio A, Watkins KE, Douaud G, James AC, James S, De SN, Matthews PM, Smith SM, Johansen-Berg H. 2008 Jan. Changes in white matter microstructure during adolescence. Neuroimage 39(1):52-61.

Giorgio A, Santelli L, Tomassini V, Bosnell R, Smith S, De SN, Johansen-Berg H. 2010 Jul. Age-related changes in grey and white matter structure throughout adulthood. Neuroimage 51(3):943-951.

Goertsches R, Baranzini SE, Morcillo C, Nos C, Camina M, Oksenberg JR, Montalban X, Comabella M. 2008 Apr. Evidence for association of chromosome

10 open reading frame (C10orf27) gene polymorphisms and multiple sclerosis. Mult Scler 14(3):412-414.

Good CD, Johnsrude IS, Ashburner J, Henson RN, Friston KJ, Frackowiak RS. 2001 Jul. A voxel-based morphometric study of ageing in 465 normal adult human brains. Neuroimage 14(1 Pt 1):21-36.

Goodman AD, Brown TR, Krupp LB, Schapiro RT, Schwid SR, Cohen R, Marinucci LN, Blight AR. 2009 Feb. Sustained-release oral fampridine in multiple sclerosis: a randomised, double-blind, controlled trial. Lancet 373(9665):732-738.

Goodman AD, Brown TR, Edwards KR, Krupp LB, Schapiro RT, Cohen R, Marinucci LN, Blight AR. 2010 Oct. A phase 3 trial of extended release oral dalfampridine in multiple sclerosis. Ann Neurol 68(4):494-502.

Gorgoraptis N, Wheeler-Kingshott CA, Jenkins TM, Altmann DR, Miller DH, Thompson AJ, Ciccarelli O. 2010 May. Combining tractography and cortical measures to test system-specific hypotheses in multiple sclerosis. Mult Scler 16(5):555-565.

Grossman RI, Gomori JM, Ramer KN, Lexa FJ, Schnall MD. 1994 Mar. Magnetization transfer: theory and clinical applications in neuroradiology. Radiographics 14(2):279-290.

Haase A, Frahm J, Matthaei D, Hanicke W, Merboldt KD. 1986. Flash imaging: rapid NMR imaging using low flip angle pulses. J Magn Reson 67:258.

Hahn EL. 1950. Spin Echoes. Phys Rev.

Haller S, Xekardaki A, Delaloye C, Canuto A, Lovblad KO, Gold G, Giannakopoulos P. 2011 Nov. Combined analysis of grey matter voxel-based morphometry and white matter tract-based spatial statistics in late-life bipolar disorder. J Psychiatry Neurosci 36(6):391-401.

Hauser SL, Waubant E, Arnold DL, Vollmer T, Antel J, Fox RJ, Bar-Or A, Panzara M, Sarkar N, Agarwal S, Langer-Gould A, Smith CH. 2008 Feb. B-cell depletion with rituximab in relapsing-remitting multiple sclerosis. N Engl J Med 358(7):676-688.

Hawker K, O'Connor P, Freedman MS, Calabresi PA, Antel J, Simon J, Hauser S, Waubant E, Vollmer T, Panitch H, Zhang J, Chin P, Smith CH. 2009 Oct. Rituximab in patients with primary progressive multiple sclerosis: results of a randomized double-blind placebo-controlled multicenter trial. Ann Neurol 66(4):460-471.

He Y, Dagher A, Chen Z, Charil A, Zijdenbos A, Worsley K, Evans A. 2009 May. Impaired small-world efficiency in structural cortical networks in multiple sclerosis associated with white matter lesion load. Brain.

Hobart J, Freeman J, Thompson A. 2000 May. Kurtzke scales revisited: the application of psychometric methods to clinical intuition. Brain 123 (Pt 5):1027-1040.

Howell OW, Reeves CA, Nicholas R, Carassiti D, Radotra B, Gentleman SM, Serafini B, Aloisi F, Roncaroli F, Magliozzi R, Reynolds R. 2011 Sep. Meningeal inflammation is widespread and linked to cortical pathology in multiple sclerosis. Brain 134(Pt 9):2755-2771.

Huijbregts SC, Kalkers NF, de Sonneville LM, de G, V, Reuling IE, Polman CH. 2004 Jul. Differences in cognitive impairment of relapsing remitting, secondary, and primary progressive MS. Neurology 63(2):335-339.

Huijbregts SC, Kalkers NF, de Sonneville LM, de G, V, Polman CH. 2006 Jun. Cognitive impairment and decline in different MS subtypes. J Neurol Sci 245(1-2):187-194.

Idris MN, Sokrab TE, Ibrahim EA, Ali HE, Elzibair MA, Abadalatif M, Osman RR. 2009 Dec. Multiple sclerosis in Sudan: a prospective study of clinical presentation and outcome. Mult Scler 15(12):1537-1538.

Ingle GT, Stevenson VL, Miller DH, Thompson AJ. 2003 Nov. Primary progressive multiple sclerosis: a 5-year clinical and MR study. Brain 126(Pt 11):2528-2536.

Ingle GT, Sastre-Garriga J, Miller DH, Thompson AJ. 2005 Sep. Is inflammation important in early PPMS? a longitudinal MRI study. J Neurol Neurosurg Psychiatry 76(9):1255-1258.

Jafari N, Hintzen RQ. 2011 Dec. The association between cigarette smoking and multiple sclerosis. J Neurol Sci 311(1-2):78-85.

Jang SH, Hong JH. 2012 Jan. The anatomical characteristics of superior longitudinal fasciculus I in human brain: Diffusion tensor tractography study. Neurosci Lett 506(1):146-148.

Jasperse B, Vrenken H, Sanz-Arigita E, de G, V, Smith SM, Polman CH, Barkhof F. 2007 Nov. Regional brain atrophy development is related to specific aspects of clinical dysfunction in multiple sclerosis. Neuroimage 38(3):529-537.

Jenkinson M, Smith S. 2001 Jun. A global optimisation method for robust affine registration of brain images. Med Image Anal 5(2):143-156.

Jensen CJ, Stankovich J, Van der Walt A, Bahlo M, Taylor BV, van der Mei IA, Foote SJ, Kilpatrick TJ, Johnson LJ, Wilkins E, Field J, Danoy P, Brown MA, Rubio JP, Butzkueven H. 2010. Multiple sclerosis susceptibility-associated SNPs do not influence disease severity measures in a cohort of Australian MS patients. PLoS One 5(4):e10003.

Johansen-Berg H, Della-Maggiore V, Behrens TE, Smith SM, Paus T. 2007. Integrity of white matter in the corpus callosum correlates with bimanual co-ordination skills. Neuroimage 36 Suppl 2:T16-T21.

Jokinen H, Ryberg C, Kalska H, Ylikoski R, Rostrup E, Stegmann MB, Waldemar G, Madureira S, Ferro JM, van Straaten EC, Scheltens P, Barkhof F, Fazekas F, Schmidt R, Carlucci G, Pantoni L, Inzitari D, Erkinjuntti T. 2007 May. Corpus callosum atrophy is associated with mental slowing and executive deficits in subjects with age-related white matter hyperintensities: the LADIS Study. J Neurol Neurosurg Psychiatry 78(5):491-496.

Jones DK, Horsfield MA, Simmons A. 1999 Sep. Optimal strategies for measuring diffusion in anisotropic systems by magnetic resonance imaging. Magn Reson Med 42(3):515-525.

Jones DK. 2009. Gaussian Modeling of the Diffusion Signal. In: Diffusion MRI: from quantitative measurement to in vivo neuroanatomy. Johansen-Berg H, Behrens T, editors, Elsevier Academic Press, Oxford. 37-54.

Kantarci OH, Schaefer-Klein JL, Hebrink DD, Achenbach SJ, Atkinson EJ, McMurray CT, Weinshenker BG. 2003 Apr. A population-based study of IL4 polymorphisms in multiple sclerosis. J Neuroimmunol 137(1-2):134-139.

Karagulle Kendi AT, Lehericy S, Luciana M, Ugurbil K, Tuite P. 2008 Mar. Altered diffusion in the frontal lobe in Parkinson disease. AJNR Am J Neuroradiol 29(3):501-505.

Kelly S, Kinsella K, Duggan M, Tubridy N, McGuigan C, Hutchinson M. 2012 Nov. A proposed modification to the McDonald 2010 criteria for the diagnosis of primary progressive multiple sclerosis. Mult Scler.

Kern KC, Sarcona J, Montag M, Giesser BS, Sicotte NL. 2010 Nov. Corpus callosal diffusivity predicts motor impairment in relapsing-remitting multiple sclerosis: A TBSS and tractography study. Neuroimage.

Kern KC, Sarcona J, Montag M, Giesser BS, Sicotte NL. 2011 Apr. Corpus callosal diffusivity predicts motor impairment in relapsing-remitting multiple sclerosis: a TBSS and tractography study. Neuroimage 55(3):1169-1177.

Khaleeli Z, Sastre-Garriga J, Ciccarelli O, Miller DH, Thompson AJ. 2007 Octa. Magnetisation transfer ratio in the normal appearing white matter predicts progression of disability over 1 year in early primary progressive multiple sclerosis. J Neurol Neurosurg Psychiatry 78(10):1076-1082.

Khaleeli Z, Cercignani M, Audoin B, Ciccarelli O, Miller DH, Thompson AJ. 2007 Augb. Localized grey matter damage in early primary progressive multiple sclerosis contributes to disability. Neuroimage 37(1):253-261.

Khaleeli Z, Altmann DR, Cercignani M, Ciccarelli O, Miller DH, Thompson AJ. 2008 Nova. Magnetization transfer ratio in gray matter: a potential surrogate marker for progression in early primary progressive multiple sclerosis. Arch Neurol 65(11):1454-1459.

Khaleeli Z, Ciccarelli O, Manfredonia F, Barkhof F, Brochet B, Cercignani M, Dousset V, Filippi M, Montalban X, Polman C, Rovaris M, Rovira A, Sastre-Garriga J, Vellinga M, Miller D, Thompson A. 2008 Junb. Predicting progression in primary progressive multiple sclerosis: a 10-year multicenter study. Ann Neurol 63(6):790-793.

Khaleeli Z, Ciccarelli O, Mizskiel K, Altmann D, Miller DH, Thompson AJ. 2010 Mar. Lesion enhancement diminishes with time in primary progressive multiple sclerosis. Mult Scler 16(3):317-324.

Koch G, Cercignani M, Pecchioli C, Versace V, Oliveri M, Caltagirone C, Rothwell J, Bozzali M. 2010 May. In vivo definition of parieto-motor connections involved in planning of grasping movements. Neuroimage 51(1):300-312.

Koch M, Kingwell E, Rieckmann P, Tremlett H. 2009 Dec. The natural history of primary progressive multiple sclerosis. Neurology 73(23):1996-2002.

Kooi EJ, Strijbis EM, van d, V, Geurts JJ. 2012 Sep. Heterogeneity of cortical lesions in multiple sclerosis: clinical and pathologic implications. Neurology 79(13):1369-1376.

Kragt JJ, Thompson AJ, Montalban X, Tintore M, Rio J, Polman CH, Uitdehaag BM. 2008 Mar. Responsiveness and predictive value of EDSS and MSFC in primary progressive MS. Neurology 70(13 Pt 2):1084-1091.

Kurtzke JF. 1983 Nov. Rating neurologic impairment in multiple sclerosis: an expanded disability status scale (EDSS). Neurology 33(11):1444-1452.

Kutzelnigg A, Lucchinetti CF, Stadelmann C, Bruck W, Rauschka H, Bergmann M, Schmidbauer M, Parisi JE, Lassmann H. 2005 Nov. Cortical demyelination and diffuse white matter injury in multiple sclerosis. Brain 128(Pt 11):2705-2712.

Langdon DW. 2011 Jun. Cognition in multiple sclerosis. Curr Opin Neurol 24(3):244-249.

Larson EB, Burnison DS, Brown WS. 2002 Apr. Callosal function in multiple sclerosis: bimanual motor coordination. Cortex 38(2):201-214.

Lassmann H, van HJ, Mahad D. 2012 Sep. Progressive multiple sclerosis: pathology and pathogenesis. Nat Rev Neurol.

Laule C, Vavasour IM, Zhao Y, Traboulsee AL, Oger J, Vavasour JD, Mackay AL, Li DK. 2010 Jun. Two-year study of cervical cord volume and myelin water in primary progressive multiple sclerosis. Mult Scler 16(6):670-677.

Law CG, Brookmeyer R. 1992 Sep. Effects of mid-point imputation on the analysis of doubly censored data. Stat Med 11(12):1569-1578.

Lazar M. 2010 Aug. Mapping brain anatomical connectivity using white matter tractography. NMR Biomed 23(7):821-835.

Le Bihan D, Breton E, Lallemand D, Grenier P, Cabanis E, Laval-Jeantet M. 1986 Nov. MR imaging of intravoxel incoherent motions: application to diffusion and perfusion in neurologic disorders. Radiology 161(2):401-407.

Leary SM, Silver NC, Stevenson VL, Barker GJ, Miller DH, Thompson AJ. 1999 Oct. Magnetisation transfer of normal appearing white matter in primary progressive multiple sclerosis. Mult Scler 5(5):313-316.

Leary SM, Miller DH, Stevenson VL, Brex PA, Chard DT, Thompson AJ. 2003 Jan. Interferon beta-1a in primary progressive MS: an exploratory, randomized, controlled trial. Neurology 60(1):44-51.

Lechner-Scott J, Kappos L, Hofman M, Polman CH, Ronner H, Montalban X, Tintore M, Frontoni M, Buttinelli C, Amato MP, Bartolozzi ML, Versavel M, Dahlke F, Kapp JF, Gibberd R. 2003 Mar. Can the Expanded Disability Status Scale be assessed by telephone? Mult Scler 9(2):154-159.

Li DK, Held U, Petkau J, Daumer M, Barkhof F, Fazekas F, Frank JA, Kappos L, Miller DH, Simon JH, Wolinsky JS, Filippi M. 2006 May. MRI T2 lesion burden in multiple sclerosis: a plateauing relationship with clinical disability. Neurology 66(9):1384-1389.

Lin F, Yu C, Jiang T, Li K, Chan P. 2007 Feb. Diffusion tensor tractography-based group mapping of the pyramidal tract in relapsing-remitting multiple sclerosis patients. AJNR Am J Neuroradiol 28(2):278-282.

Lin X, Tench CR, Morgan PS, Constantinescu CS. 2008 Apr. Use of combined conventional and quantitative MRI to quantify pathology related to cognitive impairment in multiple sclerosis. J Neurol Neurosurg Psychiatry 79(4):437-441.

Ljunggren S. 1983. A simple graphical representation of Fourier-based imaging methods. J Magn Reson 54:338.

Losseff NA, Webb SL, O'Riordan JI, Page R, Wang L, Barker GJ, Tofts PS, McDonald WI, Miller DH, Thompson AJ. 1996 Jun. Spinal cord atrophy and disability in multiple sclerosis. A new reproducible and sensitive MRI method with potential to monitor disease progression. Brain 119 (Pt 3):701-708.

Lublin FD, Reingold SC. 1996 Apr. Defining the clinical course of multiple sclerosis: results of an international survey. National Multiple Sclerosis Society (USA) Advisory Committee on Clinical Trials of New Agents in Multiple Sclerosis. Neurology 46(4):907-911.

Lucas RM, Hughes AM, Lay ML, Ponsonby AL, Dwyer DE, Taylor BV, Pender MP. 2011 Oct. Epstein-Barr virus and multiple sclerosis. J Neurol Neurosurg Psychiatry 82(10):1142-1148.

Lucchinetti C, Popescu BFG, Bunyan RF, Moli NM, Roemer SF, Lassmann H, Bruck W, Parisi J, Scheithauer B, Giannini C, Weigand SD, Mandrekar J, Ransohoff RM. 2011. Inflammatory cortical demyelination in early multiple sclerosis. N Engl J Med 365:2188-2197.

Lycklama G, Thompson A, Filippi M, Miller D, Polman C, Fazekas F, Barkhof F. 2003 Sep. Spinal-cord MRI in multiple sclerosis. Lancet Neurol 2(9):555-562.

Magliozzi R, Howell O, Vora A, Serafini B, Nicholas R, Puopolo M, Reynolds R, Aloisi F. 2007 Apr. Meningeal B-cell follicles in secondary progressive multiple sclerosis associate with early onset of disease and severe cortical pathology. Brain 130(Pt 4):1089-1104.

Magliozzi R, Howell OW, Reeves C, Roncaroli F, Nicholas R, Serafini B, Aloisi F, Reynolds R. 2010 Oct. A Gradient of neuronal loss and meningeal inflammation in multiple sclerosis. Ann Neurol 68(4):477-493.

Mansfield P, Pykett IL. 1977. Biological and medical imaging by NMR. J Magn Reson 29:355.

Martino J, Brogna C, Robles SG, Vergani F, Duffau H. 2010 May. Anatomic dissection of the inferior fronto-occipital fasciculus revisited in the lights of brain stimulation data. Cortex 46(5):691-699.

Maurer M, Ponath A, Kruse N, Rieckmann P. 2002 Oct. CTLA4 exon 1 dimorphism is associated with primary progressive multiple sclerosis. J Neuroimmunol 131(1-2):213-215.

Mazziotta J, Toga A, Evans A, Fox P, Lancaster J, Zilles K, Woods R, Paus T, Simpson G, Pike B, Holmes C, Collins L, Thompson P, MacDonald D, Iacoboni M, Schormann T, Amunts K, Palomero-Gallagher N, Geyer S, Parsons L, Narr

K, Kabani N, Le GG, Boomsma D, Cannon T, Kawashima R, Mazoyer B. 2001 Aug. A probabilistic atlas and reference system for the human brain: International Consortium for Brain Mapping (ICBM). Philos Trans R Soc Lond B Biol Sci 356(1412):1293-1322.

McDonald WI, Compston A, Edan G, Goodkin D, Hartung HP, Lublin FD, McFarland HF, Paty DW, Polman CH, Reingold SC, Sandberg-Wollheim M, Sibley W, Thompson A, van den NS, Weinshenker BY, Wolinsky JS. 2001 Jul. Recommended diagnostic criteria for multiple sclerosis: guidelines from the International Panel on the diagnosis of multiple sclerosis. Ann Neurol 50(1):121-127.

Mesaros S, Rocca MA, Riccitelli G, Pagani E, Rovaris M, Caputo D, Ghezzi A, Capra R, Bertolotto A, Comi G, Filippi M. 2009 Aug. Corpus callosum damage and cognitive dysfunction in benign MS. Hum Brain Mapp 30(8):2656-2666.

Mesaros S, Rocca MA, Pagani E, Sormani MP, Petrolini M, Comi G, Filippi M. 2011 Jun. Thalamic damage predicts the evolution of primary-progressive multiple sclerosis at 5 years. AJNR Am J Neuroradiol 32(6):1016-1020.

Miki Y, Grossman RI, Udupa JK, Wei L, Polansky M, Mannon LJ, Kolson DL. 1999 Nov. Relapsing-remitting multiple sclerosis: longitudinal analysis of MR images--lack of correlation between changes in T2 lesion volume and clinical findings. Radiology 213(2):395-399.

Miller DH, Leary SM. 2007 Oct. Primary-progressive multiple sclerosis. Lancet Neurol 6(10):903-912.

Miller DH, Chard DT, Ciccarelli O. 2012 Feb. Clinically isolated syndromes. Lancet Neurol 11(2):157-169.

Moll NM, Rietsch AM, Thomas S, Ransohoff AJ, Lee JC, Fox R, Chang A, Ransohoff RM, Fisher E. 2011 Nov. Multiple sclerosis normal-appearing white matter: pathology-imaging correlations. Ann Neurol 70(5):764-773.

Montalban X. 2004 Jun. Overview of European pilot study of interferon beta-Ib in primary progressive multiple sclerosis. Mult Scler 10 Suppl 1:S62-S64.

Montalban X, Sastre-Garriga J, Tintore M, Brieva L, Aymerich FX, Rio J, Porcel J, Borras C, Nos C, Rovira A. 2009 Octa. A single-center, randomized, double-blind, placebo-controlled study of interferon beta-1b on primary progressive and transitional multiple sclerosis. Mult Scler 15(10):1195-1205.

Montalban X, Sastre-Garriga J, Filippi M, Khaleeli Z, Tellez N, Vellinga MM, Tur C, Brochet B, Barkhof F, Rovaris M, Miller DH, Polman CH, Rovira A, Thompson AJ. 2009 Decb. Primary progressive multiple sclerosis diagnostic criteria: a reappraisal. Mult Scler 15(12):1459-1465.

Morgen K, Sammer G, Courtney SM, Wolters T, Melchior H, Blecker CR, Oschmann P, Kaps M, Vaitl D. 2006 Apr. Evidence for a direct association

between cortical atrophy and cognitive impairment in relapsing-remitting MS. Neuroimage 30(3):891-898.

Mori S. 2005. MRI Atlas of Human White Matter. Elsevier, Amsterdam, The Netherlands.

Mostert JP, Koch MW, Steen C, Heersema DJ, De Groot JC, De KJ. 2010 Dec. T2 lesions and rate of progression of disability in multiple sclerosis. Eur J Neurol 17(12):1471-1475.

Moy G, Millet P, Haller S, Baudois S, de BF, Weber K, Lovblad K, Lazeyras F, Giannakopoulos P, Delaloye C. 2011 Jul. Magnetic resonance imaging determinants of intraindividual variability in the elderly: combined analysis of grey and white matter. Neuroscience 186:88-93.

Munger KL, Levin LI, Hollis BW, Howard NS, Ascherio A. 2006 Dec. Serum 25-hydroxyvitamin D levels and risk of multiple sclerosis. JAMA 296(23):2832-2838.

Nakamura K, Fisher E. 2009 Feb. Segmentation of brain magnetic resonance images for measurement of gray matter atrophy in multiple sclerosis patients. Neuroimage 44(3):769-776.

Natarajan R, Einarsdottir E, Riutta A, Hagman S, Raunio M, Mononen N, Lehtimaki T, Elovaara I. 2012 Sep. Melatonin pathway genes are associated

with progressive subtypes and disability status in multiple sclerosis among Finnish patients. J Neuroimmunol 250(1-2):106-110.

Nelson HE. 1982. The National Adult Reading Test.

Nguyen D, Vargas MI, Khaw N, Seeck M, Delavelle J, Lovblad KO, Haller S. 2011 Mar. Diffusion tensor imaging analysis with tract-based spatial statistics of the white matter abnormalities after epilepsy surgery. Epilepsy Res.

Nichols TE, Holmes AP. 2002 Jan. Nonparametric permutation tests for functional neuroimaging: a primer with examples. Hum Brain Mapp 15(1):1-25.

Nijeholt GJ, van Walderveen MA, Castelijns JA, van Waesberghe JH, Polman C, Scheltens P, Rosier PF, Jongen PJ, Barkhof F. 1998 Apr. Brain and spinal cord abnormalities in multiple sclerosis. Correlation between MRI parameters, clinical subtypes and symptoms. Brain 121 (Pt 4):687-697.

Nijeholt GJ, Castelijns JA, Lazeron RH, van Waesberghe JH, Polman CH, Uitdehaag BM, Barkhof F. 2000 Apr. Magnetization transfer ratio of the spinal cord in multiple sclerosis: relationship to atrophy and neurologic disability. J Neuroimaging 10(2):67-72.

O'Riordan JI, Gawne CM, Coles A, Wang L, Compston DA, Tofts P, Miller DH. 1998 Oct. T1 hypointense lesion load in secondary progressive multiple sclerosis: a comparison of pre versus post contrast loads and of manual versus

semi automated threshold techniques for lesion segmentation. Mult Scler 4(5):408-412.

Ozturk A, Smith SA, Gordon-Lipkin EM, Harrison DM, Shiee N, Pham DL, Caffo BS, Calabresi PA, Reich DS. 2010 Feb. MRI of the corpus callosum in multiple sclerosis: association with disability. Mult Scler 16(2):166-177.

Pagani E, Filippi M, Rocca MA, Horsfield MA. 2005 Maya. A method for obtaining tract-specific diffusion tensor MRI measurements in the presence of disease: application to patients with clinically isolated syndromes suggestive of multiple sclerosis. Neuroimage 26(1):258-265.

Pagani E, Rocca MA, Gallo A, Rovaris M, Martinelli V, Comi G, Filippi M. 2005 Febb. Regional brain atrophy evolves differently in patients with multiple sclerosis according to clinical phenotype. AJNR Am J Neuroradiol 26(2):341-346.

Panitch H, Miller A, Paty D, Weinshenker B. 2004 Nov. Interferon beta-1b in secondary progressive MS: results from a 3-year controlled study. Neurology 63(10):1788-1795.

Park HJ, Kim JJ, Lee SK, Seok JH, Chun J, Kim DI, Lee JD. 2008 May. Corpus callosal connection mapping using cortical gray matter parcellation and DT-MRI. Hum Brain Mapp 29(5):503-516.

Parker GJ, Haroon HA, Wheeler-Kingshott CA. 2003 Aug. A framework for a streamline-based probabilistic index of connectivity (PICo) using a structural interpretation of MRI diffusion measurements. J Magn Reson Imaging 18(2):242-254.

Patani R, Balaratnam M, Vora A, Reynolds R. 2007 Jun. Remyelination can be extensive in multiple sclerosis despite a long disease course. Neuropathol Appl Neurobiol 33(3):277-287.

Patrikios P, Stadelmann C, Kutzelnigg A, Rauschka H, Schmidbauer M, Laursen H, Sorensen PS, Bruck W, Lucchinetti C, Lassmann H. 2006 Dec. Remyelination is extensive in a subset of multiple sclerosis patients. Brain 129(Pt 12):3165-3172.

Pelletier D, Nelson SJ, Oh J, Antel JP, Kita M, Zamvil SS, Goodkin DE. 2003 Jul. MRI lesion volume heterogeneity in primary progressive MS in relation with axonal damage and brain atrophy. J Neurol Neurosurg Psychiatry 74(7):950-952.

Penny S, Khaleeli Z, Cipolotti L, Thompson A, Ron M. 2010 Feb. Early imaging predicts later cognitive impairment in primary progressive multiple sclerosis. Neurology 74(7):545-552.

Pierpaoli C, Basser PJ. 1996 Dec. Toward a quantitative assessment of diffusion anisotropy. Magn Reson Med 36(6):893-906.

Pipe J. 2009. Pulse sequences for diffusion-weighted MRI. In: Diffusion MRI: from quantitative measurement to in vivo neuroanatomy. Johansen-Berg H, Behrens TE, editors, Elsevier Academic Press, Oxford. 11-35.

Plummer D. 1992. DispImage: A display and analysis tool for medical images. Rev Neuroradiol 5:489-495.

Polman CH, Reingold SC, Edan G, Filippi M, Hartung HP, Kappos L, Lublin FD, Metz LM, McFarland HF, O'Connor PW, Sandberg-Wollheim M, Thompson AJ, Weinshenker BG, Wolinsky JS. 2005 Dec. Diagnostic criteria for multiple sclerosis: 2005 revisions to the "McDonald Criteria". Ann Neurol 58(6):840-846.

Polman CH, Reingold SC, Banwell B, Clanet M, Cohen JA, Filippi M, Fujihara K, Havrdova E, Hutchinson M, Kappos L, Lublin FD, Montalban X, O'Connor P, Sandberg-Wollheim M, Thompson AJ, Waubant E, Weinshenker B, Wolinsky JS. 2011 Feb. Diagnostic criteria for multiple sclerosis: 2010 revisions to the McDonald criteria. Ann Neurol 69(2):292-302.

Pomeroy IM, Jordan EK, Frank JA, Matthews PM, Esiri MM. 2008 May. Diffuse cortical atrophy in a marmoset model of multiple sclerosis. Neurosci Lett 437(2):121-124.

Poser CM, Paty DW, Scheinberg L, McDonald WI, Davis FA, Ebers GC, Johnson KP, Sibley WA, Silberberg DH, Tourtellotte WW. 1983 Mar. New diagnostic criteria for multiple sclerosis: guidelines for research protocols. Ann Neurol 13(3):227-231.

Prinster A, Quarantelli M, Orefice G, Lanzillo R, Brunetti A, Mollica C, Salvatore E, Morra VB, Coppola G, Vacca G, Alfano B, Salvatore M. 2006 Feb. Grey matter loss in relapsing-remitting multiple sclerosis: a voxel-based morphometry study. Neuroimage 29(3):859-867.

Ramagopalan SV, DeLuca GC, Degenhardt A, Ebers GC. 2008 Sep. The genetics of clinical outcome in multiple sclerosis. J Neuroimmunol 201-202:183-199.

Ramagopalan SV, Dobson R, Meier UC, Giovannoni G. 2010 Jul. Multiple sclerosis: risk factors, prodromes, and potential causal pathways. Lancet Neurol 9(7):727-739.

Ramio-Torrenta L, Sastre-Garriga J, Ingle GT, Davies GR, Ameen V, Miller DH, Thompson AJ. 2006 Jan. Abnormalities in normal appearing tissues in early primary progressive multiple sclerosis and their relation to disability: a tissue specific magnetisation transfer study. J Neurol Neurosurg Psychiatry 77(1):40-45.

Raz E, Cercignani M, Sbardella E, Totaro P, Pozzilli C, Bozzali M, Pantano P. 2010 Nova. Gray- and white-matter changes 1 year after first clinical episode of multiple sclerosis: MR imaging. Radiology 257(2):448-454.

Raz E, Cercignani M, Sbardella E, Totaro P, Pozzilli C, Bozzali M, Pantano P. 2010 Janb. Clinically isolated syndrome suggestive of multiple sclerosis:

voxelwise regional investigation of white and gray matter. Radiology 254(1):227-234.

Reich DS, Smith SA, Jones CK, Zackowski KM, van Zijl PC, Calabresi PA, Mori S. 2006 Nov. Quantitative characterization of the corticospinal tract at 3T. AJNR Am J Neuroradiol 27(10):2168-2178.

Reich DS, Smith SA, Zackowski KM, Gordon-Lipkin EM, Jones CK, Farrell JA, Mori S, van Zijl PC, Calabresi PA. 2007 Nov. Multiparametric magnetic resonance imaging analysis of the corticospinal tract in multiple sclerosis. Neuroimage 38(2):271-279.

Reich DS, Zackowski KM, Gordon-Lipkin EM, Smith SA, Chodkowski BA, Cutter GR, Calabresi PA. 2008 Feb. Corticospinal tract abnormalities are associated with weakness in multiple sclerosis. AJNR Am J Neuroradiol 29(2):333-339.

Reynolds R, Roncaroli F, Nicholas R, Radotra B, Gveric D, Howell O. 2011 Aug. The neuropathological basis of clinical progression in multiple sclerosis. Acta Neuropathol 122(2):155-170.

Riccitelli G, Rocca MA, Pagani E, Rodegher ME, Rossi P, Falini A, Comi G, Filippi M. 2011 Oct. Cognitive impairment in multiple sclerosis is associated to different patterns of gray matter atrophy according to clinical phenotype. Hum Brain Mapp 32(10):1535-1543.

Rice GP, Filippi M, Comi G. 2000 Mar. Cladribine and progressive MS: clinical and MRI outcomes of a multicenter controlled trial. Cladribine MRI Study Group. Neurology 54(5):1145-1155.

Rocca MA, Colombo B, Falini A, Ghezzi A, Martinelli V, Scotti G, Comi G, Filippi M. 2005 Oct. Cortical adaptation in patients with MS: a cross-sectional functional MRI study of disease phenotypes. Lancet Neurol 4(10):618-626.

Rocca MA, Absinta M, Filippi M. 2012 Apra. The role of advanced magnetic resonance imaging techniques in primary progressive MS. J Neurol 259(4):611-621.

Rocca MA, Valsasina P, Damjanovic D, Horsfield MA, Mesaros S, Stosic-Opincal T, Drulovic J, Filippi M. 2012 Octb. Voxel-wise mapping of cervical cord damage in multiple sclerosis patients with different clinical phenotypes. J Neurol Neurosurg Psychiatry.

Roosendaal SD, Geurts JJ, Vrenken H, Hulst HE, Cover KS, Castelijns JA, Pouwels PJ, Barkhof F. 2009 Feb. Regional DTI differences in multiple sclerosis patients. Neuroimage 44(4):1397-1403.

Roosendaal SD, Bendfeldt K, Vrenken H, Polman CH, Borgwardt S, Radue EW, Kappos L, Pelletier D, Hauser SL, Matthews PM, Barkhof F, Geurts JJ. 2011 Sep. Grey matter volume in a large cohort of MS patients: relation to MRI parameters and disability. Mult Scler 17(9):1098-1106.

Ropele S, Fazekas F. 2009 Feb. Magnetization transfer MR imaging in multiple sclerosis. Neuroimaging Clin N Am 19(1):27-36.

Rosenfeld A, Kak AC. 1982. Digital Picture Processing 2nd edition. Academic Press, Orlando (FL).

Rovaris M, Bozzali M, Santuccio G, Ghezzi A, Caputo D, Montanari E, Bertolotto A, Bergamaschi R, Capra R, Mancardi G, Martinelli V, Comi G, Filippi M. 2001 Dec. In vivo assessment of the brain and cervical cord pathology of patients with primary progressive multiple sclerosis. Brain 124(Pt 12):2540-2549.

Rovaris M, Gass A, Bammer R, Hickman SJ, Ciccarelli O, Miller DH, Filippi M. 2005 Nov. Diffusion MRI in multiple sclerosis. Neurology 65(10):1526-1532.

Rovaris M, Judica E, Gallo A, Benedetti B, Sormani MP, Caputo D, Ghezzi A, Montanari E, Bertolotto A, Mancardi G, Bergamaschi R, Martinelli V, Comi G, Filippi M. 2006 Oct. Grey matter damage predicts the evolution of primary progressive multiple sclerosis at 5 years. Brain 129(Pt 10):2628-2634.

Rovaris M, Judica E, Sastre-Garriga J, Rovira A, Sormani MP, Benedetti B, Korteweg T, De SN, Khaleeli Z, Montalban X, Barkhof F, Miller DH, Polman C, Thompson AJ, Filippi M. 2008 May. Large-scale, multicentre, quantitative MRI study of brain and cord damage in primary progressive multiple sclerosis. Mult Scler 14(4):455-464.

Rudick RA, Lee JC, Simon J, Fisher E. 2006 Aug. Significance of T2 lesions in multiple sclerosis: A 13-year longitudinal study. Ann Neurol 60(2):236-242.

Rugg MD, Otten LJ, Henson RN. 2002 Aug. The neural basis of episodic memory: evidence from functional neuroimaging. Philos Trans R Soc Lond B Biol Sci 357(1424):1097-1110.

Santos AC, Narayanan S, De SN, Tartaglia MC, Francis SJ, Arnaoutelis R, Caramanos Z, Antel JP, Pike GB, Arnold DL. 2002 Jun. Magnetization transfer can predict clinical evolution in patients with multiple sclerosis. J Neurol 249(6):662-668.

Sastre-Garriga J, Ingle GT, Chard DT, Ramio-Torrenta L, Miller DH, Thompson AJ. 2004 May. Grey and white matter atrophy in early clinical stages of primary progressive multiple sclerosis. Neuroimage 22(1):353-359.

Sastre-Garriga J, Ingle GT, Chard DT, Cercignani M, Ramio-Torrenta L, Miller DH, Thompson AJ. 2005 Juna. Grey and white matter volume changes in early primary progressive multiple sclerosis: a longitudinal study. Brain 128(Pt 6):1454-1460.

Sastre-Garriga J, Ingle GT, Rovaris M, Tellez N, Jasperse B, Altmann DR, Benedetti B, Stevenson VL, Cercignani M, Leary SM, Barkhof F, Brochet B, Dousset V, Filippi M, Montalban X, Kalkers NF, Polman CH, Rovira A, Miller DH, Thompson AJ. 2005 Augb. Long-term clinical outcome of primary

progressive MS: predictive value of clinical and MRI data. Neurology 65(4):633-635.

Sawcer S, Hellenthal G, Pirinen M, Spencer CC, Patsopoulos NA, Moutsianas L, Dilthey A, Su Z, Freeman C, Hunt SE, Edkins S, Gray E, Booth DR, Potter SC, Goris A, Band G, Oturai AB, Strange A, Saarela J, Bellenguez C, Fontaine B, Gillman M, Hemmer B, Gwilliam R, Zipp F, Jayakumar A, Martin R, Leslie S, Hawkins S, Giannoulatou E, D'alfonso S, Blackburn H, Martinelli BF, Liddle J, Harbo HF, Perez ML, Spurkland A, Waller MJ, Mycko MP, Ricketts M, Comabella M, Hammond N, Kockum I, McCann OT, Ban M, Whittaker P, Kemppinen A, Weston P, Hawkins C, Widaa S, Zajicek J, Dronov S, Robertson N, Bumpstead SJ, Barcellos LF, Ravindrarajah R, Abraham R, Alfredsson L, Ardlie K, Aubin C, Baker A, Baker K, Baranzini SE, Bergamaschi L, Bergamaschi R, Bernstein A, Berthele A, Boggild M, Bradfield JP, Brassat D, Broadley SA, Buck D, Butzkueven H, Capra R, Carroll WM, Cavalla P, Celius EG, Cepok S, Chiavacci R, Clerget-Darpoux F, Clysters K, Comi G, Cossburn M, Cournu-Rebeix I, Cox MB, Cozen W, Cree BA, Cross AH, Cusi D, Daly MJ, Davis E, de Bakker PI, Debouverie M, D'hooghe MB, Dixon K, Dobosi R, Dubois B, Ellinghaus D, Elovaara I, Esposito F, Fontenille C, Foote S, Franke A, Galimberti D, Ghezzi A, Glessner J, Gomez R, Gout O, Graham C, Grant SF, Guerini FR, Hakonarson H, Hall P, Hamsten A, Hartung HP, Heard RN, Heath S, Hobart J, Hoshi M, Infante-Duarte C, Ingram G, Ingram W, Islam T, Jagodic M, Kabesch M, Kermode AG, Kilpatrick TJ, Kim C, Klopp N, Koivisto K, Larsson M, Lathrop M, Lechner-Scott JS, Leone MA, Leppa V, Liljedahl U, Bomfim IL, Lincoln RR, Link J, Liu J, Lorentzen AR, Lupoli S, Macciardi F, Mack T, Marriott M, Martinelli V, Mason D, McCauley JL, Mentch F, Mero IL, Mihalova T,

Montalban X, Mottershead J, Myhr KM, Naldi P, Ollier W, Page A, Palotie A, Pelletier J, Piccio L, Pickersgill T, Piehl F, Pobywajlo S, Quach HL, Ramsay PP, Reunanen M, Reynolds R, Rioux JD, Rodegher M, Roesner S, Rubio JP, Ruckert IM, Salvetti M, Salvi E, Santaniello A, Schaefer CA, Schreiber S, Schulze C, Scott RJ, Sellebjerg F, Selmaj KW, Sexton D, Shen L, Simms-Acuna B, Skidmore S, Sleiman PM, Smestad C, Sorensen PS, Sondergaard HB, Stankovich J, Strange RC, Sulonen AM, Sundqvist E, Syvanen AC, Taddeo F, Taylor B, Blackwell JM, Tienari P, Bramon E, Tourbah A, Brown MA, Tronczynska E, Casas JP, Tubridy N, Corvin A, Vickery J, Jankowski J, Villoslada P, Markus HS, Wang K, Mathew CG, Wason J, Palmer CN, Wichmann HE, Plomin R, Willoughby E, Rautanen A, Winkelmann J, Wittig M, Trembath RC, Yaouanq J, Viswanathan AC, Zhang H, Wood NW, Zuvich R, Deloukas P, Langford C, Duncanson A, Oksenberg JR, Pericak-Vance MA, Haines JL, Olsson T, Hillert J, Ivinson AJ, De Jager PL, Peltonen L, Stewart GJ, Hafler DA, Hauser SL, McVean G, Donnelly P, Compston A. 2011 Aug. Genetic risk and a primary role for cell-mediated immune mechanisms in multiple sclerosis. Nature 476(7359):214-219.

Schaefer PW, Grant PE, Gonzalez RG. 2000 Nov. Diffusion-weighted MR imaging of the brain. Radiology 217(2):331-345.

Schmahmann JD, Pandya DN. 2007 Oct. The complex history of the fronto-occipital fasciculus. J Hist Neurosci 16(4):362-377.

Schmierer K, Scaravilli F, Altmann DR, Barker GJ, Miller DH. 2004 Sep. Magnetization transfer ratio and myelin in postmortem multiple sclerosis brain. Ann Neurol 56(3):407-415.

Schmierer K, Wheeler-Kingshott CA, Boulby PA, Scaravilli F, Altmann DR, Barker GJ, Tofts PS, Miller DH. 2007 Apr. Diffusion tensor imaging of post mortem multiple sclerosis brain. Neuroimage 35(2):467-477.

Schott JM, Bartlett JW. 2012 May. Investigating missing data in Alzheimer disease studies. Neurology 78(18):1370-1371.

Sdika M, Pelletier D. 2009 Apr. Nonrigid registration of multiple sclerosis brain images using lesion inpainting for morphometry or lesion mapping. Hum Brain Mapp 30(4):1060-1067.

Sepulcre J, Sastre-Garriga J, Cercignani M, Ingle GT, Miller DH, Thompson AJ. 2006 Aug. Regional gray matter atrophy in early primary progressive multiple sclerosis: a voxel-based morphometry study. Arch Neurol 63(8):1175-1180.

Serra L, Cercignani M, Lenzi D, Perri R, Fadda L, Caltagirone C, Macaluso E, Bozzali M. 2010. Grey and white matter changes at different stages of Alzheimer's disease. J Alzheimers Dis 19(1):147-159.

Smith A. 1982. Symbol Digit Modalities Test (SDMT) Manual (revised). Los Angeles.

Smith SM, Jenkinson M, Woolrich MW, Beckmann CF, Behrens TE, Johansen-Berg H, Bannister PR, De LM, Drobnjak I, Flitney DE, Niazy RK, Saunders J, Vickers J, Zhang Y, De SN, Brady JM, Matthews PM. 2004. Advances in functional and structural MR image analysis and implementation as FSL. Neuroimage 23 Suppl 1:S208-S219.

Smith SM, Jenkinson M, Johansen-Berg H, Rueckert D, Nichols TE, Mackay CE, Watkins KE, Ciccarelli O, Cader MZ, Matthews PM, Behrens TE. 2006 Jul. Tract-based spatial statistics: voxelwise analysis of multi-subject diffusion data. Neuroimage 31(4):1487-1505.

Smith SM, Nichols TE. 2009 Jan. Threshold-free cluster enhancement: addressing problems of smoothing, threshold dependence and localisation in cluster inference. Neuroimage 44(1):83-98.

Song SK, Yoshino J, Le TQ, Lin SJ, Sun SW, Cross AH, Armstrong RC. 2005 May. Demyelination increases radial diffusivity in corpus callosum of mouse brain. Neuroimage 26(1):132-140.

Srikanth V, Phan TG, Chen J, Beare R, Stapleton JM, Reutens DC. 2010 Feb. The location of white matter lesions and gait--a voxel-based study. Ann Neurol 67(2):265-269.

Stankoff B, Freeman L, Aigrot MS, Chardain A, Dolle F, Williams A, Galanaud D, Armand L, Lehericy S, Lubetzki C, Zalc B, Bottlaender M. 2011 Apr. Imaging central nervous system myelin by positron emission tomography in multiple

sclerosis using [methyl-(1)(1)C]-2-(4'-methylaminophenyl)- 6-hydroxybenzothiazole. Ann Neurol 69(4):673-680.

Stejskal EO, Tanner JE. 1965. Spin diffusion measurements: spin echoes in the presence of a time-dependent field gradient. J Chem Phys 42:288-292.

Stevenson VL, Miller DH, Rovaris M, Barkhof F, Brochet B, Dousset V, Dousset V, Filippi M, Montalban X, Polman CH, Rovira A, de SJ, Thompson AJ. 1999 Mar. Primary and transitional progressive MS: a clinical and MRI cross-sectional study. Neurology 52(4):839-845.

Stricker NH, Schweinsburg BC, Delano-Wood L, Wierenga CE, Bangen KJ, Haaland KY, Frank LR, Salmon DP, Bondi MW. 2009 Mar. Decreased white matter integrity in late-myelinating fiber pathways in Alzheimer's disease supports retrogenesis. Neuroimage 45(1):10-16.

Stuve O, Kita M, Pelletier D, Fox RJ, Stone J, Goodkin DE, Zamvil SS. 2004 Jun. Mitoxantrone as a potential therapy for primary progressive multiple sclerosis. Mult Scler 10 Suppl 1:S58-S61.

Stys PK, Zamponi GW, van MJ, Geurts JJ. 2012 Jul. Will the real multiple sclerosis please stand up? Nat Rev Neurosci 13(7):507-514.

Tallantyre EC, Bo L, Al-Rawashdeh O, Owens T, Polman CH, Lowe J, Evangelou N. 2009 May. Greater loss of axons in primary progressive multiple

sclerosis plaques compared to secondary progressive disease. Brain 132(Pt 5):1190-1199.

Thompson A. 2004 Jun. Overview of primary progressive multiple sclerosis (PPMS): similarities and differences from other forms of MS, diagnostic criteria, pros and cons of progressive diagnosis. Mult Scler 10 Suppl 1:S2-S7.

Thompson AJ, Montalban X, Barkhof F, Brochet B, Filippi M, Miller DH, Polman CH, Stevenson VL, McDonald WI. 2000 Jun. Diagnostic criteria for primary progressive multiple sclerosis: a position paper. Ann Neurol 47(6):831-835.

Tofts PS. 2003. Quantitative MRI of the brain: measuring changes caused by disease. John Wiley and Sons.

Toosy AT, Ciccarelli O, Parker GJ, Wheeler-Kingshott CA, Miller DH, Thompson AJ. 2004 Apr. Characterizing function-structure relationships in the human visual system with functional MRI and diffusion tensor imaging. Neuroimage 21(4):1452-1463.

Tortorella C, Viti B, Bozzali M, Sormani MP, Rizzo G, Gilardi MF, Comi G, Filippi M. 2000 Jan. A magnetization transfer histogram study of normal-appearing brain tissue in MS. Neurology 54(1):186-193.

Tozer DJ, Chard DT, Bodini B, Ciccarelli O, Miller DH, Thompson AJ, Wheeler-Kingshott CA. 2012 Feb. Linking white matter tracts to associated cortical grey matter: a tract extension methodology. Neuroimage 59(4):3094-3102.

Trapp BD, Peterson J, Ransohoff RM, Rudick R, Mork S, Bo L. 1998 Jan. Axonal transection in the lesions of multiple sclerosis. N Engl J Med 338(5):278-285.

Tremlett H, Paty D, Devonshire V. 2005 Dec. The natural history of primary progressive MS in British Columbia, Canada. Neurology 65(12):1919-1923.

Tremlett H, Zhu F, Petkau J, Oger J, Zhao Y. 2012 Oct. Natural, innate improvements in multiple sclerosis disability. Mult Scler 18(10):1412-1421.

Truyen L, van Waesberghe JH, van Walderveen MA, van Oosten BW, Polman CH, Hommes OR, Ader HJ, Barkhof F. 1996 Dec. Accumulation of hypointense lesions ("black holes") on T1 spin-echo MRI correlates with disease progression in multiple sclerosis. Neurology 47(6):1469-1476.

Tsunoda I, Fujinami RS. 2002. Inside-Out versus Outside-In models for virus induced demyelination: axonal damage triggering demyelination. Springer Semin Immunopathol 24(2):105-125.

Tur C, Khaleeli Z, Ciccarelli O, Altmann DR, Cercignani M, Miller DH, Thompson AJ. 2011 Apra. Complementary roles of grey matter MTR and T2 lesions in predicting progression in early PPMS. J Neurol Neurosurg Psychiatry 82(4):423-428.

Tur C, Penny S, Khaleeli Z, Altmann D, Cipolotti L, Ron M, Thompson A, Ciccarelli O. 2011 Novb. Grey matter damage and overall cognitive impairment in primary progressive multiple sclerosis. Mult Scler 17(11):1324-1332.

Tweig DB. 1983. The k-trajectory formulation of the NMR imaging process with applications in analysis and synthesis of imaging methods. Med Phys 10:610.

Ukkonen M, Vahvelainen T, Hamalainen P, Dastidar P, Elovaara I. 2009 Sep. Cognitive dysfunction in primary progressive multiple sclerosis: a neuropsychological and MRI study. Mult Scler 15(9):1055-1061.

van der Mei I, Ponsonby AL, Dwyer T, Blizzard L, Simmons R, Taylor BV, Butzkueven H, Kilpatrick T. 2003 Aug. Past exposure to sun, skin phenotype, and risk of multiple sclerosis: case-control study. BMJ 327(7410):316.

van der Meulen P, Groen JP, Cuppen JJ. 1985. Very fast MR imaging by field echoes and small angle excitation. Magn Reson Imaging 3(3):297-299.

Van Hecke W, Nagels G, Leemans A, Vandervliet E, Sijbers J, Parizel PM. 2010 Jun. Correlation of cognitive dysfunction and diffusion tensor MRI measures in patients with mild and moderate multiple sclerosis. J Magn Reson Imaging 31(6):1492-1498.

van Waesberghe JH, Kamphorst W, De Groot CJ, van Walderveen MA, Castelijns JA, Ravid R, Nijeholt GJ, van d, V, Polman CH, Thompson AJ, Barkhof F. 1999 Nov. Axonal loss in multiple sclerosis lesions: magnetic

resonance imaging insights into substrates of disability. Ann Neurol 46(5):747-754.

van Walderveen MA, Kamphorst W, Scheltens P, van Waesberghe JH, Ravid R, Valk J, Polman CH, Barkhof F. 1998 May. Histopathologic correlate of hypointense lesions on T1-weighted spin-echo MRI in multiple sclerosis. Neurology 50(5):1282-1288.

Varade J, Comabella M, Ortiz MA, Arroyo R, Fernandez O, Pinto-Medel MJ, Fedetz M, Izquierdo G, Lucas M, Gomez CL, Rabasa AC, Alcina A, Matesanz F, Alloza I, Antiguedad A, Garcia-Barcina M, Otaegui D, Olascoaga J, Saiz A, Blanco Y, Montalban X, Vandenbroeck K, Urcelay E. 2012 Jul. Replication study of 10 genes showing evidence for association with multiple sclerosis: validation of TMEM39A, IL12B and CLBL genes. Mult Scler 18(7):959-965.

Vasconcelos CC, Fernandez O, Leyva L, Thuler LC, Alvarenga RM. 2009 Sep. Does the DRB1*1501 allele confer more severe and faster progression in primary progressive multiple sclerosis patients? HLA in primary progressive multiple sclerosis. J Neuroimmunol 214(1-2):101-103.

Vellinga MM, Geurts JJ, Rostrup E, Uitdehaag BM, Polman CH, Barkhof F, Vrenken H. 2009 Apr. Clinical correlations of brain lesion distribution in multiple sclerosis. J Magn Reson Imaging 29(4):768-773.

Voineskos AN, Rajji TK, Lobaugh NJ, Miranda D, Shenton ME, Kennedy JL, Pollock BG, Mulsant BH. 2010 Apr. Age-related decline in white matter tract

integrity and cognitive performance: A DTI tractography and structural equation modeling study. Neurobiol Aging.

Voineskos AN, Rajji TK, Lobaugh NJ, Miranda D, Shenton ME, Kennedy JL, Pollock BG, Mulsant BH. 2012 Jan. Age-related decline in white matter tract integrity and cognitive performance: a DTI tractography and structural equation modeling study. Neurobiol Aging 33(1):21-34.

Voogd J. 2003 Dec. The human cerebellum. J Chem Neuroanat 26(4):243-252.

Vrenken H, Pouwels PJ, Geurts JJ, Knol DL, Polman CH, Barkhof F, Castelijns JA. 2006 May. Altered diffusion tensor in multiple sclerosis normal-appearing brain tissue: cortical diffusion changes seem related to clinical deterioration. J Magn Reson Imaging 23(5):628-636.

Vrenken H, Pouwels PJ, Ropele S, Knol DL, Geurts JJ, Polman CH, Barkhof F, Castelijns JA. 2007 Jul. Magnetization transfer ratio measurement in multiple sclerosis normal-appearing brain tissue: limited differences with controls but relationships with clinical and MR measures of disease. Mult Scler 13(6):708-716.

Wakana S, Jiang H, Nagae-Poetscher LM, van Zijl PC, Mori S. 2004 Jan. Fiber tract-based atlas of human white matter anatomy. Radiology 230(1):77-87.

Wegner C, Esiri MM, Chance SA, Palace J, Matthews PM. 2006 Sep. Neocortical neuronal, synaptic, and glial loss in multiple sclerosis. Neurology 67(6):960-967.

Weinshenker BG, Rice GP, Noseworthy JH, Carriere W, Baskerville J, Ebers GC. 1991 Apr. The natural history of multiple sclerosis: a geographically based study. 3. Multivariate analysis of predictive factors and models of outcome. Brain 114 (Pt 2):1045-1056.

Westbrook C. 2009. MRI at a glance. Blackwell Science Ltd, Oxford.

Wheeler-Kingshott CA, Boulby PA, Symms MR, Barker GJ. 2002. Optimised cardiac gating for high-resolution whole-brain DTI on a standard scanner.

Wheeler-Kingshott CA, Barker GJ. 2003. The diffusion of water. In: Quantitative MRI: measuring changes caused by disease. Tofts P, editor, John Wiley & Sons, London. 201-255.

Wiendl H, Hohlfeld R. 2009 Mar. Multiple sclerosis therapeutics: unexpected outcomes clouding undisputed successes. Neurology 72(11):1008-1015.

Wilson M, Tench CR, Morgan PS, Blumhardt LD. 2003 Feb. Pyramidal tract mapping by diffusion tensor magnetic resonance imaging in multiple sclerosis: improving correlations with disability. J Neurol Neurosurg Psychiatry 74(2):203-207.

Wingerchuk DM, Noseworthy JH, Weinshenker BG. 1997 Nov. Clinical outcome measures and rating scales in multiple sclerosis trials. Mayo Clin Proc 72(11):1070-1079.

Wolff SD, Balaban RS. 1989. Magnetization transfer contrast (MTC) and tissue water proton relaxation in vivo. Magn Reson Med 10:135-144.

Wolinsky JS, Narayana PA, O'Connor P, Coyle PK, Ford C, Johnson K, Miller A, Pardo L, Kadosh S, Ladkani D. 2007 Jan. Glatiramer acetate in primary progressive multiple sclerosis: results of a multinational, multicenter, double-blind, placebo-controlled trial. Ann Neurol 61(1):14-24.

Woolrich MW, Jbabdi S, Patenaude B, Chappell M, Makni S, Behrens T, Beckmann C, Jenkinson M, Smith SM. 2009 Mar. Bayesian analysis of neuroimaging data in FSL. Neuroimage 45(1 Suppl):S173-S186.

Yu HJ, Christodoulou C, Bhise V, Greenblatt D, Patel Y, Serafin D, Maletic-Savatic M, Krupp LB, Wagshul ME. 2012 Feb. Multiple white matter tract abnormalities underlie cognitive impairment in RRMS. Neuroimage 59(4):3713-3722.

Zhang J, Jones M, DeBoy CA, Reich DS, Farrell JA, Hoffman PN, Griffin JW, Sheikh KA, Miller MI, Mori S, Calabresi PA. 2009 Mar. Diffusion tensor magnetic resonance imaging of Wallerian degeneration in rat spinal cord after dorsal root axotomy. J Neurosci 29(10):3160-3171.

Zivadinov R. 2007 May. Can imaging techniques measure neuroprotection and remyelination in multiple sclerosis? Neurology 68(22 Suppl 3):S72-S82.